Development of a novel MRI technique for imaging the ischaemic penumbra in experimental stroke

Craig Alan Robertson

BSc (Hons), MRes

Submitted in fulfilment of the requirements for the degree of Doctor of Philosophy to the Institute of Neuroscience and Psychology, College of Medical, Veterinary and Life Sciences, University of Glasgow

September, 2011

Abstract

In Scotland, stroke is the third most common cause of death behind heart disease and cancer. However, most strokes are not fatal and can cause severe disability, with one third of survivors still functionally dependent after one year. The advent of recombinant tissue plasminogen activator (rT-PA) as a thrombolytic modality revolutionised the treatment for ischaemic stroke, providing a treatment aimed to promptly restore nutritional blood flow to the ischaemic penumbra, a transient tissue state which is amenable to salvage. Crucially, patient ineligibility from a multitude of factors (including the narrow time window for benefit and the risk of intracranial haemorrhage) means that fewer than 10% of all stroke patients are thrombolysed.

Positive identification of penumbra is not employed in the current intravenous rT-PA administration strategy, which is instead based on two main prerequisites: stroke patients in whom intracerebral haemorrhage has been excluded with non-contrast computed tomography (CT) and who also present within 4.5 hours of symptom onset. The technical impracticalities and limited availability of the gold standard penumbral imaging modality, multitracer ^{15}O positron emission tomography (PET), and the lack of standardised thresholds to identify penumbra using non-contrast CT have hindered the development and inclusion of routine brain imaging in the management of acute stroke patients. An alternative research tool which may potentially be used in clinical practice is magnetic resonance imaging (MRI) which defines penumbra on the basis of diffusion-perfusion (DWI/PWI) mismatch. However, this provides an imprecise measure of penumbra and fails to identify tissue viability.

The T_2^* Oxygen Challenge technique

Current PET-derived definitions of penumbra use metabolic indices such as oxygen extraction fraction (OEF) and the cerebral metabolic rate of oxygen ($CMRO_2$), which are not fully incorporated into MR definitions. This thesis presents an alternative MRI method for identifying the metabolic penumbra in a rodent model of focal cerebral ischaemia. This utilises an MRI sequence similar to that used in functional MRI (fMRI) techniques, and uses 100% oxygen inhalation as a biotracer to detect penumbral tissue. Specifically, by using a blood oxygen level dependent (BOLD) T_2^*-weighted sequence in which changes in the deoxyhaemoglobin:oxyhaemoglobin ratio are detected - in conjunction with a transient

hyperoxic challenge (Oxygen Challenge (OC) paradigm: 5 minutes breathing air followed by 5 minutes breathing 100% oxygen) - penumbral tissue can be distinguished from adjacent ischaemic core and benign oligaemia (Santosh et al, 2008).

Characterisation of the T_2^* BOLD OC technique

Changes in CBF, cerebral blood volume (CBV), tissue oxygenation, and oxidative metabolism can all influence the T_2^* signal (Ramsay et al, 1993; Corfield et al, 2001), so it was important to evaluate the possibility that factors other than tissue metabolism were influencing the signal change during OC. An initial study was performed which showed that baseline CBF did not influence T_2^* signal response to OC, whilst a greater increase in the percentage change in arterial oxygen saturation following OC caused an increased magnitude in T_2^* percentage signal change in contralateral tissue and penumbra, but not in ischaemic core. Arterial oxygen levels (PaO_2) affect the magnitude of the T_2^* signal change to OC, with lower baseline PaO_2 levels amplifying the T_2^* signal response in metabolically active regions, implying that careful control of physiological variables may optimise the T_2^*OC technique.

Confirming metabolic activity in T_2^*OC-defined penumbra using [^{14}C] 2-deoxyglucose autoradiography

The first validation study used [^{14}C] 2-deoxyglucose autoradiography to determine the metabolic status of penumbra defined by T_2^*OC MRI. The results confirmed that glucose metabolism in the T_2^*OC-defined penumbra was comparable to contralateral values, whereas markedly different levels of glucose metabolism were evident in the ADC-derived ischaemic core and an adjacent region of increased 2DG phosphorylation. From this, it was concluded that metabolic information could be yielded from the ischaemic brain that may improve delineation of the penumbra using the OC technique.

Consequences of reperfusion on the T_2^*OC-defined penumbra

As penumbral tissue must fulfil the fundamental criteria of being potentially salvageable and responsive to therapy, the consequences of reperfusion on the T_2^*OC-defined penumbra was tested. This study confirmed that T_2^*OC-defined penumbra displayed a T_2^* signal change significantly higher than contralateral tissue during ischaemia which

subsequently returned to contralateral levels following reperfusion and did not progress to infarction when assessed at day 7 following stroke.

Investigating the spatiotemporal characteristics of the T_2^*OC-defined penumbra

Finally, the spatiotemporal characteristics of the T_2^*OC-defined penumbra were investigated and compared with DWI/PWI mismatch-defined penumbra. Serial scanning demonstrated that T_2^*OC penumbra behaved in a similar manner to tissue defined by traditional mismatch criterion. The spatial location and tissue volumes of penumbra were similar with both methods, showing that, in animals where mismatch tissue volume reduced over time, T_2^*OC penumbra reduced similarly, and in animals where mismatch volume remained static over time, T_2^*OC-defined penumbra behaved similarly. Additionally, an interesting finding arose in the latter study which showed that ischaemic damage continues to progress beyond 4 hours following permanent MCAO, which may be relevant to the calculation of ADC and CBF thresholds used in defining DWI/PWI mismatch.

Collectively, the preclinical data support the potential of T_2^*OC to discriminate tissue compartments in acute stroke based on metabolic status which thereby provides an alternative and improved means of defining the ischaemic penumbra.

List of contents

List of tables

List of figures

Acknowledgements

Foremost, I would like to thank my primary supervisors, Mhairi Macrae and Chris McCabe, for their excellent supervision, guidance and encouragement, and for making my PhD a very enjoyable experience. I am very appreciative of the support provided at the Wellcome Surgical Institute; in particular, Lindsay Gallagher, for experimental assistance and for passing on her considerable surgical skills; Debbie Dewar, for her constructive suggestions and discussions; Margaret Stewart, Linda Carberry and George Graham, for all their histological and practical support, and; Jim Mullin, for his technical and practical input, and especially for his enjoyable conversations.

I would also like to express gratitude to colleagues at the Southern General Hospital; Celestine Santosh, whose ideas and enthusiasm were instrumental in the formation of this thesis; Barrie Condon, my secondary supervisor; Maria del Rosario Lopez-Gonzalez, for her image analysis contributions and assistance; Keith Muir, for his intellectual input and proof-reading of publications, and those that were involved in Oxygen Challenge projects.

Much gratitude goes out to my parents, Marie and David, for supporting me through my years at university, and a big thank you to my girlfriend for her encouragement and continual support.

Declaration

I declare that, except where explicit reference is made to the contribution of others, this dissertation is the result of my own work and has not been submitted for any other degree at the University of Glasgow or any other institution

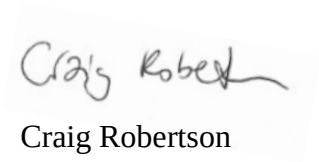

Craig Robertson

Published manuscripts

1. Robertson CA, McCabe C, Gallagher L, Lopez-Gonzalez R, Holmes W, Condon B, Muir KW, Santosh C, Macrae IM (2011) Stroke Penumbra Defined by an MRI-based Oxygen Challenge Technique: 1.Validation using [^{14}C] 2-Deoxyglucose Autoradiography. Journal of Cerebral Blood Flow & Metabolism (in press).

2. Robertson CA, McCabe C, Gallagher L, Lopez-Gonzalez R, Holmes W, Condon B, Muir KW, Santosh C, Macrae IM (2011) Stroke Penumbra Defined by an MRI-based Oxygen Challenge Technique: 2. Validation based on the consequences of reperfusion. Journal of Cerebral Blood Flow & Metabolism (in press)

3. Baskerville TA, Deuchar G, McCabe C, Robertson C, Holmes WH, Santosh C, Macrae IM (2011) Influence of 100% and 40% oxygen on penumbral blood flow, oxygen level and T_2^*-weighted MRI in a rat stroke model. Journal of Cerebral Blood Flow & Metabolism (in press)

Published abstracts

1. Robertson C, McCabe C, Lopez-Gonzalez MDR, Holmes W, Condon B, Muir KW, Santosh C, Macrae, IM (2009) Co-registration of T_2^*-weighted MRI with [^{14}C]-2-deoxyglucose autoradiography to validate delineation of the ischaemic penumbra. J Cereb Blood Flow Metab 2009*;* 29*:* 23.

2. Robertson C, McCabe C, Lopez-Gonzalez MDR, Holmes W, Condon B, Muir KW, Santosh C, Macrae, IM (2011) Stroke penumbra defined by an MRI-based Oxygen Challenge technique: validation using a focal ischaemia model with reperfusion. J Cereb Blood Flow Metab (in press)

List of Abbreviations

^{1}H	hydrogen nuclei
2DG	2-deoxyglucose
2-DG-G-P	2-deoxyglucose-6-phosphate
7T	seven tesla
ADC	apparent diffusion coefficient
AMPA	alpha-amino-3-hydroxy-5-methyl-4-isoxazolepropionate
ANOVA	analysis of variance
APAF1	apoptosis-activating factor
ASL	arterial spin labelling
ASPECTS	Alberta Stroke Program Early CT Score
ATLANTIS	Alteplase Thrombolysis for Acute Noninterventional Therapy in Ischemic Stroke
ATP	adenosine triphosphate
BOLD	blood oxygen level dependent
BP	blood pressure
Ca^{2+}	calcium ion
CASL	continuous arterial spin labelling
CBF	cerebral blood flow
CBV	cerebral blood volume
CI	confidence interval
Cl^{-}	chlorine ion
CMRglc	cerebral glucose utilisation rate
$CMRO_2$	cerebral metabolic rate of oxygen
CNS	central nervous system
CPP	cerebral perfusion pressure
CSD	cortical spreading depolarisations
CSF	cerebrospinal fluid
CT	computed tomography
CTP	computed tomography perfusion
dATP	deoxyadenosine triphosphate
D	diffusion coefficient
DC	direct current

DEFUSE	diffusion and perfusion imaging evaluation for understanding stroke evolution study
DNA	deoxyribonucleic acid
DNase	DNA-degrading enzyme
DPM	disintegrations per minute
DSC	dynamic susceptibility contrast
DWI	diffusion-weighted imaging
DWI/PWI mismatch	diffusion-perfusion mismatch
ECA	external carotid artery
ECASS III	third European Cooperative Acute Stroke Study
ECG	electrocardiogram
EPI	echo planar imaging
EPITHET	Echoplanar Imaging Thrombolytic Evaluation Trial
FLAIR	fluid-attenuated inversion recovery
FMISO	fluoromisonidazole
fMRI	functional magnetic resonance imaging
FMZ	flumazenil
H&E	haematoxylin and eosin
ICA	internal carotid artery
ICH	intracranial haemorrhage
ILF	intraluminal filament
i.v.	intravenous
K^+	potassium ion
LCMRglc	local cerebral metabolic rate of glucose
LCBF	local cerebral blood flow
LDF	laser Doppler Flowmetry
MABP	mean arterial blood pressure
MCA	middle cerebral artery
MCAO	middle cerebral artery occlusion
MHz	megahertz
MRI	magnetic resonance imaging
mRS	modified Rankin Scale
MRS	magnetic resonance spectroscopy
MTT	mean transit time
M_z	longitudinal magnetisation
Na^+	sodium ion

NAIP	neuronal apoptosis inhibitory protein
NIH	National Institute of Health
NIHSS	National Institute of Health stroke scale
NINDS	National Institute of Neurological Disorders and Stroke
NMDA	N-methyl-D-aspartate
NMV	net magnetisation vector
OC	oxygen challenge
OEF	oxygen extraction fraction
OR	odds ratio
OTT	onset to start of treatment
$PaCO_2$	arterial partial pressure of carbon dioxide
PAM	paraformaldehyde in phosphate buffered saline
PaO_2	arterial partial pressure of oxygen
PET	positron emission tomography
PGSE	pulsed gradient spin echo
PID	peri-infarct depolarisations
PWI	perfusion-weighted imaging
RARE	rapid acquisition with refocused echoes
RBC	red blood cell
rCBF	relative cerebral blood flow
RF	radiofrequency
ROI	region of interest
rT-PA	recombinant tissue plasminogen activator
SD	standard deviation
SPECT	single photon emission computed tomography
SUTC	Stroke Unit Trialists' Collaboration
T_1	longitudinal relaxation time
T_2	transverse relaxation time
T_2^*OC	T_2^* oxygen challenge
TE	echo time
TR	repetition time
TTC	2,3,5-triphenyltetrazolium chloride
TTP	time to peak

Chapter

1

Introduction

1.1 Stroke

Stroke is the second most common cause of death and the leading cause of disability worldwide (Donnan et al, 2008). In the UK, stroke accounts for 9% of all deaths and is second only to coronary heart disease. The rate of stroke deaths varies geographically, with parts of Scotland having the highest rates in the UK; for example it is ~50% higher than in London (http://www.heartstats.org, Stroke Statistics 2009). The incidence of stroke death is expected to increase exponentially in the next 20 years for males and females (Mackay and Mensah, 2004), and it has been predicted that stroke will become the leading cause of death worldwide by 2025 (Feigin, 2005). However, most strokes are not fatal and as such it is the greatest cause of severe disability, in which one third of survivors are functionally dependent after one year (Adamson et al, 2004). As a result, the economic implications are considerable. In the UK, the cost of stroke to the health care system was £2.5 billion in 2007, of which, £1.1 billion was devoted to inpatient hospital care and £900 million for residential care (http://www.heartstats.org Stroke Statistics 2009).

1.1.1 Overview, definition and classification

Stroke is defined by the World Health Organization as a rapidly developing loss of cerebral function (focal or global) originating from vascular disturbances, persisting beyond 24h or interrupted by death before 24 hours. The 24 hour time window is selected arbitrarily, although it allows differentiation between a transient ischaemic attack (in which the neurological symptoms resolve within 24 hours) and events of longer duration. Although stroke can be haemorrhagic – caused by an arterial aneurysm rupture or general arteriovenous malformation – the majority of strokes are ischaemic, accounting for approximately 80-87% of all cases of stroke (Chen et al, 2010; Rothwell et al, 2005; Donnan et al, 2008). Ischaemic stroke may be thrombotic or embolic, arising either from atherosclerotic plaques (thrombi), or from a displaced embolus such as a blood clot that travels from the heart to the brain and adheres to the arterial wall (Figure 1.1).

Atherosclerotic plaques can change morphologically, causing ulcerations, thrombosis, calcifications and haemorrhage. Unstable plaques which arise from endothelial disruption cause platelets to affix to the plaque to form a platelet-rich thrombus and the release of vasoactive substances including thromboxane A2 and serotonin, leading to further platelet aggregation and vasoconstriction (Zaman, Helft, Worthley, and Badimon, 2000). Clotting factors are also activated in the blood, and red blood cells aggregate to form a mesh of fibrin. This pathological cascade is combined with the presence of leukocytes that induce an inflammatory response, and the consequence is severe narrowing of the lumen which causes a local occlusion (Fuster et al, 1990). The result of a cerebral vascular occlusion is a severe downstream reduction in blood flow that restricts or precludes nutritive delivery, activating a cascade of deleterious biochemical and cellular events.

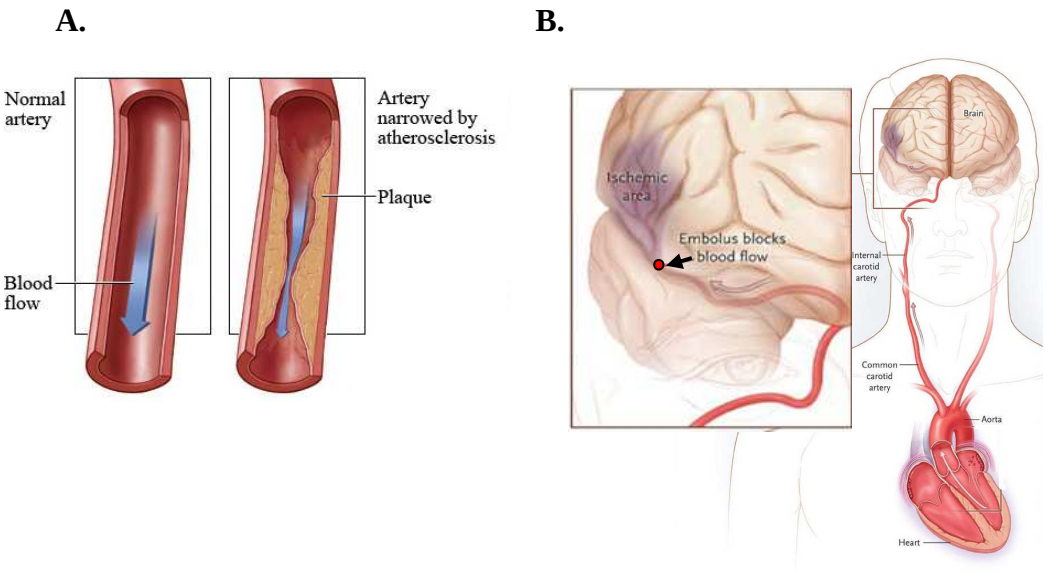

Figure 1.1. **A**. Ischaemic stroke arising from atherosclerotic plaques, in which blood flow is restricted by a thrombus and, **B**. embolic ischaemic stroke, where a travelling embolus lodges within a brain artery to preclude flow (Modified from Go, 2009)

1.1.2 The rat as a stroke model

The scope of cerebral ischaemia research is ever-expanding, ranging from the study of cultured systems such as brain cells and organotypic brain slices to the many *in vivo* models now available. Advances in our understanding of ischaemic brain damage have not translated into successful therapies to treat stroke patients, despite the completion of over 260 clinical trials of acute stroke therapies (http://www.strokecenter.org). Specific animal models have enabled compounds and factors with therapeutic potential to be discovered, although their translation to the clinical domain has been notoriously difficult (Howells et

al, 2010). O'Collins (2006) evaluated the preclinical data of 1026 treatments in acute experimental stroke, in which 603 were tested in focal ischaemia and, of which, 374 were found to be effective. Of these treatments which demonstrated efficacy in animal models, 97 were taken into clinical trials, and only 1 was shown to be effective; thrombolysis with recombinant tissue plasminogen activator (rT-PA). This questioned whether or not the most efficacious drugs were chosen for clinical trials, and suggested that potential drugs must exhibit both evidence supporting clinical application and a very high level of experimental efficacy.

The heterogeneity and complexity of human stroke may prevent a unitary animal model from being developed, and as such, there is no universal animal stroke model that can incorporate all the factors implicated in human stroke. Candidate species for human stroke models include sub-human primates, cats, rabbits and rodents (Tamura et al, 1996). Sub-human primates with gyrencephalic brains are behaviourally and anatomically similar to humans, but their preclinical use is stunted by ethical and economic concerns (Cenci et al, 2002). Most preclinical experiments are performed in homogenous cohorts of young, male rodents, and rodents are often bred for genetic homogeneity to ensure relatively reproducible infarcts. Highly controlled experiments can assure consistency in the arterial occlusion site, the severity and duration of ischaemia, and pre- and post-ischaemia care. Rodent models of stroke are popular in the research domain due to the similarities in the cerebral vasculature of humans and rodents (Macrae, 1992), the resultant sensorimotor deficits and the pathophysiological processes associated with ischaemic damage (Cenci et al, 2002). However, human stroke is very heterogeneous, in which the occlusion site, the duration of ischaemia and the extent of collateral supply varies between patients.

The causative mechanisms of ischaemic damage occur rapidly following blood vessel occlusion and they are relatively short-lived, and as such, many crucial early events of the ischaemic cascade may only be investigated using monitored animals. Multiple non-invasive imaging techniques at the disposal of preclinical laboratories can be readily used for monitored animals in a controlled environment, and it would be unethical to expect a patient with a stroke to endure a prolonged scanning session in the acute phase of stroke. Additionally, in modalities that emit ionising radiation (computed tomography (CT), positron emission tomography (PET) and single photon emission computed tomography (SPECT)), multiple scans result in unacceptable radiation exposure in humans. It is common for stroke patients to present with high blood pressure, abnormal glucose or abnormal blood gases immediately following stroke. In animals, stroke outcome can be

somewhat controlled by careful monitoring and manipulation of physiological variables to maintain physiological limits or be adjusted to mimic abnormal levels. These factors all contribute to the problems in translation from preclinical rodent studies to the complexities of acute human stroke.

Cerebrovasculature

Brain tissue is supplied by four major arteries that form an intricate communicating network. From the neck, the two common carotid arteries bifurcate into the internal (ICA) and external carotid (ECA) arteries, which join the circle of Willis and supply the facial muscles, respectively. The circle of Willis is a formation of several arteries at the base of the brain, from both internal carotid arteries and the basilar artery. The basilar artery – which supplies the cerebellum and brainstem - divides into the right and left posterior cerebral arteries. The internal carotid arteries branch into the anterior cerebral artery, the middle cerebral artery and the posterior communicating artery. The circle of Willis is completed when the two anterior cerebral arteries are joined by the anterior communicating artery and two posterior arteries are joined by the posterior communicating artery (Figure 1.2). The significance of this configuration is that distal collateral arteries can potentially preserve brain perfusion if part of the circle is stenosed, effectively acting as anastomoses. The main difference between the human and rat cerebrovasculature is that the ICA does not form part of the Circle of Willis in the human, which it does in the rat.

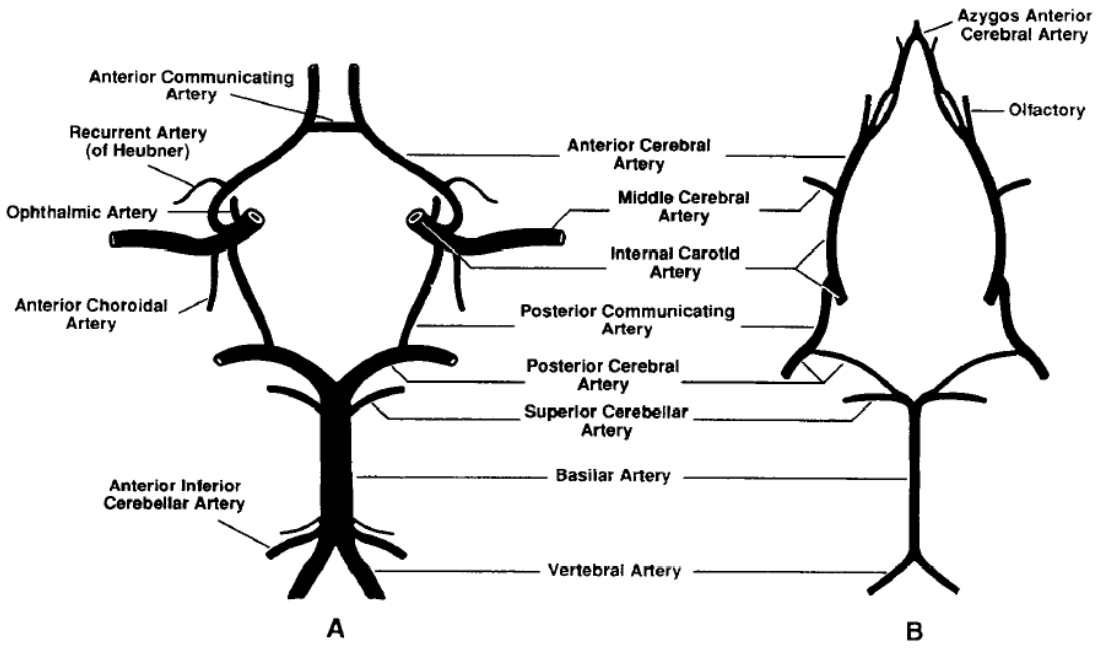

Figure 1.2. Organisation of blood vessels in the brain for **A**. Human, and **B**. Rat (taken from Lee, 1995)

1.1.3 Rodent models of focal ischaemia

Most strokes involve the middle cerebral artery (MCA) territory (Barnett, Mohr, Stein et al, 1992, Figure 1.3), accounting for 80% of cases in Caucasians (Derouesne et al, 1993; Warlow et al, 2003), and animal models of focal ischaemia usually involve occlusion of the MCA (McAuley, 1995).

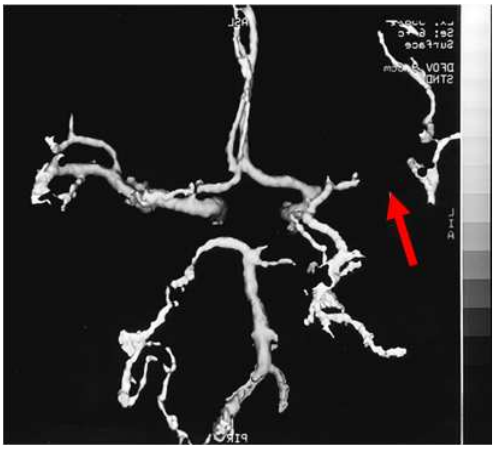

Figure 1.3. CT angiography displaying MCA occlusion (red arrow) in a stroke patient. Modified from Wong et al (1996)

The susceptibility of the core MCA territory to damage following MCA occlusion is in part due to the severity of the ischaemic insult. The small, penetrating arterial branches of the MCA that supply core tissues (much of the ventral cortex and striatum) are not supported by a collateral circulation, and therefore occlusion of one of these arteries is likely to cause uncompromised infarction (Ringelstein et al, 1992; Marinkovic et al, 1985). As such, a number of models of MCA occlusion have been developed to reproduce human stroke (Figure 1.5).

Intraluminal filament model (ILF)

The most commonly used method of inducing permanent or transient focal ischaemia is the intraluminal filament (ILF) model (Koizumi et al, 1986). This involves the insertion of a silicon rubber-coated monofilament into the external carotid artery, where it is introduced into the ICA and advanced to block the origin of the middle cerebral artery. The filament can remain in this position permanently, or retracted and removed to induce reperfusion. The ILF model is advantageous because it does not require a craniotomy, although adherence of the filament to the blood vessel walls may cause mechanical endothelial

damage. Additionally, the infarcts tend to be more variable than with some other middle cerebral artery occlusion (MCAO) models, with higher mortality often reported (Tamura et al, 1996; Minematsu et al, 1992). A typical pattern of ischaemic damage using the ILF method is shown with Magnetic Resonance Imaging (MRI) (Figure 1.4).

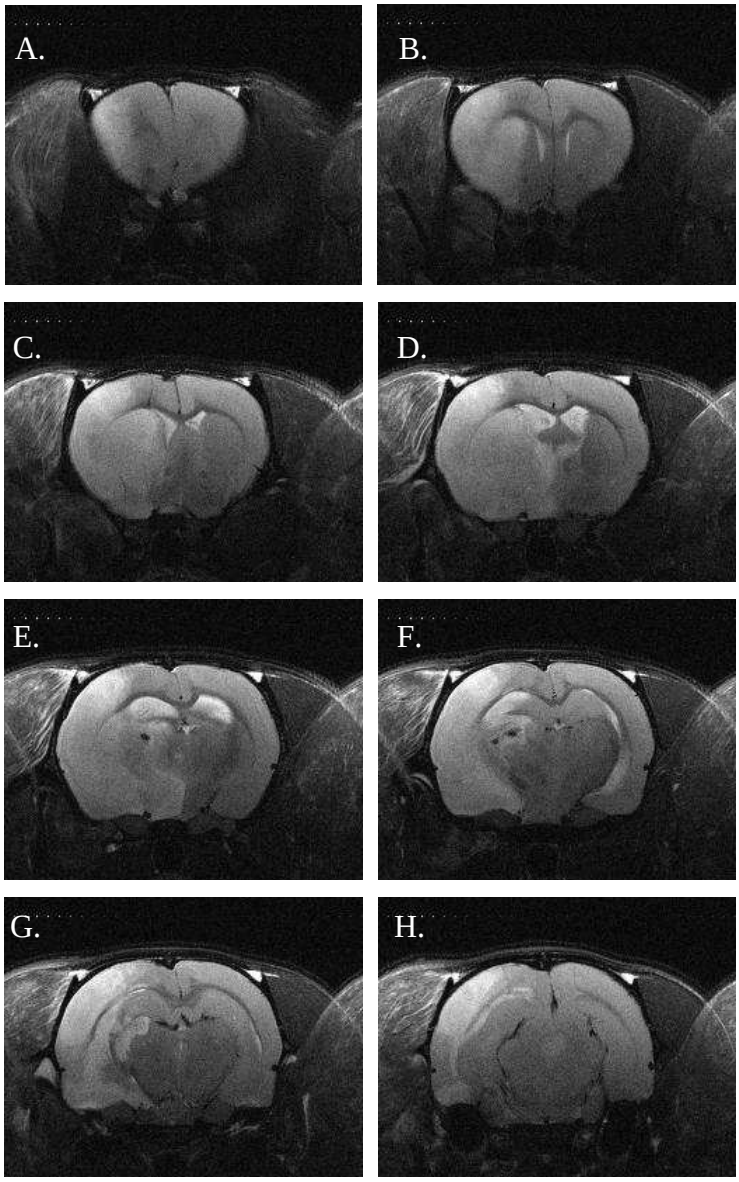

Figure 1.4. T_2-weighted coronal rat brain images at 24 hours following the intraluminal filament model of permanent MCAO (rostral (A) to caudal (H)). On T_2 images, ischaemic tissue appears hyperintense due to its high water content, causing the cerebrospinal fluid (CSF) in the ventricles to also appear bright. Considerable brain swelling is evident in the ipsilateral hemisphere at this time point due to cerebral oedema, and this accounts for the midline shift. Small haemorrhages are also common in this model, for example in the caudate nucleus on Image E & F. As shown, the introduction of the intraluminal filament may also result in damage to tissue supported by the posterior cerebral artery and the posterior communicating artery

Electrocoagulation model

A second MCAO model involves electrocoagulating the MCA following a craniotomy, which was developed by Robinson and colleagues (1975) and further modified by Tamura and colleagues (1981). Specifically, the Tamura model electrocoagulates a proximal region of MCA at the origin of the lenticostriatal branches and induces both cortical and striatal damage, whereas the technique by Robinson and colleagues involves electrocoagulation of a more distal region of the MCA which induces cortical damage only. Thus, the extent of ischaemic damage is dependent upon the position and length of the occlusion. The craniotomy diminishes the deleterious consequences of brain swelling following ischaemia, making this method popular due to the low mortality and high reproducibility. However, it cannot be used to study transient focal ischaemia.

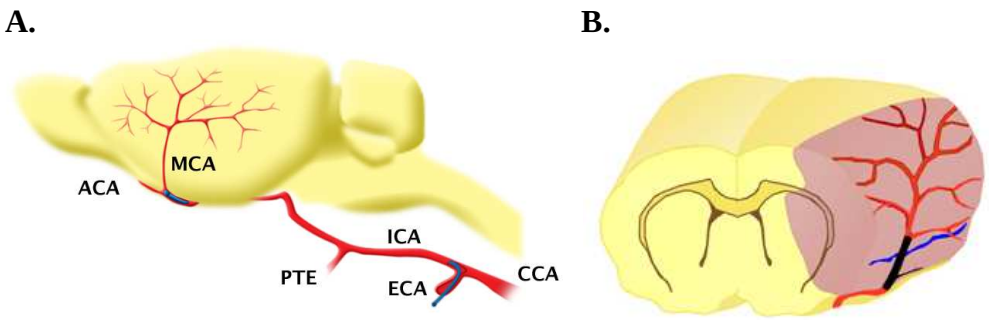

Figure 1.5. Two commonly used rodent MCAO models. **A**. Sagittal representation of the intraluminal filament method of MCAO, where the bulbed monofilament is introduced through the external and internal carotid arteries to the origin of the MCA, thus precluding flow and inducing ischaemia, and **B**. Coronal representation of the electrocoagulation method of MCAO, in which the MCA destroyed by electrocoagulation is coloured black. The pink shading represents the ischaemic territory following MCA occlusion. Illustration **A** courtesy of Chris Stock, University of Manchester

Transient MCAO

Identifying the permanence of the MCA occlusion in humans is complicated. Stroke patients also tend to experience varying levels of reperfusion which therefore offers another complex facet to its reproduction in animal models. Spontaneous reperfusion – partially or totally – accounts for ~24% of all stroke cases (Rha and Saver, 2007). In large arteries, persisting distal emboli and occlusions in the microcirculation may inhibit successful tissue reperfusion. The ILF model of MCAO is particularly useful for inducing

transient focal ischaemia. In this model, the filament can be left in place for a set period of time, and reperfusion can then be induced by slow and careful retraction of the filament to induce restoration of flow to the previously ischaemic tissue. This can also uncover possible injury associated with late reperfusion into ischaemic tissue (reperfusion injury) and therefore reflects more closely the situation that occurs in the majority of human ischaemic strokes.

1.1.4 Stroke pathophysiology

Ischaemic stroke initiates a constellation of pathophysiological processes, including energy failure, increased intracellular calcium, excitotoxicity and secondary pathogenic mechanisms which increase the profundity of the insult, such as peri-infarct depolarisations, inflammation and apoptosis (Figure 1.6).

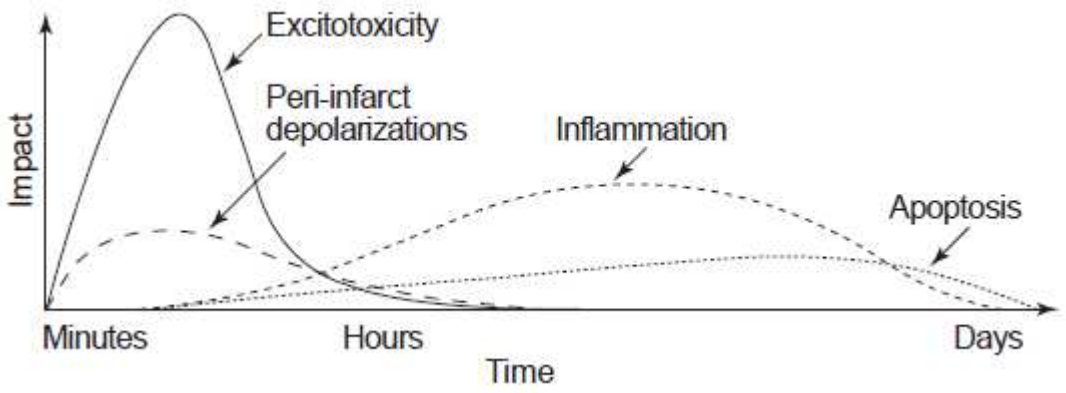

Figure 1.6. The time course and impact of the pathophysiological cascade following cerebral ischaemia (Dirnagl et al, 1999)

Energy Failure

Focal ischaemia due to the blockage of an intracranial artery induces compromised cerebral metabolism associated with hypoxia and declining glucose provision. An incipient effect of nutritive deprivation is the detectable and immediate silence in electrical activity (Astrup et al, 1977). In the initial phase, ischaemia triggers energy failure through a loss of adenosine triphopshate (ATP). As a consequence, this initiates an elevation in extracellular potassium (K^+) levels, due to leakage of K^+ through the K_{ATP} channels, which are normally blocked by ATP. Depletion of high-energy phosphates rapidly leads to membrane ion pump failure (Wu, and Fujikawa, 2002), in which there is decreased activity of the Na^+/K^+-ATPase and Ca^{2+}/H-ATPase pumps, as well as the reversal of the Na^+-Ca^{2+}

exchanger (Phan et al, 2002). Consequently, this causes an elevation of intracellular Na^+, Ca^{2+}, and Cl^- which results in cytotoxic oedema and leads to events triggered by excess intracellular Ca^{2+} (Durukan, and Tatlisumak, 2007).

Elevation of intracellular Ca^{2+}

There is an accumulation of free calcium in the cell following the failure of the ion pumps that would normally transport the calcium back out of the cell. Both neuronal and non-neuronal cells become depolarised and voltage-dependent Ca^{2+}-channels are activated. Depolarisation also initiates the release of neurotransmitters such as excitatory amino acids (glutamate) from presynaptic axon terminals into the synaptic cleft (Kristián and Siesjö, 1996). In addition to changes in water, sodium and energy change, calcium is released from the mitochondria and endoplasmic reticulum to increase the concentration of free calcium within the cytosol. The rise in intracellular calcium ions activates membrane phospholipases A and C, which break down membrane phospholipids, resulting in the release of free arachidonic acid which directly increases membrane permeability and also has profound secondary metabolic events. It is presumed that cellular oedema occurs as an almost immediate consequence of cerebral ischaemia (Kristián and Siesjö, 1996).

Excitotoxicity

Excitotoxicity is the pathological process triggered by depletion of cellular energy by which nerve cells are damaged and killed by glutamate and similar substances. Following the perturbation of energy production and exhaustion of cellular ATP, the membrane potential is completely lost, resulting in depolarisation of neurons and glia (Dirnagl, Iadecola, and Moskowitz, 1999). In normal conditions, energy-dependent processes remove glutamate – which is stored in the synaptic terminals – from the extracellular space. During the stage of energy exhaustion, glutamate transporters cannot remove glutamate from the extracellular space due to the loss of ion gradients. As glutamate cannot be readily cleared, there is an opening of calcium channels due to the activation of the glutamate receptors (N-methyl-D-aspartate (NMDA), the alpha-amino-3-hydroxy-5-methyl-4-isoxazolepropionate (AMPA) and metabotropic glutamate receptors (Durukan, and Tatlisumak, 2007).

Excitotoxins like NMDA and kainic acid which bind to these receptors, as well as pathologically high levels of glutamate, can cause excitotoxicity by allowing high levels of

calcium ions to enter the cell. Calcium can also cause the release of more glutamate which exacerbates the insult. Ca^{2+} influx into cells activates a number of enzymes, including phospholipases, endonucleases and proteases, including calpain. These enzymes succeed in damaging cell structures such as components of the cytoskeleton, mitochondria, endoplasmic reticulum, plasma membrane and DNA. When free radicals and leukotrienes are formed, irreversible mitochondrial damage and necrotic and programmed cell death occur following increases in intracellular Ca^{2+} (Durukan, and Tatlisumak, 2007).

Spreading depolarisations

In the subsequent subacute phase, secondary mechanisms cause an expansion of the ischaemic damage into surrounding tissue. These include electrochemical waves called spreading depolarisations or depressions, and their incidence has been shown to correlate with infarct size in the rat (Dijkhuizen et al, 1999). With accumulations in glutamate and elevated extracellular K^{+} and Ca^{2+}, tissue regions adjacent to the ischaemic core actively propagate recurring waves of depolarisations, ionic imbalances and glutamate beyond the ischaemic core to the at-risk, less hypoperfused tissue termed the ischaemic penumbra, thus expanding the lesion size (Hartings et al, 2003). Such waves are termed peri-infarct depolarisations in this context, and in MCAO rat studies, up to eight peri-infarct depolarisations have been observed over 3 hours post-stroke (Mies et al, 1993; Back et al, 1996). Lastly, a cascade of injurious mechanisms that further recruit tissue into the infarct may persist for a few days, including cytotoxic oedema (ionic disturbances largely due to sodium, calcium, lactate and hydrogen ions), inflammation and apoptosis.

Apoptosis

Apoptosis – or programmed cell death – is a genetically controlled series of events which acts to save biological components of a cell about to die. This enables utilisation of these parts through either macrophages or phagocytes and it is vital for the sustenance of the organism. For example, the P53 gene – a tumour suppressor – prevents tumour growth by inducing apoptosis in tumour cells as they begin proliferating (Lee and Bernstein, 1995). This mechanism occurs when a cell has been exposed to an environment in which it cannot survive – e.g., an environment undergoing oxygen and glucose depletion (Feril, 2005). By triggering ‘cell-suicide’ (Tortora and Grabowski, 2000: p94) genes, a number of enzymes begin attacking the cell, resulting in cell fragmentation and phagocytic uptake. The initiation of apoptosis enables the body’s immune reaction to be minimal, which in turn

saves energy (Albert, 2004). There is not an immune response because the cell's contents are phagocytosed before they get the opportunity to leak into surrounding spaces, unlike necrosis – where the cells burst and spill their contents into the neighbourhood (Raff, 1998). Also, a cell with considerable injury would begin to procure nutrients from its host, and therefore it is advantageous to destroy one cell as opposed to weakening a multitude of cells. Apoptosis differs from necrosis – accidental cell death as opposed to programmed death – in that it is controlled and orderly, and requires energy. Apoptosis requires caspases, which act to cleave proteins in the cell for easy phagocytotic ingestion. They cleave a protein that normally holds a DNA-degrading enzyme (a DNase) in an inactive form, freeing the DNase to carve the DNA in the cell's nucleus (Enari, Sakahira, et al, 1998). They also cleave protein constituents of the cell's skeleton and other proteins involved in the attachment of cells to their neighbours, thereby helping the dying cell to detach and round up, making it easy to ingest (Raff, 1998).

Both caspase-dependent and caspase-independent pathways in apoptosis have been implicated following stroke. The genes for caspases as well as genes that suppress (such as Bcl2, Iap) or augment (Bax, Trp53) cell death are activated in both early and late stages of ischaemia. Caspases 1 and 3 are known to play a fundamental role in apoptosis during ischaemia. Since the capases are protein cleavers, they have been shown to modify homeostasis and repair proteins that end up disassembling and killing the cells. Capsases become activated when cytochrome C, released from mitochondria, activates an apoptosome complex (apoptosis-activating factor (APAF1) plus pro-caspase 9) in the presence of deoxyadenosine triphosphate (dATP), a nucleotide used in cells for DNA synthesis. Cytochrome C can enter the cytosol from its location on the external side of the inner mitochondrial membrane. The formation of the apoptosome complex, which is suppressed by BCL2L1, promotes clipping and activation of caspase 3 (Hara et al, 1997). Following ischaemia, neurons are particularly susceptible to cell death due to the action of caspases. After MCA occlusion in rodents, cytochrome C release and caspase processing are evident between 6 and 9 hours, and apoptotic cell death is shown between 24 and 72 hours (Dirnagl, Iadecola, and Moskowitz, 1999).

1.1.5 Neuroprotectants

Ca^{2+} channel blockers

In short, following ischaemia, the lack of oxygen affects the production of ATP in the neurons, which in turn induces failure of ATP-reliant ion transfer pumps. This causes cellular depolarisation, and the intracellular influx of calcium, sodium cations and chloride anions. The ion pumps can no longer transport calcium out of the cell, and intracellular calcium levels increase significantly. Consequently, the presence of calcium triggers the release of the excitatory amino acid neurotransmitter glutamate and activates enzymes which lead to increased free radical production. The rationale behind giving Ca^{2+} blockers is to decrease the influx of Ca^{2+} through ion channels into cells. Buchan and colleagues (1994) presented evidence that SNX-111, a selective N-type (neuronal type) calcium channel blocker, reduced neuronal injury in a model of forebrain ischaemia in rats after a recovery interval of 7 days. SNX-111 was highly neuroprotective, even when administered after a delay of 24 hours following reperfusion. However, upon assessing injury at 4 weeks post-ischaemia, neuronal protection was no longer apparent. Overall, it failed to provide neuroprotection, indicating its ability to delay neuronal death instead of prevent it. It may have offered a role to extend the therapeutic window, and although it reached phase II trials, it was discontinued due to its ability to induce severe hypotension which exacerbated injury (Buchan et al, 1994). Also, the L-type calcium channel blocker nimodipine has reduced ischaemic damage in animal models (Mandir et al, 2000), although it did not have a beneficial effect in patients when administered 24 to 48 hours after stroke. It seemed more efficacious when taken within 12 hours, although it again induced hypotension (Weinberger, 2006).

Glutamate receptor antagonists

Glutamate-receptor antagonists such as MK-801 (a potent anticonvulsant) have demonstrated efficacy in decreasing neuronal damage in animal models. The NMDA receptor-mediated calcium influx is blocked using MK-801, a non-competitive NMDA antagonist. NMDA antagonists do not, however, improve outcome in clinical trials, as they do not protect against oxidative stress that damages the surrounding neuropil (Weinberger, 2006). The effect of MK-801 was physiological rather than pharmacological, as the effect was facilitated by inducing hypothermia in the animals and increasing the blood flow, rather than blocking the NMDA receptor channel. Neuroprotectants such as MK-801 have

a number of contraindications, including deleterious cardiovascular events and expressed toxicity in certain areas of the brain such as the cingulate cortex.

Anaesthetics and anticonvulsants

Anaesthetics and anticonvulsants act to inhibit the release of neurotransmitters during ischaemia. Pentobarbital in gerbil models has reduced ischaemic damage, and this may be due to a reduction in metabolic demand and inhibited release of catecholamine in the striatum (Levy and Brierly, 1979). Ketamine has been shown to reduce extracellular plasma catecholamines in rat models with cerebral ischaemia (Hoffman, Pelligrino, Werner, et al, 1992). Other anticonvulsants, including lubeluzole (Grotta, 1997), clomethiazole (Wahlgren, et al, 1999) and gavestinel showed initial promise, but subsequent trials denigrated their potential utility (Diener et al , 2000; Lyden et al, 2002; Sacco et al, 2001).

Caspase inhibitors

The blocking of apoptosis is the rationale behind the development of caspase inhibitors, and they have been shown to suppress cell death (Han et al, 2002). The therapeutic window seems to be temporally related to the onset of caspase activation, and caspase inhibitors attenuate ischaemic brain injury and neurological function when administered up to the point of protease activation (Lo, Dalkara and Moskowitz, 2003; Fink et al, 1998). However, caspase inhibitors do not reduce infarct size in all brain ischaemia models.

1.2 The ischaemic penumbra

1.2.1 Definition

Much of our understanding of the acute period of MCA stroke derives from models established in animal studies. Using a primate model, the ischaemic brain was initially compartmentalised by Lindsay Symon and colleagues in the 1970s, whom identified a mismatch between electrical cerebral function and blood flow at various thresholds, in which there was an area of hypoperfused tissue with cellular dysfunction but not death – demonstrated by somato-sensory evoked potentials (Symon, Pasztor and Branston, 1974). Importantly, they established that reduced cerebral function in hypoperfused tissue had the potential to return to normal following full restoration of blood flow.

As such, the pathophysiology of the ischaemic brain was defined in terms of four distinct tissue compartments (Figure 1.7); brain tissue unaffected by stroke, an ischaemic core which will ultimately die, tissue destined to survive (benign oligaemic tissue), and functionally impaired but structurally intact tissue with the potential to die or survive (Astrup, Siesjo and Symon, 1981). This latter region was termed the ischaemic penumbra (from the latin paene 'almost' and umbra 'shadow' – an astronomical sobriquet explaining the outer region of a shadow cast by earth during a partial eclipse) because of its location around the ischaemic core and its transitory nature (Figure 1.8).

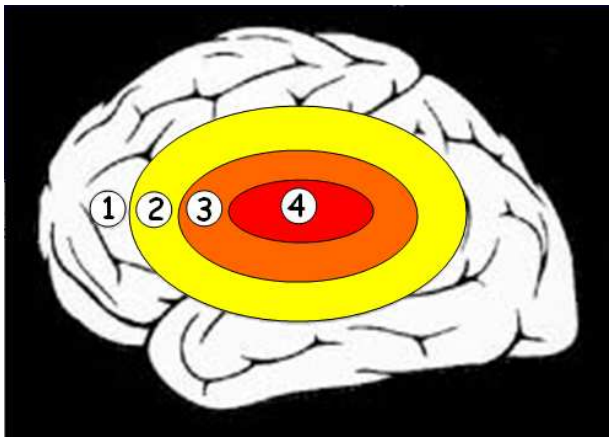

Figure 1.7. The compartmental model of ischaemic brain injury. The unaffected site (**1**) is the outermost region, followed by an area of benign oligaemia (**2**) that does not require reperfusion to survive. The ischaemic penumbra (**3**) is at risk of irreversible cell death, and surrounds the irreversibly damaged ischaemic core (**4**).
Adapted from Lee et al (2005)

Hakim (1987) further broadened the definition and outlined the clinical relevance by explaining that penumbra is 'fundamentally reversible', presenting a therapeutic window of opportunity. However, over time and without intervention, this penumbral tissue becomes incorporated into the irreversibly damaged, ischaemic core. Thus, an all-encapsulating definition of penumbra is that it is functionally impaired ischaemic tissue potentially destined for infarction which, unless salvaged by reperfusion or otherwise supported, will become incorporated into the infarct core. For the penumbra to be classified as a clinical measure, the salvage of the tissue must improve clinical outcomes (Donnan et al, 2007).

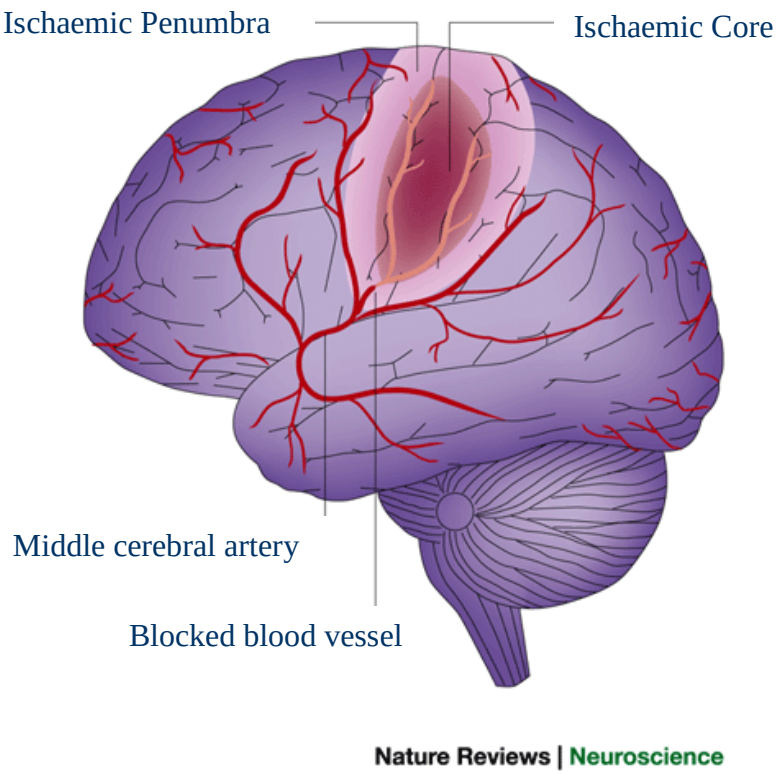

Figure 1.8. Depiction of the nature of ischaemic injury, with penumbral tissue surrounding an ischaemic core following blockage of a cerebral artery. Adapted from Allan and Rothwell (2001)

1.2.2 Cerebral blood flow following stroke

Whilst the brain comprises 2% of total body weight in humans, its utilisation of both oxygen and glucose is not correlated with its size, accounting for ~20% of oxygen consumption and ~25% glucose consumption in the blood. Due to such a high metabolic demand, the brain acquires 15% of the resting cardiac output (Winn, Dacey, and Mayberg, 1989). These characteristics of the brain, coupled with its inability to hold appreciable,

endogenous energy reserves (Marieb, 1998) make this organ reliant on the continual delivery of oxygen and nutrients by circulating blood and particularly vulnerable to changes in blood supply. If its blood supply is impeded, irreversible cell death ensues as quickly as 5 minutes.

The cerebral vessels possess the ability to deliver a constant supply of blood despite systemic blood pressure (BP) fluctuations. The mean arterial blood pressure (MABP) can be altered over a fairly wide range – between about 50 and 150 mmHg without affecting cerebral blood flow (CBF). This phenomenon is called 'autoregulation' and can be defined as the ability of cerebral resistance vessels to alter in response to changes in perfusion pressure (Stan et al, 2004). Specifically, this attains constancy in blood flow, allowing consistent nutritive delivery to the brain (Johnson, 1964). Autoregulation is basically an inhibitory feedback system, and as mean arterial blood pressure can enter high and low limits due to hypertension or hypotension, the change in calibre of cerebrovascular vessels counteracts these phenomena by constricting or dilating, respectively. When blood pressure falls, physiological mechanisms attempt to maintain flow to prevent ischaemia. Similarly, when blood pressure rises, the same mechanism stops the blood flow from increasing to excessive levels. If this did occur, cerebral oedema could develop and the brain would enlarge because of the increase in cerebral arterial blood volume.

Autoregulation and stroke

Cerebral autoregulation is also a major self-defence mechanism against secondary ischaemic insults after traumatic brain injury and subarachnoid haemorrhage, and impairment of cerebral autoregulation has been shown to affect prognosis (Czosnyka et al, 1996). Stroke can induce a loss of cerebral autoregulation, and the complications associated with this are, in part, responsible for consequential brain damage post-ischaemic insult, indicative of oedema formation and secondary ischaemia. Thus, the loss of autoregulation may play a vital role in secondary deterioration of stroke patients (Dohmen, 2006).

Cerebral vasoregulation involves several complex mechanisms adapting blood flow to fluctuations of systemic blood pressure. Autonomic BP and metabolic vasoregulation are impaired after stroke and cerebral blood flow then depends on systemic BP (Dawson, Panerai and Potter, 2003). With severe strokes, autoregulation has been seen to remain preserved despite failure of the plethora of regulatory mechanisms. This presentation of

preserved autoregulation is false, however, and may possibly be due to several interacting mechanisms including changes in cerebral tissue pressure and changes in blood flow (Paulson, 1972). Loss of autoregulation in acute cerebral lesions tends to be due to tissue ischaemia and/or acidosis. Cerebral resistance vessels then dilate in an attempt to increase blood flow. The actual level of the blood flow in such regions not only depends on the degree of vasodilatation, but also on other factors such as intracranial pressure, local cerebral oedema and vascular obstruction.

The major factor responsible for adjustments in intrinsic blood flow is the metabolic demand of the tissue, and thus blood flow is related to the requirement of the local neurons to expend energy for activity – the principal consumer of energy in the brain. Therefore, blood flow is controlled by the extent of neuronal activity at certain brain regions, which gives rise to autoregulatory mechanisms that enable such flow modifications. In short, the more functionally active a region of brain is, the greater the metabolic demand and the greater the blood flow. Cerebral blood flow is measured in millilitres per 100g of brain tissue per minute. These values vary between species, and CBF and cerebral glucose utilisation rate (CMRglc) are inversely proportional to the size of the animal (Table 1.1).

Species	CBF (mL/100g/min)	CMRglc (mL/100g/min)
Human	54	31
Rat	107	69

Table 1.1. CBF and CMRglc of the rat and human. Adapted from Harper (1990)

Following stroke, in terms of blood flow, there is a significant topographical gradient of CBF reduction across the vascular territory. Tissue in end artery territory has the greatest severity of ischaemia, where total or profound loss of CBF represents tissue that will progress to infarct. As the brain has a complex array of anastomosing vasculature, the region adjacent to the core is marginally supplied by collaterals, which represents tissue experiencing less-severe ischaemia.

Perfusion thresholds for functional integrity

Astrup, Siesjo and Symons (1979) implemented a three-part model with the thresholds of cerebral blood flow associated with normal functioning, penumbral tissue, and ischaemic core, identified by inducing ischaemia in a primate MCA occlusion model. Tissue compartments of the brain following stroke can be classified by the extent and duration of ischaemia. Following the blockage of a vessel, the end artery territory (ischaemic core) has CBF of <10 to 15 mL/100 g per min in primates. Ischaemic damage occurs rapidly – often under 1 hour – and the morphological changes in the tissue are irreversible. Intermediate tissue around the periphery of this core – the penumbral region – experiences a more modest reduction in CBF, where flow is ~15% to 40% of normal levels. Unless blood flow is restored, penumbral tissue will eventually become incorporated into the infarct, and this evolution can take a number of hours (Pulsinelli, 1992). Thirdly, benign oligaemic tissue - classified as tissue which is not expected to progress to infarction under normal circumstances in humans - can range from normal CBF values down to ~20 mL/100g/min (Baron et al, 2001). This tissue survives within the hyperacute stage following stroke (within 12 hours), but its fate is less definite following persistent occlusion. One may expect this region to enter a less severely hypoperfused state (above 30 mL/100g/min), which prevents the tissue undergoing infarction (Linskey et al, 1994). The benign oligaemic region is not completely invulnerable to infarction, as accompanying factors such as hyperglycaemia, fever and hypotension may induce progressive damage.

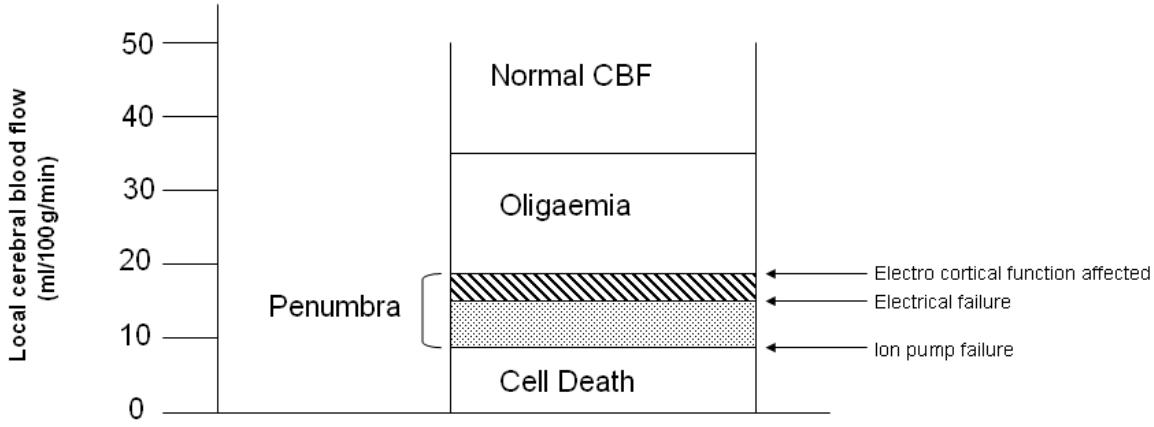

Figure 1.9. CBF thresholds shown depict the situation in sub-human primates. Adapted from Astrup et al (1977)

The CBF thresholds (Figure 1.9) to differentiate between normal, penumbral and infarcted core are based on animal experiments, although their diagnostic accuracy in humans are poorly established (Latchaw et al, 2003). The human thresholds are:

1. Normal, unaffected tissue (including benign oligaemia): CBF ~50 mL/100g/min (Muir et al, 2006)
2. Penumbra: 10 to 17 mL/100g/min
3. Infarct core: <10 mL/100g/min (Moustafa and Baron, 2007)

1.2.3 Autoregulatory responses in the ischaemic brain

Unaffected brain tissue following stroke

In the unaffected, normal region of the brain (Region 1, Figure 1.10), the regional CBF is about 50-60 mL/100g/min in humans (~100 mL/100g/min in rats). A reduction in blood flow is associated with a reduction in cerebral perfusion pressure (CPP), which induces a vasodilatory reaction in the blood vessels affected (Region 2, Figure 1.10). In the autoregulated area, this introduces more blood to the region, which attempts to maintain CBF, and this mechanism will remain intact if the BP remains between about 50 and 150 mmHg. In this region, autoregulation is sufficient to sustain an adequate CBF.

The benign oligaemic region

In benign oligaemic tissue (Region 3, Figure 1.10), there is neither functional impairment nor morphological abnormality. The region is indicative of reduced cerebral perfusion

pressure (CPP), moderately reduced CBF, an increased oxygen extraction fraction (OEF), and a normal cerebral metabolic rate of oxygen ($CMRO_2$). OEF refers to the matching of cerebral blood flow to metabolism, and the $CMRO_2$ reflects oxygen consumption, which is the difference of oxygen flowing in and out of a region (Boas et al, 2003). The increased OEF is the compensatory mechanism – known as the 'perfusion reserve' – and it allows normal $CMRO_2$ to be maintained.

Penumbral region

As CPP decreases further, the $CMRO_2$ cannot be maintained, even when the OEF increases. This is because the perfusion reserve is depleted, and the neurons become impaired when metabolism is critically impaired. This penumbral tissue (Region 4, Figure 1.10) is metabolically exhausted yet the integrity of the cells is maintained. There are a number of established markers of the ischaemic penumbra; a region with increased OEF (Baron et al, 1984), a mismatch between neuronal integrity and CBF (Heiss et al, 1997) and a mismatch of cerebral protein synthesis and energy depletion (Hata et al, 1998).

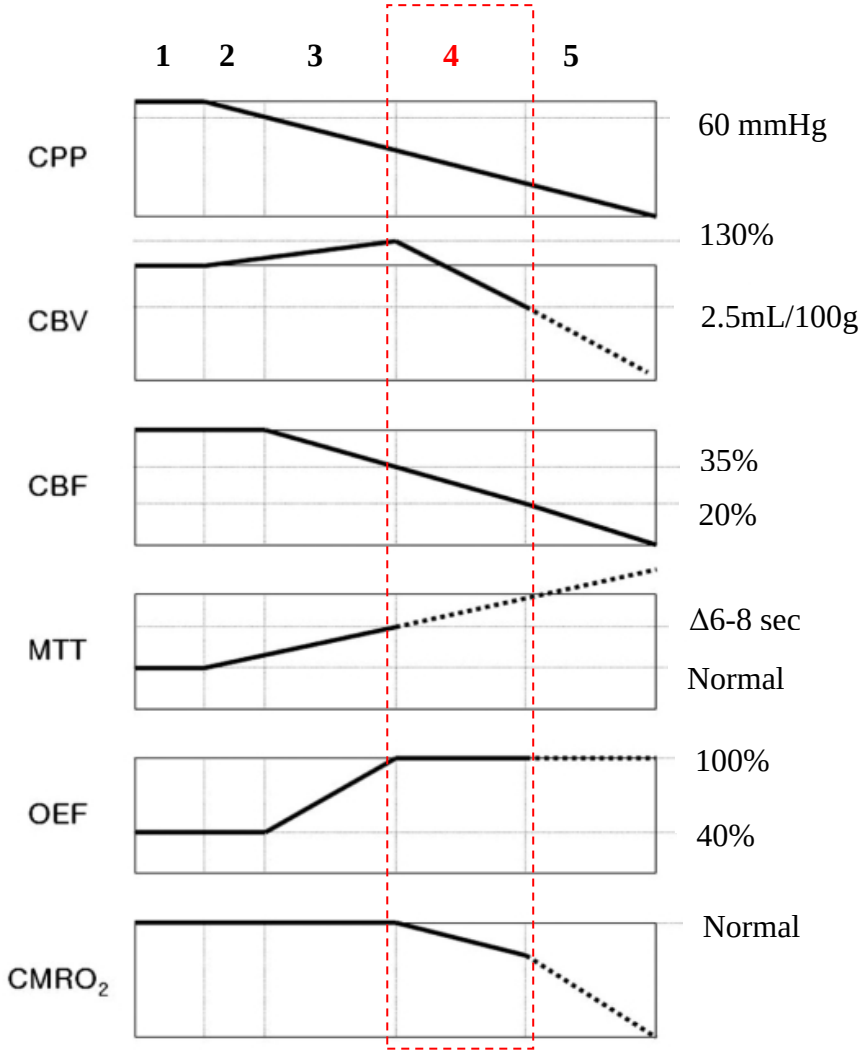

Figure 1.10. Haemodynamic and metabolic changes in various tissue compartments following ischaemia, represented as; **1.** Unaffected area, **2**. The autoregulated region, **3**. The benign oligaemic, **4**. The ischaemic penumbra, and **5**. The ischaemic core. Adapted from Maeda et al (1993)

CPP = cerebral perfusion pressure; CBV = cerebral blood volume; CBF = cerebral blood flow; MTT = mean transit time; OEF = oxygen extraction fraction; and $CMRO_2$ = cerebral metabolic rate of oxygen

1.2.4 Biochemical and metabolic thresholds for definition of penumbra

A number of established markers (Figure 1.11) have been employed to characterise the ischaemic penumbra. Major vascular occlusion is a dynamic and complex phenomenon, in which the severity and duration thresholds for tissue viability are dependent upon factors including cell type, the health of the collateral vessels, residual flow, and biochemical events. Demarcating penumbra from intact tissue is more complex at lower flow rates, since increasingly more pathophysiological disturbances occur. The advent of multimodal

imaging methods to identify these biochemical processes and thresholds has further complicated penumbra definition and contributed to the idea of multiple penumbras (Sharp et al, 2000) by characterising its molecular expression pattern, as opposed to the classically described blood flow and physiologic descriptions.

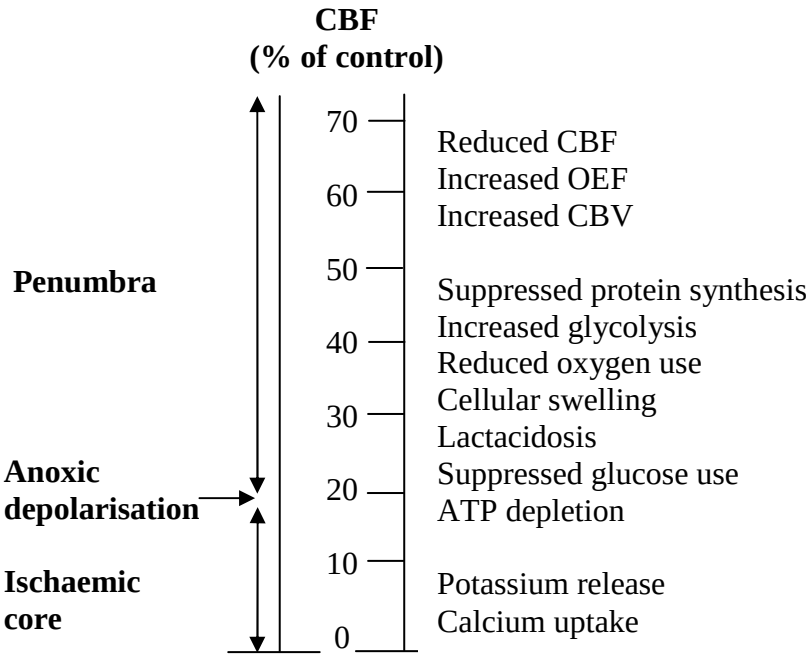

Figure 1.11. The pathophysiological disturbances that occur within the penumbra and ischaemic core as blood flow levels decrease (Adapted from Hossmann and Mies (2007))

As the markers for identifying penumbra tend to be generated from animal models - often identified using invasive, terminal tissue-sectioning procedures - there is a difficulty in translating this information and establishing the relationship between penumbra salvage and improved clinical outcome. Such is the complexity and heterogeneity of stroke, the reason that there is no established penumbral marker is because research groups tend to focus on a specific biological process in the ischaemic model. Instead of studying the characteristics of the penumbra, many groups have a biochemical process in mind that may complement the body of work on an ischaemic insult as a whole. Whilst a group may focus on the significance of suppressed protein synthesis following an ischaemic insult, another group may study the mismatch between stimulation of anaerobic glycolysis and CBF. Although both groups satisfy the criteria for the ischaemic penumbra identification, the rationale for their studies varies, their regions of interest are variable and the thresholds of cerebral blood flow in the rat differ for protein synthesis (at 55 mL/100g/min) and anaerobic glycolysis (at 35 mL/100g/min), for example (Hossmann, 1994).

1.2.5 Difficulties in defining the ischaemic penumbra in stroke patients

A fundamental issue that hinders the development of a sophisticated predictive model of tissue viability is the lack of standardised parameters. Warach (2001) notes that there are no absolute viability thresholds that are independent of time, and also that there is no time window of tissue viability. Warach (2001) suggests that the various markers of tissue viability such as apparent diffusion coefficient (ADC) and CBF must be combined to improve their predictive power, and that they need to be tested on the stroke population as a whole. Then, the models can be compared, and if there are no significant differences, the model of least complexity will be the gold standard in the clinical domain.

For preclinical MR imaging of acute stroke, the simplest research tool is diffusion-perfusion (DWI/PWI) mismatch. However, this has still to be validated both preclinically and clinically, and at present there is no consensus as to what thresholds should be used for diffusion and perfusion. Therefore, until a more accurate MR model is characterised and validated, positron emission tomography (PET) (see section 1.3.2 for definition) will continue to represent the gold standard for imaging the penumbra.

Bandera and colleagues (2006) performed a systematic review to assess the evidence available on CBF thresholds for differentiating between ischaemic core and penumbra in adult stroke patients. They found that out of 237 reviewed papers, only 7 satisfied their inclusion criteria. Papers were excluded for a number of reasons; data were recorded from animal studies/experimental models, studies were on paediatric patients, the clinical diagnosis was not stroke, unreported CBF thresholds, review papers, and studies where there was no comparison with the gold standard. Within the seven papers, CBF thresholds for penumbra and ischaemic core varied, from 14.1 to 35.0 and from 4.8 to 8.4 mL/100g/min, respectively.

The ischaemic penumbra can be defined in animal models by directly relating flow measurements to the functional state of the tissue. To enable penumbra definition to be transferrable to the clinical situation, there are three measurements required (Heiss, 2003):

1. Quantification of flow in the ischaemic core and adjacent hypoperfused regions;
2. The integrity of the tissue in the affected areas with regards to irreversible damage or preserved viability;
3. The duration and extent of reduced blood flow in the various tissue compartments

At present, there is an inability to generate a real-time measure of blood flow. Only momentary measurements of tissue characteristics can be observed, when the progression of infarct and the imminent recruitment of the penumbra to the ischaemic core are of vital importance. The upshot of measuring real-time haemodynamic parameters is that they can allow us to make predictions about the fate of the tissue.

1.2.6 Salvaging the ischaemic penumbra

By improving blood flow or interfering with the ischaemic cascade, penumbra has the potential for rescue. Penumbral salvage is associated with neurological improvement and recovery, and therefore it is the target for acute stroke therapy (Molina and Saver, 2005). There is no direct treatment measure to reduce the extent of neurologic injury (The National Institute of Neurological Disorders and Stroke rT-PA Stroke Study Group, 1995). For ischaemic injury, blockage removal and blood flow restoration take primacy. The penumbra takes a central role in therapeutic interventions.

1.2.6.1 Reperfusion therapies

Of all the therapeutic strategies for acute ischaemic stroke, the most dramatically effective intervention is reperfusion (Molina and Saver, 2005). Ischaemic stroke refers to the sudden loss of blood flow in a cerebral artery due to a blockage. Mechanical or drug-induced restoration of blood flow with its accompanying nutritive delivery by reperfusion enables salvage of previously injured (penumbral) tissue (Figure 1.12). As a result, adequate tissue viability is retained in this penumbral tissue, and infarct evolution is halted. Rapid reperfusion of the artery by thrombolysis has been shown to produce a favourable clinical outcome such as reduced final infarct volume and improved clinical outcome scores (Felberg et al, 2002; Uchino et al, 2005) in selected patients (NINDS rT-PA Stroke Study Group, 1995).

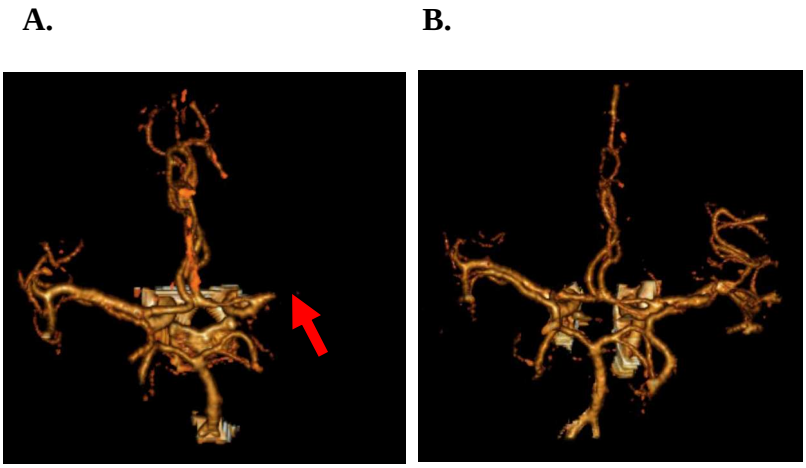

Figure 1.12. 3D CT image of the Circle of Willis of an acute stroke patient with an occluded middle cerebral artery identified by the missing vessel (red arrow) (**A**) and following thrombolysis (**B**), where flow is restored to previously ischaemic regions (Images provided by Professor K Muir, Southern General Hospital)

Disability and mortality are reduced by admission to specialised stroke units (Rudd et al, 2005). Other than this, the only widely approved drug treatment for acute cerebral ischaemia is recombinant tissue plasminogen activator (rT-PA). Before thrombolysis was approved by the US Food and Drug Administration for acute ischaemic stroke in 1996 (i.v rT-PA; therapeutic time window of less than 3 hours of stroke onset) (Adams et al, 1996), stroke was considered to have a bleak prognosis, and patients were treated non-urgently. Since then, clinical experience and randomised i.v (intravenous) rT-PA trials have shown a time-dependent effectiveness, in that patients experience the greatest benefit within the first 90 minutes (Donnan et al, 2004). However, many patients are ineligible for thrombolytic therapy, in that fewer than 10% of all stroke patients can be thrombolysed (Cocho et al, 2005; Molina and Saver, 2005). The low treatment rates with i.v. rT-PA (for example 1-7% in the USA following FDA approval (Wardlaw et al, 2009)) partly reflects delays in presentation and institutional barriers to rapid medical assessment (Katzan et al, 2004, Kahn et al, 2005), but also that clinical uncertainty prevents treatment in many circumstances, including patients awaking with symptoms in whom onset time is unclear, rapidly improving or mild symptoms, and perceived concern about bleeding risks in treating patients with mild strokes (Barber, 2001).

RT-PA is an enzyme that catalyses the conversion of plasminogen to plasmin, which can then degrade and dissolve the clot. Within the acute stages of ischaemia, the benefit of such therapy is at least an order of magnitude greater than aspirin – another

pharmacological agent with a proven (modest) efficacy for treating ischaemic stroke (Molina and Saver, 2005). According to the National Institute of Neurological Disorders and Stroke (NINDS) trials, for every 1000 patients treated with rT-PA, around 323 will attain a better outcome (Saver, J.L, 2004). It has been shown, from randomised i.v. rT-PA trials, that its effectiveness is time-dependent.

Initially, as further clinical trials showed no benefit of rT-PA treatment after the 3-h limit (Clark et al, 1999; Hacke et al, 1998), it was thought that the risk/benefit ratio did not justify its use beyond 3 hours (Intercollegiate Stroke Working Party, 2004). However, studies have reported substantial delays in presentation following stroke (Katzan et al, 2004; Lacy et al, 2001) including a study based in Oxford which showed only 31% of stroke patients presenting within 3 hours (Salisbury et al, 1998).

Barber and colleagues (2001) analysed eligibility for thrombolysis in patients admitted to all four Calgary hospitals in Canada. They categorised the patients according to the time of presentation; within the 3 hour time window and presenting beyond it. They noted that, of the 27% of patients presenting within the time window, only 27% received i.v rT-PA, the majority were excluded according to the criteria in (Figure 1.13). As such, 31% of patients were not given i.v rT-PA because their symptoms were either considered too mild or were rapidly improving. Overall, a third of this 31 percentile were left either dependent or dead.

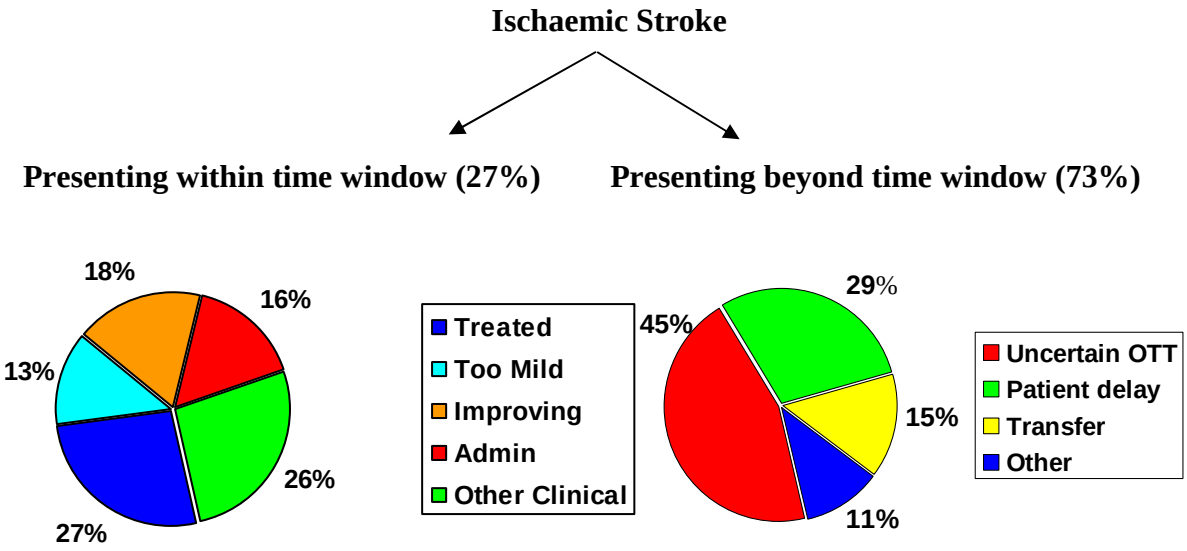

Figure 1.13. Pie charts representing the percentage of ischaemic stroke patients presenting within the time window and the clinical outcomes, and the reasons for presenting out with the time window (Barber et al, 2001). OTT – uncertain time of onset. Admin and other clinical reasons refer to clinical uncertainty – such as patients awaking with symptoms in whom onset time is unclear, perceived concern about bleeding risks in treating mild strokes, emergency department referral delay and significant comorbidity

In May 2009, the American Heart Association (AHA)/American Stroke Association (ASA) extended the window for acute ischaemic stroke, approving rT-PA as a treatment between 3 and 4.5 hours post-symptom onset. The decision was primarily based on findings from the third European Cooperative Acute Stroke Study (ECASS III) trial, which confirmed a significant reduction in disability at the 90 day time period after rT-PA treatment between 3-4.5 hours (Hacke et al, 2008). The exclusion criteria applied in the trial design included patients over 80, a National Institutes of Health (NIH) stroke scale score>25, history of previous stroke or diabetes, or if taking oral anticoagulants.

More recently, a time profile of benefit and harm for rT-Pa in a pooled analysis of eight randomised trials concluded that one in three patients had improved outcomes when treated between 1 and 3 hours from symptom onset, whilst one in six benefitted in the 3-4.5 h time window. Significantly, risk may outweigh benefit beyond the 4.5h time point (Lees et al, 2010), and this finding was supported by a previous Cochrane meta-analysis (Wardlaw et al, 2009).

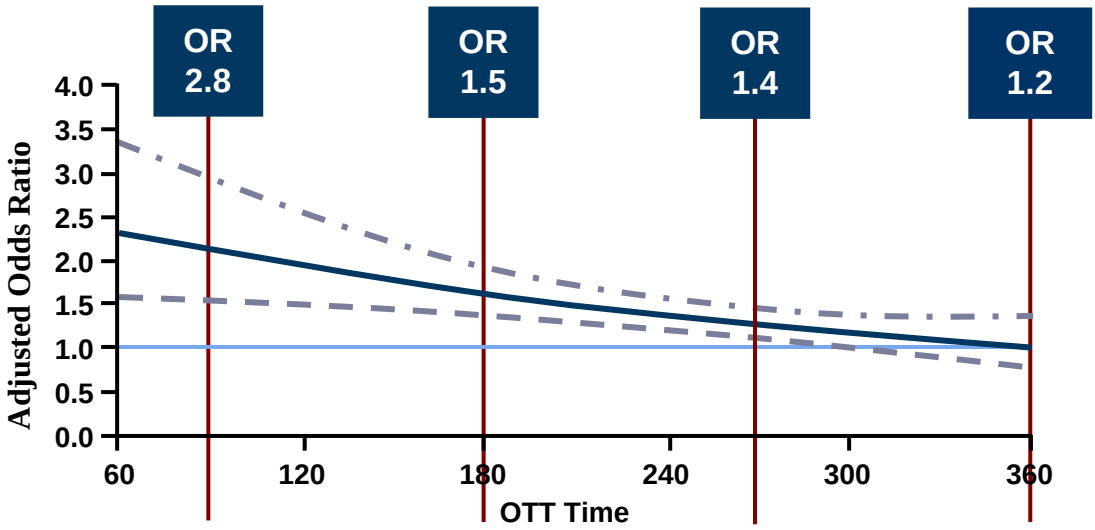

Figure 1.14. Combined data from NINDS, ECASS and ATLANTIS investigators observing the effects of timing of thrombolysis on stroke outcome. Patients treated within 90 min had the most improved 3-month outcomes, whilst patients treated between 90 and 360 min also experienced improvements. Beyond 360 min, the effect is not evident (NINDS, ECASS and ATLANTIS investigators, 2004) OR: Odds ratios, OTT: onset to start of treatment. The dark blue slope is the odds ratio estimated by the model, and the dashed lines represent the upper and lower 95% confidence intervals (CI). The light blue line at 1.0 reflects the adjusted odds ratio where the outcome of thrombolysis group is equal to the placebo group

NINDS, ECASS and ATLANTIS (Alteplase Thrombolysis for Acute Noninterventional Therapy in Ischemic Stroke) investigators combined data for a pooled analysis (2004) which reported the effects of timing on outcome. It showed that patients treated within 90 min had improved 3-month outcomes and in patients treated up to the 360 min time point, improved outcomes were still observed. However, the odds of favourable 3-month outcome increases as onset to start of treatment (OTT) decreased. Interestingly, if the OTT is beyond 4.5 hours, the beneficial effect may no longer be evident. The researchers divided the OTT into 90 min intervals (0–90, 91–180, 181–270, and 271–360) and the ratio of patients with a favourable outcome (modified Rankin Scale (mRS) 0, 1, or 2; National Institutes of Health Stroke Scale 0-1 and Barthel Index 95-100) was analysed in 2779 patients. There was a significant correlation of outcome with time from symptom onset. The odds ratios for the favourable outcome were 2.81, 1.55, 1.4 and 1.15, respectively, with the last OR missing statistical significance. Figure 1.14 shows the odds ratio for a favourable outcome at 3 months in rT-PA-treated patients compared with controls by OTT.

It showed that the lower 95% CI intersects with 1.0 at 285 min after symptom onset and the point estimate of the odds of a favourable outcome is close to 1·0 at 360 min, suggesting reduced probability of benefit beyond this time. The lower 95% CI defines the lower range of the CI, and when the OR reaches 1.0, the odds of a favourable outcome in the thrombolysis treatment group is the same rate as the placebo group. The findings suggest that the beneficial effect of rT-PA might extend beyond 3 h since the odds ratio for a favourable outcome was 1·40 (1·05–1·85) for thosetreated within 181–270 min. Within the first 3 hours there were significant OR changes at 10-minute increments (Fiebach and Schellinger, 2003).

Despite a good likelihood of an excellent neurological outcome with early reperfusion, late reperfusion may paradoxically induce a serious of pathophysiological responses which result in potentially fatal outcomes, including cerebral oedema or intracranial haemorrhage (ICH) (The NINDS t-PA Stroke Study Group, 1997). Haemorrhagic transformation, identified 24-36 hours following stroke is more frequent after reperfusion, regardless of the modality used to induce recanalisation, such as anti-thrombotics, mechanical recanalisation and intravenous lytics (Khatri et al, 2007). Regarding animal models, reperfusion following a prolonged period of ischaemia may actually increase final infarct size, compared to permanent ischaemia models (for example, ischaemia lasting 120-300 mins (Aronowski et al, 1997) and 180 mins (Yang and Betz, 1994)). As such, thrombolytic therapy can potentially exacerbate ischaemic injury for certain patients, whilst dramatically improving clinical outcomes in others. rT-PA is contraindicated for haemorrhagic strokes and carries a risk for increased ICH in ischaemic stroke potentially inducing 1 fatal ICH in every 20 patients treated (Figure 1.15) (Wardlaw, del Zoppo, and Yamaguchi, 2003).

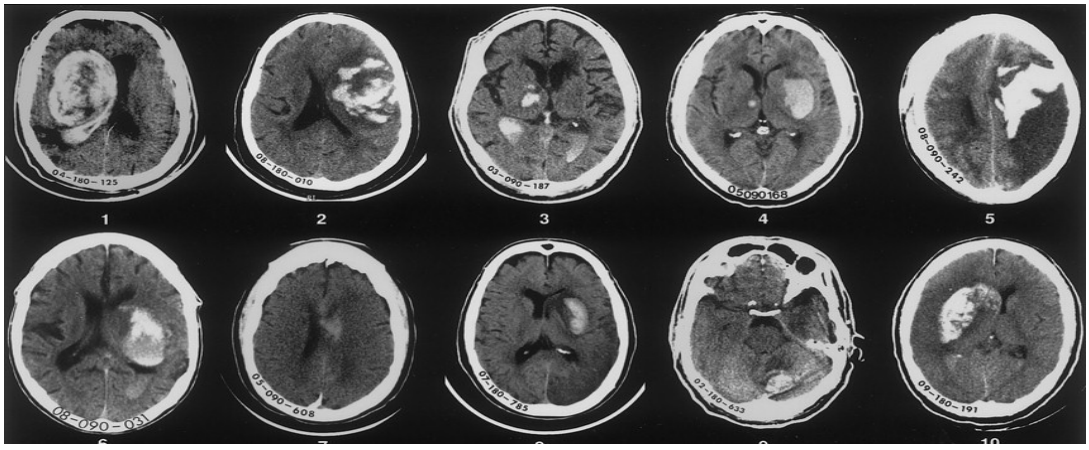

Figure 1.15. Evidence of intracerebral haemorrhage following stroke on 10 stroke patients treated with rT-PA. The NINDS t-PA Stroke Study Group (1997). Haemorrhages are displayed as hyperintense regions in this MRI sequence

1.2.6.2 Influence of admission to specialised stroke units on outcome

Admission to a specialised stroke unit has been shown to improve the neurological outcome from stroke. Rudd and colleagues (2005), using data from the 2001 to 2002 National Stroke Audit, assessed the effectiveness of stroke unit care in England, Wales, and Northern Ireland in delivering effective processes of care and in reducing case fatality and disability (Rudd et al, 2005). They found that the risk of death in patients receiving stroke unit care was estimated to be ~75% that of the risk from having no stroke unit care. This favourable outcome was in agreement with previous studies, including clinical trials by the Stroke Unit Trialists' Collaboration (SUTC), where there were fewer deaths and less morbidity in patients residing in stroke units (Stroke Unit Trialists' Collaboration, 2002).

In 2002, stroke unit care in the UK only accounted for one third of stroke victims (Intercollegiate Working Party for Stroke, 2001-02: http:// www.rcplondon.ac.uk/college/ceeu/strokeconciseauditreport.pdf). Given that there are approximately 120,000 first strokes per year with a 30% mortality rate after one year (in England and Wales), only 40,000 receive care from specialised units. Non-specialised units are responsible for mortality rates 14-25% higher than stroke units (Stroke Unit Trialists' Collaboration, 2002). Thus, stroke unit care availability for all patients would translate to potentially saving 3500-6000 lives a year.

1.3 Multimodal identification of penumbral tissue

Advancements in brain imaging modalities may introduce more stringent prerequisites for patients to qualify for penumbral salvage either with current therapy or recruited into clinical trials to test new therapies. Criterion such as perfusion status and the physiological and biochemical condition of ischaemic tissue are becoming more accurately defined to improve patient selection (Table 1.3).

The evolution of the ischaemic penumbra for individual patients is dependent upon time from onset, the adequacy of collateral blood flow, temperature, and systemic metabolic disturbances (e.g., glucose level, acidosis) (Fisher, 1997). This implies that the volume and concomitant loss of penumbral tissue varies between patients, and thus the time window for thrombolytic treatment is entirely subjective. The processes that advance loss of penumbra into ischaemic core may differ from patient to patient, and thus in the future, clinical intervention may be specific to the individual.

Failure to identify efficacy in both thrombolysis and neuroprotection trials (Kidwell et al, 2001) could have arisen from treatment being administered in some patients at a time point when no salvageable (penumbral) tissue remained, but potentially also to recruitment of patients lacking target penumbral tissue even within conventional time windows (Muir, 2002). The possible improvement in safety with selection for thrombolysis based on more advanced penumbral imaging has been suggested (Schellinger 2003). Neuroimaging techniques have influenced the ability to evaluate the extent of stroke damage, as well as introducing a surrogate for treatment outcome assessment and criteria for treatment administration.

1.3.1 Computed tomography (CT)

Computed tomography is currently the most accessible clinical technique for identification of the ischaemic penumbra due to its speed of image generation, its wide availability and practicality. Plain CT scans cannot identify the penumbra, but CT perfusion (CTP) techniques using injection of a contrast medium bolus are showing promise. CT perfusion imaging defines penumbra using changes in CBV, CBF and MTT (mean transit time). Using CT, the ischaemic core has been defined as a region with CBV below 2 mL/100g and relative MTT above or equal to 145% of the contralateral value. Autoregulation is

compromised in the ischaemic core, which results in lowering of CBV. CTP defines penumbral tissue as a region with increased cerebral blood volume (relative to the ischaemic core due to local vasodilatation, where autoregulatory processes compensate for reduced relative (rCBF)), as well as reduced CBF and increased MTT. However, it suffers similar problems to MRI-based perfusion-weighted imaging (Chapter 1.3.3.4) as there are no proven thresholds for defining the outer limit of the penumbra to differentiate it from benign oligaemic tissue. It may perhaps be less accurate than the diffusion-perfusion mismatch technique (an established MR research tool) (Chapter 1.3.3.5), as there is no equivalent to DWI data of injured tissue on CTP. CT is therefore still incompletely validated for penumbral identification in acute stroke treatment studies, and whole brain coverage is not yet readily available. Radiation exposure may prevent serial scanning, and iodinated contrast agent administration may cause nephropathy and allergy (Ebinger et al, 2009).

1.3.2 Positron Emission Tomography (PET)

The gold standard for clinical assessment of penumbra is PET, which detects gamma rays emitted indirectly by a positron emitting radioisotope bound to a ligand. A 3D image can be tomographically reconstructed that is based on the concentration of the administered tracer. Multitracer PET using ^{15}O or $H_2{}^{15}O$ as ligands can quantitatively identify tissue metabolic state and can be used to characterise the penumbra as tissue with reduced CBF, preserved $CMRO_2$ and an increased OEF (Baron, 1999; Ebinger et al, 2009) (Figure 1.16). This signature of penumbral tissue was termed ‘misery perfusion’ by Baron and colleagues (1981). In humans, oxygen metabolism and CBF thresholds of irreversibly damaged tissue have been defined as 65 µmol/100g/min and 12 mL/100g/min, respectively (Heiss, 2003).

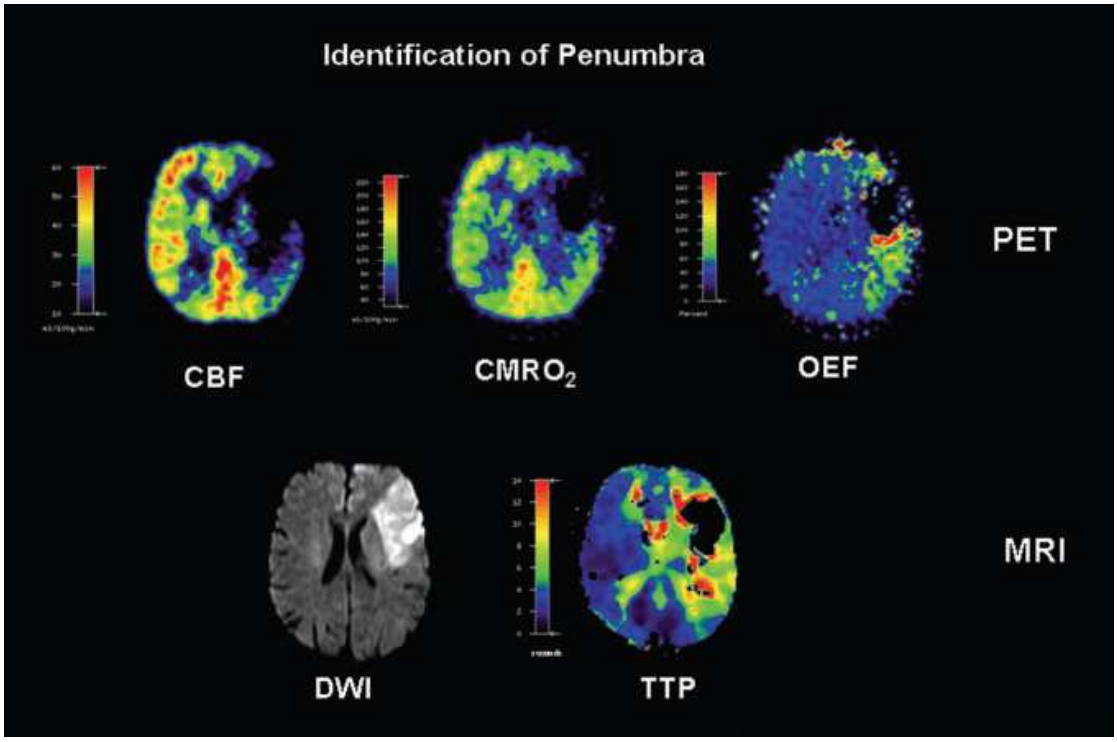

Figure 1.16. Multimodal imaging 5 hours post-stroke in a human patient. Penumbra is defined as a region with reduced CBF, preserved $CMRO_2$ and increased OEF, which correlates approximately with MRI findings (DWI hyperintensity and time to peak (TTP) delay of 4 seconds). Adapted from Heiss et al (2004)

Serial PET has been used experimentally which demonstrates the spatial and temporal evolution of penumbra following MCAO (Heiss, 1994; Touzani et al, 1995). Perfusion and non-perfusion based markers of ischaemic tissue (such as the hypoxic ligand [^{18}F]-fluoromisonidazole (FMISO) and the neuronal receptor ligand [^{11}C]-flumazenil (FMZ)) are becoming more accurately defined to improve patient selection (Takasawa et al, 2008). FMZ can identify the integrity of neurons and it can detect damage in the acute phase post-stroke, whereas FMISO identifies hypoxic tissue expressed as regions of increased tracer uptake (Heiss, 2003). The technique was supported by Takasawa and colleagues (2007), who noted increased FMISO uptake in the first hours in a MCAO rat model when reperfusion was not induced and the tissue was not yet irreversibly damaged. However, increased FMISO uptake has been shown 20 hours post-stroke in the peri-infarct tissue in the rat (Saita et al, 2004) despite reversal of MCAO following reperfusion. The authors suggested that peri-infarct oedema, small vessel occlusion, or the ‘no-reflow’ phenomenon may have caused persistent hypoxia. This may also have been a methodological problem, in that the intraluminal filament MCAO technique may have induced vascular injury or resulted in incomplete reperfusion.

Although PET is an accurate means of physiological monitoring which permits quantitative measurements, it is impractical for clinical use (Schellinger et al, 2003; Muir and Santosh, 2005). It necessitates arterial catheterisation for blood sampling, and it is prohibited when the administration of thrombolytics is planned (Heiss et al, 1998). Additionally, multiple scans cannot be performed due to the radiation dose administered, and it is expensive, technically challenging and of limited availability in stroke units (Schellinger et al, 2003; Muir and Santosh, 2005). As such, MRI is preferred for penumbral imaging in the experimental research domain.

1.3.3 Magnetic Resonance Imaging (MRI)

The emergence of MRI as a potent and robust modality for imaging anatomy, pathology, organ function and even neural activity has elevated it to the technique of choice for assessing many diseases of the central nervous system. By affording such high resolution of anatomical structures, as well as enabling manipulation of image appearance due to the multitude of sequences available, MRI offers a high degree of specificity in the neuroscience domain.

MRI is a non-invasive method of imaging the human body, based on the electromagnetic activity of atomic nuclei. The presence of a strong external magnetic field takes advantage of the intrinsic characteristics of hydrogen nuclei (^{1}H), which are abundant in the body. Each hydrogen nucleus consists of a single positively charged proton which rotates around its own axis - a property known as spin. The positive charge inherent in these particles causes their spins to induce a small magnetic field referred to as the magnetic moment. When a subject is placed in a magnetic field such as an MRI scanner, the protons are forced to align in one of two possible positions - protons will align either parallel or anti-parallel with the magnetic field. When radio waves are sent toward these hydrogen atoms, the alignment of the magnetisation is altered. This causes the emittance of a weak radio signal that can be amplified and detected by a scanner. Different types of tissues send back different signals, allowing differentiation between internal structures, which leads to a reconstruction of the image of the body. Specific MRI techniques can be used to depict specific attributes of the tissues of interest, enabling disease processes to be suitably characterised.

To enable structural imaging, the MR system requires the following components:

1. A large magnet to generate the magnetic field;
2. Shim coils to make the magnetic field as homogeneous as possible;
3. A radiofrequency (RF) coil to transmit a radio signal into the body part being imaged;
4. A receiver coil to detect the returning radio signals;
5. Gradient coils to provide spatial localisation of the signals, and;
6. A computer to reconstruct the radio signals into the final image

The magnetic field is achieved by generating a current with the use of a superconducting electromagnet. This current is introduced through a superconducting wire – resistance is eliminated by cooling the wire with liquid helium to 4K (−269°C). For example, seven Tesla (7T) refers to the magnetic field strength of the scanner, which is 175,000 times more powerful than the magnetic field of the Earth. The rationale for providing a scanner with such high magnetic fields is to enable the best signal to noise ratio in samples of small dimension (such as a rat or mouse brain). The 7T scanner which was used in this thesis is shown in Figure 1.17.

Figure 1.17. The Bruker Biospec 7 Tesla MRI scanner at the Glasgow Experimental MRI Centre (GEMRIC), University of Glasgow.
(http://www.gla.ac.uk/departments/glasgowexperimentalmricentre)

The translation of MRI to medicine is aided by the fact that water makes up more than two thirds of the weight of the human body. MRI harnesses the intrinsic nature of this water by delineating between the various water content of tissue and organs. Crucially, changes in water content are indicative of a number of pathologies – reflected in MR images. The signal-influencing characteristics of interest are the relaxation time constants; the

longitudinal (T_1) and transverse (T_2) relaxation times. The relaxation times vary for different tissues and structures. For example, water protons move rapidly, and this prevents them from relinquishing their energy with ease. This means that the relaxation time is long, and because the tissues of the body have varying water contents, the T_1 and transverse T_2 relaxation times differ.

1.3.3.1 Relevant MRI physics

MRI signals are generated by nuclei with a positive charge, such as ^{31}P and ^{1}H. This indicates that the nucleus has an excess proton which is unpaired, unlike the remaining positively charged protons that are attached to a negatively charged electron. The constituent parts of water are OH^- and H^+. H^+ is an elementary particle that has both a positive and negative pole (the respective distributive charges from the single orbiting proton and electron) and the positive charge causes the particle to possess spin, and thus generates a magnetic field.

The spin of a particle causes the subject's protons in an MR magnet to align in a high or low energy state. The high energy state refers to when the north pole of the spin is aligned with the south pole of the magnetic field, and the low energy state indicates when the north pole of the spin aligns with the north pole of the magnet. As the proton has an electrical charge, it has a magnetic moment, which gives it a magnetic property. This latter characteristic therefore makes it particularly reactive to external magnetic fields and electromagnetic waves. As MR scanners require the reception of a signal via a receiver coil, images can be generated when a voltage is applied – this occurs when the proton moves as a result of the application of external fields and waves.

The movement of the proton can be explained in a vector model that uses a standard coordinate system (Figure 1.18). The force is represented as an arrow, in which the strength is represented by the length of the arrow. The X, Y and Z coordinates enable the positional changes of the proton to be depicted under the influence of the magnetic field. The main magnetic field is often represented as B_0, and its direction is in the z plane, from bottom to top.

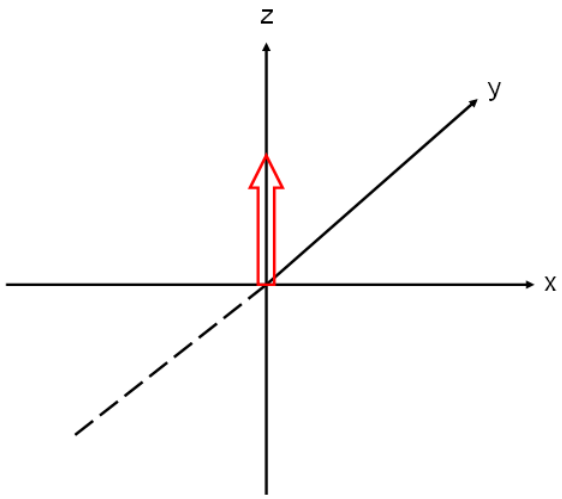

Figure 1.18. The dimensions of the magnetic field are shown as x, y and z. Z refers to the main magnetic field, whilst the xy-plane is perpendicular to the z-axis

The z axis corresponds to the direction of the bore of the magnet, and this is known as the longitudinal direction (shown as the red arrow in Figure 1.18). As the protons spin, they are being forced into alignment by the magnetic field. This induces a torque that provides an angular momentum, enabling it to retain the spatial orientation of its rotation axis. The angular momentum affects the movement of the rotational axis of the spins, and the nuclei undergo precession that is proportional to the frequency of the applied magnetic field strength – this is called the Larmor frequency, shown as;

$$\omega_0 = \gamma_0 \cdot B_0$$

where;

ω_0, is the Larmor frequency in megahertz [MHz],

γ_0, the gyromagnetic ratio, a constant specific to a particular nucleus, and,

B_0, the strength of the magnetic field in tesla [T].

Longitudinal magnetisation, M_Z, accumulates in the z-direction when the spin system relaxes and retains its initial stable state. This occurs because the magnetic vectors representing the individual magnetic moments amass. The magnetic resonance signal is very faint, and therefore the strength of the magnet is required to be sufficiently powerful to obtain any signal at all. The spins can be parallel or anti-parallel to the magnetic field, although most are in the parallel state. The net magnetisation is actually due to this difference, and is named the net magnetisation vector (NMV). In the magnetic field of an

MRI scanner at room temperature, there is approximately the same number of proton nuclei aligned with the main magnetic field B_0 as counter-aligned. The aligned position is slightly favoured, as the nucleus is at a lower energy in this position. For every one-million nuclei, there is about one extra nucleus aligned with the B_0 field as opposed to the field. This results in a net or macroscopic magnetization pointing in the direction of the main magnetic field.

An electromagnetic wave can then be introduced to this environment. This wave of energy is proportional to the Larmor frequency and is known as the resonance condition. This is applied by generating an electromagnetic wave with a radio transmitter, and via an antenna coil. The energy absorption can be quantified by the extent to which the longitudinal magnetisation is tipped from the z-direction towards the xy-plane. If the radiofrequency (RF) pulse is strong enough, and applied for long enough, then all of the longitudinal magnetisation is tipped exactly 90^o (Figure 1.19), which is known as transverse magnetisation.

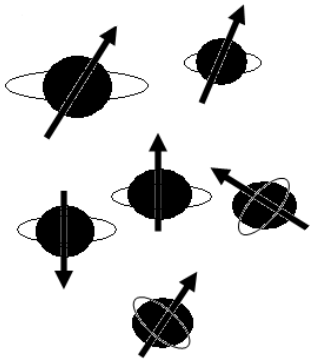

A With no magnetic field, the spins rotate around their axes in random directions

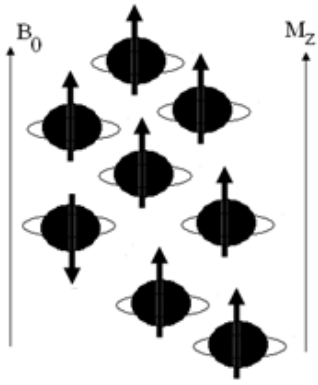

B Slightly more spins align parallel to the magnetic field when it is present

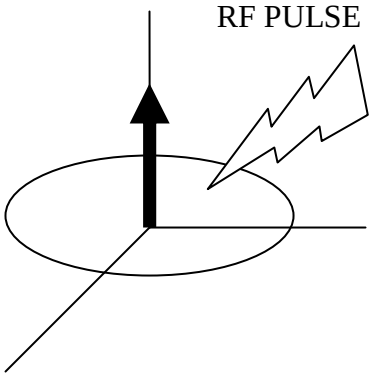

C An RF pulse, when the spins are aligned parallel to the magnet, causing directional spin changes

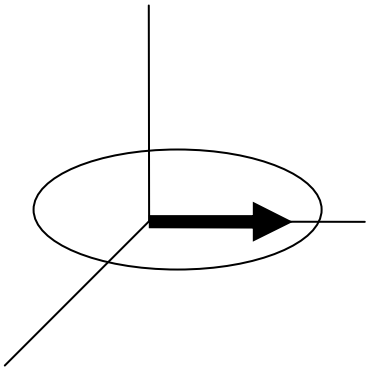

D The pulse shifts the direction of the spins by exactly 90^{o}, causing transverse magnetisation, M_{xy}

Figure 1.19. Protons spin randomly when there is no magnetic field (**A**), and soon align mainly in the low energy state in a magnetic field (**B**). This causes longitudinal magnetisation (**C**) until an RF pulse can be generated to induce transverse magnetisation (**D**). (Weishaupt, Kochli, and Marincek, 2006: p1-5)

Relaxation

Spin lattice relaxation time (T_1) and spin-spin relaxation time (T_2) weighted imaging are commonly used techniques. For image contrast, these methods are dependent upon the longitudinal and transverse relaxation of different tissue types, respectively. Water has a long relaxation time because the protons are moving too fast to easily give up their energy. Different tissues contain various amounts of water; therefore, they will experience different

T_1 and T_2 relaxation times. Transverse magnetisation is weakened by spin-lattice interaction and spin-spin interaction.

T_1 relaxation

T_1 is the decay constant for the recovery of the z component of the nuclear spin magnetization, as it retains its stable, longitudinal position. The magnetisation on the xy-plane decreases and the MR signal fades in proportion. The restoration of the M_z magnetisation results and this is known as longitudinal relaxation, or T_1 recovery, which always increases with time (Figure 1.20).

The time constant for this recovery is T_1 and is dependent on the strength of the external magnetic field, B_0, and the internal motion of the molecules (Brownian motion). Biological tissues have T_1 values of half a second to several seconds at 1.5T (Weishaupt, Kochli, and Marincek, 2006: pp7).

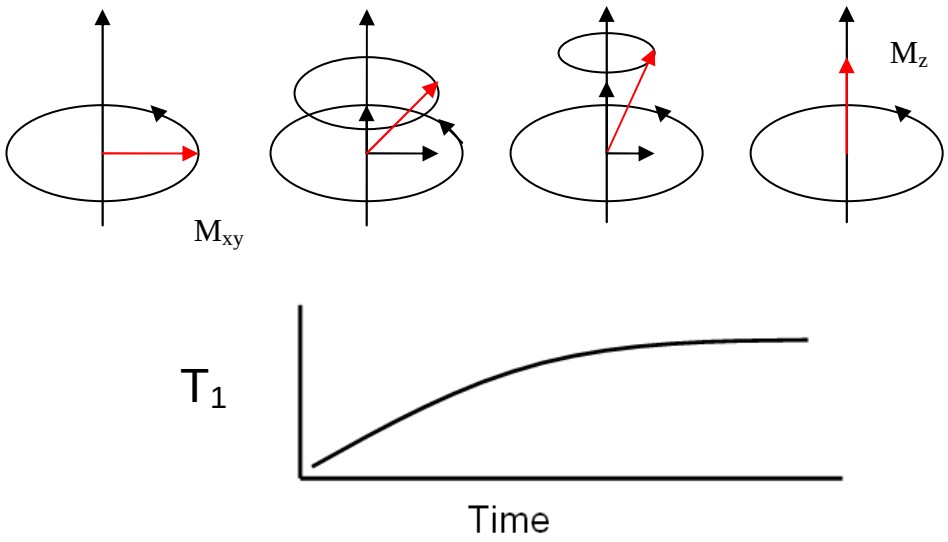

Figure 1.20. A depiction of T_1 relaxation, where the flip angle gradually decreases. The regrowth of Mz magnetisation is achieved as transverse magnetisation decays. Relaxation is shown as a function of time as Mz magnetisation is restored. (Weishaupt, Kochli, and Marincek, 2006: p8)

T_2 and T_2^* relaxation

Phase refers to the position of a magnetic moment on its circular processional path, and is expressed as an angle. If there are two spins, A and B, precessing at the same speed in the

xy-plane, and if B is ahead of A in its angular motion by 10^{o}, then we say B has a phase of +10 relative to A. Conversely, a spin C that is behind A by 30^{o} has a phase of -30^{o}.

Immediately after excitation, part of the spins precesses synchronously. These spins therefore have a phase of 0^{o}, and are said to be in phase. This state is known as phase coherence.

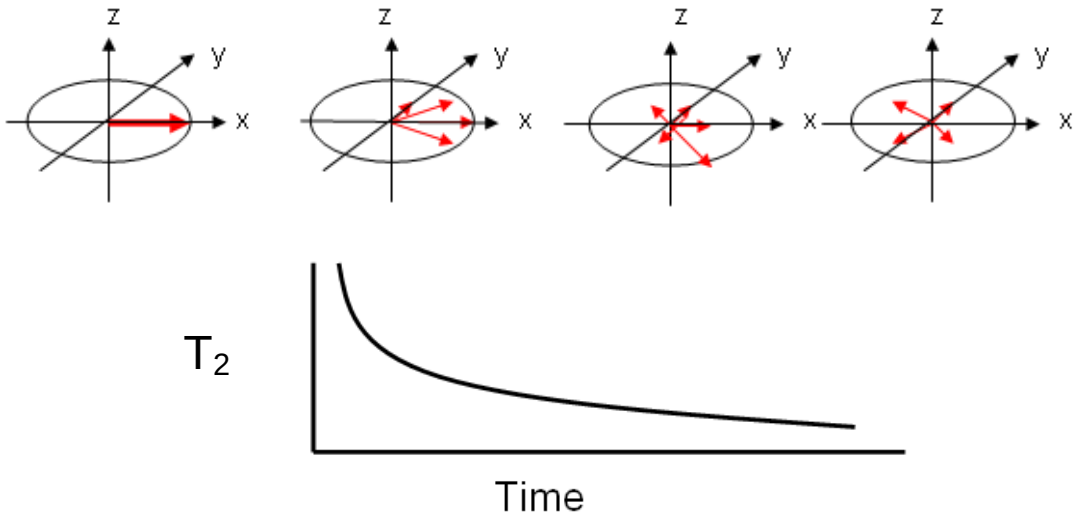

Figure 1.21. The spins dephase when they lose energy to one another, resulting in the loss of transverse magnetisation. T_2 signal decreases with time

Phase coherence is gradually lost, as some spins advance while others fall behind on their precessional paths. There is a reduction of magnetisation as the energy is shifted from the high energy state to the low energy state, causing the MR signal to fade. The rate at which transverse magnetisation relaxes is known as T_2 relaxation, and this decreases with time (Figure 1.21). Transverse relaxation differs from longitudinal relaxation in that the spins do not dissipate energy to their surroundings but instead exchange energy with each other. T_2 denotes the process of energy transfer between spins, whilst T_2^{*} refers to the effects of additional field inhomogeneities contributing to dephasing. T_1 and T_2 occur independently, but also occur more or less simultaneously.

Repetition Time (TR)

T_1 influence

To generate an image, the signal at the tissue has to be measured numerous times. Repetition time (TR) is the amount of time that exists between successive pulse sequences applied to the same slice. When TR is long, more excited spins rotate back to the z-plane

and contribute to the return to longitudinal magnetisation. The more magnetisations that can be excited with the next RF pulse, the larger the MR signal that can be collected.

When TR is short (less than 600 msec), image contrast is strongly affected by T_1. Tissues with a short T_1 therefore undergo relaxation rapidly, and more nuclei are ready to experience excitation when the next pulse is initiated. Therefore, they give off a large signal, and the images appear bright. Tissues with long T_1 have fewer nuclei that retained their longitudinal magnetisation after the first pulse, and so less are available for the next pulse. They emit a weak signal, and appear as dark images. An image acquired with a short TR is T_1-weighted because it contains mostly T_1 information.

By measuring the signal very soon after the last 90° pulse (a short TR), a discrepancy between the magnetisation of each tissue develops. Conversely, by allowing a longer time to pass (a longer TR), the magnetisation between the tissues reduces. By having a short TR, the magnetisation of tissues will be most diverse, allowing differentiation of structures to be achieved.

T_2 influence

Signal differences between tissue types arise from differences in T_2. This is achieved by waiting for different amounts of signal decay to occur before taking a signal measurement. When the echo time (TE) is altered, the change in signal resulting from differences in the T_2 of tissues is either enhanced or attenuated. Echo time relates to the time taken to collect the MR signal once the excitation pulse has been generated. Thus, a short TE would reduce the time required for the signal amplitudes in different tissue to change. A larger difference would exist if the TE was longer, as more time passes to enable signal amplitudes in the tissues to vary. In short, increasing the TE enhances differences in signal arising from differences in the T_2 of tissues.

Tissue	T_1-weighted image	T_2-weighted image
Fat	Bright	Bright
Aqueous liquid	Dark	Bright
Tumour	Dark	Bright
Inflammatory tissue	Dark	Bright
Muscle	Dark	Dark
Connective tissue	Dark	Dark
Haematoma, acute	Dark	Dark
Haematoma, subacute	Bright	Bright
Fibrous cartilage	Dark	Dark
Hyaline cartilage	Bright	Bright
Compact bone	Dark	Dark
Air	No signal	No signal

Table 1.2. MR signal intensities of various tissues under T_2- and T_1-weighted sequences

Echo-planar imaging (EPI)

EPI is a very fast MR imaging technique capable of acquiring an entire MR image in only a fraction of a second. In single-shot echo-planar imaging, all the spatial-encoding data of an image can be obtained after a single radio-frequency excitation, whereas multishot echo-planar imaging results in high-quality images comparable to conventional MR images. Additionally, echo planar imaging offers major advantages over conventional MR imaging, including reduced imaging time, the elimination of motion artefacts, and the ability to image rapid physiologic processes of the human body (Poustchi-Amin et al, 2001).

There are a numerous physiological and logistical constraints in performing diffusion-weighted imaging (DWI) and perfusion-weighted imaging (PWI), so EPI is used. EPI can be thought of as an ‘add on’ to a pulse sequence, to acquire more signals from each excitation pulse. It requires strong and rapidly switched frequency-encoding gradients. An echo train consisting of up to 128 echoes can be acquired. In this way, it is possible to obtain an image with a resolution of 256 x 128 after a single excitation pulse in 70 msec, corresponding to 16 images per second. Although EPI is ultrafast, it cannot compensate for

field inhomogeneities, causing the signal to decay with T_2^*. Also, a very strong and fast gradient is required due to this T_2^* signal decay because there is limited time for echo collection.

EPI for stroke

EPI is a recent technique that can be used to visualize physiologic parameters in addition to measuring diffusion coefficients of the ischaemic brain. Changes in brain oxygenation can be monitored by using gradient echo and EPI, in which deoxygenated blood acts as a susceptibility contrast agent. EPI can be used in conjunction with bolus injection of intravenous paramagnetic agents to assess cerebral perfusion and functional changes in cerebral blood volume (CBV)
(Sen, 2007 at http://www.emedicine.com/neuro/topic431.htm).
The major advantage of using EPI for stroke imaging is its insensitivity to patient movement artefacts of brain bulk motion, which severely compromises the quality of DWI scans. Incorporating EPI, DWI and PWI into an acute stroke protocol that includes rapid MR angiography, T_1-weighted, T_2-weighted, proton density, susceptibility-weighted and fluid-attenuated inversion recovery (FLAIR) sequences can take only 20 to 25 mins to perform. An acute stroke protocol using only EPI, DWI and PWI may be completed in 5 to 10 mins.

1.3.3.2 MRI in experimental stroke

In terms of prevalence, MR imaging in acute stroke is currently second to CT. A significant factor in CT taking precedence is the longer acquisition times needed for some MRI techniques. However, technical improvements in MRI software and hardware now mean that a plethora of MRI scans can be obtained within 15 minutes providing vital information, including evidence of intracerebral haemorrhage, location of thrombus, the perfusion status, an approximation of the duration of the ischaemic event, location and extent of ischaemic injury, and blood brain barrier breakdown. MRI techniques can also be used as surrogate markers to assess patient outcomes following therapeutic intervention. In the investigation of ischaemic stroke, conventional, structural magnetic resonance imaging techniques are valuable for the assessment of infarct size and location beyond the first 12 to 24 hours after stroke onset, and can be combined with MR angiography to non-invasively assess the intracranial and extracranial vasculature. However, during the critical first 6 to 12 hours, the probable period of greatest therapeutic opportunity, these methods

do not adequately assess the severity and extent of ischaemia (Baird and Warach, 1998; Kidwell et al, 2003).

Developments in MR imaging are showing great promise for the detection of developing focal cerebral ischaemic lesions within the first hours. These include:

1. Diffusion-weighted imaging (DWI), which provides physiologic information about the diffusion of water, thereby detecting one of the first elements in the pathophysiologic cascade leading to ischaemic injury;
2. Perfusion imaging (PWI), which depicts blood flow, and thus provides information on the severity and extent of ischaemia.

1.3.3.3 Diffusion-weighted imaging (DWI)

Diffusion is regarded as the redistribution of molecules from a region of high concentration to a region of low concentration. Applied to MRI, it is the technique that shows the signal intensity changes that are due to water motion by diffusion (Weishaupt, Kochli, Marincek, 2006). In a magnetic field, protons carried by moving water correspond to the relative intensity of diffusion of water molecules in each voxel. DWI is based on the sensitivity of magnetic resonance to motion, which shows the signal intensity changes that are due to water motion by diffusion. Water has isotropic diffusion properties, meaning that the molecules are free to move in any direction. The rate of diffusion, termed the diffusion coefficient (D) is measured in millimetres squared per second (mm^2/sec). This rate is influenced by the cellular architecture in terms of anisotropy versus isotropy (where the diffusion rate appears to be the same when measured along any axis). As such, to include these factors that affect observed diffusion, the rate of diffusion is termed the ‘apparent diffusion coefficient’ (ADC). A high value of D, or ADC, indicates a region of high motion and as such, there will be a lower signal in DWI. The corresponding ADC map will display this as a bright region (as it has a high self-diffusion coefficient).

A commonly used technique for generating diffusion-weighted images is with Pulsed Gradient Spin Echo (PGSE), which was invented by Stejskal and Tanner (1965). This consists of a 90^o-180^o spin-echo pair of RF pulses with equal gradients on either side of the 180^o pulse; the first pulsed gradient induces protons to precess at different rates, which will dephase and cause signal loss. The second gradient will rephase the proton spins. As some protons have moved between pulse times, the signal is attenuated. Therefore, the pulse

sequence is sensitive to diffusion. The Stejskal-Tanner equation simply relates diffusion related measurements (S) to measurements without diffusion weighting (S0);

$$S = S(0)\exp(-bD)$$

Where;
b is a known property of the gradient pulse sequence (the 'diffusion weighting factor'), S(0) relates to measurements without diffusion weighting, and D is the diffusion coefficient - the property of the tissue which you want to affect the image. DWI can be performed as little as twice with different DW gradients to create an 'apparent diffusion coefficient'.

Cerebral ischaemia below a critical cerebral blood flow threshold results in disruption of energy metabolism with a consequent failure of ion pumps and anoxic cell membrane depolarisation. The activity of the ion pumps (e.g. Na^+/K^+ ATPase pump) is ATP dependent. As local cerebral blood flow drops below a critical threshold the energy supply to such cells becomes inadequate, resulting in pump failure since it is ATP dependent. The membrane permeability is increased and water shifts from the extracellular space to the intracellular space resulting in cytotoxic oedema, cell swelling and restricted diffusion (Kesavadas et al, 2003). Under normal conditions, water protons have the ability to diffuse relatively freely in the extracellular space resulting in a lower signal on DWI images. Following ischaemia, hyperintensity on DWI signifies restriction of the ability of water protons to freely diffuse due to the reduced extracellular space caused by the development of cytotoxic oedema. It is possible to obtain a quantitative measure relating to the properties of diffusion occurring within a particular voxel (volume picture element). This value, the ADC, can then be mapped as an image, using diffusion as the contrast. These are known as ADC maps, and an area of acute ischaemic damage that is bright on a diffusion-weighted image (reduced mobility of water protons) will appear dark on the corresponding ADC map (smaller diffusion constant). A decrease in the ADC of the ischaemic brain tissue has been shown to coincide with the onset of cytotoxic oedema (Davis et al, 1994). Regions of reduced ADC have been taken as a guide to irreversibly damaged tissue, but evidence shows that rapid reperfusion can salvage some tissue within the ADC-defined lesion (Hassegawa et al, 1994). ADC values in ischaemic areas can be lower by 50% or more than those of normal brain areas. Diffusion weighted imaging can identify ischaemic changes in under an hour following stroke, whereas CT scans and T_2-weighted MRI can

only identify ischaemic damage between 3 and 12 hours post-stroke, respectively, which is useful in the acute period following stroke (Roberts et al, 2002). Sample ADC map and T_2- and diffusion-weighted imaging post-ischaemia is shown in Figure 1.22.

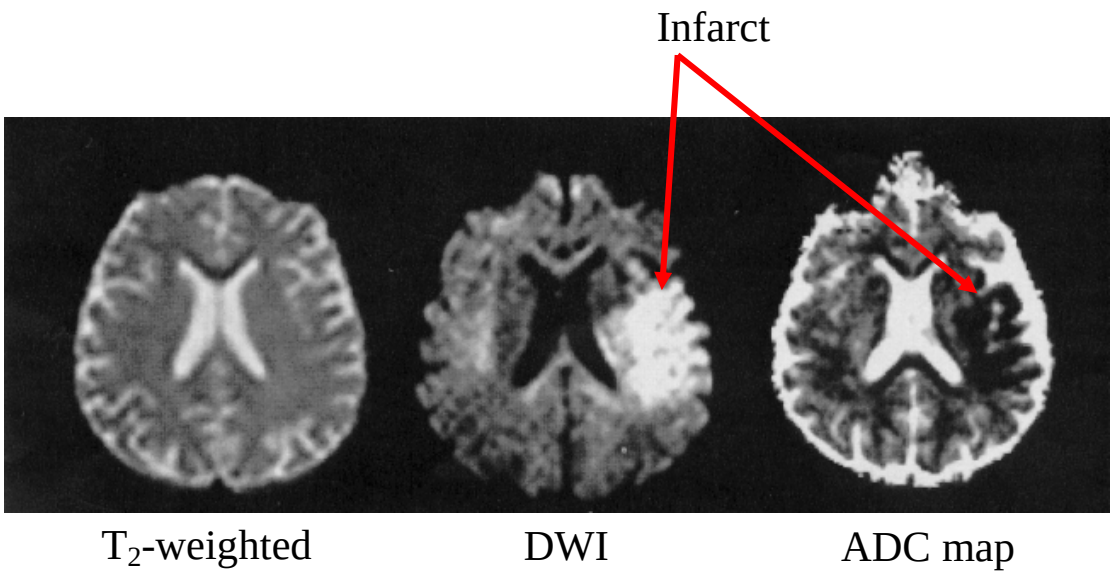

Figure 1.22. T_2-weighted image, diffusion-weighted image (DWI), and apparent diffusion coefficient (ADC) map of hyperacute ischaemic stroke in a human studied 2 hours after the onset of a right hemiparesis and global aphasia. Ischaemic damage appears bright on DWI and dark on ADC maps in left MCA territory, whereas the T_2-weighted image appears normal. (Baird and Warach, 1998)

In humans, ADC values tend to remain unchanged until CBF drops below 20 mL/100g/min. The most severely ischaemic tissue generally has the lowest ADC value, which the values increase outwardly as the CBF deficit reduces. Therefore, ADC can be used as a surrogate marker of tissue viability (Kraemer et al, 2005). There is a proportional relationship between ADC and the $CMRO_2$ in the severe ischaemic core, but variability in ADC values in penumbra undermines its utility in predicting the fate of this tissue (Guadagno et al, 2006). Despite this, ADC is a useful research tool – albeit a poor predictor of stroke outcome – and in concert with perfusion imaging, it can provide further information on tissue at risk.

1.3.3.4 Perfusion-weighted imaging (PWI)

MR imaging can be used to quantitatively assess the extent of tissue perfusion. Blood flow is measured *in vivo* by monitoring the signal changes that are induced by a tracer entering the tissue of interest. Commonly-used PWI techniques include monitoring the signal

changes following the introduction of a non-diffusible tracer such as gadolinium (known as dynamic susceptibility contrast (DSC)) or by using blood itself as an endogenous tracer (arterial spin labelling (ASL)). DSC bolus tracking is commonly used clinically, whereby patients are given an intravenous contrast agent. However, CBF values generated with this technique tend to overestimate the region of perfusion deficit when compared with PET techniques (Zaro-Weber et al, 2009).

Arterial Spin Labelling

ASL is a multislice modality that does not require the injection of a contrast agent to quantify cerebral blood flow. Instead, it is a noninvasive technique that uses electromagnetically labelled arterial water as an endogenous contrast agent. The effects of arterial tagging on distal images can be quantified in terms of tissue perfusion because the regional changes in signal intensity are determined.

A continuous ASL (CASL) sequence employs a special RF labelling scheme known as flow-driven adiabatic inversion. ASL acts by continuously magnetically inverting (or labelling) the spins at a specific location (tagging slice) – using an inversion pulse – before they enter the slice to be imaged. In short, spins entering the tissue with higher flow are labelled first, and spins entering at lower flows are labelled later (Figure 1.23).

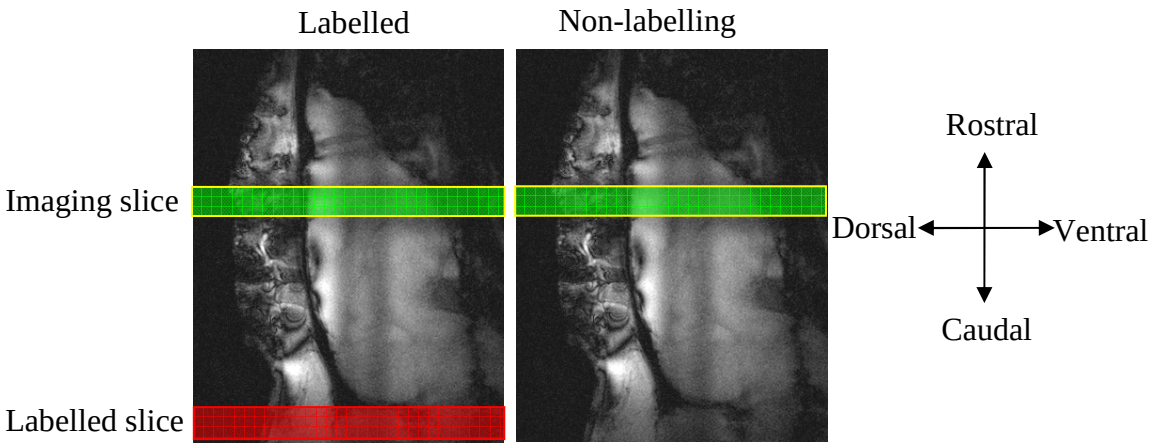

Figure 1.23. Concept of arterial spin labelling, shown on a sagittal scan of a rat brain

Quantitative perfusion maps can be calculated if other parameters (such as tissue T_1 and the efficiency of spin labelling) also are measured. In order to produce a CBF map, the T_1 signal intensity is plotted as a function of time for both the selective and non-selective slice images. The signal difference between the two images is due to the water that was inverted

during the total inversion from the non-selective pulse moving into the slice; which is in turn proportional to the amount of inflowing blood. Effects of cerebral perfusion are assessed by comparing images obtained with and without arterial spin labelling. The subtraction image (the labelled image subtracted from the non-labelled image) is dependent on the tagged blood that flowed into the imaging plane. The resulting CBF map is calculated from the difference between the two images and a mathematical equation (Figure 1.24).

$$CBF = \frac{\lambda}{T_1} \frac{(S_0 - S_1)}{2\alpha S_0}$$

Figure 1.24. Formula for continuous labelling, where; λ is the blood/tissue partition function (assumed to be 0.9), T_1 is the tissue longitudinal relaxation time which introduces the time component, S_0 and S_1 are the image signals with inversion pulses applied to non-labelled and labelled, respectively, and α is the efficiency of the inversion pulses. CBF is measured in millilitres per 100g of tissue per minute.

The difference in signal between the labelled and unlabelled images is proportional to the inflow of blood (CBF) to the selected brain slice (Calamante, Gadian and Connelly, 2002). This is a relatively new technique which has not yet been tested on many clinical scanners, and therefore, its predictive value in stroke patients has not yet been validated. In rodent models, the utility of PWI as a predictor of outcome is less ambiguous, possibly due to the homogeneity of rodent stroke models compared to patients. Shen and colleagues (2004) used the absolute CBF values of <30 mL/100g/min as critically damaged tissue expected to evolve to infarct. This was supported by Meng and colleagues (2004), who set the abnormal perfusion threshold at 30±9 mL/100g/min, and described it as a 57±11% reduction in CBF, relative to mean contralateral hemisphere values.

1.3.3.5 Diffusion-perfusion mismatch

The introduction of diffusion-weighted and perfusion-weighted MRI into the clinical stroke domain in the 1990s transformed the field of acute stroke neuroimaging. One of the most promising concepts that arose from early reports of combining diffusion and perfusion imaging was the notion that diffusion–perfusion mismatch could identify the operational ischaemic penumbra (Baird and Warach, 1998; Kidwell, Alger and Saver, 2004). In this model, the diffusion abnormality on the DWI represents irreversibly injured ischaemic

core tissue – indicative of reduced mobility of water protons with oedema, causing restricted diffusion (high signal on DW images), whilst the perfusion deficit – which maps rCBF and thus estimates the total region at risk of infarction – represents areas of abnormal perfusion (Figure 1.25).

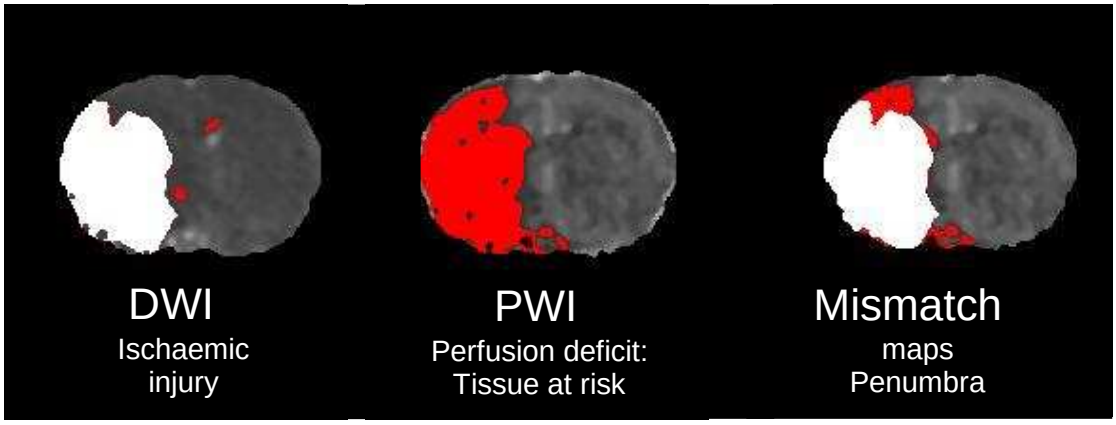

Figure 1.25. Coronal images of acute permanent MCAO in the rat 1 hour post-stroke. The thresholded PWI (57% reduction of mean contralateral CBF values) illustrates the perfusion deficit, whilst the thresholded DWI (16.5% reduction in mean contralateral ADC values) is an indication of ischaemic damage. The thresholded area on the DWI is subtracted from the region of hypoperfusion, the mismatch corresponding to the ischaemic penumbra

Typically, the hypoperfused area initially exceeds the area of reduced ADC generated from the DWI image – and this diffusion-perfusion mismatch (DWI/PWI mismatch) is taken as an approximation of the ischaemic penumbra (Schlaug et al, 1997). There is a dearth of research offering explanatory descriptions of DWI/PWI mismatch patterns in stroke patients who present at later timepoints after onset of symptoms, and also information as to whether the presence of mismatch in these patients also holds the potential for beneficial therapeutic interventions (Neumann-Haefelin et al, 1999). In experimental animal studies, mismatch can be used to ascertain the efficacy of neuroprotectants, and has been used in clinical trials to characterise therapeutic efficacy in groups of stroke patients with similar lesion size and location (Baird & Warach, 1998).

The use of DWI/PWI to select patients for thrombolysis up to 9 h after stroke-onset has been shown to improve clinical outcomes (Hacke, 2005), but there is no consensus as yet on the ADC and CBF viability thresholds that differentiate infarct, penumbra and healthy tissue (Warach, 2001). If the CBF threshold used to define the perfusion deficit is set too low, there will be an underestimation of penumbral tissue. Equally, if the threshold is not

low enough, the penumbra will be overestimated and may include benign oligaemic tissue. The ADC threshold is similarly crucial, as if the ADC threshold is too low, then the ischaemic core is underestimated and therefore the area of mismatch will be overestimated and *vice versa*. The existence of a DWI/PWI mismatch has been documented within 6 hours of onset in ~70% of individuals with MCA occlusion (Barber et al, 1999). The mismatch tends to resolve after 24-48 hours (Perez et al, 2006), indicative of the penumbra becoming incorporated into the ischaemic core or oligaemic tissue being reperfused.

The results of the diffusion and perfusion imaging evaluation for understanding stroke evolution (DEFUSE) study (Albers et al, 2006) support the validity of the mismatch hypothesis in patients treated with rT-PA therapy in the 3 to 6 h time window. This study showed that early reperfusion is associated with a more favourable clinical response in patients with the DWI/PWI mismatch profile, whereas patients without mismatch did not appear to benefit from reperfusion. There has been variation in the criteria used to determine the presence of mismatch (Parsons et al, 2002; Schellinger et al, 2000; Darby et al, 1999). In many studies, mismatch has been defined as PWI lesion volume of >120% of DWI lesion, but this threshold was chosen arbitrarily (Kakuda et al, 2008).

Recent MRI research using DWI/PWI mismatch to identify penumbral tissue in patients presenting 3-6 hours after stroke onset suggested that phase III trials beyond 3 h after treatment onset were warranted. It showed that reperfusion was more common with rT-PA than with a placebo and was associated with less infarct growth (Davis et al, 2008). In thrombolysis studies, patients with penumbral tissue identified by DWI/PWI mismatch experienced improved clinical outcomes up to 6 h after symptom onset, compared to the standard non-contrast CT–guided therapy (Köhrmann et al, 2006; Schellinger et al, 2007).

Schellinger and colleagues (2007) compared the safety and efficacy of MRI- and CT-based thrombolysis within and beyond the 3 hour time window. The criterion for CT-based thrombolysis was to exclude patients with evidence of intracerebral haemorrhage. CT scan exclusion criterion (according to European Cooperative Acute Stroke Study [ECASS]) were intracranial tumours except small meningioma, hemorrhage of any degree or location, significant mass effect with midline shift, and acute hypodense parenchymal lesion or effacement of cerebral sulci in more than one third of the MCA territory criteria. The latter criteria stemmed from a retrospective evaluation of CTs from the ECASS study (1995) which suggested that if ischaemic changes were present in greater than 33% of the MCA territory, the patients had an increased risk of ICH. Safety outcomes were predefined as

symptomatic intracranial haemorrhage and mortality, whilst primary efficacy outcome was a favourable outcome (modified Rankin Scale (mRS) 0 to 1) at the 3-6 hour time point. They found that the use of MRI significantly reduced symptomatic intracranial haemorrhage. Additionally, MRI significantly predicted a favourable outcome (Figure 1.26). It showed that 40% of patients had a mRS of 0-1 with MRI-based rT-PA administration within the 3-6 hour time point, and overall it appeared to be safer and more clinically efficacious compared to standard CT.

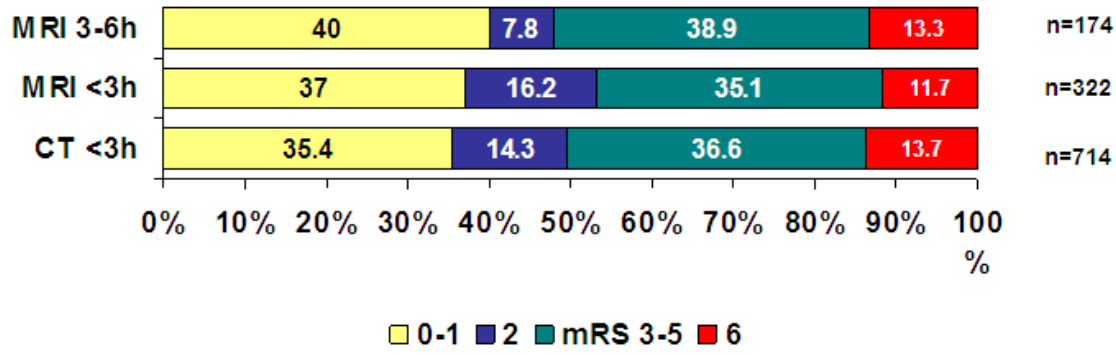

Figure 1.26. 3-month outcome according to the mRS. MRI-based rT-PA within 3h of stroke onset was more clinically efficacious than CT –based rT-PA and MRI-based rT-PA at the 3-6h time point

0. No symptoms at all
1. No significant disability despite symptoms; able to carry out all usual duties and activities
2. Slight disability; unable to carry out all previous activities, but able to look after own affairs without assistance
3. Moderate disability; requiring some help, but able to walk without assistance
4. Moderately severe disability; unable to walk without assistance and unable to attend to own bodily needs without assistance
5. Severe disability; bedridden, incontinent and requiring constant nursing care and attention
6. Dead (Schellinger et al, 2007)

1.3.3.6 Challenges to the mismatch model

When mismatch was used to select patients for thrombolysis, it identified patterns that may define treatment responsiveness (DEFUSE study, Albers, Thijs & Wechsler et al, 2006) and it has been used to select patients for an extended time window (Hacke, 2005). However, the technique has not been validated clinically and has a number of limitations.

No DWI or ADC threshold has been determined which can differentiate between irreversibly damaged and potentially recoverable tissue (Guadagno et al, 2004) and when DWI/ADC thresholds are applied, the lesions identified can be fully or partially reversed by reperfusion in animal models and man (Kidwell et al, 2000) (Figure 1.27). This suggests that penumbral tissue may be within the ADC lesion (Figure 1.28).

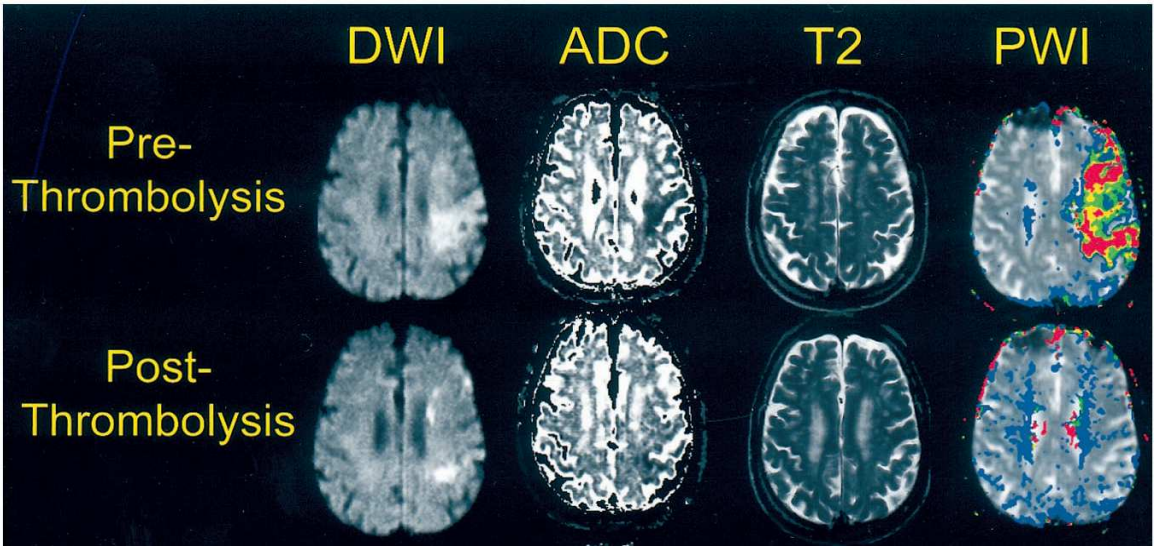

Figure 1.27. Evidence of reversible DWI-defined lesion in a human stroke patient following thrombolysis. Note the reduction in the DWI-defined lesion post-thrombolysis (Kidwell et al, 2000)

Interestingly, after reversal of the DWI lesion in humans following thrombolysis, secondary injuries may result in the return of the DWI lesion (Kidwell et al, 2000). As a consequence, thrombolysis may also benefit patients with no evidence of mismatch. Also, defining a threshold for the perfusion deficit is equally difficult and may include benign oligaemic tissue which is not at risk (Butcher et al, 2005; Takasawa et al, 2008).

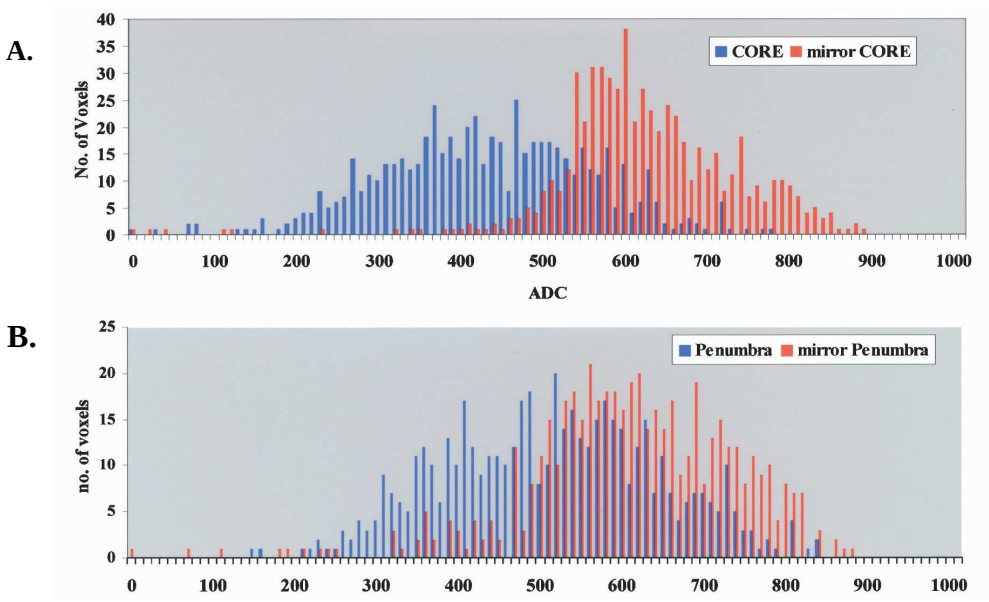

Figure 1.28. Histograms of ADC voxel values within core (**A**) and penumbra (**B**) regions of interest (ROIs) and their mirror ROIs. There is an overlap of low ADC values between core and penumbra voxel populations, but also the reduced ADC in both core and penumbra relative to mirror ROIs (Guadagno et al, 2004)

In animal stroke models, the amount of mismatch tissue has been shown to be very variable, and dependent upon the thresholds applied to ADC and CBF. Mismatch evolution varies between animal strains (Bardutzky et al, 2005) and the techniques applied to induce stroke (Henninger et al, 2006). These are crucial factors, as embolic MCAO models show the presence of penumbra for a long period of time compared to the intraluminal filament model (Zhang et al, 2001; Wang et al, 2001), suggesting that therapeutic time windows may be subjective.

Selection of patients for thrombolysis using DWI/PWI has been attempted (DEFUSE and the Echoplanar Imaging Thrombolytic Evaluation Trial (EPITHET)) in phase II trials which suggested that patients with large mismatch may have improved clinical outcomes following thrombolysis, although the DIAS-2 study indicated otherwise (Donnan et al, 2009; Albers et al, 2006; Hacke et al, 2009; Davis et al, 2008). DIAS-2 defined the PWI deficit volume as >20% of the DWI lesion volume, whereas the DEFUSE and EPITHET volumetric measurements of mismatch were generated at a later time point. This highlighted the problem of quantifying CBF and mismatch, as there is no consensus over the thresholds to define the terms. Thresholds often tend to be in-house measurements, and the introduction of standardised parameters may simplify findings between groups and studies.

The penumbra *per se* is defined not only as a region of perfusion deficit but also of some remaining metabolic activity. The absence of a marker of tissue metabolism for penumbral definition in current MRI paradigms renders comparability with standard PET findings difficult and leaves interpretation susceptible to the varied approaches used to define the perfusion deficit. As such, technological advancements are in place which introduce a measurement of metabolic activity to mismatch estimation, including MRI assessments of $CMRO_2$ (Xu et al, 2009) and MR-PET technology (Beyer and Pichler, 2009).

Technique	**Infarct**	**Penumbra**	**Advantage**	**Disadvantage**
PET	Reduced CBF	Reduced CBF but preserved $CMRO_2$ and raised OEF	Combines information on perfusion and metabolism, quantitative, physiologically accurate	Technically challenging, expensive, limited availability, radiation, arterial catheterization
SPECT	>70% reduction of tracer signal	40–70% reduction of tracer signal	Complementary to CT and MRI, inexpensive	No information about metabolism, semi-quantitative, low resolution, radiation
Computed Tomography perfusion	Reduced CBV (<2 mL/100g)	Reduced CBV & CBF, increased MTT	Fast, inexpensive, widely available, practical	Variable software, radiation, contrast agent, limited spatial coverage
DWI/PWI mismatch	DWI lesion volume	PWI- volume minus DWI-lesion volume	No radiation, excellent resolution, early ischaemic changes, practical	No agreed mismatch definition, contrast agent, no information on metabolism
Clinical DWI/PWI mismatch	DWI lesion volume	NIHSS $\geqslant$ 8 DWI lesion $\leqslant$ 25 mL	No radiation, no perfusion scan, clinical information included	MR contraindications
Clinical-CT mismatch	CT lesion volume	ASPECTS > expected based on NIHSS	No perfusion scan, clinical information included, CT availability	Radiation, low sensitivity for early ischaemic changes

Table 1.3. Imaging modalities, the criteria used to identify ischaemic penumbra, and the advantages and disadvantages of each method
ASPECTS = Alberta Stroke Program Early CT Score, CBF = cerebral blood flow, CBV = cerebral blood volume, $CMRO_2$ = cerebral metabolism of oxygen, DWI = diffusion-weighted imaging, MR = magnetic resonance, MTT = mean transit time, NIHSS = National Institute of Health Stroke Scale, OEF = cerebral oxygen extraction fraction, PET = positron emission tomography, SPECT = single photon emission computed tomography. Adapted from Ebinger et al (2009)

1.3.3.7 Functional MRI (fMRI)

The fact that haemodynamics are intricately linked to neural activity has been known for over a century (Roy and Sherrington, 1890). This phenomenon has led to the development of functional MRI (fMRI) in which the activation of neural cells triggers an increase in local blood flow and oxygenation and can produce a small signal increase due to the magnetic properties of deoxyhaemoglobin – a by-product of oxidative metabolism.

fMRI measures the haemodynamic response related to neural activity in the brain. The activity of neural cells in response to an external stimulus (e.g., visual or sensorimotor) results in an increased oxygen consumption. The brain region activated by an external stimulus locally consumes more oxygen which induces an increase in capillary blood flow and blood volume by local vasodilatation in order to meet this increased oxygen demand. This oxygen utilised by the neural cells is carried in the bloodstream by haemoglobin. Also, it is assumed that excess oxygen is supplied to the activated area because the increased blood flow exceeds the metabolic needs after some time. In response to functional activation, there is an increase in local CBF within 1-5 seconds. The increase in blood flow peaks after ~4-5 seconds before returning to basal levels. As a result, the concentrations of oxyhaemoglobin and deoxyhaemoglobin change from the normal range.

Oxyhaemoglobin and deoxyhaemoglobin in the blood have differing magnetic properties which can be utilised as an endogenous contrast to identify the changes in local blood oxygenation following neural activation. Specifically, as CBF increases with neural activation, the paramagnetic deoxyhaemoglobin levels are reduced which then causes an increased signal intensity in T_2^*-weighted MRI images (Niemi et al, 1996).

1.3.3.8 The Blood Oxygen-Level Dependent (BOLD) effect

The T_2^* relaxation rate of blood depends on whether or not the haemoglobin is bound with oxygen. Haemoglobin not combined with oxygen (deoxyhaemoglobin) is paramagnetic because of unpaired electrons which shorten the T_2^* of surrounding water. In contrast, oxyhaemoglobin is slightly diamagnetic because all electrons are paired and thus it has a negligible effect on the relaxation times of surrounding water. The higher proportion of haemoglobin molecules bound with oxygen (oxyhaemoglobin) prolongs the T_2^* time of the surrounding water, which is indicative of a signal increase on T_2^* weighted images. By exposing rodents to varying concentrations of inspired oxygen, Ogawa and colleagues

(1993) were the first to demonstrate this blood oxygen level dependent (BOLD) MRI response. They showed that during cerebral hypoxia, the deoxyhaemoglobin levels were high, which caused a darkening of contrast in the veins which was much more pronounced when compared to hyperoxic changes. As a result, BOLD imaging may permit identification of tissue compartments within the ischaemic brain following stroke, such as penumbra and ischaemic core.

T_2 and T_2^* signal changes have been reported in animal stroke models (Kavec et al, 2001; Roussel et al, 1995) in response to reductions in CBF. The T_2 reductions have been thought to be due to the increased levels of deoxyhaemoglobin and increased oxygen extraction fraction in the penumbra (Geisler et al, 2006). These changes were evident in the ADC lesion, in the periphery of the lesion, and in the surviving tissue, although the discrepancies in signal change in these regions of interest were not significant enough to provide adequate demarcation between ischaemic core and penumbral tissue.

Additional information on metabolic state may improve penumbral definition. BOLD MRI offers information on oxygen consumption and delivery (Baird & Warach, 1999; Kavec et al, 2001), but static T_2^*-weighted MRI under normoxic conditions has not adequately delineated penumbra in ischaemic stroke patients (Tamura et al, 2002; Grohn & Kauppinen, 2001), possibly because deoxyhaemoglobin is not rapidly cleared in ischaemic conditions (Giesler et al, 2006). A new method using sequential T_2^*-weighted images with transient hyperoxia may dynamically alter the oxyhemoglobin: deoxyhaemoglobin balance with the aim of distinguishing tissue compartments which have different metabolic activity and therefore different relative concentrations of deoxyhaemoglobin. By providing the additional measure of the rate of contribution of deoxyhemoglobin to the measured pool, this may remove the potential confound observed by Geisler and colleagues.

Higher BOLD signal intensities arise from increases in the concentration of oxygenated haemoglobin since the blood magnetic susceptibility now more closely matches the tissue magnetic susceptibility. The BOLD contrast changes can be either positive or negative depending upon the relative changes in both CBF and $CMRO_2$. Increases in CBF that outstrip changes in oxygen consumption will lead to increased BOLD signal, conversely decreases in CBF that outstrip changes in oxygen consumption will cause decreased BOLD signal intensity.

1.3.3.9 The T_2^*- weighted Oxygen Challenge

A new MRI technique in which oxygen is employed as a metabolic biotracer to detect tissue metabolism may enable a more precise definition of the penumbra. The technique uses the BOLD premise that is based on the different magnetic properties of deoxyhaemoglobin and oxyhaemoglobin in blood. Oxygen is carried in the blood in two forms: when breathing air (~21% oxygen) most O_2 combines with haemoglobin to generate oxyhaemoglobin but a very small amount dissolves in the plasma (paramagnetic free oxygen). By breathing normobaric hyperoxia (100% oxygen, oxygen challenge, OC), additional oxygen will dissolve in the plasma at a rate of 0.003 ml O_2/100ml of blood /mmHg pO_2) (Law and Bukwirwa, 1999).

By detecting changes in deoxy: oxyhaemoglobin ratio during OC, T_2^* signal change may provide an index of tissue oxidative metabolism and hence viability in ischaemic brain. In metabolising tissue, oxyhaemoglobin gives up its oxygen to the tissue to become deoxyhaemoglobin. The more paramagnetic deoxyhaemoglobin present in blood, the lower the T_2^* signal from the tissue. Following stroke, penumbral oxidative metabolism ($CMRO_2$) is maintained in the face of reduced cerebral perfusion pressure by increasing oxygen extraction fraction (OEF). During OC, additional O_2 converts deoxy- to oxyhaemoglobin, thereby increasing T_2^* signal. An increase in OEF in penumbra results in increased conversion of deoxy- to oxyhaemoglobin in penumbra, thus resulting in an amplified T_2^* signal change. This increase in signal should reflect the amount of oxygen being taken up by the tissue from the blood. At the end of the OC, free unbound O_2 is no longer present to maintain oxyhaemoglobin levels and so deoxyhaemoglobin levels will increase as blood flows through the tissue, and the T_2^* signal will return to the pre-OC baseline. Therefore, the increase in T_2^* signal, its maintenance during the OC and its return back to baseline when the OC is complete, should indicate metabolism within the tissue.

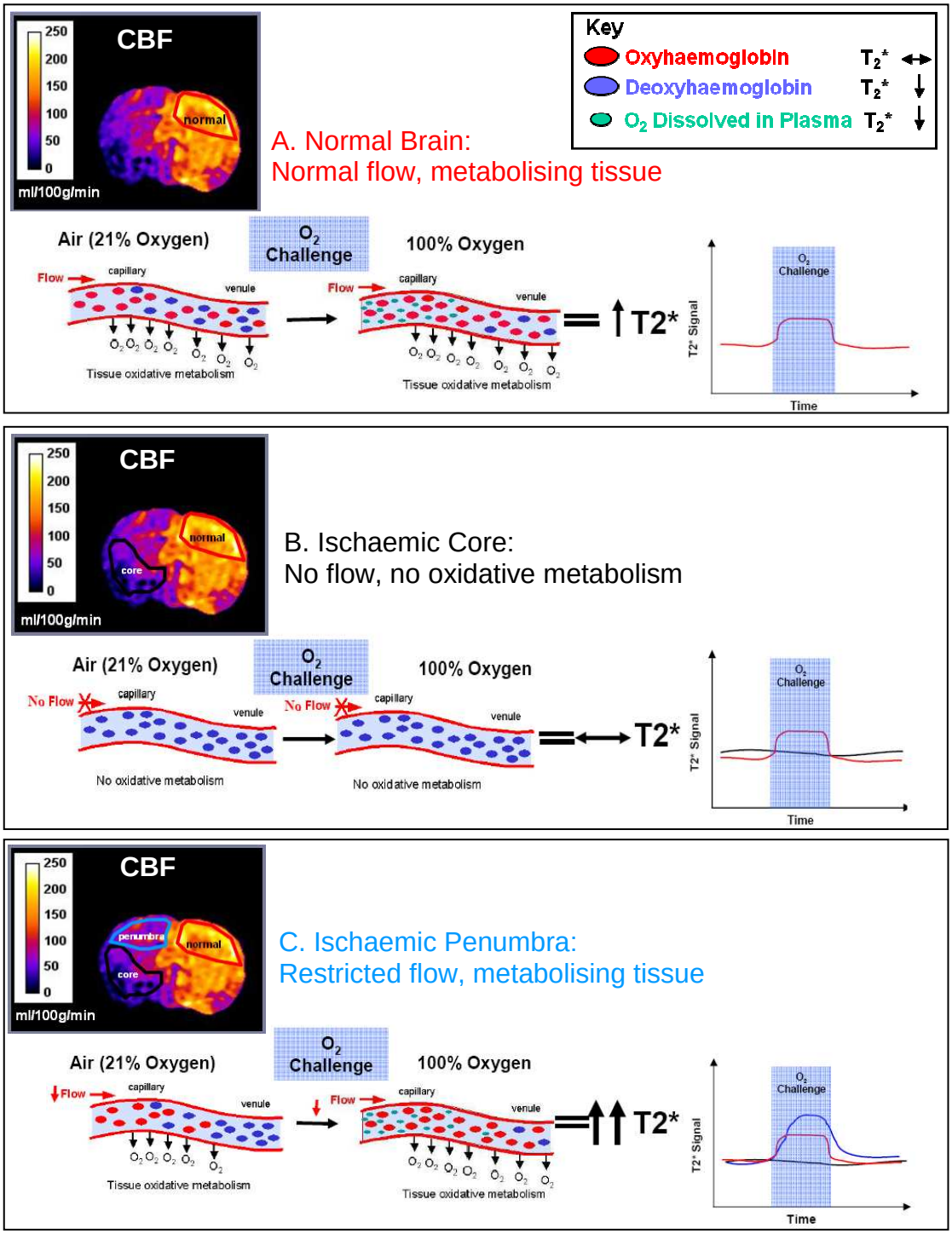

Figure 1.29. The Oxygen Challenge Paradigm

1. O_2 taken up by normal tissue for oxidative metabolism results in oxyhaemoglobin converting to deoxyhaemoglobin and thus lowering the T_2^* value for the tissue. With normobaric hyperoxia (oxygen challenge, OC), extra oxygen dissolved in plasma reduces deoxyhaemoglobin levels, increasing the T_2^* value for the tissue.

2. With permanent MCAO, where flow is not restored to the ischaemic core, haemoglobin has given up its oxygen to the tissue. Switching ventilation to 100% oxygen will have minimal effects on T_2^* as this tissue is not perfused.

3. In tissue with an increased oxygen extraction fraction, such as the penumbra, blood flow is restricted but the tissue is still metabolically active, resulting in higher levels of

deoxyhaemoglobin within the blood and a lower T_2^* signal from the tissue. Switching ventilation to 100% oxygen will convert this deoxyhaemoglobin back to oxyhaemoglobin, resulting in a greater increase in T_2^* than in normal metabolising tissue. (Santosh et al, 2008)

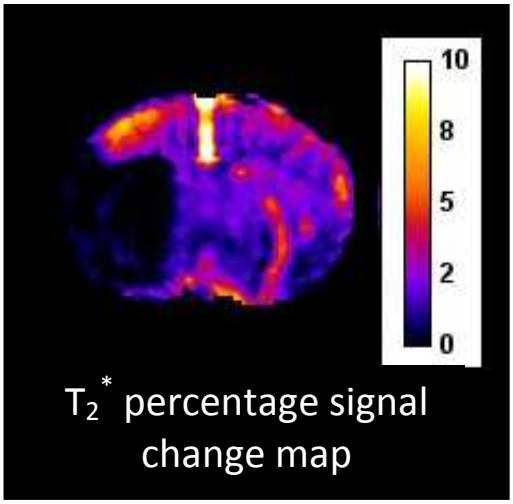

Figure 1.30 T_2^* percentage signal change map 1 hour following permanent MCAO. Penumbral tissue displays the greatest T_2^* percentage signal change, which is reflective of an increased oxygen extraction fraction. The ischaemically damaged tissue displays a negligible signal change, whereas the contralateral hemisphere exhibits normal metabolism. High signal change is evident in the large veins of the contralateral hemisphere and the venous sinuses seen in the midline, where more deoxyhaemoglobin is available for conversion

T_2^* maps can be generated that locate and quantify the percentage change in T_2^* signal to oxygen challenge throughout the territory of the occluded artery. In addition, the maintenance of this increased signal during the oxygen challenge and its return back to baseline following OC is consistent with T_2^* signal change indicating oxygen consumption. Therefore, detecting deoxyhaemoglobin *in vivo* would indicate oxygen utilisation and therefore metabolism. This technique may therefore yield information on oxygen metabolism that more closely correlates with PET definitions of the penumbra

If confirmed, this new non-invasive MRI technique should be able to discriminate between metabolically active and inactive tissues in the ischaemic brain, and enable serial imaging of penumbra, thereby providing an improved means of defining the ischaemic penumbra.

1.4 Aims of the thesis

1. Validation of the oxygen challenge T_2^* technique by confirming tissue identified as penumbra is viable using [^{14}C] 2-deoxyglucose autoradiography to provide information on glucose metabolism in a rat model of permanent focal ischaemia

2. Technique validation by confirming tissue identified as penumbra recovers with prompt restoration of blood flow

3. Characterising the technique by serial scanning and comparison with alternative MRI techniques for penumbral identification (diffusion-perfusion mismatch)

Chapter

2

Materials and Methods

2.1 Rodents

All experiments were performed using male Sprague-Dawley rats (Harlan, Bicester UK), under license from the UK Home Office (Project License number: 60/3759) and were subject to the Animals (Scientific Procedures) Act, 1986. Water and food were available *ad libitum* to all rats, housed in a temperature (21 ± 2°C), humidity (55 ± 15%), and light (12/12 hour light/dark cycle) controlled environment.

2.2 Surgery

Aseptic conditions were maintained throughout all surgical procedures. In the procedures that required recovery, animals were administered two 1 mL subcutaneous injections of sterile saline post-surgery to prevent dehydration and were given wet baby food to encourage eating.

2.2.1 General anaesthesia

Animals were initially anaesthetised with 5% inhaled isofluorane delivered in oxygen–nitrous oxide (30:70) in an induction chamber at room temperature. In the experiments that required recovery, animals were intubated with a 16 gauge (1.3mm inner, 1.8mm outer diameter, and 45 mm in length) sterile plastic Anicath i.v. cannula (Millpledge Veterinary, Nottingham, UK) and artificially ventilated. Upon intubation, gases were changed to air to limit the effect of oxygen on the baseline physiology during T_2^* scans. Animals were given a subcutaneous 0.4 mL dose of atropine sulphate (Martindale Pharmaceuticals, UK) post-intubation to prevent a build up of mucous secretions in the trachea. During surgery, isoflurane was maintained at ~2% anaesthetic dose, and animals were artificially ventilated with a 7025 rodent ventilator (Ugo Basile, Italy) with a respiratory rate of 60 breaths per min and a tidal volume of 3-4 mL.

For experiments that did not require recovery, animals underwent a surgical tracheotomy. Following initial anaesthetic in the induction chamber, anaesthesia was maintained with a face mask whilst a ventral incision was performed in the neck to expose the muscle surrounding the trachea. Blunt dissection of the muscle was performed to expose the trachea. Loose ties were placed around the trachea, an incision made, and a tracheal tube (13 gauge (2.5 mm) x 150 mm, Solomon Scientific, USA) was quickly inserted into the trachea and tied in place and connected to the ventilator. Artificial ventilation was maintained at a rate of 50 breaths per min with a respiratory volume of 3-4 mL.

2.2.2 Cannulation of blood vessels

Femoral artery cannulation was performed to monitor blood gases and mean arterial blood pressure (MABP). The femoral artery was exposed by blunt dissection and isolated with 4.0 silk threads (United States Surgical, USA). The artery was cannulated with 1% heparinised (1000 units/mL, Wockhardt UK Ltd, UK) saline-filled polythene catheters (Portex: external diameter 0.96 mm; internal diameter 0.58 mm; 70 cm long). Femoral vein cannulation was performed for the study that required radioisotope administration (Chapter 4).

2.2.3 Intraluminal filament model of middle cerebral artery occlusion

MCA occlusion

Permanent middle cerebral artery occlusion (pMCAO) was induced using the intraluminal filament method (Figure 2.1), first described by Koizumi and colleagues in 1986. A ventral midline incision was made in the neck, to the left of the trachea. Blunt dissection exposed the underlying muscle that covers the carotid artery. The common carotid artery was exposed by retraction of the triumvirate of the multidirectional pretrachial strap musculature, the sternomastoid muscle and the mandibular gland. Just below the internal and external bifurcation, the common carotid was ligated using a 4-0 nylon suture. The external carotid artery (ECA) was then tied above the occipital branch, and the ascending pharyngeal and superior thyroid arteries were isolated and permanently occluded using diathermy forceps. Following this, the ECA was occluded by diathermy distal to the tie, and cut to enable introduction of the intraluminal filament for stroke inducement. The internal carotid artery (ICA) was also loosely tied above the occipital artery, which was also diathermied, and the pterygopalatine artery was isolated and tied around its bifurcation

from the internal carotid, preventing the filament from entering the extracranial branch instead of reaching the origin of the MCA. A small incision was made into the remaining ECA stump, and a 3-0 nylon monofilament with a bulb (0.28-0.3 mm in diameter for 300-350 g rats) fashioned using a cauterising pen, was gently advanced through the incision in the ECA, through the ICA to the origin of the MCA for a distance of ~22 mm. When slight resistance was felt, this indicated that the origin of the MCA was reached, occluding the blood flow and inducing a stroke within the MCA territory.

To induce transient MCAO, the filament was left in position for a specific time period, and then reperfusion was performed by filament withdrawal, electrocoagulation of the incision site on the ECA stump, and loosening of the tie around the common carotid artery and pterygopalatine branch to restore blood flow to MCA territory. Restoration of cerebral blood flow on filament withdrawal was confirmed on MRI cerebral blood flow maps.

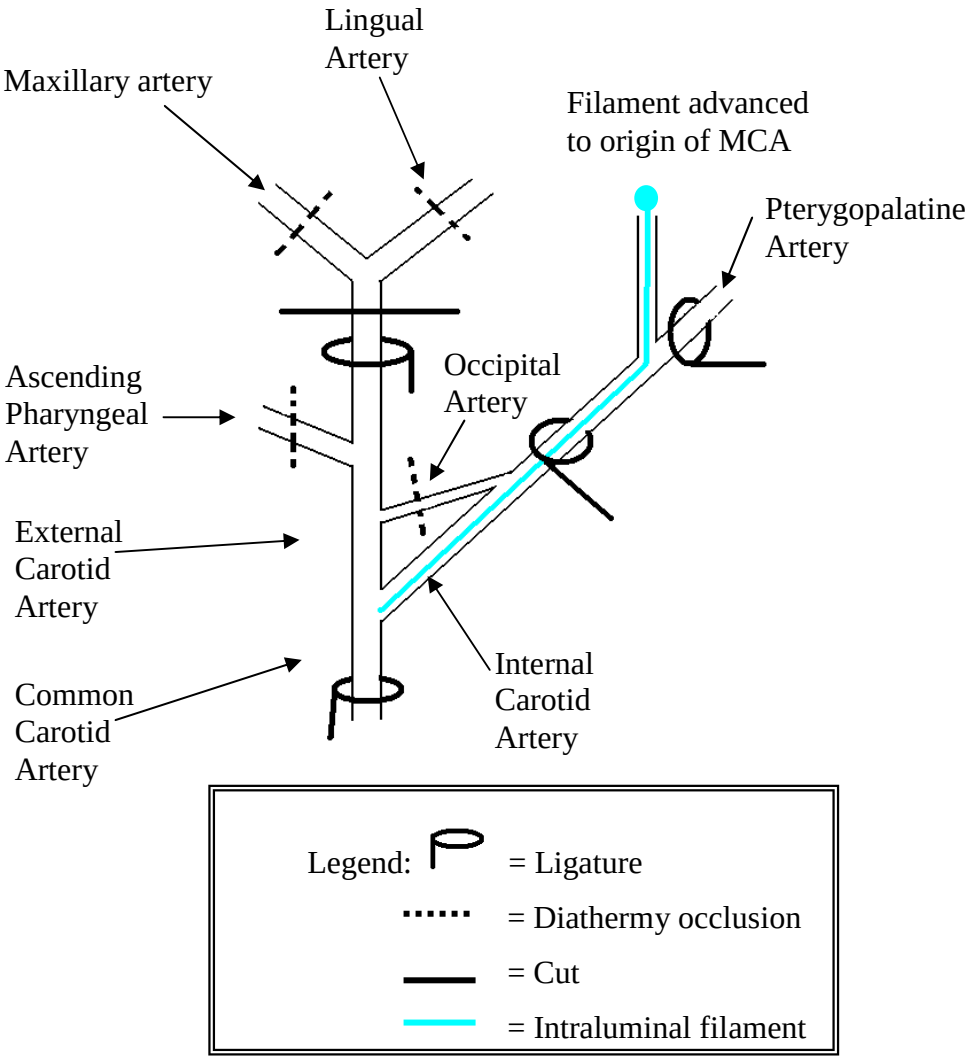

Figure 2.1. Diagram showing the intraluminal filament method for MCAO. The following arteries were ligated in this order with 4-0 surgical sutures (illustrated in figure by a black circle): the common carotid artery (at the internal and external bifurcation), the internal carotid artery and the pterygopalatine artery (at its bifurcation from the internal carotid)

2.2.4 Testing reperfusion

Laser Doppler Flowmetry (LDF) generally allows the surface monitoring of blood flow although flow probes can also be implanted into the brain. The principle of laser Doppler involves directing a monochromatic light source in the form of a laser beam at the region under investigation. The light is reflected from both moving red blood cells (RBC) and from static sources. Photons are scattered and undergo a frequency shift (known as the Doppler shift) according to the Doppler principle. Reflected light is then collected and directed to a photodetector. The electrical output of the photodetector is processed to yield a continuous recording proportional to the blood flow. However, the actual unit is one of velocity or flux and the results are usually quoted as a percentage change from baseline values (Dirnagl et al, 1989).

To test the reperfusion technique, a laser Doppler experiment was performed on one animal, where LDF probes were placed on the fronto-parietal ipsilateral and contralateral cortices following stroke. Probe calibration was performed using a flux agent with a pre-determined microsphere size of 0.33 mm (Moor Instruments). The prone animal was immobilised in a stereotaxic frame. A midline head incision through the skin and fascia exposed the skull. Burr holes were drilled into the skull 5 mm lateral and 1 mm posterior to bregma. Care was taken to preserve a thin layer of bone to avoid injury to the cortex. Two DP5b stainless steel 0.8 mm diameter probes bent at a 90° angle (Moor Instruments) were attached to the arms of the stereotaxic frame, enabling accurate manipulation of the probes in the x,y and z planes. The face probes were placed perpendicular to the exposed parietal cortex (Figure 2.2).

The animal was subjected to MCAO for 60 mins, followed by 3 hours of reperfusion. The filament was gently advanced until LDF indicated adequate MCA occlusion by a sharp decrease in ipsilateral flow (Figure 2.3).

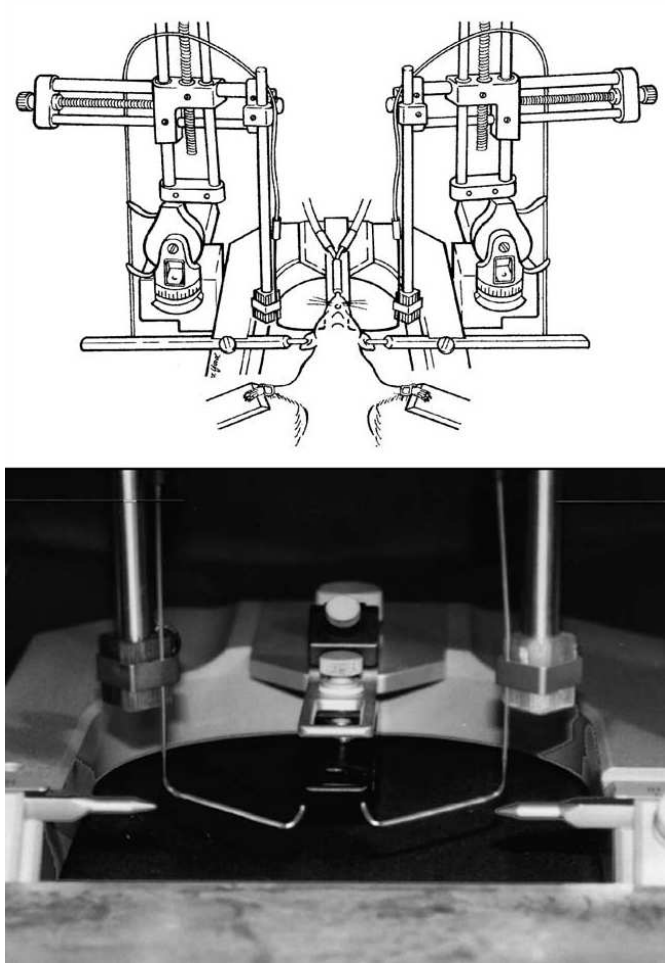

Figure 2.2. Experimental setup for cerebral blood flow measurements using laser Doppler Flowmetry (Image from Hungerhuber (2006)

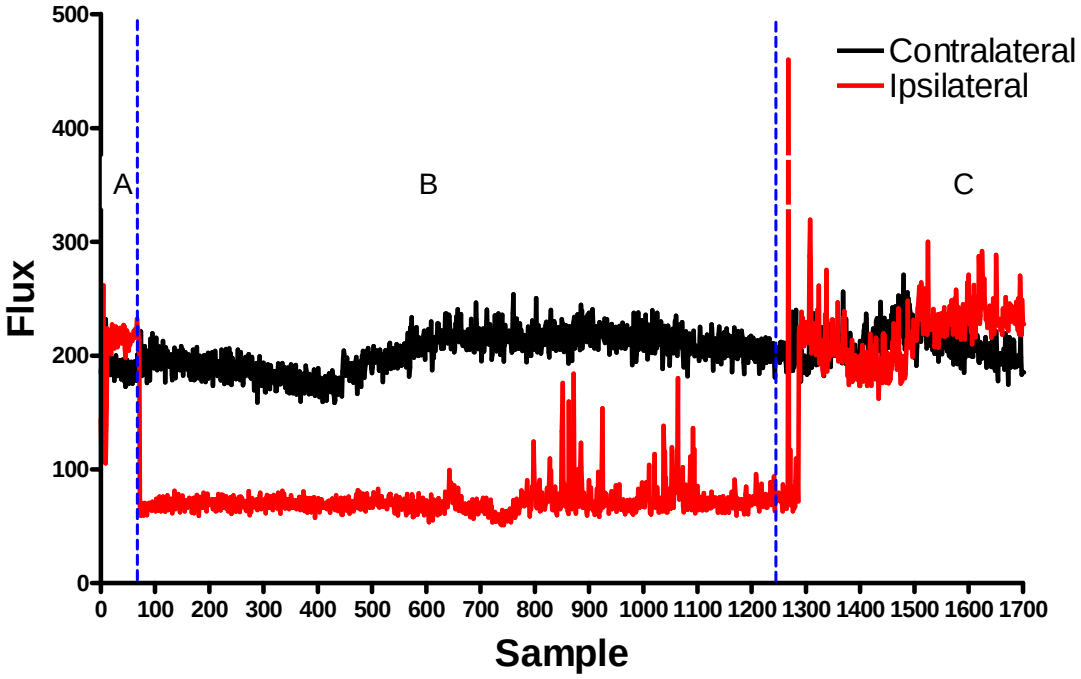

Figure 2.3. LDF measurements in the fronto-parietal ipsilateral and contralateral cortices **A**. Before filament insertion, **B**. Following filament insertion, and **C**. Following reperfusion. The blue dashed lines represent the point when filament was inserted and withdrawn, respectively

2.2.5 Physiological monitoring

Following stroke, the animal was immediately transferred to the imaging cradle, and instrumented for monitoring of physiological variables such as MABP, heart rate, body temperature and blood gases. Ventilation parameters were adjusted and imaging delayed until the animal was physiologically stable and blood gases were within a defined range [Mean arterial BP 80-100 mmHg, $PaCO_2$ 35-45 mmHg and PaO_2 80-100 mmHg, body temperature 37^oC]. Mean arterial blood pressure was monitored with MP150 Biopac and AcqKnowledge software (Linton). A rectal thermocouple (Physitemp Thermalert TH-5) provided continual monitoring of core body temperature which was controlled (37^oC) with a heated lamp during surgery and with a heated water jacket during imaging.

2.3 Brain tissue processing

2.3.1 Perfusion fixation

For assessment of ischaemic brain damage on Haematoxylin and Eosin (H&E) stained sections, the animals were killed by perfusion fixation with 4% paraformaldehyde in phosphate buffered saline (PAM). Rats were deeply anaethetised (5% isoflurane) and placed in the supine position. The chest was opened with scissors in order to expose the heart and a 16 gauge needle was inserted directly into the apex of the left ventricle and advanced into the ascending aorta for perfusion fixation. The needle position was secured with a clamp and heparinised saline was delivered at a pressure of ~100-150 mmHg. The right atrium was then cut with sharp scissors. When blood was cleared from body with heparinised saline (~200 ml), 4% paraformaldehyde solution (~200 ml) was perfused at the same pressure. Spontaneous movement on switching from saline to fixative and a lightened colour of the liver provided good indicators of effective perfusion fixation.

2.3.2 Tissue processing

Following perfusion fixation, animals were decapitated and the heads immersed in PAM for 24 hours. The brains were then removed from the skull, and post-fixed in PAM for a further 24 hours before being placed in a processor (Tissue-Tek VIP, Miles Scientific), which took them through cycles of alcohols to dehydrate the tissue and to allow clearance with xylene over a 59 hour period (Table 2.1). Brains were then submerged in liquid paraffin wax at 60^oC.

Station	Solution	Temperature	Time
1	70% Alcohol	35^{o}C	2 hours
2	80% Alcohol	35^{o}C	3 hours
3	96% Alcohol	35^{o}C	4 hours
4	Absolute Alcohol	35^{o}C	4 hours
5	Absolute Alcohol	35^{o}C	5 hours
6	Absolute Alcohol	35^{o}C	5 hours
7	Absolute Alcohol	35^{o}C	6 hours
8	Xylene/ Abs Al	35^{o}C	4 hours
9	Xylene 1	35^{o}C	5 hours
10	Xylene 2	35^{o}C	5 hours
11	Paraffin wax 1	60^{o}C	5 hours
12	Paraffin wax 2	60^{o}C	5 hours
13	Paraffin wax 3	60^{o}C	6 hours

Table 2.1. The tissue processing procedure

2.3.3 Tissue embedding and sectioning

The brains were then embedded in small containers containing liquid paraffin wax, left to cool, then removed and mounted onto wooden blocks. Coronal sections (6 µm) were cut using a microtome (Leica RM 2135), and mounted onto poly-L-lysine glass slides.

2.3.4 Haematoxylin and Eosin staining

Following removal of wax in 100% Histoclear for ~15 min (National Diagnostics) and rehydration through a series of graded alcohols (100%, 90% and 70%) and water, sections were placed in 100% haematoxylin (Surgipath, Peterborough) for 5 minutes and then washed in running water (Table 2.2). The sections were differentiated in acid alcohol and washed again. The sections were placed in Scots Tap Water Substitute for 2 minutes, washed again in running water and placed in eosin (Surgipath, Peterborough) for 3 minutes. The tissue was then dehydrated in absolute alcohol, cleared in Histoclear for 12 minutes and mounted using DPX mounting medium (Raymond A Lamb Laboratory Supplies, East Sussex).

Solution	Time
Histoclear 1	4-5 mins
Histoclear 2	4-5 mins
Histoclear 3	4-5 mins
Absolute Alcohol 1	3 mins
Absolute Alcohol 2	3 mins
90% Alcohol	3 mins
70% Alcohol	3 mins
Wash in running water	4 mins
Haematoxylin	4 mins
Wash in running water	1-2 mins
Differentiate in acid alcohol	A few dips
Wash well in running water	3 mins
Scott's Tap Water Substitute	2 mins
Wash in running water	2 mins
Dehydrate in 70% Alcohol	2 mins
Dehydrate in 90% Alcohol	2 mins
Stain in Alcoholic Eosin (95%)	4 mins
Dehydrate in Absolute Alcohol 1	4 mins
Dehydrate in Absolute Alcohol 2	4 mins
Dehydrate in Absolute Alcohol 3	4 mins
Clear in Histoclear 1	4 mins
Clear in Histoclear 2	4 mins
Clear in Histoclear 3	4 mins

Table 2.2. Chronological list of agents used for the staining procedure

2.3.5 Determination of ischaemic damage and quantification of infarct size

The haematoxylin and eosin stained sections were viewed under a light microscope at a range of magnifications (x5, x10, x20 and x40) to accurately determine the boundary of the infarct. Morphological characteristics of ischaemic neurons compared to non-ischaemic neurons, and pallor/vacuolisation of the neuropil were identified on stained sections to delineate areas of infarction. Ischaemic neurons were identified as pyknotic (shrunken and triangular in shape) with cellular incrustations most evident at x20 magnification. Pyknotic neurons also showed an eosinphilic cytoplasm and the surrounding neuropil was disrupted and displayed pallor. Identification of the boundaries between ischaemic core, border zone and normal tissue was achieved by studying the neuronal morphology combined with changes in the neuropil in the form of pallor of staining and microvacuolation. Regions of interest (ROIs) representing the ischaemic core (where the majority of cells and neuropil showed the irreversible features of ischaemic cell change, Figure 2.4B), border zone (mixed population of cells with abnormal and normal morphology, Figure 2.4C) and adjacent normal zone (normal cell morphology and neuropil, Figure 2.4A) are shown in Figure 2.4.

Areas of infarct were transcribed onto line diagrams of 8 pre-determined coronal levels (Figure 2.5) throughout the MCA territory, and quantified using image analysis (MCID, Imaging Research Inc., Canada) based on the original method by Osborne and co-workers (1987).

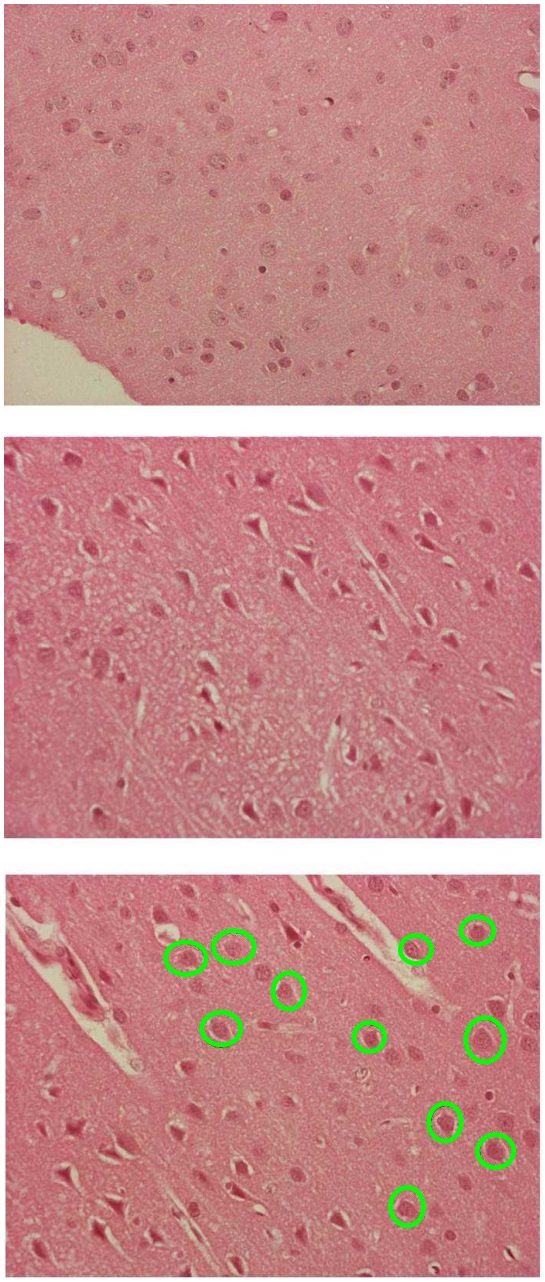

A. Normal zone (x40)

B. Ischaemic core (x40)

C. Border zone (x40)

Figure 2.4. Differentiation between the normal zone (**A**), ischaemic core (**B**) and border (**C**) zone. Histological photomicrographs of ROI in dorso-lateral cortex ipsilateral to permanent MCAO from a representative animal. Pictures from haematoxylin & eosin stained sections have been captured at x 40 magnification:

a) Normal Cortex. Neurons display normal morphology;

b) Ischaemic Core. Note darkly stained triangular neurons that have the features of the ischaemic cell process within microvacuolated, pale stained neuropil;

c) Border Zone. Scattered throughout the ischaemic cortex are normal neurons (circled) which display a normal morphology

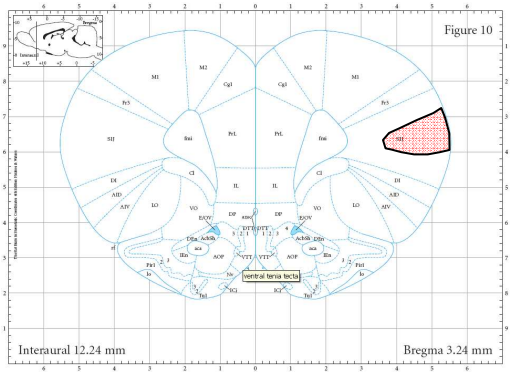

Level 1. Bregma = 3.24 mm

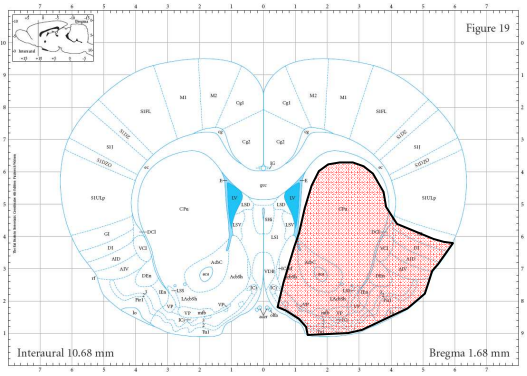

Level 2. Bregma = 1.68 mm

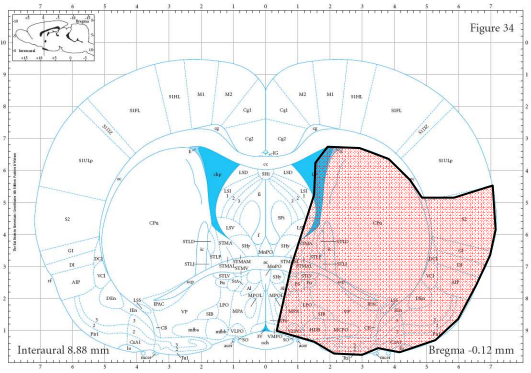

Level 3. Bregma = -0.12 mm

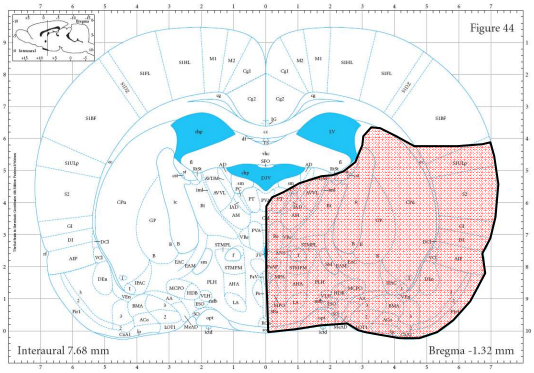

Level 4. Bregma = -1.32 mm

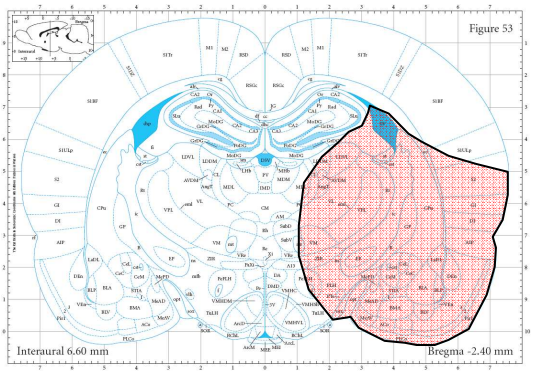

Level 5. Bregma = -2.40 mm

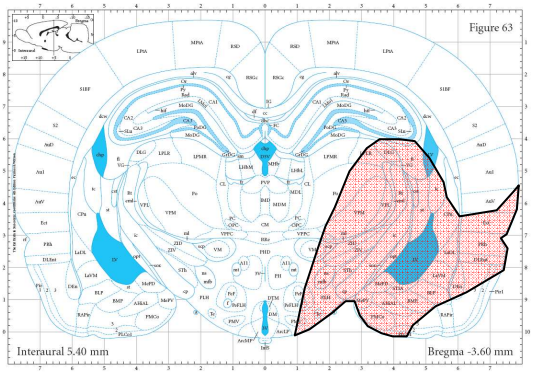

Level 6. Bregma = -3.60 mm

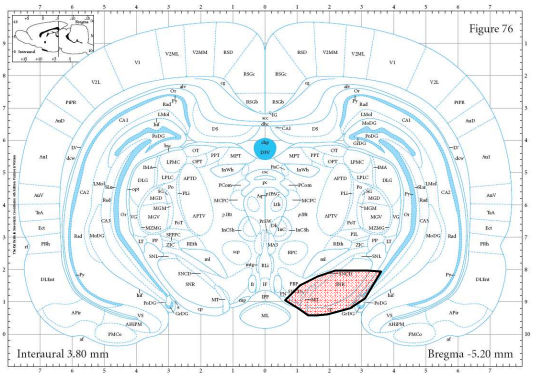

Level 7. Bregma = -5.20 mm

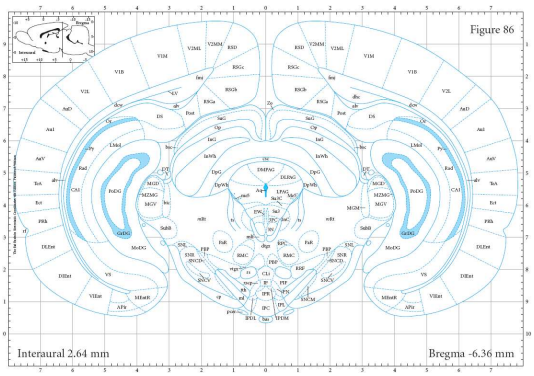

Level 8. Bregma = -6.36 mm

Figure 2.5. Line diagram comprising 8 pre-determined coronal levels with the distance from bregma of each level adjacent to it. Brain sections were collected at these levels and areas of infarct (in pink) were transcribed onto the diagram (Paxinos and Watson, 2007)

The areas of ischaemic damage were measured directly from the line diagrams for each coronal level. The volume of damage for each brain was calculated from the integration of these areas using the known distance between the stereotaxic coordinates of the coronal levels. The integration end points of 3.24 mm anterior and -6.36 mm posterior to bregma were used. Provided the origin of the MCA is occluded by the filament and the cardiovascular and respiratory status of the animal are controlled rigorously, then a reproducible lesion results. This type of occlusion would be classed as a proximal MCAO and since the lenticulostriate branches of the MCA lie distal to the occlusion site, and the model produces both subcortical and cortical ischaemic damage. Distal occlusions, which are uniquely produced with the electrocoagulation model of ischaemia, also produce reproducible lesions which are limited to the cortical regions, whilst a proximal occlusion blocks the lenticulostriate arteries and induce a subcortical lesion. Relatively minor differences in operative technique affect significantly the extent of ischaemic damage and the stroke outcome in the rat model. It is dependent upon good microsurgical technique, well-controlled anaesthesia and close physiological monitoring and control within physiological limits (Osborne et al, 1987).

2.3.6 2, 3, 5 Triphenyltetra-zolium chloride (TTC) staining

2,3,5-triphenyltetrazolium chloride (TTC) is a colourless, water-soluble salt which is oxidised to a lipid soluble bright red formazan by mitochondrial enzyme systems. In undamaged tissue, dehydrogenase reduces TTC to formazan which stains a deep red. The intensity of the stain reflects the functional activity of the mitochondria. In infarcted tissue, where the mitochondrial systems have been incapacitated, dehydrogenase activity is reduced or eliminated and so such areas remain unstained (Figure 2.6). TTC is effective in assessing infarct volume at 24 hours after stroke. It is not an accurate assessment of infarction at 4 hours post-stroke but was used when training in stroke surgery to give a quick assessment of the extent of ischaemic damage. The stroke was allowed to progress for 4 hours, allowing evolution of ischaemic damage. The animal was then anaesthetised with 5% isoflurane and decapitated for brain removal. The brain was placed in a rat brain matrix (World Precision Instruments, Hertfordshire, UK) and chilled with ice. Continuous bathing with ice-cold saline prevented the brain from sticking to the matrix. Razor blades were placed 2 mm apart to section the brain into coronal slices. The slices were then incubated in 2% TTC at 37^{o}C for 15 minutes. TTC staining after 4 hours of focal ischaemia displays deep red staining of normal brain tissue and white non-staining of ischaemically-injured tissue with a distinct border.

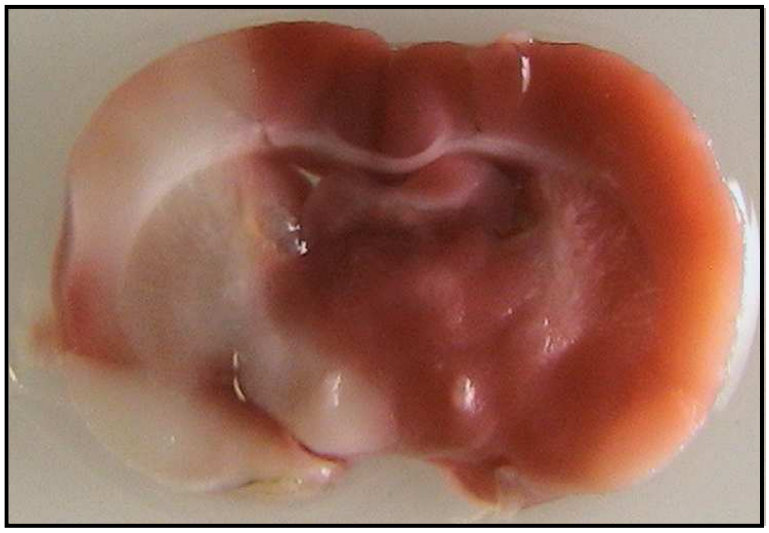

Figure 2.6. TTC stained coronal slice of tissue from an animal 4 hours after permanent MCAO. The white area represents ischaemic damage

TTC has been validated for use 24 hours after injury (Bedersen et al, 1986), but it cannot accurately delineate areas of infarcted tissue as early as 4 hours after permanent MCAO. However, after 36 hours of ischaemia, infiltration of macrophages and microglia, neovasculisation and astrocytic reactions occur (Hudgins and Garcia, 1970) which can obscure the margin of ischaemic damage. Also, although the extent of ischaemic damage can be assessed using this technique, there is no differentiation of grey and white matter structures, or the ability to study the consequences of ischaemia on individual cells.

Digital photographs of both sides of the slices were taken with a Canon Camcoder Mv750i. The photographs were analysed using ImageJ v1.39 (http://rsb.info.nih.gov/ij/). The entire contralateral hemisphere, and the stained area of the ipsilateral hemisphere, were manually traced and measured on two separate occasions and the mean calculated.

2.4 [^{14}C] 2-Deoxyglucose autoradiography

Quantification of local glucose utilisation in the brain can be achieved with the [^{14}C] 2-deoxyglucose autoradiography technique ([^{14}C] 2DG). 2DG is an analogue of glucose and it is unique in that it is metabolised through part of the pathway of glucose metabolism at a rate relative to glucose. Unlike glucose, however, its product, 2-deoxyglucose-phosphate, is trapped in the tissues as it is not a substrate for phosphoglucose isomerise. Therefore, this can provide a quantitative indication of glucose utilisation locally. The rate of glucose utilisation is proportional to the concentration of radioactivity ([^{14}C]) in the tissues and this can be visualised in cerebral structures with autoradiographical methods.

2.4.1 Theory

[^{14}C] 2DG autoradiography assumes that energy requirements of cerebral tissue are exclusively obtained by the aerobic catabolism of glucose (Sokoloff, 1977), and also that, within the CNS, functional activity is associated with local energy consumption. The technique is essentially measuring the rate of glucose phosphorylation within a region of cerebral tissue. As this is equivalent to the oxidative catabolism of glucose, it therefore corresponds to the generation of energy and its consumption.

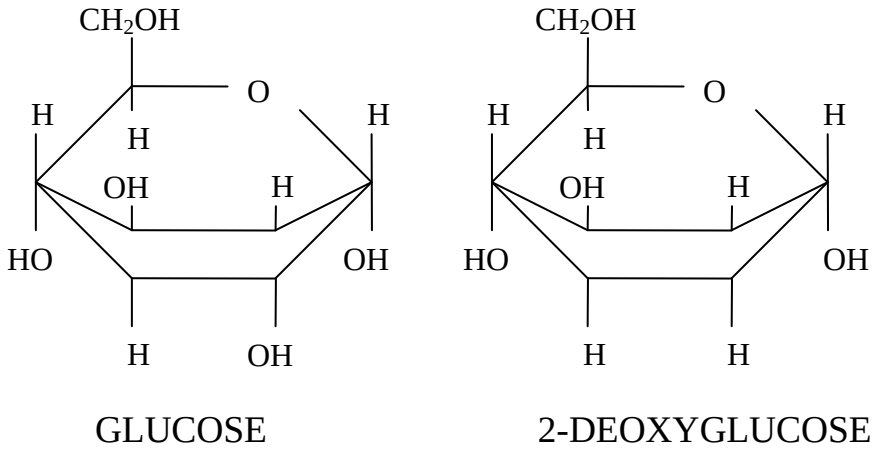

Figure 2.7. The structural differences between glucose and 2-deoxyglucose. 2-deoxyglucose and glucose are almost identical. The only difference is on the second carbon atom in which a hydroxyl group is replaced by a hydrogen atom

2DG and glucose can be transferred between the blood and the brain in both directions. Within the CNS, they become substrates for metabolism and are phosphorylated by hexose-6-phosphates. 2DG is phosphorylated by hexokinase to 2-deoxyglucose-6-phosphate (2-DG-6-P). Glucose-6-phosphate is metabolised further and thus does not accumulate in cerebral tissue, with the final products being CO_2 and water (Sokoloff, 1981).

2-DG-6-P differs from glucose-6-phosphate in that it is not a substrate for the next enzyme in the glycolytic cycle (isomerise), allowing the 2-DG-6-P to be trapped in the brain long enough to be measured (Figure 2.8). 2-DG-6-P can undergo glucose-6-phosphatase metabolism, although the low levels of glucose-6-phosphatase prevents it from interfering with the present experiment. Regions with more metabolic activity that require more glucose will accumulate more 2-DG-6-P (Sokoloff, 1981). ^{14}C is isotopically labelled with 2DG, enabling the radioactive substrate to be identified and quantified by autoradiographic measures.

An operational equation was derived by Sokoloff and colleagues (1977) which enabled quantification of the rate of glucose utilisation (Figure 2.9). For the duration of the experiment, it exploits the rate of glucose utilisation in relation to the arterial plasma concentration of glucose (Cp) and [^{14}C]-2-DG (Cp^*), and the total concentration of ^{14}C tracer within cerebral tissue at the end of the experiment (Ci^*).

The operational equation depends on the following assumptions:

1. A steady state for glucose – the arterial plasma concentration and the rate of glucose consumption remain constant throughout the experimental period;
2. Tissue is homogenous within which the concentrations of [^{14}C] 2-deoxyglucose and glucose are uniform and exchange directly with the plasma, and;
3. [^{14}C] deoxyglucose-6-phosphate and [^{14}C] 2-deoxyglucose are present in a tracer amount

(Sokoloff, 1977)

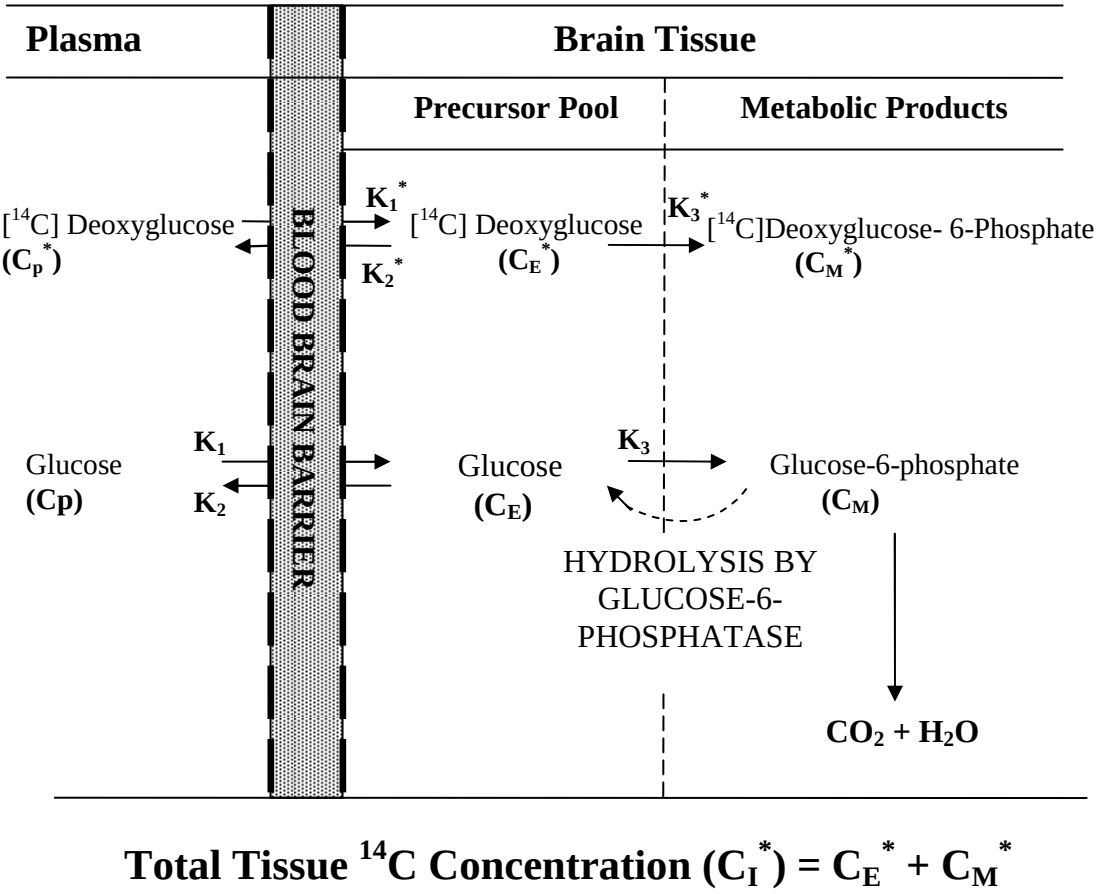

Figure 2.8. Diagrammatic representation of the theoretical model that forms the basis for the 2-deoxyglucose method

C_I represents the total ^{14}C concentration in a single homogenous tissue of the brain

C_P and C_P^* represent the concentration of glucose and [^{14}C]-2-deoxyglucose in the arterial plasma

C_E and C_E^*represent the concentrations of glucose and [^{14}C]-2-deoxyglucose in tissue pools serving as substrates for hexokinase

CM^* represents the tissue concentration of [^{14}C]-2-deoxyglucose

K_1^* is the rate constant for carrier-mediated transport of [^{14}C]-2-DG from plasma to tissue

K_2^* is the constant for carrier-mediated transport back from the tissue to plasma

K_3^* is the constant for phosphorylation by hexokinase

K_1, K_2, and K_3 are the equivalent constants for glucose

Adapted from Sokoloff et al (1977)

Three rate constants, K_1^*, K_2^* and K_3^* and the lumped constant (K) were predetermined by Sokoloff and colleagues (1977), and, as such, they are not measured in every experiment. The rate constants define the distribution of tracer between plasma and brain tissue compartments, and the lumped constant (k) corrects for the relative preference of the glucose transporters and enzyme systems for glucose as opposed to 2-deoxyglucose (Figure 2.8).

The rate of glucose consumption (Ri, Figure 2.9) is calculated in terms of the total [^{14}C] in the tissue at the end of the experimental period (Ci^*T) and the concentrations of [^{14}C] 2-deoxyglucose and glucose in the plasma (Cp^* and CP, respectively). The K_1^*, K_2^* and K_3^* rate constants are for the carrier-mediated transport of [^{14}C] 2-deoxyglucose from plasma to tissue and for phosphorylation by hexokinase. The lumped constant is composed of the ratio of the distribution space for deoxyglucose in the tissue relative to that of glucose, a factor which corrects for the fraction of glucose which, once phosphorylated, continues down the glycolytic pathway and the Michaelis-Menten kinetic constants of hexokinase for deoxyglucose and glucose (Sokoloff et al, 1977).

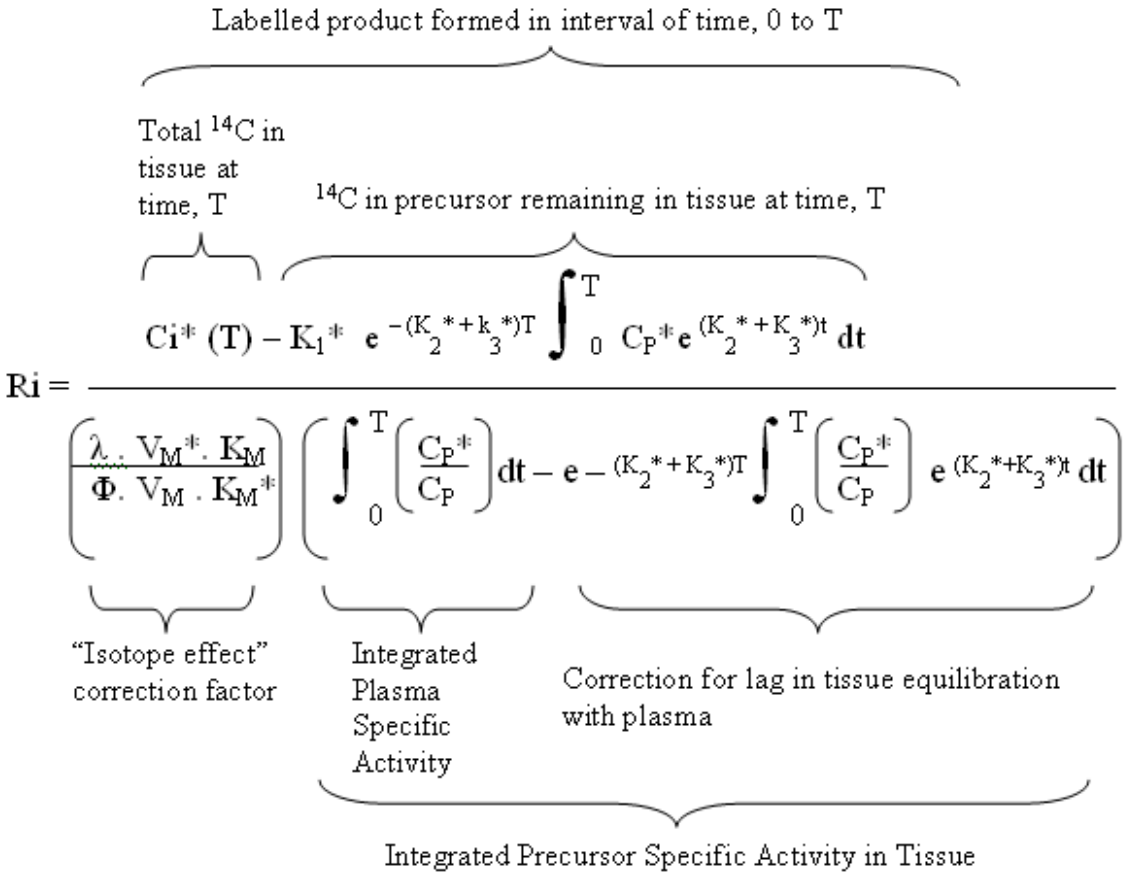

Figure 2.9. The operational equation of [^{14}C]-2-deoxyglucose method

Ri = the rate of glucose utilisation

T = duration of the experimental period

λ = ratio of distribution space of DG in the tissue to that of glucose

Φ = fraction of glucose-6-phosphate, once formed, continues down glycolytic and pentose phosphate shunt pathways (e.g., with zero G-6-Pase activity = 1)

Km^* and Vm^* are the Michaelis-Menten kinetics constants of hexokinase for DG

Km and Vm are the equivalent kinetic constants for glucose.

Adapted from Sokoloff (1978)

2.4.2 Animal preparation for [^{14}C] 2-deoxyglucose autoradiography

Male Sprague-Dawley rats were initially anaesthetised with 5% inhaled isofluorane delivered in oxygen–nitrous oxide (30:70) in an induction chamber at room temperature. The animals were artificially ventilated following a surgical tracheotomy, with air slightly enriched in oxygen (30%) to maintain physiological stability under anesthesia (~2% isofluorane). A rectal thermocouple provided continual monitoring of core body temperature which was controlled (37^{o}C) with a heated lamp. Polyethylene catheters (Portex: external diameter 0.96 mm; internal diameter 0.58 mm; 70 cm long) were placed in both femoral arteries, to continuously monitor blood pressure and conduct blood gas analysis, and a femoral vein for 2DG administration.

Physiological parameters were maintained within the normal range under anaesthesia apart from increased arterial partial pressure of oxygen (PaO_2) during the oxygen challenge. $PaCO_2$ was maintained between 35-45 mmHg in order to minimise cerebrovascular reactivity. Mean arterial blood pressure was maintained between 70-90 mmHg by manipulating the isoflurane level.

2.4.3 Experimental protocol for LCMRglc measurement

Immediately after the MRI scanning session, the animal was removed from the magnet for LCMRglc measurement. This was initiated by the intravenous (i.v) injection of [^{14}C] 2DG (125 µCi/kg in 0.6 mL heparinised saline (approximately 0.4 mL [^{14}C] 2DG and 0.2 mL heparinised saline), Perkin-Elmer, Waltham, MA, USA) at a steady rate over 30 seconds. Over the subsequent 45 minutes of the experiment, a series of 14 blood samples, approximately 50 µL per sample, were collected into heparinised centrifuge tubes at pre-determined time intervals (Table 2.3). In order to avoid hypovolaemia, each blood sample was replaced by a similar volume of saline. The collection of samples was timed in such a way as to ensure full characterisation of the peak in plasma [^{14}C] 2DG concentration during the first 5 mins of the experiment and the full arterial profile of plasma [^{14}C] 2DG over the course of the whole experimental period (Figure 2.10).

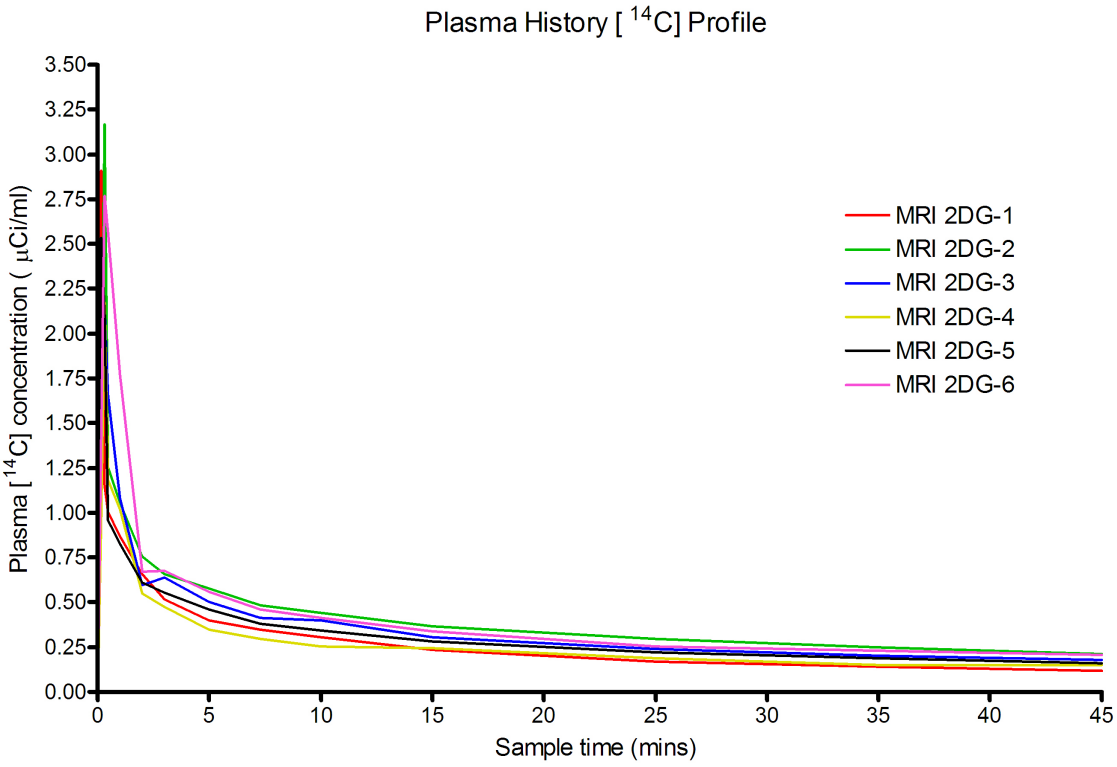

Figure 2.10. Complete plasma history profile determined in quantitative 2-deoxyglucose autoradiography from infusion of isotope to the terminal plasma sample at 45 min. Data from 6 representative animals

A 45 minute time course limited the influence of exponential factors in the operational equation, as well as making sure that there was minimal loss of [^{14}C]-DG-6-phosphate from the tissues resulting from glucose-6-phosphatase activity (Sokoloff et al, 1977). Samples were immediately centrifuged and aliquots of plasma removed for the determination of plasma glucose (Cp) and ^{14}C concentrations (Cp^*) by glucose oxidase assay (Beckman glucose analyser) and liquid scintillation analysis, respectively. At 45 minutes, animals were rapidly killed by i.v injection of sodium pentobarbitone and the brains rapidly dissected out, frozen (isopentane, -40ºC) and processed for quantitative autoradiography. The brain was mounted on a microtome chuck encased in a plastic embedding matrix (Lipshaw). Coronal brain sections (20 μm thick) were cut on a cryostat maintained at -22°C. Three sections were thaw-mounted onto a glass coverslip, and then the coverslip was immediately placed on a hotplate (60ºC) for 5 mins. Rapid drying prevents diffusion of the trapped [^{14}C] from the cells. Coverslips were glued onto card and apposed to x-ray film (Kodak Biomax MR film 8”x10”, Eastman Kodak Company, Rochester, NY, USA) in light-tight cassettes with [^{14}C]-labelled polymer autoradiographic microscales (40-1070 nCi/g, Amersham, GE healthcare) and exposed for 3 days. Films were then developed using a standard Kodak automatic processor.

The three parameters generated from the experiment are used in the operational equation of the technique to determine LCMRglc; the time-course of arterial [^{14}C] 2DG concentration; time-course of arterial plasma glucose concentration and; tissue concentration of [^{14}C], as determined by autoradiography. LCMRglc within discrete brain regions was measured from local tissue calculations of [^{14}C] (Ci^*) and the plasma [^{14}C] 2-deoxyglucose (Cp^*) and glucose (Cp) concentrations according to the operational equation.

	A	B	C	D	E	F	G	H	I	J	L	M
1	*Date: 10/02/09*											
2	*Treatment: 2DG*										*Animal ID: MRI 2DG-6*	
3												
4	*2DG dose: 125µ/kg*				*Weight: 283.5 g*							
5	Volume (ml): 0.4				*Isotope Injected:*							
6	*Overall MBq = 1.452*											
7												
8	Sample	Sample	Start	Stop	Mean	DPM1	DPM2	DPM3	Mean	Plasma Glucose	Plasma glucose	Plasma 14C conc
9	Number	Time	Time	Time	time				DPM	(mg/ml)	(mg%)	(µCi/ml)
10										Pre-glucose: 6.8		
11	1	0	0.00	0.05	0.042	48.8	54.5	55.2	52.9	6.5	118.04	0.00119
12	2	0.15	0.17	0.25	0.350	62452.4	62527.8	62318.6	62432.9	7.5	136.2	1.40615
13	3	0.3	0.32	0.38	0.583	122616.0	123192.0	122610.0	122806.0	8.1	147.096	2.76590
14	4	0'45	0.50	0.55	0.875	113784.0	113810.0	113893.0	113829.0	8	145.28	2.56372
15	5	1'00	1.02	1.08	1.083	78607.1	78599.7	78246.7	78484.5	8	145.28	1.76767
16	6	2'00	2.10	2.15	2.208	29701.4	29674.8	29734.9	29703.7	6.8	123.488	0.66900
17	7	3'00	3.10	3.16	3.216	29895.9	29950.4	29984.1	29943.5	8	145.28	0.67440
18	8	5'00	5.01	5.06	5.058	24862.4	24807.7	24774.3	24814.8	8.2	148.912	0.55889
19	9	7'30	7.32	7.37	7.575	20478.6	20428.6	20450.5	20452.6	8.5	154.36	0.46064
20	10	10'00	10.04	10.10	10.120	18265.3	18370.2	18370.5	18335.3	8.6	156.176	0.41296
21	11	15'00	15.02	15.10	15.100	14988.9	15119.2	15071.2	15059.8	8.8	159.808	0.33918
22	12	25'00	25.02	25.07	25.075	11249.0	11092.6	11230.1	11190.6	9.6	174.336	0.25204
23	13	35'00	35.03	35.08	35.092	10182.9	10176.1	10123.2	10160.7	10.5	190.68	0.22885
24	14	45'00	45.01	45.06	45.058	9208.8	9167.2	9206.0	9194.0	11	199.76	0.20707
25	Kill Time	45.1										

Table 2.3. Representative example of a [^{14}C] 2-deoxyglucose data sheet displaying the sample times (inputted in deciminutes (1/100th of a minute) for the MCID analyser), the measure of radioactivity (disintegrations per minute (DPM)), plasma glucose values and the plasma [^{14}C] concentrations (from a 20 µL sample)

2.4.4 Densitometric analysis and LCMRglc calculation

Densitometric analysis of autoradiograms was performed using an MCID Basic image analysis system (7.0 Rev 1.0, build 207; Imaging Research Inc.). The MCID system was calibrated at the start of each session to standardise the film background using the range of [^{14}C] standards. The optical densities of the pre-calibrated [^{14}C] standards were measured to produce a calibration curve. Measured grey level values (from 0 (black) to 255 (white)) within designated regions of interest (ROI) were then converted to optical density values. Optical density measurements were measured on the film and using the ^{14}C standards, measurements were converted into ^{14}C concentrations and measured in discrete brain regions by placing autoradiograms (Figure 2.11) on a light box under a closed circuit camera (using the same magnification and light intensity used for calibration) and positioning a frame over each ROI. The mean [^{14}C] value was calculated from the average of the value of the ROI from 5 brain sections per rat.

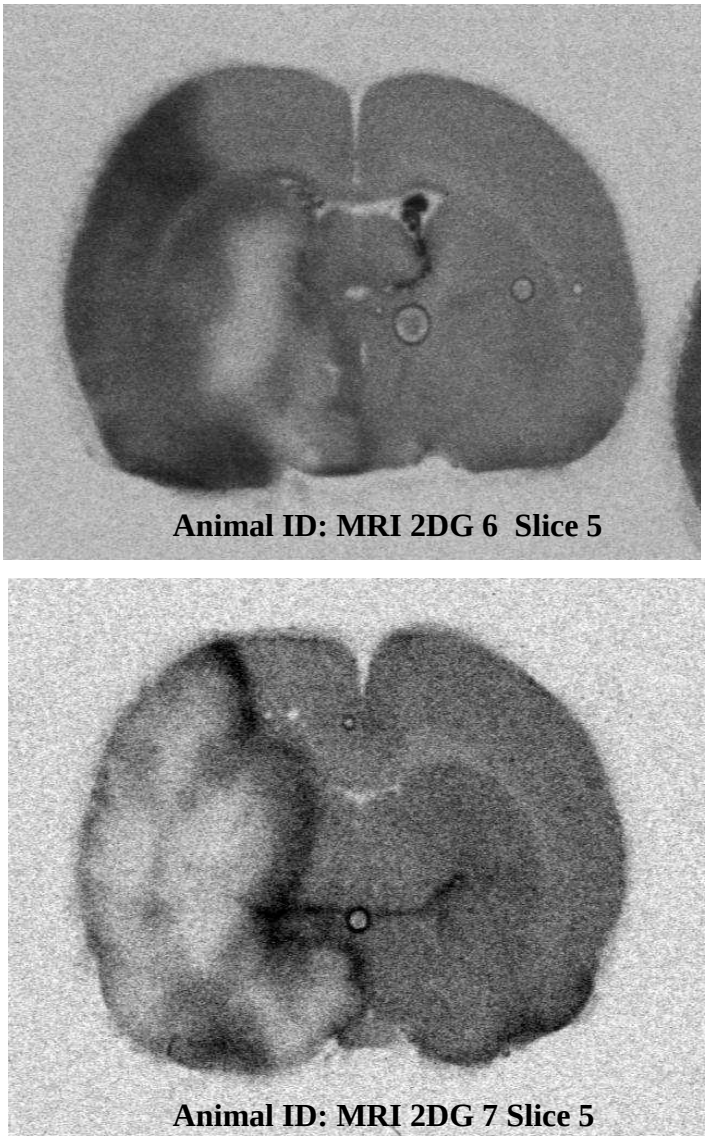

Figure 2.11. Two separate representative autoradiograms photographed on the MCID analyser in animals that under went the MCAO model of ischaemia. The white region represents a region of critically reduced glucose use which corresponds to the ischaemic damage. The dark area surrounding the region of reduced glucose use represents a region of increased 2DG phosphorylation. White matter is notable for its reduced glucose utilisation compared to the grey matter, whilst the choroid plexus within the ventricle displays a high glucose utilisation value

2.5 Magnetic resonance imaging scanning

2.5.1 Magnet specifications

All animals were scanned in a Bruker Biospin Avance 7T (300MHz) Magnetic Resonance Imaging (MRI) and Magnetic Resonance Spectroscopy (MRS) system, equipped with an inserted gradient coil (121 mm ID, 400mT/m) and a 72 mm birdcage resonator.

2.5.2 Physiological monitoring during MRI scans

Following surgery to induce MCAO, animals were placed prone in a Perspex cradle, with the head restrained using ear and tooth bars to limit movement. A linear surface receiver coil (2 cm diameter) was placed above the head of the animal. The base of the cradle, and a cover placed over the rat's body, contained water channels with circulating warm water connected to a temperature controlled combined heater and water pump. This could be pre-set for a given temperature to maintain body temperature at 37ºC. Physiological variables including core body temperature, electrocardiogram (ECG) and respiration rate were monitored with a BioTrig system (Bruker, BioSpin) which had both a command and acquisition module. Physiological input was acquired by attaching electrocardiogram leads (3M innovation) to the rat with conductive electrode gel (Sigma) and electrode adhesive pads; two were attached to the animal's chest and a third to the inner right thigh. A rectal thermocouple was reinserted for continual temperature monitoring. The system was connected to a laptop and AcqKnowledge software used to display the cardiac and respiratory waveforms. Stability of physiological variables was determined from the waveform patterns and temperature readout, and manual control of anaesthetic levels and water heater temperature ensured maintenance of variables within the physiological range. MABP was monitored by cannulating the femoral artery and attaching the cannula to a blood pressure transducer, which was in turn connected to Biopac (Bruker, Biospin) software.

2.5.3 Diffusion-weighted scans

Technical specifications for DWI scans

Spin Echo planar (EPI) diffusion-weighted scans consisted of eight contiguous coronal slices of 1.5 mm thickness which were generated with an in-plane resolution of 260 μm. The field of view was 25 x 25 mm^2 and the matrix size was 96 x 96 mm. The gradient strengths (B values) were 0 and 1000 s/mm^2 and gradient directions were x, y and z. The repetition time (TR) was 4000.3 ms and the echo time (TE) was 43 ms. A DWI scan over the whole brain takes approximately 3 minutes.

ADC maps were generated for each of the 8 contiguous coronal slices throughout the brain (Figure 2.12). Raw datasets were initially processed using Paravision v5 (Bruker Biospin). Subsequent analysis of ADC maps was carried out using ImageJ (http://rsb.info.nih.gov.ij) software.

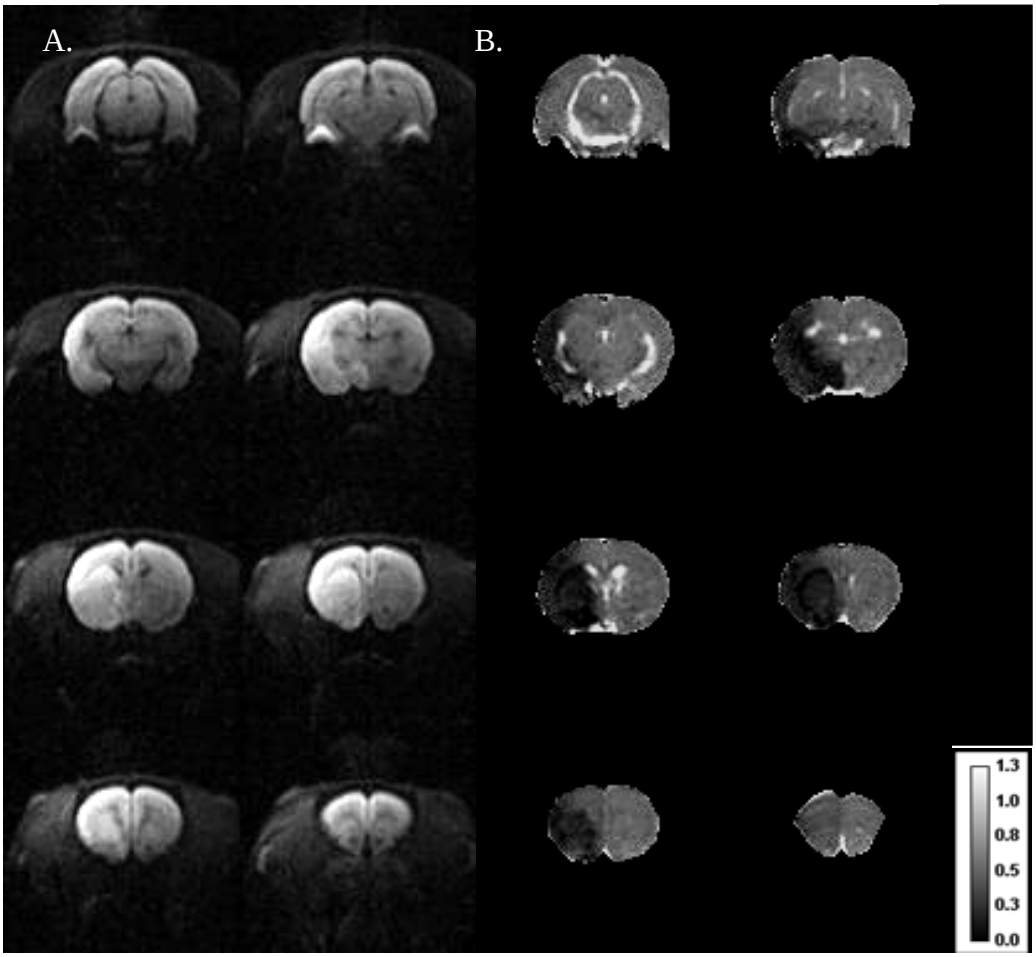

Figure 2.12. A. DWI images of eight coronal slices from a rat brain 2.5 h following intraluminal filament model of permanent MCAO (pMCAO) and **B**. Equivalent ADC maps. The ischaemic damage appears bright on the DWI images and dark on acute ADC maps. ADC values expressed as $x10^{-3}$ mm^2/sec

2.5.4 Arterial spin labelling

Technical specifications

Non-invasive quantitative CBF was carried out on coronal slices within the MCA territory during ischaemia, and immediately following reperfusion for Chapter 5, using a form of pseudo-continuous ASL based on a train of adiabatic inversion pulses (Moffat et al, 2005). The sequence employs a spin-echo echo-planar-imaging (EPI) imaging module (TE 20 ms, TR 7000 ms, matrix 96 x 96, FOV 25 x 25 mm^2, slice thickness 1.5 mm, 16 averages, 4 shots) preceded by 50 hyperbolic secant inversion pulses in a 3 second train. The time taken to generate data for a single slice is approximately 5 minutes. In addition to this, a T_1-weighted image (scan time 10 minutes for the whole brain) was performed to allow quantification of CBF in mL per 100 g per minute.

Post-processing

CBF maps were generated for each of the 4 contiguous slices throughout the brain (Figure 2.13D). Raw datasets were processed ImageJ software. Quantification of the CBF images was performed with use of methods described. The labelled CASL images were first subtracted from the averaged control images (subtracted CASL) (Figure 2.13A) and then divided by the signal intensity to generate a relative CBF map (Figure 2.13B). Fully quantitative CBF maps (Figure 2.13D) were generated by dividing the relative CBF map by the T_1 values generated from the T_1 map (Figure 2.13C). A perfusion deficit map can then be generated from the quantitative CBF map by applying a relevant threshold (e.g. 57% reduction of the mean contralateral hemisphere excluding the ventricles (Figure 2.13E)).

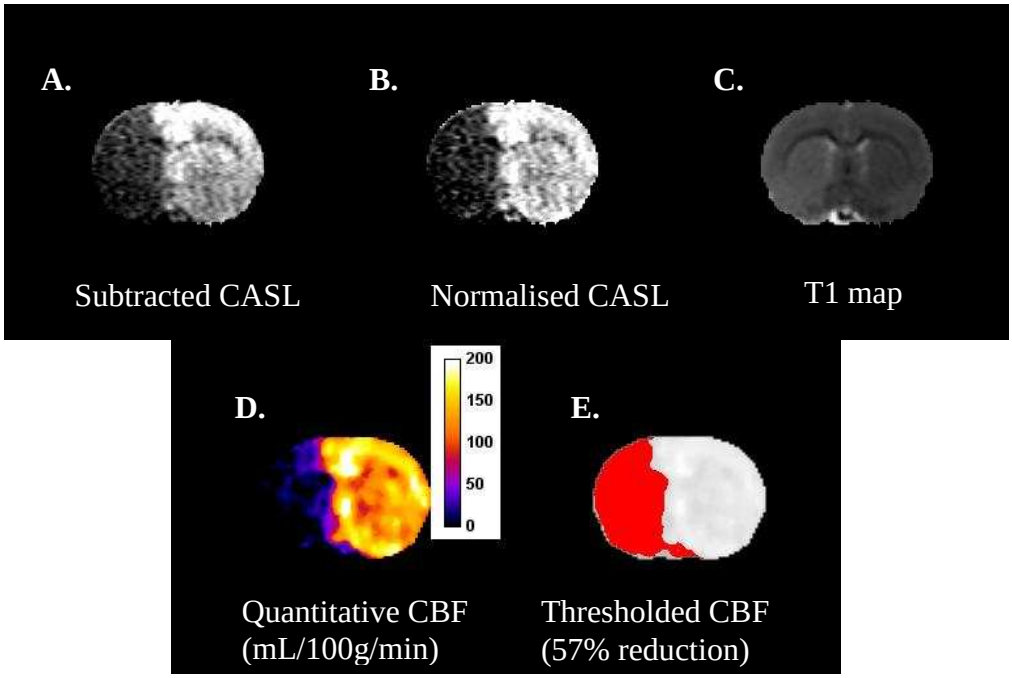

Figure 2.13. ASL Images and the corresponding T_1 map generated from a rat 1 h following intraluminal filament-induced MCAO

2.5.5 T_2-weighted scanning

T_2-weighted scans were generated for two reasons; first, sagittal T_2 scans were performed to identify neuroanatomical landmarks and second, coronal scans were generated for final infarct measurements. The need for neuroanatomical landmarks was particularly important for the reperfusion study (Chapter 5), where the animal was removed from the magnet to induce reperfusion, and then placed back in to scanner (the reperfusion phase), and again at 7 days to assess final infarct. Using the rhinal fissure, the brain can be repositioned to match the initial acute scan geometry as closely as possible. During acute scanning and at 7 days following reperfusion, a sagittal RARE (rapid acquisition with refocused echoes) T_2 scan (effective TE: 46.8 ms, TR: 5000 s; in plane resolution of 97 μm; 18 slices of 0.5 mm thickness) was performed, in which the rhinal fissure was used as the neuroanatomical landmark for the first slice position (Figure 2.14).

Second, a coronal RARE T_2 sequence (effective TE: 46.8 ms, TR: 5000 s; in plane resolution of 97 um; 16 slices of 0.75 mm thickness) enabled T_2-derived final infarct measurements. ImageJ was used to separate the images (8 slices are displayed in Figure 2.15) and the hyperintense region that represented the infarct was manually delineated using the freehand function. Measurement of individual images gave the infarct areas in millimetres squared, and infarct volume was calculated by adding up the 16 areas and multiplying by the slice thickness (0.75 mm).

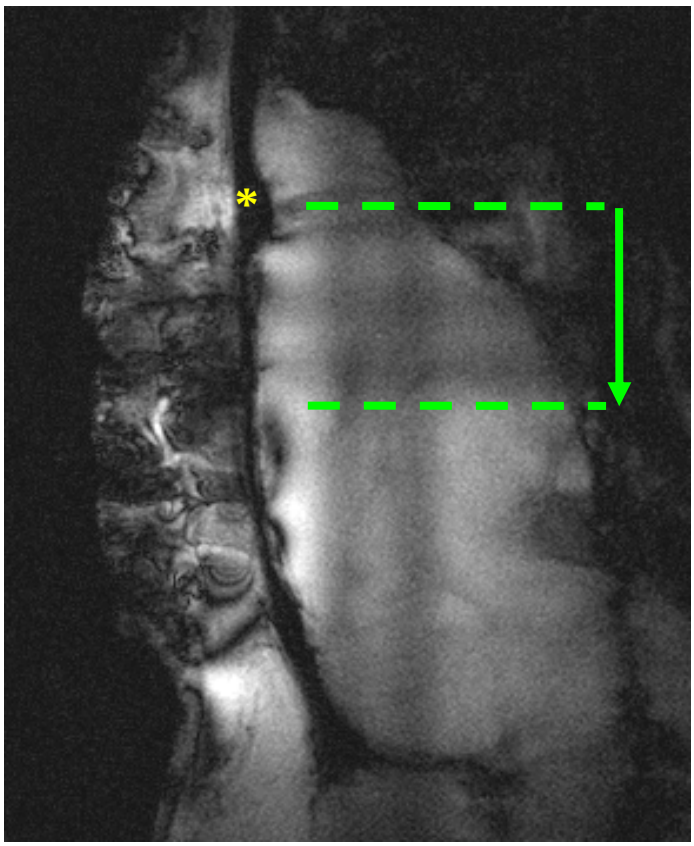

Figure 2.14. Sagittal T_2 scan of a rat brain (direction of arrow represents the rostro-caudal position of the brain. The dashed lines display the imaging window for which 18 slices of 0.5 mm thickness were generated (yellow asterisk marks the rhinal fissure)

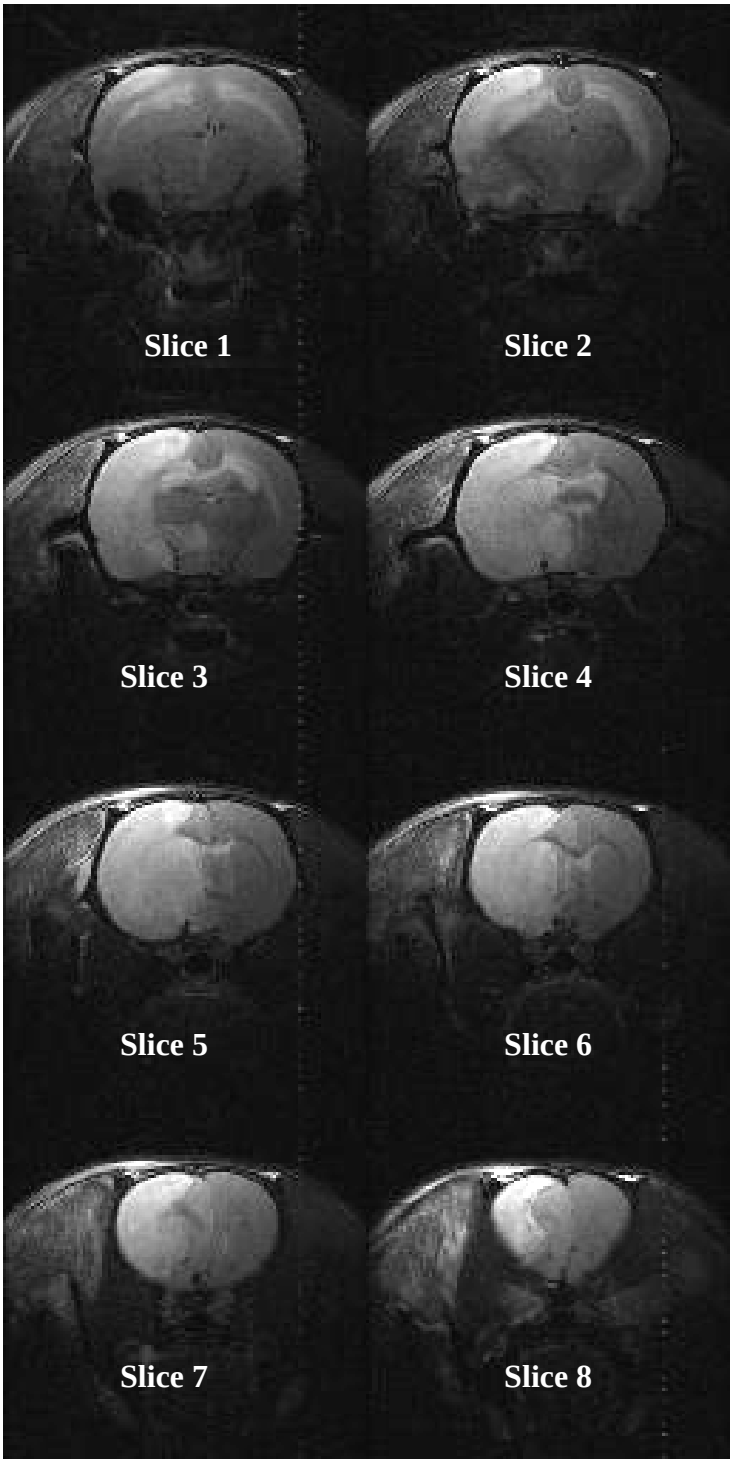

Figure 2.15. T_2-weighted images of eight coronal slices (caudal to rostral) from a rat brain following intraluminal filament induced permanent MCAO at 24 hours post-ischaemia. Ischaemic damage appears bright on RARE T_2 images

2.5.6 T_2^*- weighted scans

The sequence used to measure T_2^* changes during an oxygen challenge (OC, ventilation changed from ~22% to 100% O_2 for a short and transient period) was a single shot, gradient echo (echo planar imaging) sequence: TE: 20 milliseconds, TR: 10 seconds, matrix 96 x 96, FOV 25 x 25 mm^2, eight contiguous slices of 1.5 mm thickness, two averages, temporal resolution 20 seconds, 75 repetitions). Two MRI slices which corresponded to the territory supplied by the MCA were selected for analysis (Figure 2.16). Three paradigms were used for the generation of data during the T_2^*-weighted OC sequence:

1) 5 minutes breathing air, followed by 5 minutes breathing 100% oxygen, and then 15 minutes breathing air;

2) 5 minutes breathing air followed by 5 minutes breathing 100% oxygen; or

3) 5 minutes breathing air, followed by 5 minutes breathing 100% oxygen, and then 10 minutes breathing air

For the former paradigm ([^{14}C] 2-deoxyglucose study, Chapter 4) a stack of 600 images were generated (75 images per slice, for a total of 8 slices). For the second paradigm, (Reperfusion study, Chapter 5, 240 images were generated (30 images per slice, for a total of 8 slices). For the latter paradigm (Serial OC study, Chapter 6) a stack of 960 images (120 images per slice, total of 8 slices) was generated over 10 mins.

T_2^* image processing

The time course and size of the T_2^* signal change during OC was analysed using the ImageJ percentage signal change plugin. T_2^* percentage signal change within selected regions of interest was calculated from time course graphs (Figure 2.18B), where the average baseline signal (over 5 minutes) was subtracted from the peak signal during OC. This value was then divided by the average baseline signal and multiplied by 100. T_2^*OC percentage signal change maps were then generated (Figure 2.17).

T_2^* image analysis

T_2^* percentage signal change within selected regions of interest were determined by first manually drawing round a region of interest (such as the ADC-derived ischaemic core) (Blue ROI on Figure 2.18A), and then generating the time course data by plotting a z-axis profile of the raw 75 images (Figure 2.18B)

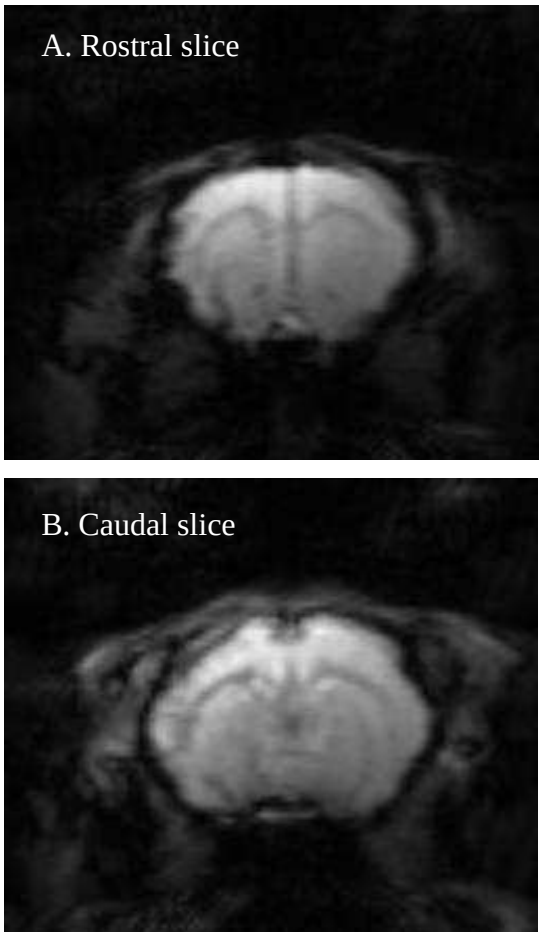

Figure 2.16. Example of raw T_2^*-weighted images of a rostral (**A**) and caudal (**B**) slice within MCA territory 1 hour post-MCAO. The oxygen challenge involved 4 min air inhalation followed by 6 mins 100% oxygen inhalation

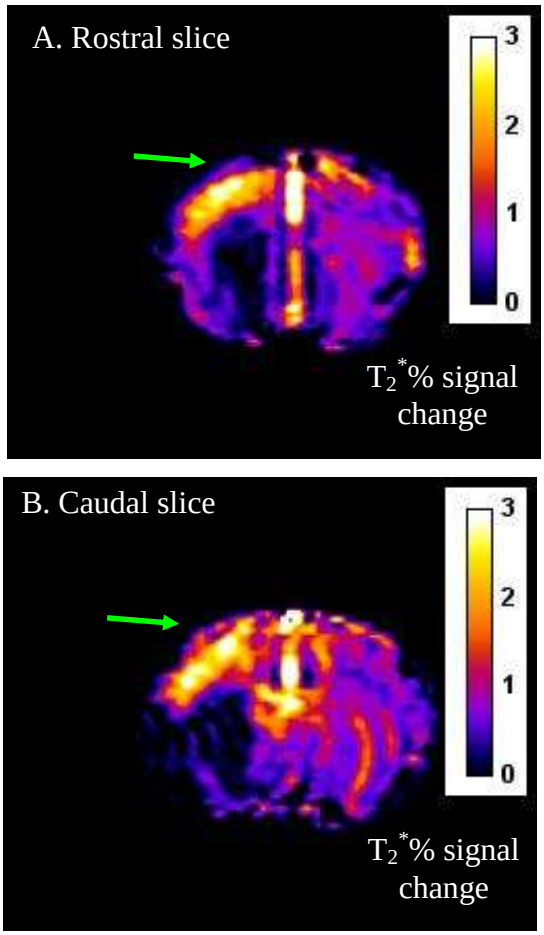

Figure 2.17. T_2^* percentage signal change maps from a rat 1 hour post-pMCAO, generated from the time course data (corresponding maps of the rostral and caudal slices displayed in Figure 2.16). Note the low T_2^* % signal change within the ischaemic core, and the high signal change within the sensorimotor cortex (presumed penumbra, green arrow) and large veins and sinuses

A.

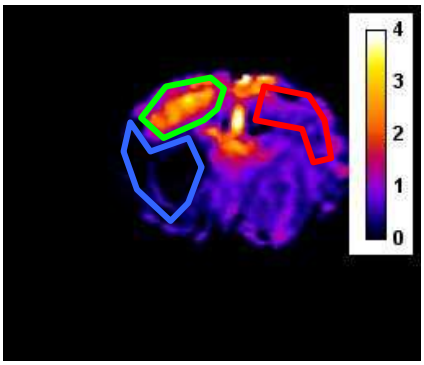

B.

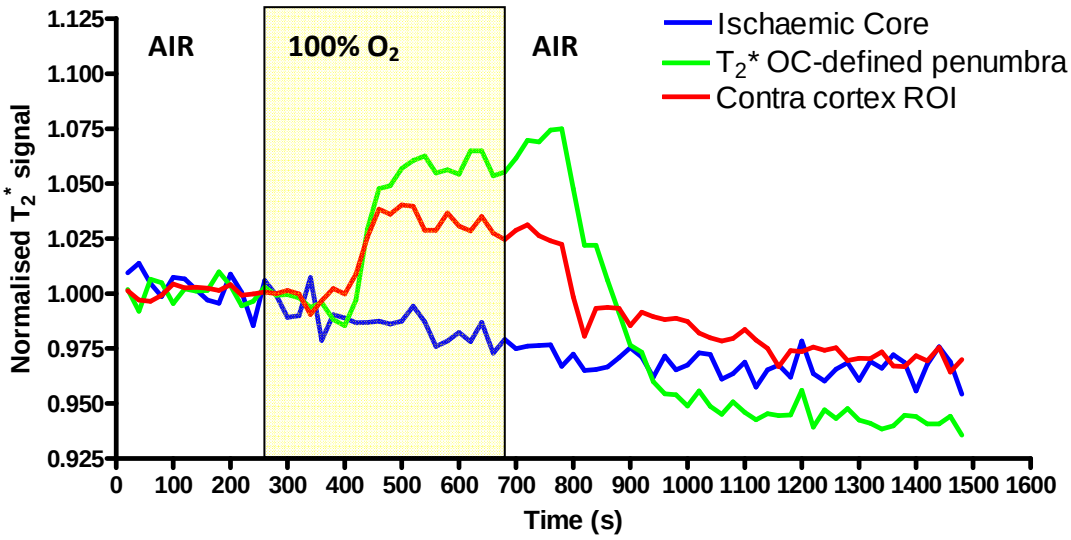

Figure 2.18. Images and T_2^* data from a representative rat 1 hour after pMCAO. **A**. Manually selected ROIs (ADC-derived ischaemic core – blue, T_2^*OC-defined penumbra – green, and contralateral cortex – red), and **B**. the corresponding T_2^* time course data for the selected ROIs. Y-axis scale is normalised T_2^* signal

Thresholding T_2^* % signal change images

Penumbral tissue was defined using a threshold based on the empirical rule: the mean plus 2 SD of the T_2^* value of the contralateral hemisphere, excluding the ventricles (Figure 2.19).

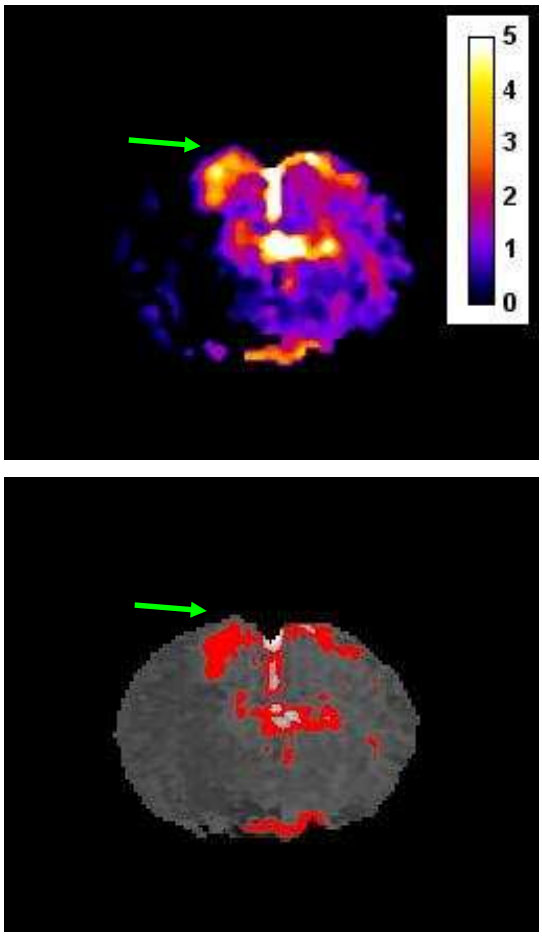

Figure 2.19. The non-thresholded (**A**) and thresholded (**B**) T_2^* percentage signal change map for a sample slice at 1 hour post-pMCAO. Scale bar in units of T_2^* percentage signal change. Presumed penumbra shown by green arrow

2.5.7 Co-registration of scans

EPI sequences - such as the T_2^*OC sequence - are susceptible to high levels of artefacts which manifest themselves as image and signal distortion. Small magnetic field differences will result in spatial distortion. Regions of the brain close to the nasal sinus, such as the auditory meatus, frontal and temporal lobes are particularly affected. In order to compare data on T_2^* scans with ADC, T_2 and ASL scans, linear coregistration was performed using Analyze software (AnalyzeDirect, Inc).

Processed ADC maps were used as a template for co-registering the raw T_2^*OC stack. A single slice was separated from the T_2^*OC stack and the distorted slice was manually coregistered and aligned to fit the spatial location of the ADC template using the 3D voxel registration plugin (Figure 2.20). The coregistered matrix data was saved and 2D voxel registration was used to warp the remaining T_2^*OC stack. The coregistered matrix data was used to coregister raw datasets with scans performed at later time points (in Chapters 5 and 6).

Using the co-registration software (Analyze), only rotation and translation of the images were required to accurately co-register the data. This did not involve warping (stretching) the images which would cause co-registration errors (by introducing subjectivity).

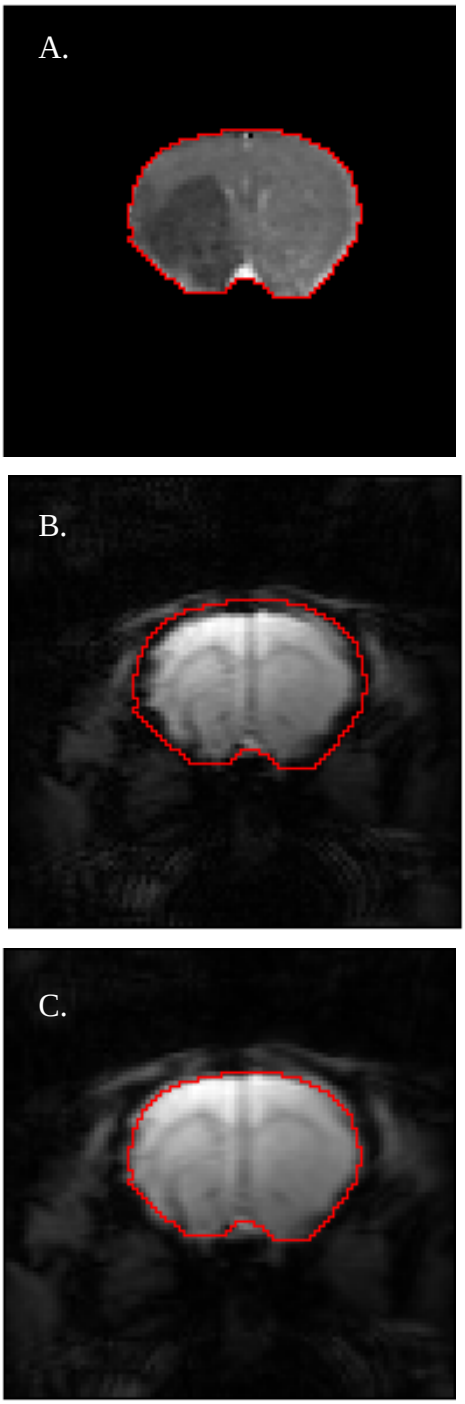

Figure 2.20. An example ADC coronal slice (**A**) at 1 hour post-pMCAO, used as a template for co-registration with T_2^* scans. The unwarped OC slice (**B**) was manually warped and aligned with the ADC slice to generate a warped T_2^*OC slice (**C**). The red line on the ADC map has been superimposed on the unwarped slice and the warped slice

Chapter

3

Characterisation of the T_2^* Oxygen Challenge technique

In this chapter data are presented to illustrate reproducibility achieved in inducing experimental stroke along with optimisation and characterisation of the Blood Oxygen Level Dependent (BOLD) MRI response to oxygen challenge (OC). The first aim was to achieve a reproducible volume of ischaemic damage using the intraluminal filament method to induce permanent MCAO in the rat and to establish methods of infarct quantification. Secondly, the effect of physiological variables on the BOLD signal response to OC was assessed. It was important to identify factors, other than tissue metabolism, which could influence the T_2^* signal change during OC.

3.1 Establishing reproducibility in the MCAO model using TTC and H&E to quantitatively assess infarct volume

3.1.1 Introduction

Infarct volume is an important outcome measure for assessing irreversible ischaemic damage. 2,3,5-triphenyltetrazolium chloride (TTC) and haematoxylin-eosin (H&E) staining were used, which are commonly used to detect infarct volumes in animal models. Experiments were performed to assess the MCAO surgical technique with TTC staining initially carried out as a quick method of confirming success of MCAO surgery and for quantifying infarct volume reproducibility. Once proficiency in stroke surgery was achieved, H&E staining was used to accurately measure infarct volume.

Using TTC staining, two different methods can be implemented that do not necessarily produce the same results (Dettmers et al, 1994). TTC can be transcardially perfused *in vivo* or incubated with brain slices *ex vivo.* Using the perfusion technique, in the acute phases of ischaemia, staining mainly reflects changes in perfusion of the stain due to altered blood flow rather than ischaemic (mitochondrial) damage (Liszczak et al, 1984). The latter

technique was used in the first *in vivo* experiments, as this was simpler and provided a crude but quick estimate of infarct. TTC does not accurately define infarct size until 24 hours after permanent MCAO (Bedersen et al, 1986) but provides sufficient information 4-6 hours post-MCAO to determine if the MCA has been sufficiently occluded by the intraluminal filament.

Cerebral ischaemia causes changes to the general morphology of cells which can be detected with the commonly used histological stain haematoxylin and eosin (H&E). Specifically, haematoxylin stains basophilic structures with a blue-purple hue, and eosin is the counterstain which stains the eosinophilic structures, such as the cytoplasm and extracellular components a sharply contrasting pink. The basophilic structures contain nucleic acids, such as the ribosomes and the chromatin-rich cell nucleus.

3.1.2 Methods

Male Sprague-Dawley rats (300-343 g, Harlan, Bicester, UK) were initially anaesthetised with 5% inhaled isoflurane delivered in oxygen–nitrous oxide (30:70) in an induction chamber at room temperature. The rats were then intubated and artificially ventilated, with anaesthetic maintained at ~2% isoflurane. A polyethylene catheter (Portex: external diameter 0.96 mm; internal diameter 0.58 mm; 70 cm long) was surgically inserted in a femoral artery to continuously monitor blood pressure and for sampling to conduct blood gas analysis. Twelve rats were used overall (6 for TTC staining and 6 for H&E histological assessment of infarct), and the intraluminal filament method of permanent (pMCAO) was performed. H&E and TTC staining were performed using the methods described in Chapter 2.3). Data are displayed as the mean±SD.

Ischaemic damage assessed with TTC staining

The MCAO surgical technique was first mastered on cadavers before progressing to *in vivo* (anaesthetised throughout) experiments with assessment 4 hours after MCAO with TTC. At 4 hours post-stroke, the animal was killed by anaesthetic overdose and the brain removed, chilled, sliced in the coronal plane on a brain matrix and slices incubated in TTC. The area of ischaemic damage was measured on TTC stained tissue slices (See Chapter 2.3.6). Slice 0 to 7 refers to the most rostral to caudal slices, respectively (Figure 3.1), and two measurements of infarct area were made on each slice and the mean plotted. As slice

thickness was 2 mm, areas were converted into volumes by summing all the slice areas and multiplying by the slice thickness (2 mm).

Ischaemic damage assessed with H&E staining

Animals underwent perfusion fixation, and brains were removed for tissue processing, paraffin wax embedding and microtome sectioning (Chapters 2.3.2 and 2.3.3). Following H&E staining (Chapter 2.3.4) sections were selected at 8 stereotaxic levels throughout the MCA territory and viewed by light microscopy at x20 magnification. Areas of ischaemic damage were transcribed onto line diagrams from the rat stereotaxic atlas. Volumetric measurements were calculated three times, and the three values were averaged and infarct volume calculated by plotting the areas against the Bregma coordinates (level 1 (3.24 mm) to level 8 (-6.36 mm)) and area under the curve was calculated (Figure 3.2).

3.1.3 Results

3.1.3.1 TTC-derived ischaemic volume analysis

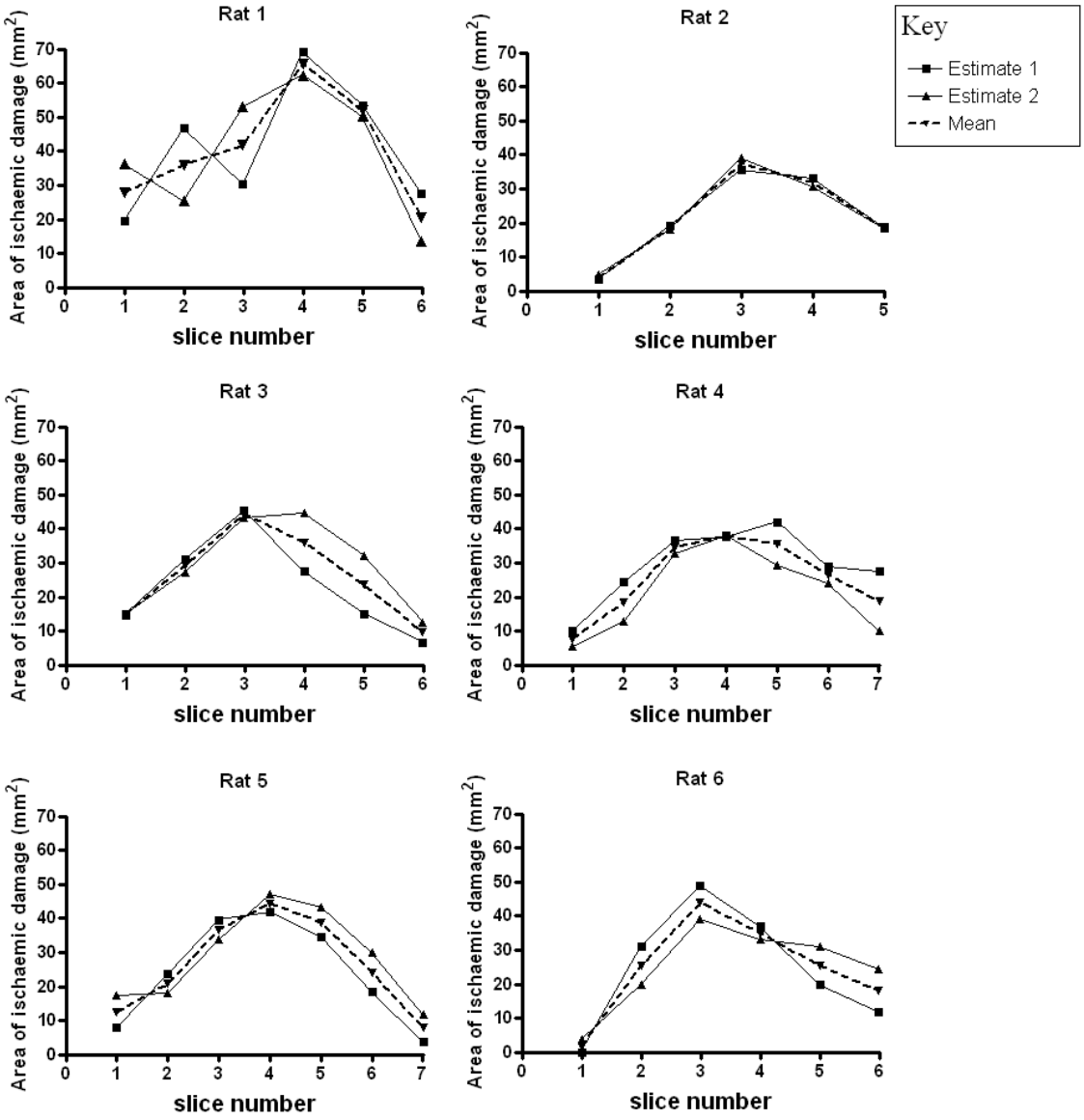

Figure 3.1. Area of ischaemic damage on TTC stained tissue slices throughout the MCA territory. Note that the region within end artery MCA territory (between slices 2-5) tended to have larger areas of ischaemic damage, whereas the slices in the more rostro-caudal regions with more collateral supply experienced less damage

3.1.3.2 H&E-derived ischaemic volume analysis

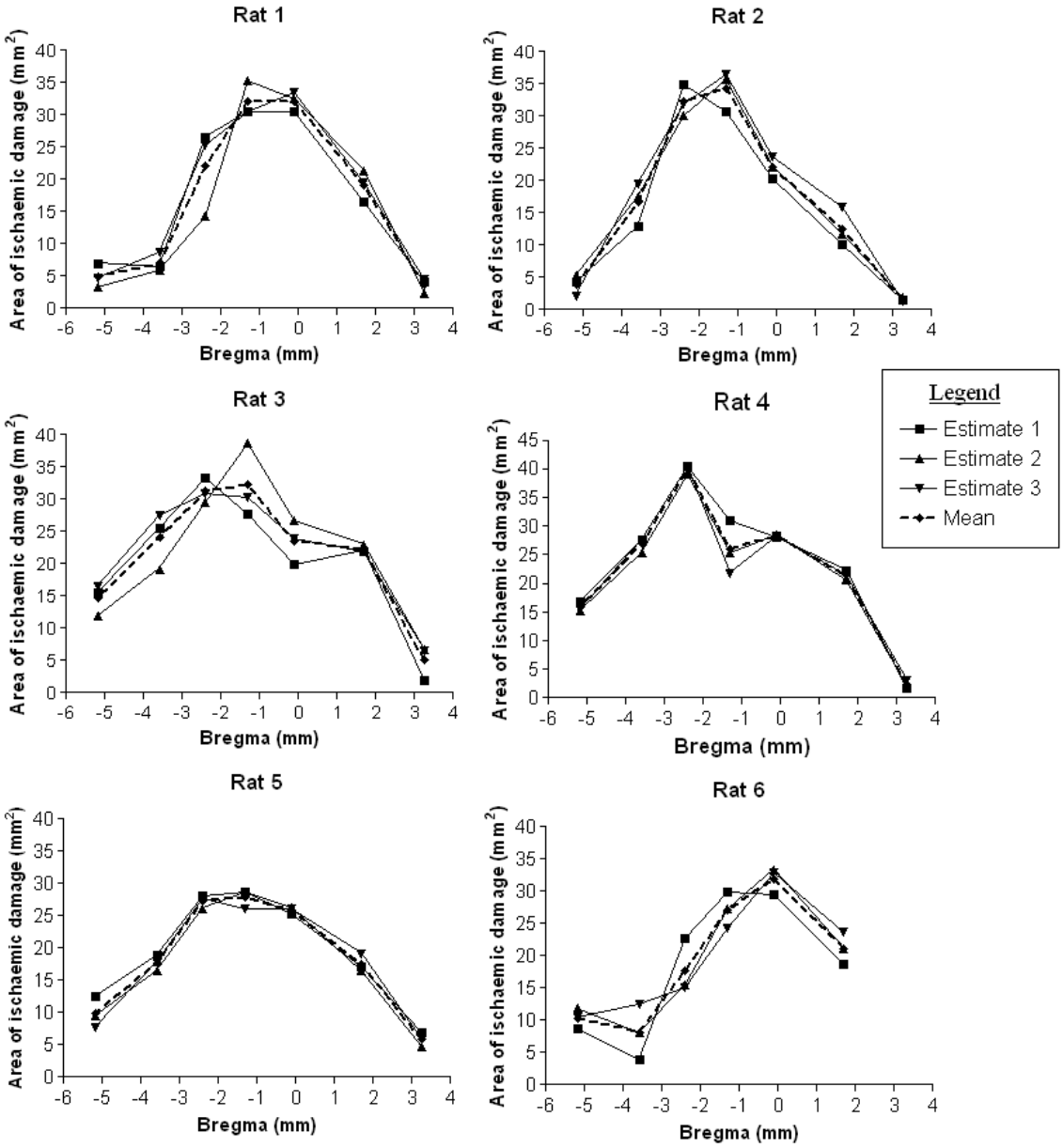

Figure 3.2. Areas of ischaemic damage per stereotaxic level according to Bregma coordinates measured on H&E stained sections. At each level, 3 sections were each measured 3 times and the average value plotted

3.1.3.3 Ischaemic damage volume comparison

The mean lesion volume using TTC staining was 308±86 mm^3 and the mean lesion volume using H&E staining was 171±25 mm^3 (Figure 3.3). The TTC method appeared to have a larger variation of results compared to histology which may reflect inexperience with the technique at this time. To determine the presence of brain swelling, the volumes of the ipsilateral and contralateral hemispheres for the TTC slices were compared (Figure 3.4), but at 4 hours post stroke there was no evidence of significant brain oedema and brain swelling (p=0.1427).

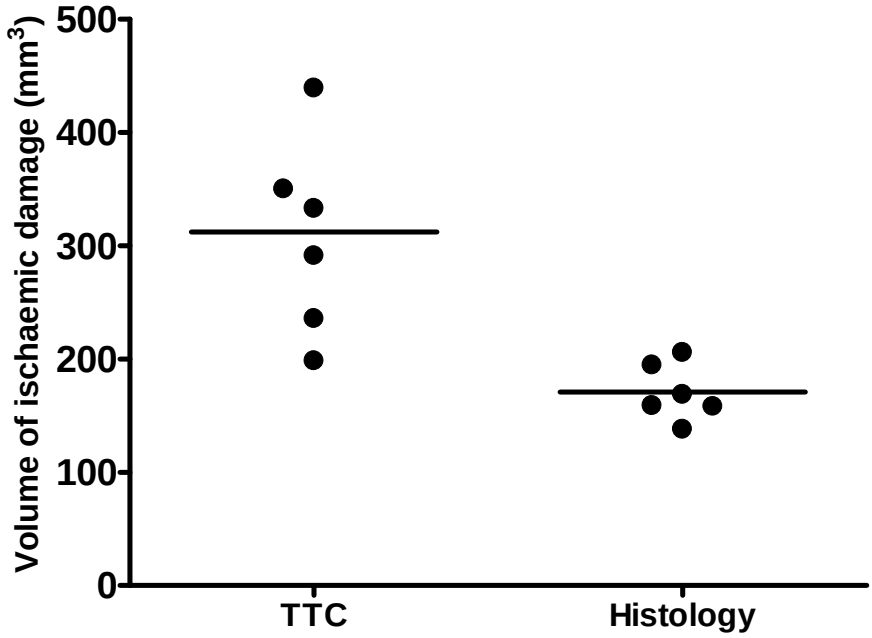

Figure 3.3. Scatterplot illustrating infarct volumes measured on TTC slices (early experiments) and histology at 4 hours following permanent MCAO. The horizontal line represents the mean

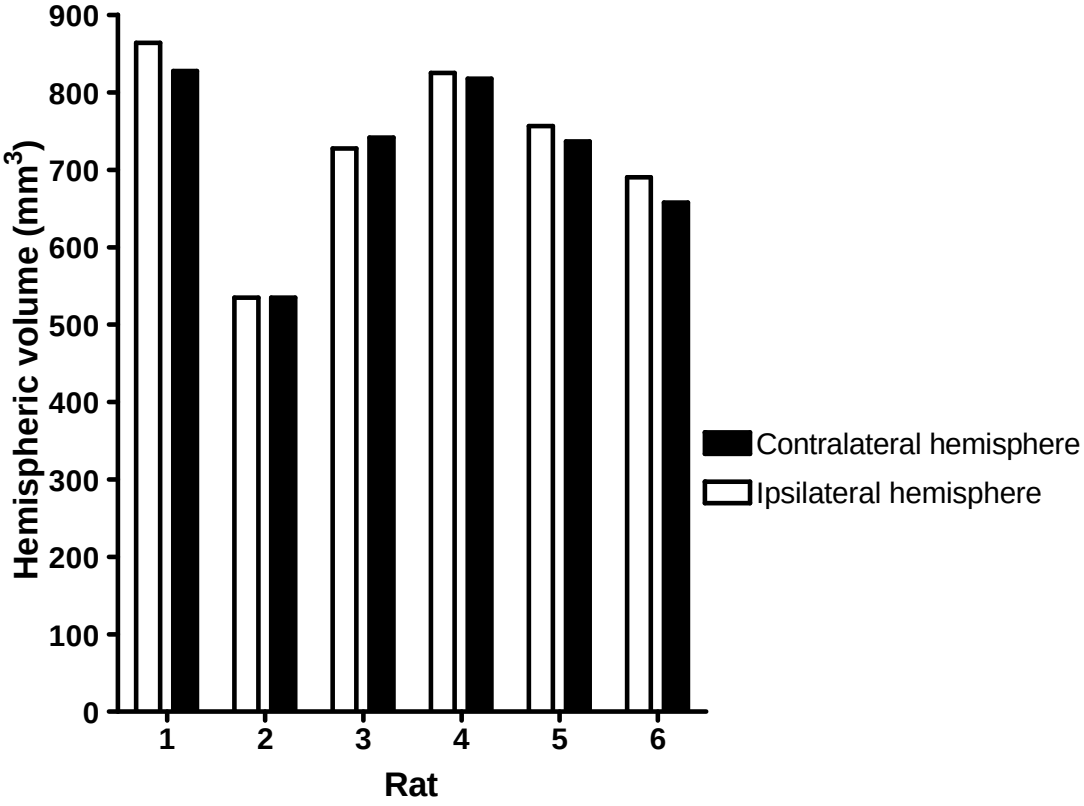

Figure 3.4. Comparing the ipsilateral and contralateral hemisphere volumes in the TTC-stained brains to determine presence of brain swelling at 4 hours post-stroke. With Rat 2, due to tissue damage to the rostral region of the brain during sectioning, only 5 slices were measured compared to the 6 or 7 slices measured in the other 5 animals. This explains the smaller measurements for total hemispheric volumes

3.2 Optimisation of the BOLD T_2^*OC technique

3.2.1 Introduction

Blood oxygen level dependent (BOLD) signal changes in MRI were initially reported in relation to cerebral blood vessels, where it was found that changes in the oxygenation of venous blood altered the T_2^* MR signal response (Ogawa et al, 1990). Acceptance and validation of the technique was aided by evidence of global signal changes following a number of respiratory challenges (Turner et al, 1991). Following on from this, human studies confirmed the concept - first described by PET studies - that during functional brain activation, the oxygen content of venous blood increases. The simple explanation for this phenomenon was that the increase in oxygen delivery outweighs the smaller increase in neuronal oxygen metabolism. The effect is that the venous blood contains less deoxyhaemoglobin which gives rise to a concomitant BOLD MRI signal increase produced by a change in T_2^* (Ogawa et al, 1992), which is useful in assessing cerebral function non-invasively. The premise is similar to that for O^{15} PET, where the detection of brain activation is based on measuring rCBF by O^{15} water injection (Volkow, Rosen and Farde, 1997).

The emergence of functional MRI (fMRI) – which measures the haemodynamic response to neural activation - was an important corollary of the initial BOLD studies which provided additional information on function to the structural neuroimaging methods, and high speed acquisition of multi-shot techniques was made possible with EPI. A robust feature of fMRI is its ability to map signal change in real time, despite the fact that temporal and spatial resolution is determined by factors associated with the haemodynamic response (Menon et al, 1997; Menon et al, 1993). However, the BOLD response originally depended on a number of underlying assumptions including factors such as baseline states remaining uniform between subjects. We now know that there are a number of factors in addition to brain function that influence the magnitude of the BOLD signal change. For example, baseline physiological parameters, such as blood gases and haematocrit, plus CBF and cerebral blood volume can influence this BOLD response. Rostrup and colleagues (Rostrup et al, 1995; Rostrup et al, 1994) verified this in humans by varying the respiratory status (the partial pressure of oxygen and carbon dioxide). The baseline CBF was shown to be a fundamental factor influencing the BOLD response by Bandettini and colleagues (1997) who noted attenuation in signal intensity when baseline CBF was high.

The role of the baseline physiological state has been complicated by reports that functional BOLD response remains constant (Bandettini and Wong, 1997) or decreases (Rostrup et al, 2005) during reduced PaO_2 (hypoxia), or increases (Cohen et al, 2002) or decreases (Posse et al, 2001) during increased $PaCO_2$ (hypercapnia).

3.2.2 Influence of baseline physiological state and CBF on T_2^*OC signal response to OC

A number of factors must be considered when interpreting alterations in T_2^* response. They may relate to the physiological responses such as vascular reactivity, in that blood vessels dilate or constrict in response to the amount of oxygen delivered. The factors may also be biophysical; venous oxygenation may change when blood flow is altered, the levels of deoxy- and oxyhaemoglobin in the blood, and the actual tissue requirements of oxygen in relation to metabolism (oxygen extraction factor, OEF), affect T_2^* response.

In normal conditions, the T_2^* signal intensity following brain activation would increase in proportion to a decrease in deoxyhaemoglobin (Ogawa et al, 1990; Ogawa et al, 1992; Lin et al, 1998; Kwong et al, 1992). Introducing a hyperoxic challenge will increase the content of arterial oxygen by increasing the oxygen saturation of haemoglobin and the levels of O_2 dissolved in the plasma. Therefore, increasing arterial O_2 content will decrease the amount of venous deoxyhaemoglobin, and thus increase the BOLD signal (Rostrup et al, 1995). Also, fluctuations in CBF, without an accompanying increase in $CMRO_2$ has the effect of changing the amount of deoxyhaemoglobin in the blood, which therefore alters the local magnetic susceptibility and affects the T_2^* response.

3.2.2.1 Aims

The aim was to identify the factors that could influence the T_2^* response and magnitude to oxygen challenge. Changes in CBF, CBV, tissue oxygenation, and oxidative metabolism can all influence the T_2^* signal (Ramsay et al, 1993; Corfield et al, 2001), so it was important to discount the possibility that factors other than tissue metabolism were influencing the signal change during OC. To develop and validate OC as an accurate penumbral marker, the relationship between T_2^*, baseline physiological state and CBF was tested since changes in these parameters may contribute to the T_2^* response. To assess the magnitude of the CBF component, correlations between T_2^* and CBF were assessed. Since T_2^* is sensitive to changes in oxy:deoxyhaemoglobin ratios, the influence of baseline

arterial partial pressure of oxygen (PaO_2) on T_2^* response was tested. Lastly, since baseline oxygen saturation (the percentage of haemoglobin binding sites in the blood occupied by oxygen) may give an indication of the extent to which deoxyhaemoglobin can be converted to oxyhaemoglobin following OC, the effect of oxygen saturation was assessed, in which the percentage change in oxygen saturation (from post-OC to during-OC) and T_2^* percentage signal change in ROIs were correlated.

3.2.2.2 Methods

Animal preparation

Male Sprague Dawley rats were anaesthetised (2% isoflurane), ventilated (air), the middle cerebral artery occluded by an intraluminal filament, and MR imaging was performed throughout MCA territory. A polyethylene catheter (Portex: external diameter 0.96 mm; internal diameter 0.58 mm; 70 cm long) was placed in a femoral artery to continuously monitor blood pressure and collect blood samples for blood gas analysis. Using arterial blood gas sampling, baseline PaO_2 (n=35) and the percentage change in oxygen saturation from baseline to during OC was measured (n=27).

Magnetic resonance imaging scanning

Magnetic resonance imaging data were acquired on the scanner described in Chapter 2.5.1. After stroke surgery, animals were placed prone in a rat cradle, with the head restrained using ear and tooth bars to limit movement, and a linear surface receiver coil (2 cm diameter) placed above the head of the animal.

T_2^* scanning

The sequence used to measure T_2^* changes during OC is described in Chapter 2.5.6. One coronal MRI slice (slice 5, Figure 3.5) within core middle cerebral artery territory was selected for analysis. The paradigm for the T_2^* weighted OC sequence was 4 minutes ventilation on air, followed by 6 minutes ventilation on 100% oxygen. The T_2^* % signal change was calculated and correlated with the baseline (pre-OC) PaO_2 (n=35) to identify the extent to which PaO_2 modulates BOLD response.

Diffusion-weighted imaging

DWI was performed to identify ischaemically injured tissue, using the sequence described in Chapter 2.5.3.

Arterial Spin Labelling

Perfusion-weighted imaging (PWI, by continuous arterial spin labelling) was used to generate quantitative CBF maps (n=17). Non-invasive quantitative CBF was carried out on 1 of the 8 coronal slices (slice 5, Figure 3.5) within the MCA territory using a form of pseudo-continuous ASL based on a train of adiabatic inversion pulses (Moffat et al, 2005). The sequence is described in Chapter 2.5.4.

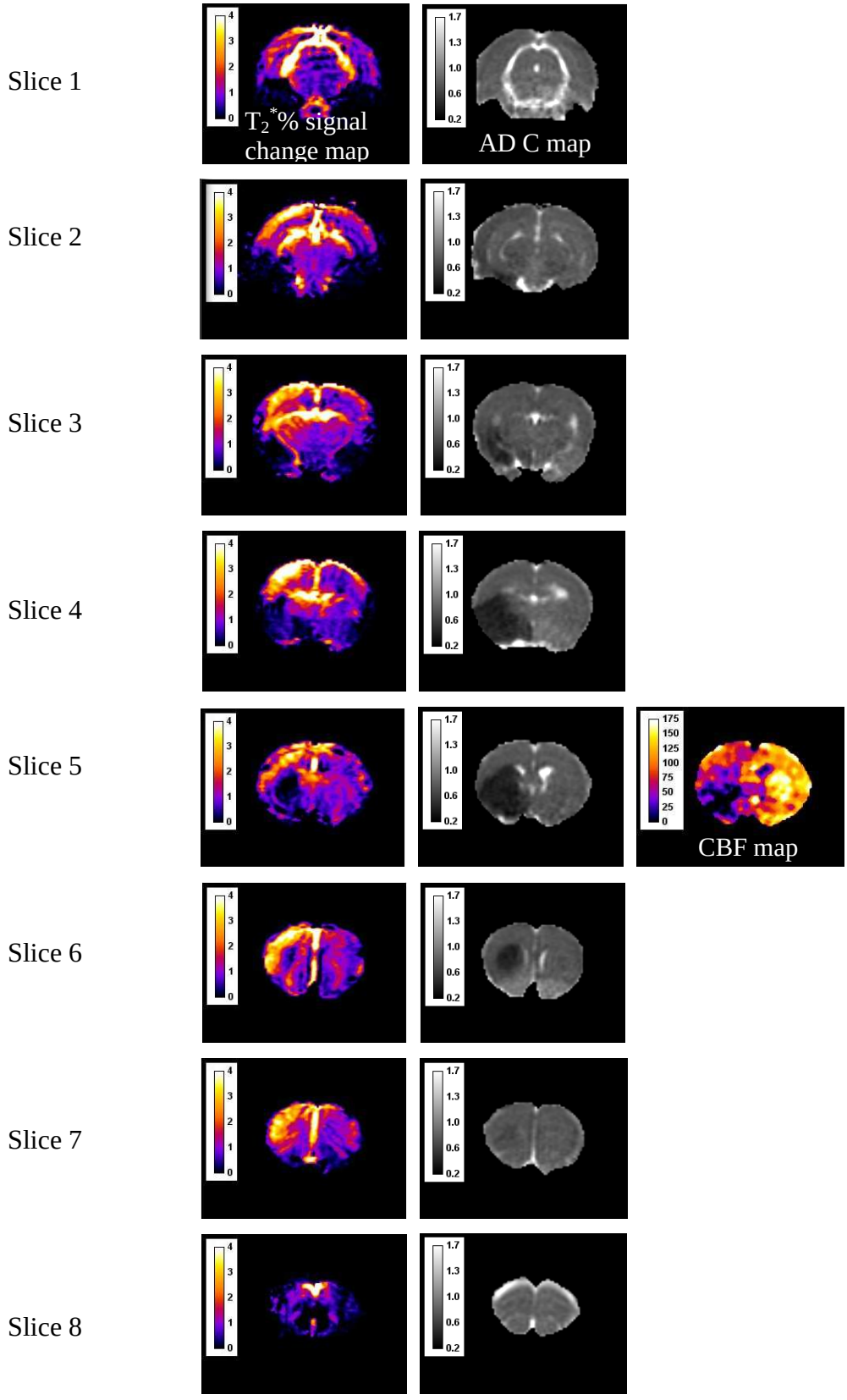

Figure 3.5. T_2^*OC (shown as % signal change) maps and equivalent ADC (in $x10^{-3}mm^2/sec$) maps across the 8 caudal-to-rostral extent (slice 1-8), including the CBF (ml/100g/min) map at slice 5. Image analysis was performed on slice 5. Note region of increased T_2^* % signal change on right hemisphere identified as penumbra, situated out with the ADC lesion (expressed as the dark region on the ADC maps in the regions within MCA territory)

ROI analysis

CBF and T_2^* % signal change values were analysed from MRI-defined regions of interest (ROI) (Figure 3.6): Ischaemic core was defined as the ADC lesion (with a threshold set at an 16.5% reduction of the mean contralateral ADC value excluding the ventricles), OC-defined penumbra (thresholded using the empirical rule – the mean plus 2SD) and mirror regions in contralateral caudate and cortex. T_2^* percentage signal change was calculated from time course graphs, where the average baseline signal over 4 minutes was subtracted from the peak signal during oxygen challenge. This value was then divided by the average baseline signal and multiplied by 100. The relationship between the different variables (T_2^* percentage signal change with PaO_2, oxygen saturation and CBF) was assessed using the Pearson *r* correlation test.

3.2.2.3 Results

Baseline CBF and T_2^*OC

In the four regions of interest, there was no correlation between T_2^* percentage signal change to OC and CBF, suggesting that baseline CBF is not implicated as a factor influencing T_2^* response (within T_2^*OC defined penumbra r^2=0.08579, p=0.2539; ADC-derived ischaemic core r^2=0.00003, p=0.98; Contralateral cortex r^2=0.0005, p=0.93; Contralateral caudate r^2=0.024, p=0.56; Figure 3.7). T_2^* signal change was not higher when lower CBF values were recorded in any of the regions analysed and *vice versa*.

PaO_2

In penumbra (r^2=0.1935, p=0.0092) and in tissue unaffected by ischaemia (r^2=0.5197, p<0.0001 in contralateral cortex and r^2=0.5395, p<0.0001 in contralateral caudate), the magnitude of the T_2^* response is influenced by the baseline PaO_2, whereas baseline PaO_2 does not influence the T_2^* response in the ischaemic core caudate (r^2=0.0455, p=0.2186). Lower baseline PaO_2 gives rise to greater T_2^* signal responses and *vice versa* in ROIs still metabolically active (Figure 3.8).

Oxygen saturation

In the ischaemic core (r^2=0.00006, p=0.49), the percentage change in O_2 saturation from baseline to during OC did not affect the T_2^* response, whereas in tissue regarded as normal (contralateral cortex r^2=0.43, p=0.0002 and contralateral caudate r^2=0.45, p=0.0001 in contralateral caudate), and in penumbra (r^2=0.6525, p=0.0001), the magnitude of the T_2^* response is influenced by the change in O_2 saturation. Lower percentage change in O_2 saturation gives rise to a lower T_2^* signal response and vice versa in ROIs on the contralateral hemisphere (Figure 3.9).

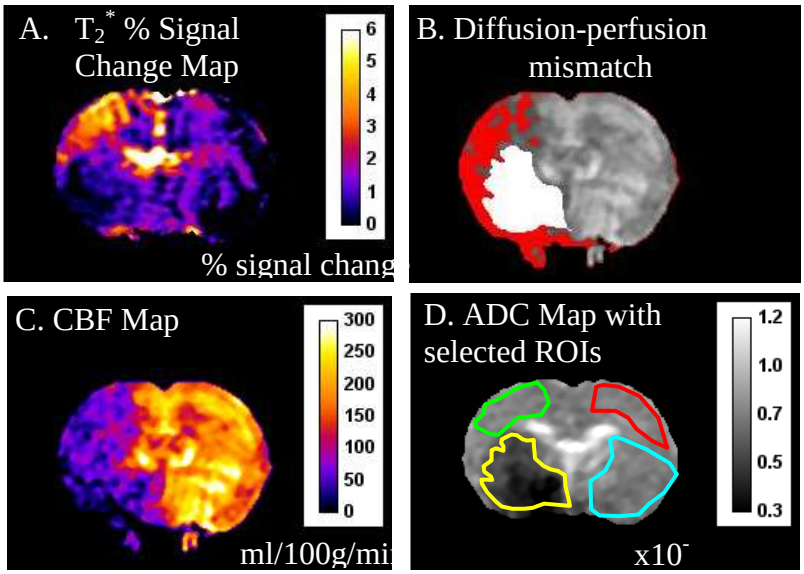

Figure 3.6. MRI scans used for data analysis. Regions of interest (shown in **D**) selected from a single MRI slice, where green ROI represents the T_2^*OC defined penumbra (from T_2^* % signal change map (**A**), the yellow ROI is the ADC-derived ischaemic core (from the ADC map), and the red and sky blue ROIs are the contralateral cortex and caudate, respectively. Penumbra defined from diffusion-perfusion mismatch is included for comparison (**B**)

CBF

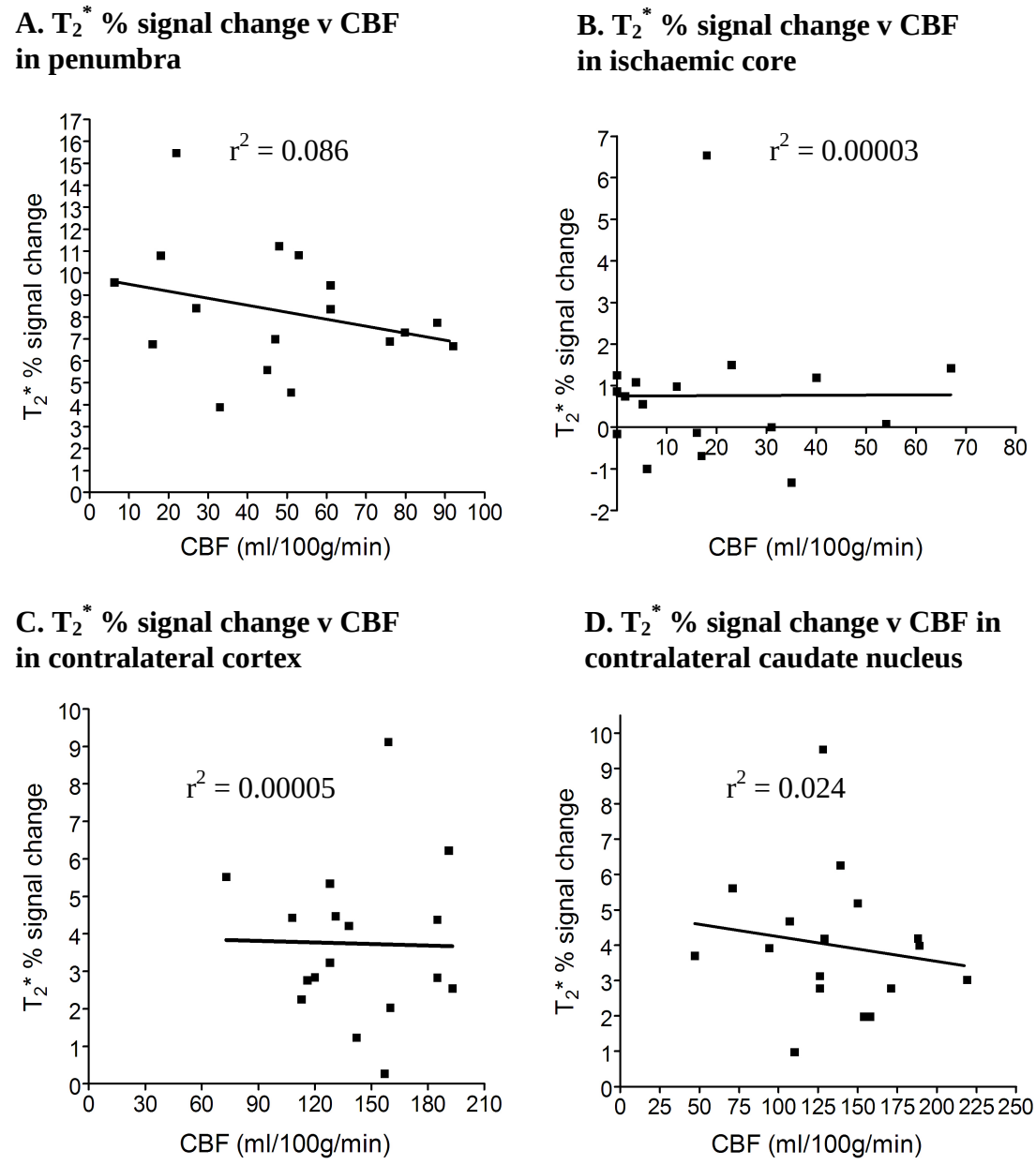

Figure 3.7. Correlation analysis between baseline CBF and T_2^* percentage signal change in; **A**. T_2^*OC defined penumbra, **B**. ADC-derived ischaemic core, **C**. Contralateral cortex and **D**. Contralateral caudate nucleus. n= 17. No significant correlations were found in the ipsilateral or contralateral cortex ROIs

Baseline PaO_2

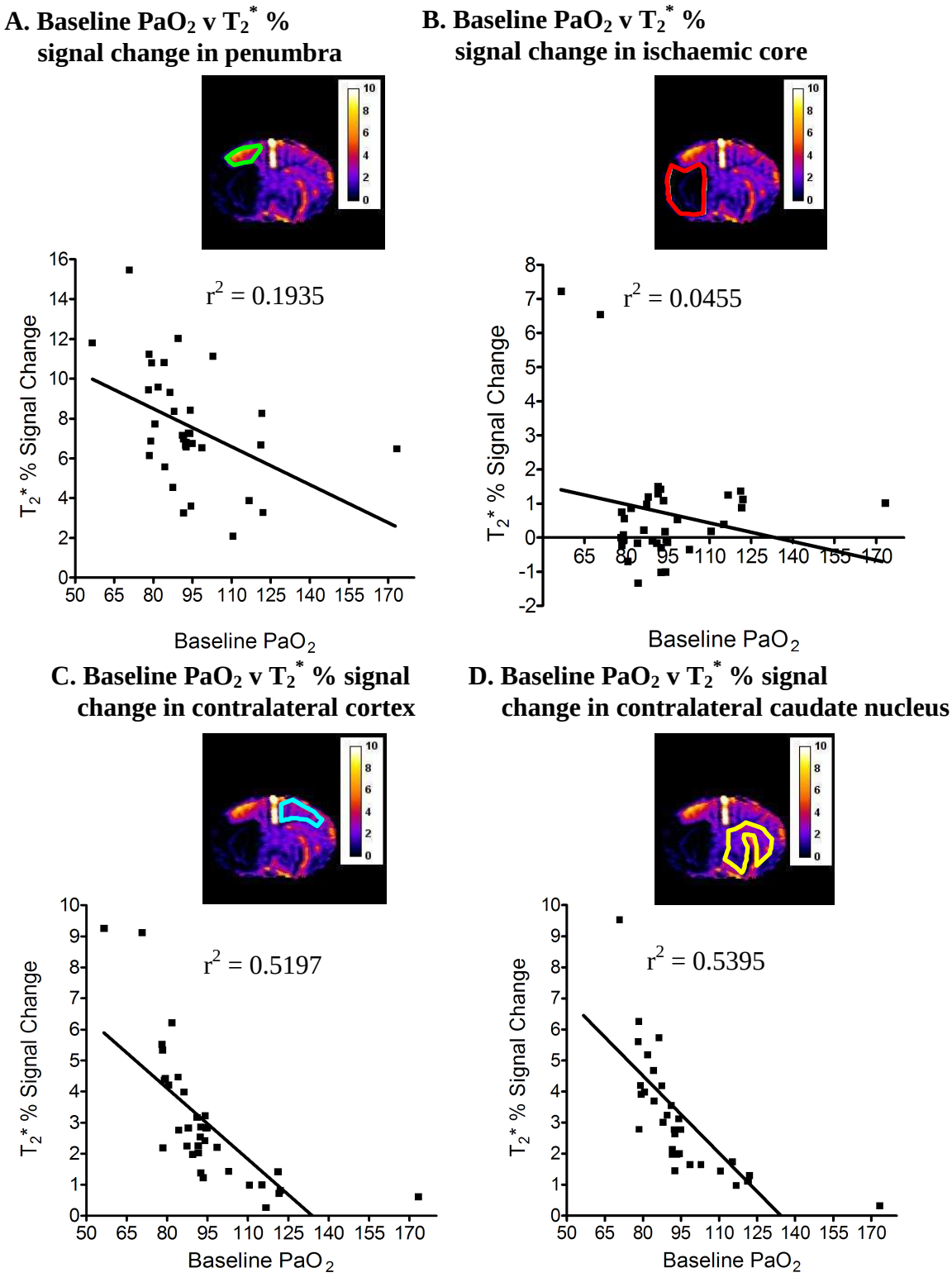

Figure 3.8. Correlation between baseline PaO_2 and T_2^* percentage signal change in; **A**. T_2^*OC defined penumbra, **B**. ADC-derived ischaemic core, **C**. contralateral cortex and **D**. contralateral caudate nucleus. The accompanying T_2^* % signal change maps show the regions of interest selected for analysis, n=35. A significant correlation was found in the penumbra and both contralateral ROIs, whereas no significant correlation was found in the ischaemic core

Oxygen Saturation

A. T_2^*% signal change v %O_2 saturation change in T_2^*OC defined penumbra

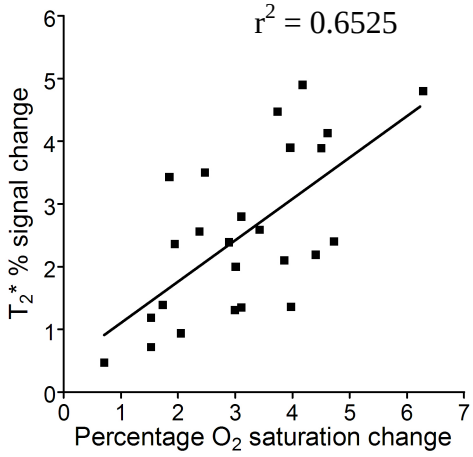

B. T_2^* % signal change v %O_2 saturation change in ischaemic core

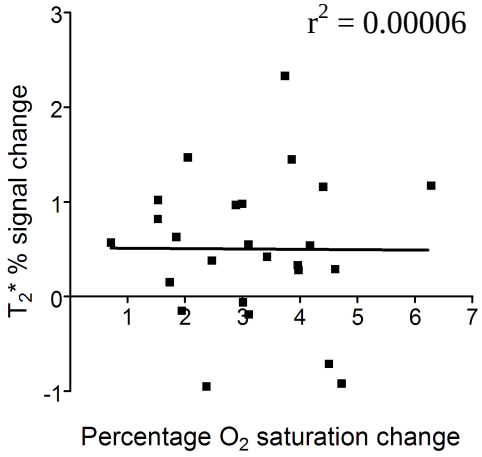

C. T_2^* % signal change v %O_2 saturation change in contralateral cortex

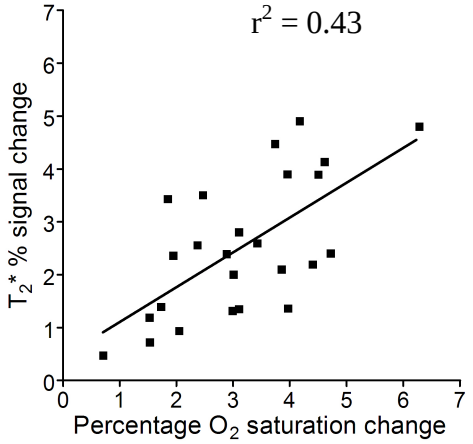

D. T_2^* % signal change v %O_2 saturation change in contralateral caudate nucleus

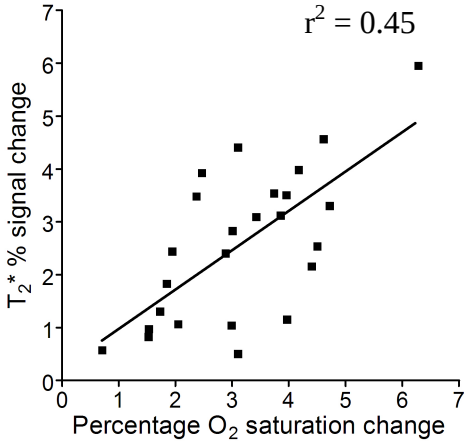

Figure 3.9. Correlation analysis between the percentage change in O_2 saturation from pre- to during-OC and T_2^* percentage signal change in; **A**. T_2^*OC defined penumbra, **B**. ADC-derived ischaemic core, **C**. Contralateral cortex and **D**. Contralateral caudate nucleus, n=25. A significant correlation was found in the contralateral ROIs, whereas no significant correlation was found in the ipsilateral ROIs

3.3 Discussion

3.3.1 Establishing reproducibility in the MCAO model using TTC and H&E to quantitatively assess infarct volume

The aim of the study was to achieve proficiency in the MCAO surgical technique and to successfully induce reproducible ischaemic lesions. The TTC immersion technique was performed to demonstrate the ability to occlude the middle cerebral artery using the intraluminal filament method, and to rapidly assess ischaemic damage. It was shown by the subsequent H&E dataset that reproducibility improved with practice, in that there was less variation in ischaemic lesion volume in these experiments.

The pilot study also allowed the comparison of two currently used methods to determine ischaemic damage, and to assess the merits and disadvantages of each. The main finding of this study was that the quantification of the infarct volume using TTC and histology differed. The result of the current study was in agreement with those found by Park and colleagues (1988), in which the TTC-measured ischaemic volume was significantly larger than the volumes measured histologically. There are considerable differences in the volumes of ischaemic damage determined by TTC and H&E histology due to the fact that histology involves the dehydration of the brain tissue which causes significant tissue shrinkage. Conversely, TTC immersed tissue slices retain their original size, and thus the TTC-stained tissue is larger than the histology-analysed tissue. This explains why the ischaemic volumes of the histological samples were consistently smaller than the TTC samples. Also, quantifying the infarct is subjective at the 4 hour mark, and tends to be based on individual interpretation when there is no sufficient, sharp demarcation between normal and infarcted tissue (Gerriets et al, 2004). The sharp gradient is more evident in TTC staining 24 hours post-stroke compared to 4 hours post stroke (Figure 3.10)

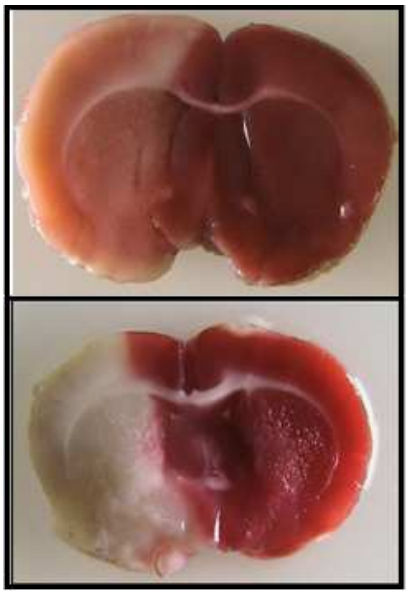

Figure 3.10. Comparison of TTC staining carried out at 4 hours and 24 hours post-stroke. Ischaemic damage is represented by paler or white tissue. Although the boundary of ischaemic damage is not clearly defined at 4 hours post-stroke, the staining is sufficient to determine if the MCA has been successfully occluded and damages both subcortical and cortical tissues

Benedek and colleagues (2006) noted that TTC staining can both under- and overestimate infarct volume due to marked metabolic changes over the course of evolution of brain infarction. Due to the fragile nature of brain tissue, there is a danger of the samples becoming damaged when sliced with the rat brain matrix. This introduces non-uniformity, in which the infarcted zone may become fragmented.

TTC immersion

TTC immersion is often preferred to H&E staining as it is inexpensive, technically simple, reliable and quicker. TTC has been validated for use 24 hours after injury (Bedersen et al, 1986). However, after 36 hours of ischaemia, infiltration of macrophages and microglia, neovascularisation and astrocytic reactions occur (Hudgins and Garcia, 1970) which can obscure the margin of ischaemia. However, according to Okuno and colleagues (2001), it should be generally accepted that the TTC immersion method requires a longer period than 4 hours of ischaemia for valid determination of infarcts. Bederson and colleagues (1986) compared the TTC immersion method and H&E staining in a rat MCA occlusion model over various periods of ischaemia. For accurate quantification of the infarct area, the ischaemia had to have lasted for at least 5–6 hours. Hatfeld and colleagues (1991) demonstrated that the TTC immersion method could not accurately determine rat brain ischaemic injury lasting 4 hours or less and they indicated that TTC immersion staining should only be used as a reliable marker of cerebral ischaemia damage with post-occlusion survival periods of 24 hours. Also, although the size of infarction can be measured using this technique, there can be no visualisation of the microscopic grey and white matter structures or individual cells.

H&E staining

In sections stained by H&E, the border between ischaemic damage and intact brain at 4 hours post-stroke was somewhat unclear, and was frequently designated by a zone, rather than a line, making the results for infarct size equivocal. Additionally, the transcribing onto line diagrams for quantification of ischaemic damage is difficult and subjective. This may give rise to slight errors in defining the zone of ischaemic damage.

3.3.2 Influence of baseline physiological state and CBF on T_2^*OC signal response to oxygen challenge

CBF

The data have shown that baseline CBF value did not influence T_2^* % signal change to OC. Further analysis of CBF during an OC protocol was performed by colleagues from our department (Baskerville et al, 2011) and this is presented in Chapter 7.

PaO_2

This study highlights the influence arterial oxygen levels have on the size of the T_2^* signal change to OC, with lower baseline PaO_2 levels amplifying T_2^* signal response and *vice versa* in ROIs still metabolically active, implying that control of physiological variables may optimise the T_2^*OC technique. The implications were that, for the subsequent studies, ventilation parameters were adjusted and OC imaging delayed until the animal was physiologically stable and blood gases were within a defined range [$PaCO_2$ 35-45 mmHg and PaO_2 80-100 mmHg]. Specifically, as T_2^* response was augmented at lower PaO_2 levels, ventilation parameters were adjusted to ensure that baseline PaO_2 was at the lower end of the normal range (~80 mmHg). This was particularly important for the serial scanning study (Chapter 6), in which signal responses were assessed at pre-determined time points and the effect of baseline physiology had to be minimised.

Oxygen saturation

It has been shown that the total deoxyhaemoglobin content and oxygen saturation has an effect on the BOLD response (Ogawa et al, 1992; Ogawa et al, 1993). The current study has shown that an increase in the percentage change in oxygen saturation following OC causes an increase in the T_2^* % signal change and *vice versa*, suggesting that the BOLD response is affected by baseline oxygen saturation. The signals within the blood vessels vary linearly with the venous concentration of deoxyhaemoglobin (Li et al, 1998), whereas extra-vascular signals depend on the total deoxyhaemoglobin content within a voxel, which becomes a larger component of the BOLD signal as field strengths increase (Obata et al, 2004). Thus, the BOLD signal would be expected to vary as a function of both oxygen saturation and blood volume (Huppert et al, 2006; Ogawa et al, 1993; Buxton et al, 1998).

In the current study, the baseline oxygen saturation often varied from 96-98% and went up to approximately 99% on OC. This may be more varied than what would be expected in human clinical presentation because of the effect of the rat's anaesthesia and artificial ventilation. If the baseline oxygen saturation could be fixed (using a pulse oximeter to measure oxygen saturation) throughout the experiments, it may be possible to standardise the technique.

3.4 Summary

Proficiency in inducement of middle cerebral artery occlusion using the intraluminal filament was achieved, and the effect of various parameters on the extent of the T_2^* response to OC was examined. It was found that both PaO_2 and oxygen saturation have significant influences on T_2^* signal change in metabolising tissue – within the contralateral hemisphere and in tissue identified as penumbra. With this in mind, these parameters were monitored and controlled in subsequent studies to limit variability in the T_2^* response.

Chapter

4

Validating T_2^*OC using [^{14}C] 2-Deoxyglucose Autoradiography

4.1 Introduction

The gold standard physiologic imaging technique used to identify penumbral tissue is PET, which measures both metabolic activity and perfusion (Marchal et al, 1993). PET can identify that penumbral oxidative metabolism ($CMRO_2$) is maintained in the face of reduced cerebral perfusion pressure by increasing oxygen extraction fraction (Powers, 1991; Baron, 1999; Marchal et al, 1993). This, in turn, increases the deoxy: oxyhaemoglobin ratio in the vasculature, resulting in a decreased T_2^* signal within penumbra. Increased oxygen delivery during OC will convert deoxyhaemoglobin back to oxyhaemoglobin with a resultant increase in T_2^* signal - the magnitude of which should be greatest in regions with greatest oxygen extraction fraction (OEF).

Whilst the OC predicates that $CMRO_2$ and OEF are the components responsible for the elevated T_2^* signal response in the penumbra, they cannot be directly measured with MRI. However, indirect measurements of metabolism can be employed to confirm the viability of discrete brain regions, including [^{14}C] 2-deoxyglucose (2DG) autoradiography. Glucose plays a fundamental role in the mammalian brain, in that it is - along with oxygen - a principle fuel for energy metabolism, and it is the only substrate able to completely sustain neural activity (Siesjo, 1978). In the basal and activated state, cerebral glucose utilisation fuels neuronal activity via oxidative metabolism. Since cerebral blood flow is intricately linked to the cerebral metabolic rate of oxygen, $CMRO_2$, there is a coupling of flow and metabolism under normal conditions (Roy and Sherrington, 1890; Sokoloff, 1976; Sokoloff et al, 1977). There are comparable functional increases in blood flow and 2DG uptake which in turn is directly related to neuronal activity (Magistretti, 2006).

In a previous study (Santosh et al, 2008), the OC technique applied to a rodent MCAO model defined an inner boundary between metabolically inactive ischaemic core (no T_2^* signal increase to OC) and metabolically active penumbra (T_2^* signal increase to OC),

which overlapped approximately with DWI/PWI mismatch, and correlated with histological evidence for neuronal integrity. The differences in magnitude of T_2^* signal in ischaemic core, penumbra and normal cortex during OC may differentiate between core, hypoperfused penumbra and benign oligaemic tissue on the basis of differences in $CMRO_2$, thereby providing a means of defining the boundaries of the penumbra.

The aim of this study was to provide further validation for the T_2^*OC MRI technique, first by determining the viability of tissue within regions defined as penumbra using OC. This was achieved by co-registering T_2^*OC maps with corresponding [^{14}C] 2-deoxyglucose autoradiograms, which provide information on local cerebral glucose utilisation (LCMRglc) as a quantitative representation of metabolic activity. Second, regions of interest (ROIs) identified on 2DG autoradiograms and MRI scans were investigated to determine the LCMRglc and MRI signatures of different tissue compartments in the ischaemic hemisphere.

4.2 Materials and methods

4.2.1 Rodent MCAO Surgery

Experiments were performed under license from the UK Home Office and were subject to the Animals (Scientific Procedures) Act, 1986. Male Sprague Dawley rats (289±13 g, n=6, Harlan, Bicester, UK), fasted overnight, were initially anaesthetised with 5% inhaled isoflurane in an induction chamber at room temperature. Following a surgical tracheotomy, animals were artificially ventilated with 2% isoflurane delivered in air, slightly enriched with oxygen (30%) to maintain physiological stability throughout the experiment. Blood gases were sampled at baseline in the 5 min before the start of OC, and half way through 100% O_2 inhalation. Blood gases were maintained within the normal physiological range apart from increased PaO_2 during the oxygen challenge. $PaCO_2$ was maintained between 35 - 45 mm Hg to minimise cerebrovascular reactivity (Table 4.1). A rectal thermocouple provided continual monitoring of core body temperature which was maintained at 37±0.5^{o}C.

Polyethylene catheters (Portex: external diameter 0.96 mm; internal diameter 0.58 mm; 70 cm long) were placed in both femoral arteries, to continuously monitor blood pressure and conduct blood gas analysis, and the femoral vein was cannulated for [^{14}C] 2-deoxyglucose

administration. Middle cerebral artery occlusion was achieved by the intraluminal filament technique (Longa et al, 1989), where a 3-0 nylon monofilament with a bulbed tip was introduced through the internal carotid artery and advanced to block the origin of the middle cerebral artery (described in Chapter 2.2.3).

4.2.2 Magnetic Resonance Imaging scanning

Magnetic resonance imaging data were acquired on the system as described in Chapter 2.5.1.

T_2 scanning

A RARE T_2 provided the neuroanatomical template for co-registration of T_2^* scans with DWI and PWI scans and 2DG autoradiograms (Figure 4.1A & B).

T_2^* scanning

The sequence used to measure T_2^* changes during OC is described in Chapter 2.5.6. Two coronal MRI slices which corresponded to territory supplied by the middle cerebral artery were selected for analysis. The paradigm for the T_2^* weighted oxygen challenge sequence was 5 minutes ventilation on air, followed by 5 minutes ventilation on 100% oxygen, and then 15 minutes ventilation on air.

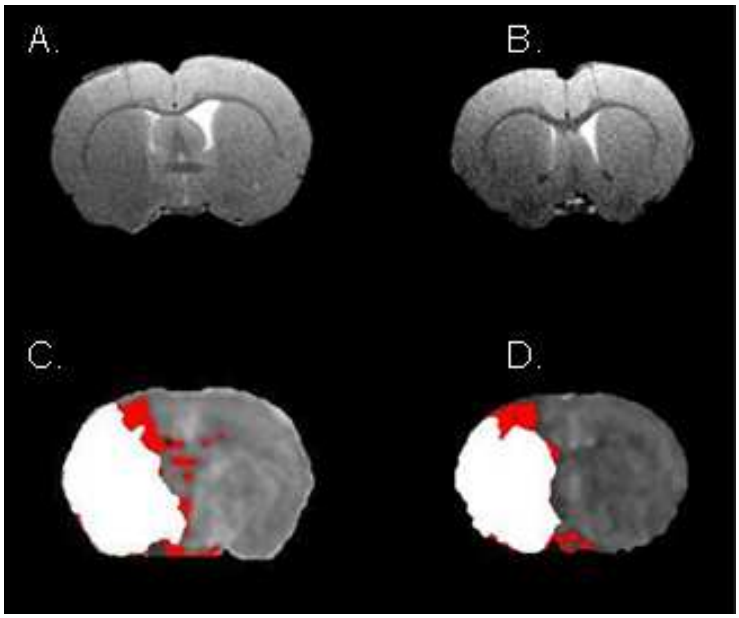

Figure 4.1. RARE T_2 neuroanatomical templates for caudal (**A**) and rostral (**B**) middle cerebral artery territory coronal slices of interest. Corresponding coregistered perfusion-weighted imaging (PWI) and diffusion-weighted imaging (DWI) thresholded images displaying DWI lesion (white) superimposed on perfusion deficit (red), revealing DWI/PWI mismatch areas for caudal (**C**) and rostral (**D**) slices. ASL scans were thresholded using a 57% reduction in the mean contralateral values (Meng et al, 2004); whereas the ADC maps were thresholded using a 16.5% reduction in the mean contralateral values (Lo et al, 1997)

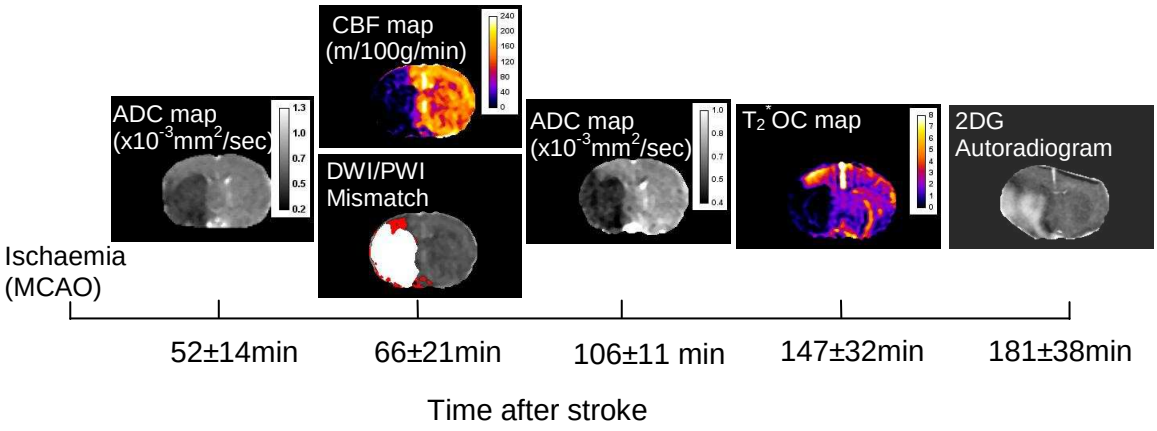

Figure 4.2. Time line of experimental protocol. Following stroke, the animals were placed in the magnet and a DWI scan was performed to identify ischaemic damage. An ASL scan was then performed to generate fully quantitative CBF maps and mismatch images were generated using these data. A second DWI scan allowed the evolution of ischaemic damage to be assessed. OC scanning was then performed to derive T_2^* percentage signal change maps, and finally, [^{14}C] 2DG autoradiography produced glucose utilisation images

Diffusion-weighted imaging

DWI was performed using the sequence described in Chapter 2.5.3 to identify ischaemically injured tissue.

Arterial Spin Labelling

Non-invasive quantitative CBF was carried out on 2 of the 8 coronal slices (slices 5 & 6, moving rostro-caudally) within the MCA territory as described in Chapter 2.5.4.

4.2.3 [^{14}C] 2-deoxyglucose autoradiography

[^{14}C] 2-deoxyglucose autoradiography was performed according to Chapter 2.4. Quantitative optical density measurements were taken from five ROIs (defined in detail in section 4.2.4 and in the legend for Figure 4.3): (1) ischaemic core; (2) penumbra; (3) an intermediate region of increased 2DG phosphorylation within the boundary of the ischaemic core (see Figure 4.32C); (4) and (5) contralateral regions homotopic to the penumbra and ischaemic core, respectively. Optical density values were converted into ^{14}C tissue concentrations using the calibration curve derived from the set of ^{14}C standards. The ^{14}C tissue concentrations along with the plasma glucose and ^{14}C plasma concentrations were used to calculate LCMRglc (μmol per 100g per minute) in ROIs using the operational equation of Sokoloff et al (1977) (Figure 2.9).

Glucose utilisation for each ROI was generated from 10 autoradiographic images covering the rostro-caudal extent of each MRI slice (1.5 mm) to accurately equate T_2^* signal change maps with glucose utilisation.

[^{14}C] 2-deoxyglucose autoradiography in conscious rats

LCMRglc values generated in our study were considerably lower than values documented in the literature, which are almost exclusively from conscious animal experiments. Anaesthetic presence and duration (approximately 6 hours) is the most likely explanation for the lower values as it is known to significantly inhibit metabolism. Consequently, [^{14}C] 2-deoxyglucose autoradiography was carried out on a conscious naive rat and conscious stroke rat in order to confirm this point. Rats were anaesthetised for approximately 45

minutes during surgery and given 2 hours to recover from anaesthesia before beginning the 2DG experiment.

4.2.4 Regions of interest analysis

Circular ROIs were selected according to specific features on the images (Figure 4.3). To ensure placement solely within the areas of interest and uniformity in ROI size, ROIs were chosen manually (spanning 80 pixels). During ROI placement, I was blinded to the autoradiography data and *vice versa*. MRI-based ROIs were defined and placed within (1) ischaemic core in caudate nucleus within the thresholded ADC lesion (Figure 4.3E, red); (2) its mirror contralateral region (sky blue), manually designated; (3) penumbra as defined by thresholded T_2^* percentage signal change (Figure 4.3B, green); (4) equivalent contralateral cortex (white), and (5) a cortical region of increased 2DG phosphorylation selected from the 2DG autoradiogram (Figure 4.3C, yellow).

Coregistration and regions of interest analysis

The processed data from the T_2^*OC, 2DG, thresholded ADC and CBF maps, were coregistered to: (1) generate ROI data and; (2) identify the location of the DWI/PWI mismatch (Figures 4.3C and D). Linear coregistration was first performed using Analyze (AnalyzeDirect, Inc. Overland Park, KS, USA) and then DWI, ASL, T_2^*- and 2DG images were warped to their corresponding RARE T_2 slices using AIR 5.2.6 (Automated Image Registration (Woods et al, 1998).

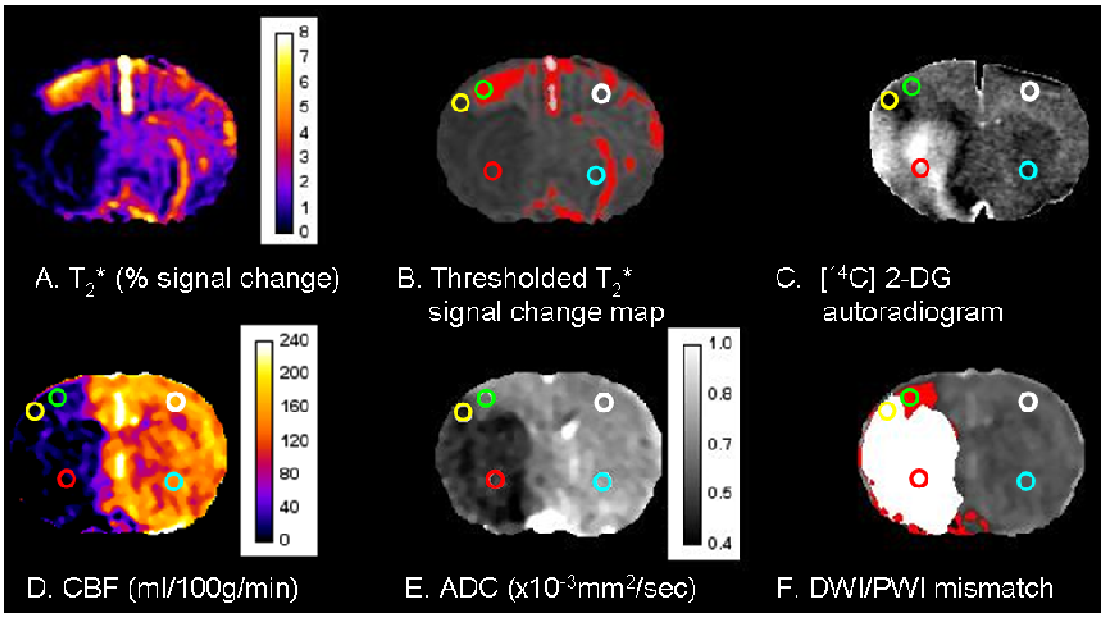

Figure 4.3. Representative MRI maps and 2DG autoradiograms from a rostral slice (slice 6 moving rostro-caudally) in a stroke rat; (**A**) T_2^* oxygen challenge (OC) percentage signal change map; (**B**) Thresholded T_2^*OC map; (**C**) [^{14}C] 2DG autoradiogram; (**D**) CBF map in mL/100g/min; (**E**) ADC map (x10^{-3} mm^2/sec) and; (**F**) DWI/PWI overlay (mismatch tissue is shown in red). ROIs were defined as follows: Green ROI: penumbra—the thresholded region displaying the greatest T_2^* percentage signal change excluding veins and ventricles (**B**). Yellow ROI: region of increased 2DG phosphorylation—identified by the dark band within the ipsilateral cortex on the 2DG autoradiogram (**C**). Red ROI: ischaemic core—within the ADC-derived lesion in the caudate nucleus (**E**). White ROI: contralateral cortex—homotopic to the penumbra ROI. Sky Blue ROI: contralateral caudate nucleus—homotopic to the ischaemic core ROI

4.2.5 Defining the ischaemic penumbra with T_2^*OC

The time course and size of the T_2^* signal change was analysed within ROIs (Chapter 2.5.6). T_2^* percentage signal change was calculated from time course graphs, where the average baseline signal during the first 3 min of the MRI scanning was subtracted from the peak signal during OC. This value was then divided by the average baseline signal and multiplied by 100 to generate a percentage signal change. T_2^*OC percentage signal change maps were generated using Image J software. Penumbral tissue was defined on T_2^* maps using a threshold based on the empirical rule: the mean plus 2 SD of the T_2^* value of the contralateral hemisphere, excluding the ventricles (see Figure 4.3B).

4.2.6 Defining the ischaemic penumbra with DWI/PWI Mismatch

DWI and PWI (using ASL) were used to define mismatch, before the T_2^*OC data were analysed, on two selected coronal slices within the MCA territory (Figure 4.1). The DWI/PWI mismatch method was included as an alternative indirect technique currently used to identify penumbra. It was used to compare the location of presumed penumbra between the two techniques. However, there are a number of limitations to the mismatch technique, which will be discussed further in Chapter 6. Quantitative ADC maps, in units of square millimeters per second, were calculated using the Stejskal–Tanner equation (Stejskal and Tanner, 1965). ADC and CBF maps were generated using ImageJ software. A 16.5% reduction of mean contralateral ADC was used to determine ischaemic lesion volume, which has been shown to match closely the final infarct size following permanent MCAO in Sprague-Dawley rats (Lo et al, 1997). Perfusion-weighted imaging was performed on the fifth and sixth coronal slices within core MCA territory and the perfusion deficit area was calculated based on a 57% reduction of mean contralateral CBF (Meng et al, 2004). ADC and CBF maps were overlaid to identify the DWI/PWI mismatch area defined as the difference between the perfusion deficit and the ADC lesion area on the corresponding slice. For analysis, the data for the rostral and caudal slices were combined.

4.2.7 Volumetric analysis of penumbra, hypo- and hyperglycaemic tissues

Volumetric analysis of penumbra (from DWI/PWI mismatch and the T_2^*OC), ADC-defined lesion, perfusion deficit and hypo- and hyperglycaemic tissue on 2-deoxyglucose autoradiograms were performed and data expressed as the mean volume over the rostro-caudal extent of the ASL scans. For 2DG autoradiograms, images were analysed to cover

the same rostro-caudal extent as the MR images, and were thresholded to determine the region of severely reduced glucose use (glucose values below 10 μmol per 100g per minute) and the region of increased 2DG phosphorylation (tissue with glucose values above 60 μmol per 100g per minute). The thresholds were determined by retrospectively analysing the glucose utilisation data points (Figure 4.6), and it found that all regions regarded as normal in the contralateral hemisphere had glucose values above 10 μmol per 100g per minute. Similar thresholding was used for the region of increased 2DG phosphorylation, in which all values in this rim had glucose values above 60 μmol per 100g per minute, and the values in the contralateral and penumbra did not exceed this.

4.2.8 Statistical analysis

All data are presented as mean±SD. All data were tested to confirm normal distribution using the D'Agostino and Pearson normality test. Data were found to be normally distributed, and as such, physiological variables at baseline (pre-OC) and during OC were analysed by Student's paired t-test. T_2^* signal, ADC, CBF, and LCMRglc values in different ROIs were analysed by one-way analysis of variance followed by Student's paired t-test with a Bonferroni correction for multiple comparisons. A paired t-test was used to analyse the temporal evolution of the ADC-derived lesion volume.

4.3 Results

4.3.1 Physiological variables

Mean time to commence OC was 147±32 minutes after MCAO. Physiological variables were recorded immediately before and during OC (Table 4.1). PaO_2 increased significantly (262%, $p<0.0001$) as expected during OC, $PaCO_2$ did not change significantly and mean arterial blood pressure increased significantly (11%, $p<0.05$). The mean plasma glucose before scanning was 9.8±2.7 mmol/L.

4.3.2 T_2^* percentage signal change to OC

T_2^* percentage signal change during OC was measured over two coronal slices. Thresholded T_2^* maps revealed a region of increased signal, which corresponded approximately with the DWI/PWI mismatch (Figures 4.3B & F, respectively). Examining the individual T_2^* time course data (Figure 4.4), T_2^* signal increase in this penumbral ROI was 9.2±3.9%, significantly greater than in the contralateral ROI (2.76±0.3%, $p<0.001$; Figure 4.5). In ischaemic core, mean T_2^* signal during OC was reduced (−0.49±1.6%) compared with the contralateral caudate nucleus ROI (3.56±0.94%, $p<0.01$). In the ROI with increased 2DG phosphorylation, there was a small T_2^* signal increase of 1.4±0.6%, significantly smaller than the response in the contralateral cortex ($p<0.05$) and penumbral ROIs ($p<0.001$).

Physiological Data (n=6)		
	Baseline	During OC
MABP (mmHg)	82.4±7	91.4±6.7*
$PaCO_2$ (mmHg)	34.8±7	36.3±8.5
PaO_2 (mmHg)	85.8±7.4	310.6±84.1**
Blood pH	7.32±0.04	7.32±0.04

Table 4.1. Physiological variables at baseline (the 5 min of air inhalation immediately before OC) and during oxygen challenge. Data expressed as mean±SD, * $p<0.05$ and ** $p<0.0001$, Student's paired t-test

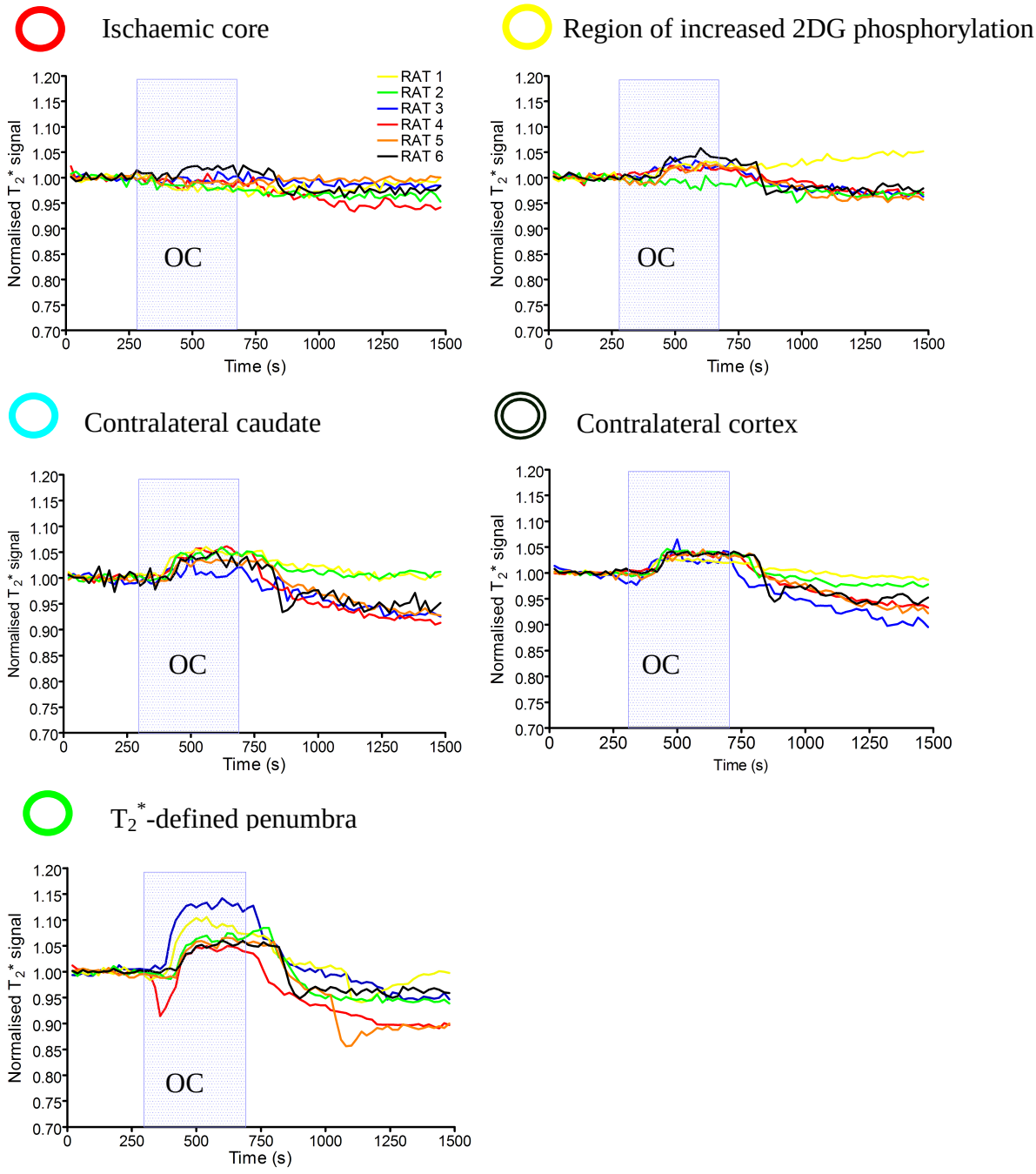

Figure 4.4. EPI T_2^* oxygen challenge (OC) signal time course: time course showing T_2^* signal change during OC in: ADC-derived ischaemic core (red circle); cortical region of increased 2DG phosphorylation from 2DG autoradiogram (yellow circle); a region corresponding to the greatest T_2^* percentage signal change increase adjacent to region of increased 2DG phosphorylation (green circle); corresponding regions on the contralateral cortex (black circle) and caudate nucleus (sky blue circle). Each line represents data from a single animal. Within each animal, all data were normalised to the average signal over the 5-minute before OC. Blue box represents the period of 100% oxygen inhalation

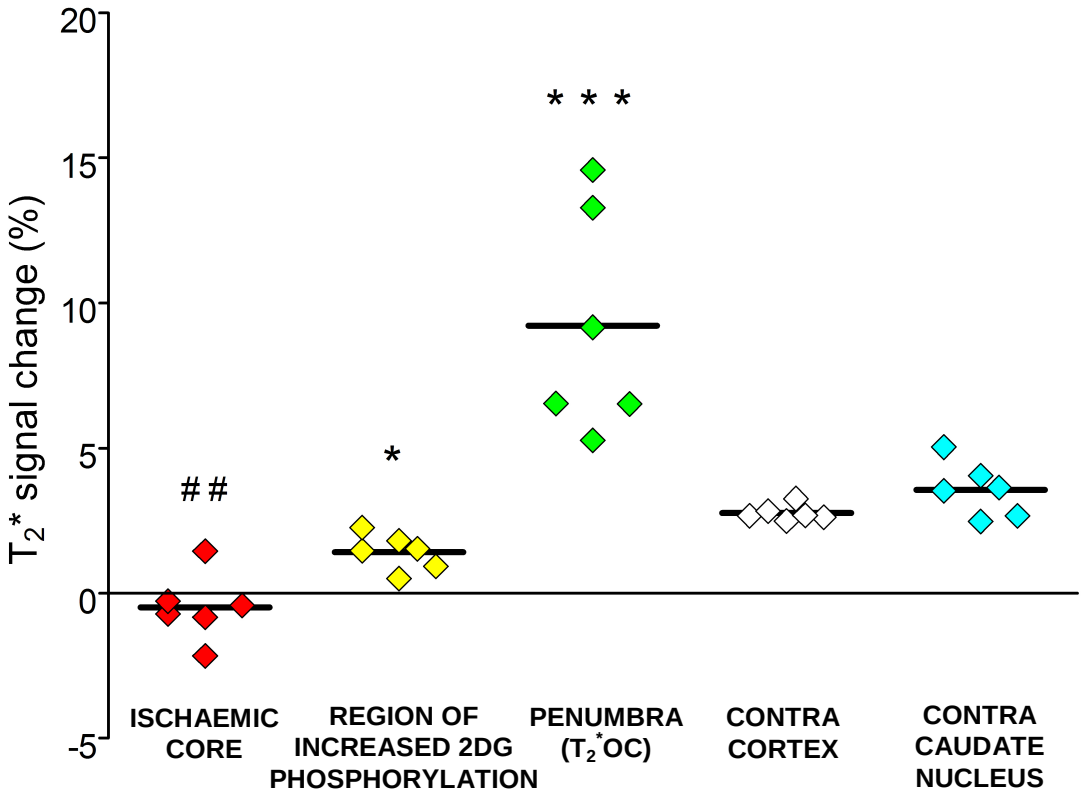

Figure 4.5. T_2^* percentage signal change from baseline in ROIs. These are individual animal data with horizontal lines representing means. ***p<0.001 and *p<0.05 relative to contralateral cortex ROI. ## p<0.01 relative to contralateral caudate nucleus. Contra = contralateral

4.3.3 Glucose use values in ROIs

[^{14}C] 2-deoxyglucose autoradiography revealed at least three different glucose use values in the ischaemic hemisphere; the ischaemic core registered severely reduced glucose values, a region of increased 2DG phosphorylation on the periphery of the ischaemic core, and an adjacent region which displayed glucose utilisation values equivalent to the contralateral values. The contralateral hemisphere displayed relatively heterogeneous glucose utilisation apart from the white matter, which registered low glucose utilisation values. [^{14}C] 2-deoxyglucose autoradiography confirmed glucose use within the T_2^*OC-defined penumbra, which was not significantly different from the contralateral ROI (22.67±2.1 μmol per 100g per minute compared with 20.1±2.3 μmol per 100g per minute; Figure 4.6). Glucose use was below the limit of detection in ischaemic core (Figures 4.3C and 4.6) and it was markedly increased in the region of increased 2DG phosphorylation (79.7±12 μmol per 100g per minute, compared with contralateral cortex 20.1±2.3 μmol per 100g per minute, $p<0.001$). The region of increased 2DG phosphorylation (279% increase in LCMRglc compared to the contralateral cortex) was located within the boundary of the ADC lesion. It displayed a small increase in T_2^* signal to OC, which was significantly smaller ($p<0.05$) than the T_2^* increase observed in the contralateral cortex (Figure 4.5).

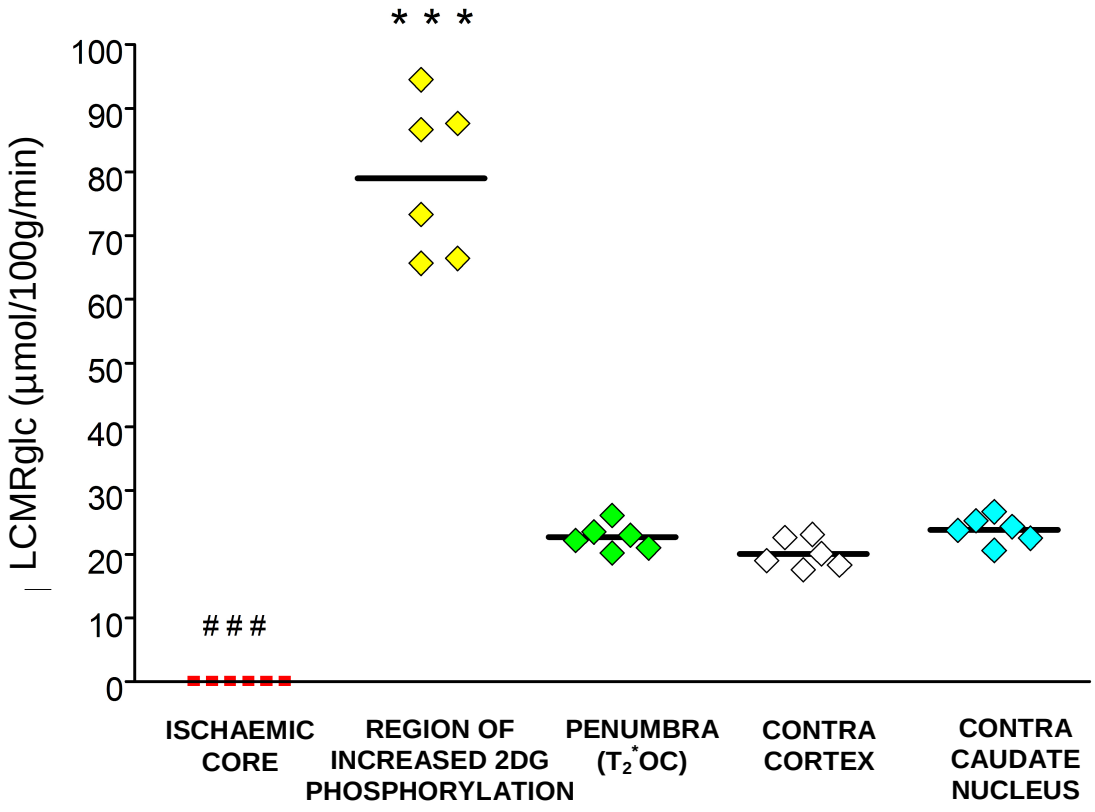

Figure 4.6. Local cerebral glucose utilisation (LCMRglc) in ROIs. These are individual animal data with horizontal lines representing means. ***p<0.001 relative to contralateral cortex. ### p<0.001 relative to contralateral caudate nucleus

Absolute glucose utilisation values in the hemisphere contralateral to the stroke were low compared with most values from the literature, which are generated from conscious animals. To confirm the validity of our 2DG technique, in an additional animal, anesthesia was withdrawn following MRI scanning and 2DG autoradiography performed 2 hours later when the animal was fully conscious (Figure 4.7). Glucose use values were similar to reported values and proportionally higher in each ROI when compared with anesthetised animals (Table 4.2). The contralateral cortex and caudate registered an LCMRglc value of 41.67 and 46.7 μmol per 100g per minute and penumbral and region of increased 2DG phosphorylation LCMRglc values displayed a 66% and 118% increase relative to contralateral cortex, respectively. Conversely, the ischaemic core had a 97% decrease in LCMRglc relative to contralateral caudate nucleus. Therefore, the low glucose utilisation values in the MRI study were most likely due to the level and duration of anesthesia

To dismiss the possibility that the presence of the region of increased 2DG phosphorylation may be a confound of O_2 administration, an additional rat underwent MCAO, and when fully conscious, 2DG autoradiography was performed without OC (Figure 4.8). The region of increased 2DG phosphorylation was present, suggesting the OC *per se* was not responsible for generating increased 2DG phosphorylation.

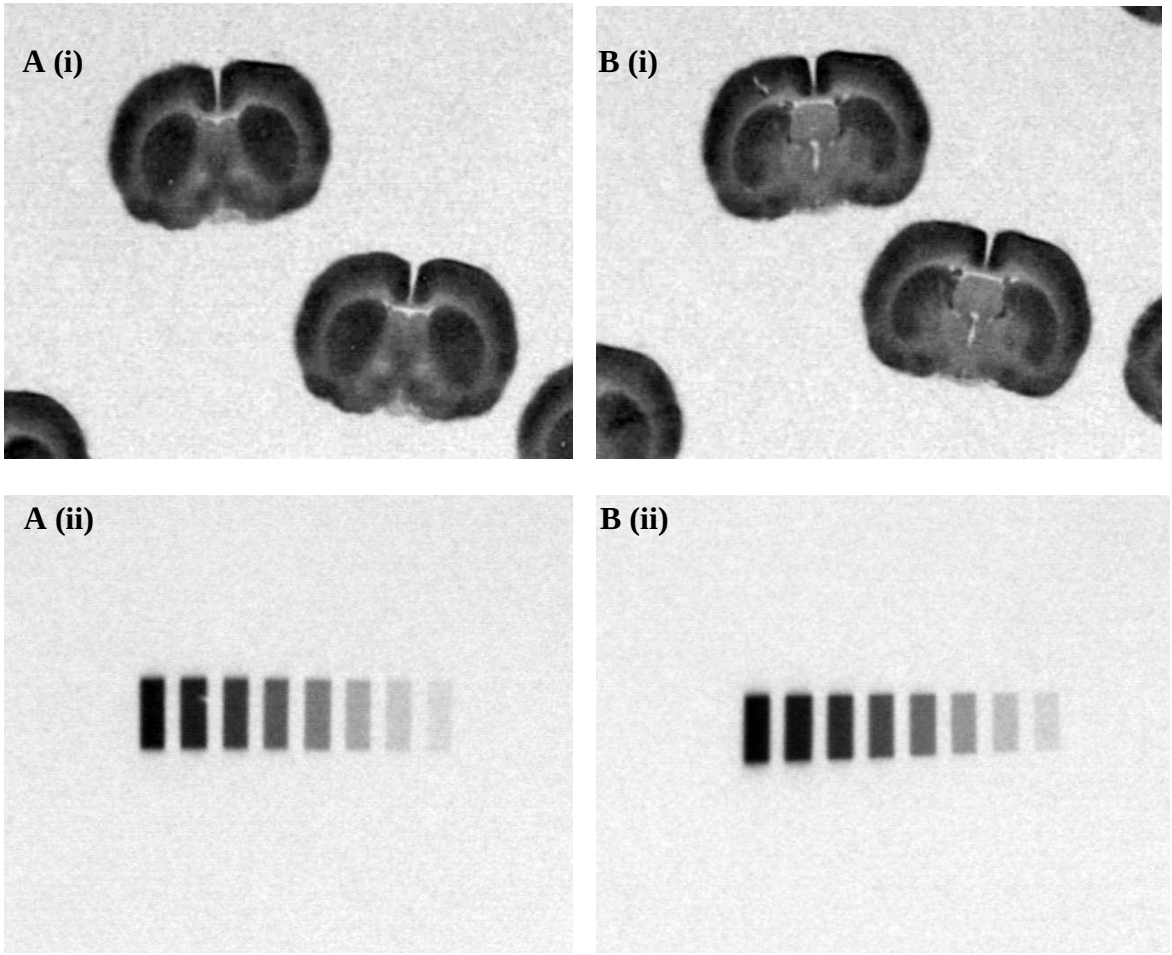

Figure 4.7. Example 2DG autoradiograms from animals that did not undergo MCAO. **A (i)** A normal conscious rat and accompanying [^{14}C] calibration standards (**A (ii)**). **B (i)** A normal anaethetised rat (RHS), and the accompanying [^{14}C] calibration standards **(B (ii)).** LCMRglc values generated from the conscious animal were similar to values in the literature

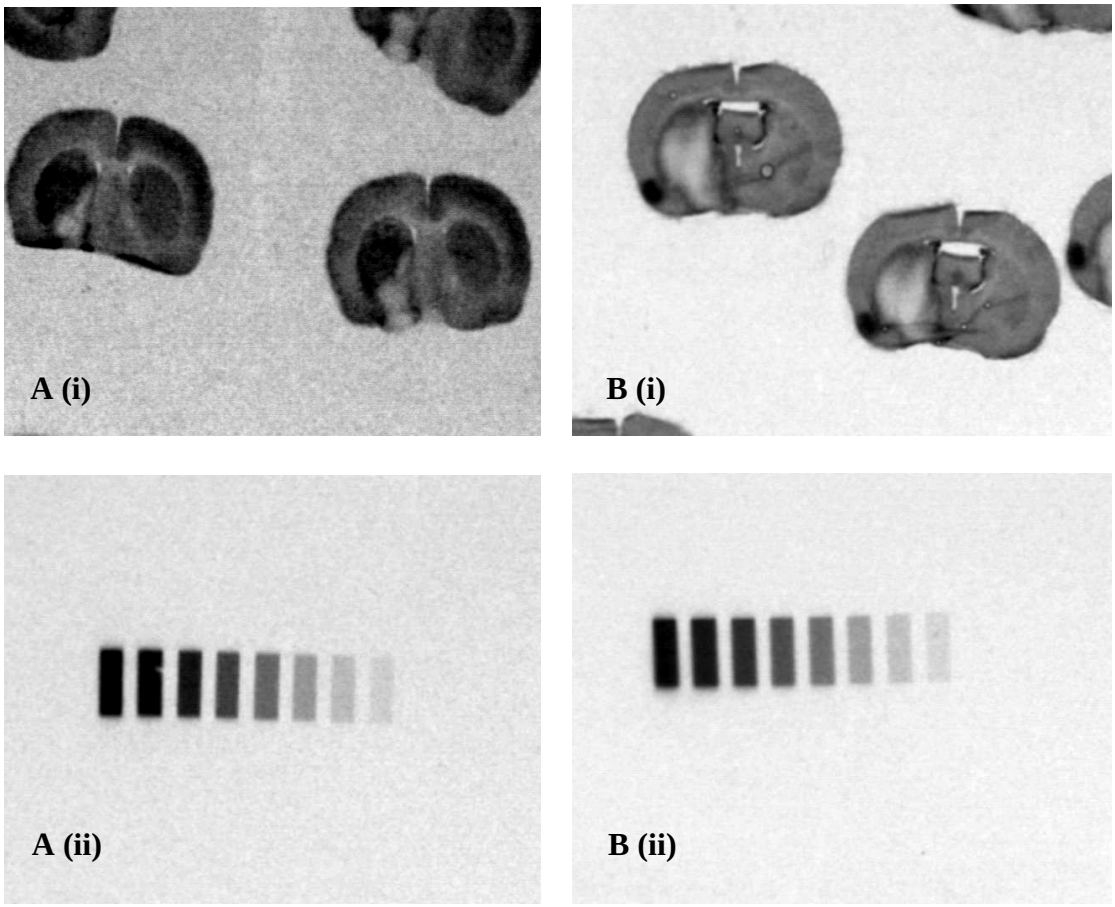

Figure 4.8. Example 2DG autoradiograms from animals that underwent MCAO. A (i) Conscious rat and accompanying [^{14}C] calibration standards **(A (ii)**). **B (i)** An anaesthetised rat with accompanying [^{14}C] calibration standards **(B (ii)).** The dark region of increased 2DG phosphorylation adjacent to the region of critically reduced glucose use which corresponds to the ischaemic damage

A.

	Glucose Utilisation Values (µmol/100g/min)
Region of Interest	**Conscious Normal Rat**
Left Cortex	45.1
Left Caudate Nucleus	48
Right Cortex	42.6
Right Caudate Nucleus	50.3

B.

	Glucose Utilisation Values (µmol/100g/min)
Region of Interest	**Conscious Stroke Rat**
T_2^*OC defined penumbra	69
Contralateral Cortex	41.7
Contralateral Caudate Nucleus	46.7
Increased 2DG phosphorylation region	91
Ischaemic Core	1.43

Table 4.2. Glucose utilisation values (µmol/100g/min) for **A**. a fully conscious control rat and **B**. a fully conscious rat 1 hour after MCAO

4.3.4 Severity of Ischaemia and tissue viability

On quantitative CBF maps (Figure 4.3D), contralateral cortex and caudate nucleus ROIs had mean CBF values of 185±45 and 165±31 mL per 100g per minute, respectively. In the ipsilateral hemisphere, there was severe or critically reduced CBF within MCA territory that matched spatially with the ADC-derived ischaemic core, and there were incremental gradations in CBF from the MCA territory outward. Cerebral blood flow within ischaemic core, region of increased 2DG phosphorylation and penumbra ROIs was significantly reduced (7.9±4.7, 21±0.2 and 37±66 mL per 100g per minute, respectively, all $p<0.001$) relative to the equivalent contralateral ROI (Figure 4.9A).

On ADC maps (Figure 4.3E), ROIs in contralateral cortex and caudate nucleus had a mean ADC of 0.73±0.06 and 0.74±0.02 $x10^{-3}mm^2/s$, respectively (Figure 4.9B). Apparent diffusion coefficient values were significantly reduced in ischaemic core and region of increased 2DG phosphorylation ROIs (0.47±0.04 and 0.51±0.08 $\times10^{-3}mm^2/s$, respectively, $p<0.001$), while in the T_2^*OC-defined penumbral ROI, mean ADC value (0.71±0.04 $x10^{-3}mm^2/s$) was not significantly reduced compared with contralateral cortex ($p>0.05$; Figure 4.9B).

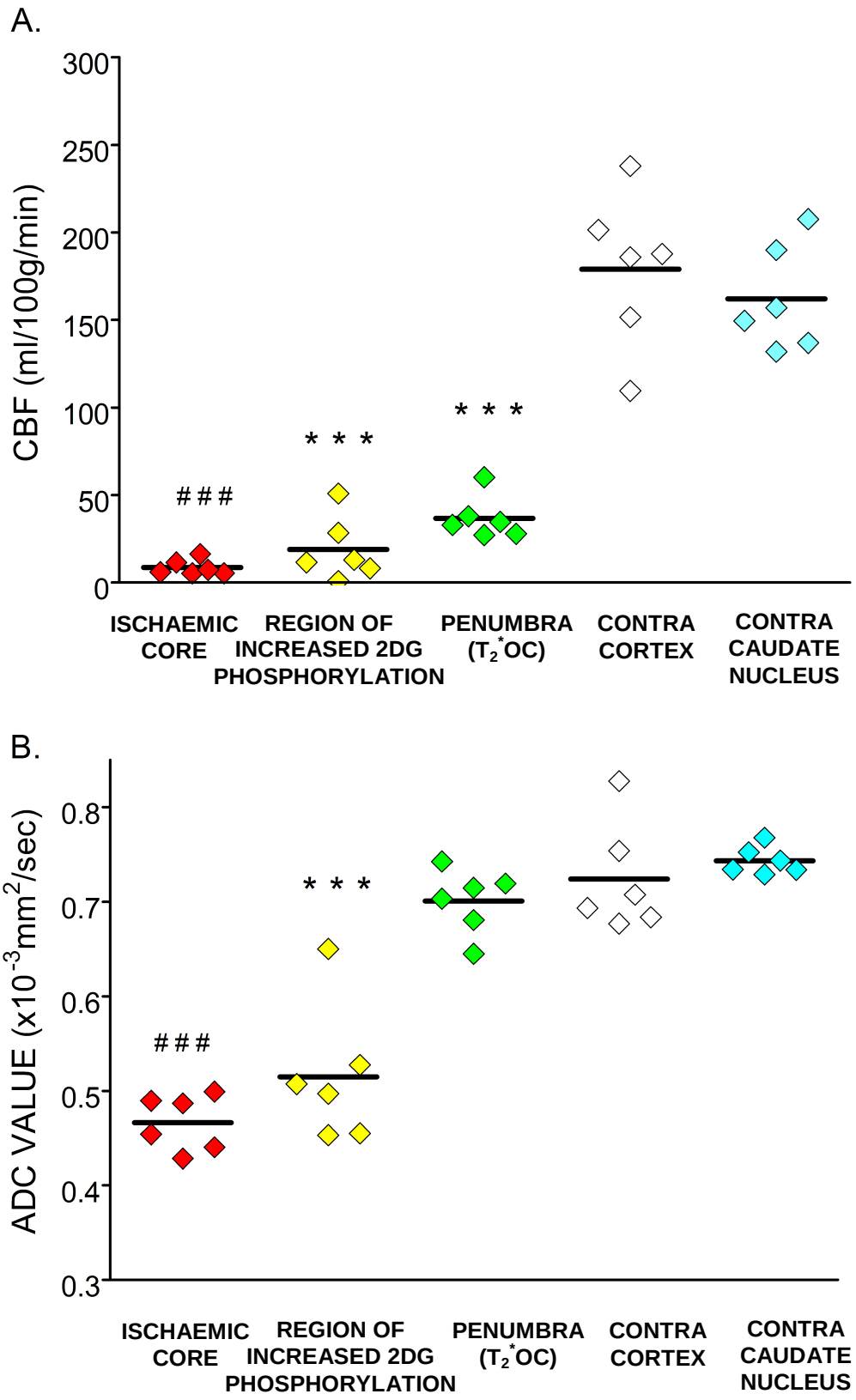

Figure 4.9. CBF (**A**) and ADC (**B**) in ROIs. Individual animal data with horizontal lines representing means. ***, ### ($p<0.001$) relative to contralateral cortex and contralateral caudate nucleus, respectively

4.3.5 Volumetric analysis of penumbra, hypo- and hyperglycaemic tissues

For comparison, penumbra as defined by DWI/PWI mismatch, was mapped over two coronal slices from the coregistered ADC and ASL scans (Figures 4.3C & D and 4.3F). The volume of perfusion deficit determined at 76.4±13.2 minutes after stroke, was 103.1±21 mm^3, the ADC lesion volume, determined at 106±8 minutes after stroke was 80.7±30 mm^3, generating a DWI/PWI mismatch volume of 22.3±19 mm^3. The thresholded T_2^*OC-defined penumbra, determined at 147±32 minutes, was 15±9 mm^3. Mismatch- and T_2^*OC-defined penumbral volumes were ~28% and 19% of the volume of the ADC-defined ischaemic core, respectively. The volume of tissue with severely reduced glucose use in ischaemic core was 52.8±18 mm^3 and the volume of the region of increased 2DG phosphorylation was 21.1±16 mm^3.

4.3.6 Evolution of ADC-derived lesion volume

Diffusion-weighted imaging scans generated at the start and conclusion of the MRI scanning session (Figure 4.2) provided information on the evolution of ischaemic injury over time. A significant increase in the ADC-derived lesion volume (106±66 mm^3 at 52±11 minutes compared with 185±130 mm^3 at 106±8 minutes after stroke, $p<0.05$) highlighted the progression of damage in the acute stroke period and the concomitant loss of penumbral tissue (Figures 4.10 and 4.11).

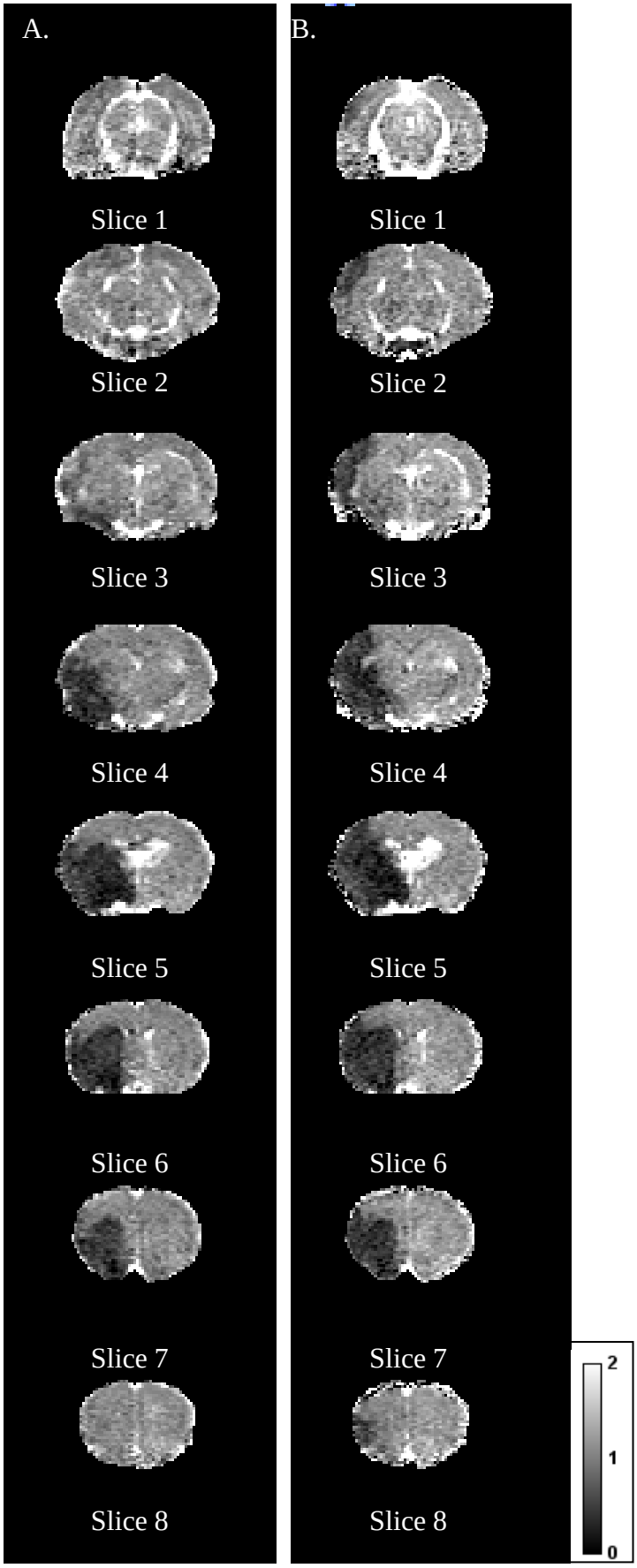

Figure 4.10. ADC maps from one animal at **A**. 47 min and **B**. 107 min to illustrate the neuroanatomical location and evolution of the ischaemic damage over time. Absolute ADC values measured in $x10^{-3}$ mm^2/sec

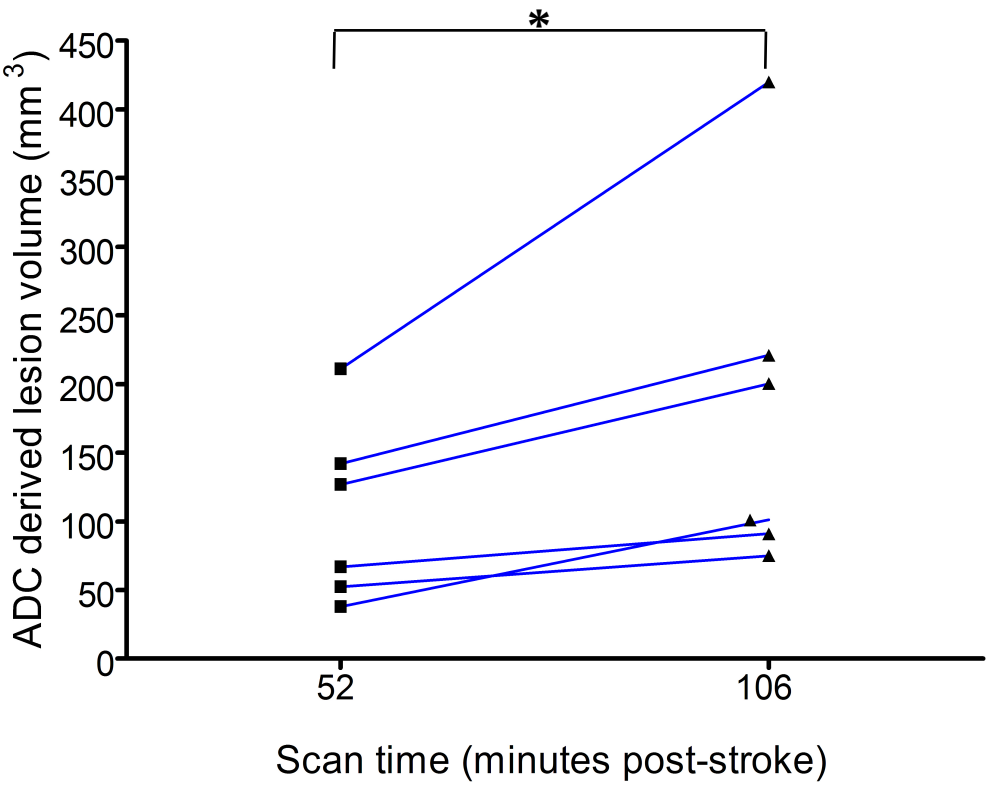

Figure 4.11. Evolution of the ADC-derived lesion volume. Lesion volumes at the two time points in individual animals are displayed, *p<0.05

4.4 Discussion

Information on metabolic state should improve penumbral definition. BOLD MRI offers information on oxygen consumption and delivery (Baird and Warach, 1999; Kavec et al, 2001), but static T_2^*-weighted MRI under normoxic conditions has not adequately delineated penumbra in ischaemic stroke patients (Tamura et al, 2002; Grohn and Kauppinen, 2001); possibly because deoxyhaemoglobin is not rapidly cleared in ischaemic conditions (Giesler et al, 2006). However, mapping dynamic changes in T_2^* in response to an oxygen challenge may improve discrimination between penumbra and surrounding tissue compartments (Santosh et al, 2008).

The T_2^*OC MRI technique for detection of the ischaemic penumbra was originally described and data generated in a permanent focal cerebral ischaemia model. Validation was based on comparison with DWI/PWI mismatch and histologically defined neuronal morphology (Santosh et al, 2008), and the feasibility of translation of the technique for clinical use in acute stroke has subsequently been demonstrated (Dani et al, 2010). The current study provides more direct validation for the technique, with evidence of ongoing glucose metabolism within the normal range in T_2^*OC-defined penumbra. In addition, coregistration of 2DG autoradiography with MRI has provided detailed information on the adjacent tissue compartments within the ischaemic hemisphere, which show markedly different levels of glucose metabolism. The hypothesis is that the T_2^*OC technique indirectly identifies penumbra from its higher oxygen extraction fraction, which influences deoxy: oxyhaemoglobin ratios and consequently T_2^* signal.

4.4.1 Limitations of the 2DG technique

The [^{14}C] 2DG method may not have accurately defined LCMRglc because the increase in radioactivity registered may either be a result of real glucose consumption or a methodological artefact from an increase in the lumped constant. In normal conditions, the lumped constant used for the 2DG technique is stable over a large spectrum of plasma glucose concentrations (Sokoloff et al, 1977). With reduced glucose supply - such as during ischaemia - the lumped constant may increase considerably (Suda et al, 1990; Vannucci et al, 1989; Gilland and Hagberg, 1996). As there is reduced glucose availability, the glucose distribution volume decreases and the lumped constant increases because 2DG is the preferred sugar for phosphorylation by hexokinase. As such, local values of the

lumped constant should be estimated, which may be derived by measuring the brain uptake of methlyglucose (Dienel et al, 1991; Gjedde et al, 1985). Another limitation is the lack of a gold standard or independent identification method for penumbra to compare T_2^*OC with. The previous preclinical and human studies by Santosh and colleagues (2008) and Dani and colleagues (2010), respectively, implicate $CMRO_2$ and OEF as the components responsible for T_2^*OC penumbral identification, but these cannot be directly measured with the imaging modalities used. Ultimately, microPET co-registered with MRI would provide a more definitive assessment of the metabolism – compared to 2DG – in the tissue defined by T_2^*OC as penumbra.

4.4.2 Glucose utilisation profiles in the ischaemic brain

Under ischaemic conditions, the coupling of blood flow and metabolism is compromised in some regions. Following focal ischaemia, regions of severely reduced blood flow exhibit markedly reduced glucose utilisation, whereas a consistent pattern of hypermetabolism is evident in the hypoperfused periphery using the 2DG autoradiography technique (Nedergaard et al, 1986; Shigeno et al, 1983; Tanaka et al, 1985). This suggests a metabolism-flow uncoupling in tissue adjacent to the ischaemic core, in which the uncoupling is considered a contributing factor to the evolution of ischaemic damage. This may occur because neural tissue appears to be more sensitive to reductions in oxygen than glucose (Astrup et al, 1981; Cox et al, 1983).

The contralateral hemisphere

A smaller T_2^* signal increase to OC in normal metabolising tissue compared with penumbral tissue would be expected (Santosh et al, 2008), and in all six animals, the hemisphere contralateral to MCAO showed measurable increases in T_2^* signal intensity during OC (Figures 4.4 and 4.5). By co-registering thresholded T_2^* maps with glucose use autoradiograms, a metabolic signature of normal tissue was generated to allow comparison with the ischaemic hemisphere.

The ischaemic core

The MR findings were consistent with the previous study (Santosh et al, 2008), in which the ischaemic core, defined by ADC, was notable as a region with negligible T_2^* signal change. It registered undetectable glucose use values, thus confirming metabolic inactivity

in this tissue compartment where $CMRO_2$ and oxygen extraction fraction would be expected to be markedly reduced or absent.

The ischaemic penumbra

The results show a region of significant T_2^* increase during OC localised to a cortical boundary zone between the MCA and anterior cerebral artery territories, which is hypoperfused and overlaps with the DWI/PWI mismatch area. This region displayed metabolism on co-registered autoradiograms not significantly different from contralateral normal tissue, and significantly greater than infarct core, which is consistent with previous 2DG studies in acute focal ischaemia (Belayev et al, 1997; Tohyama et al, 1998). Previous 2DG studies suggest penumbra metabolism within the normal range at 2 hours after stroke, with loci of hypermetabolism evident on autoradiograms (Belayev et al, 1997; Tohyama et al, 1998).

The region of increased 2DG phosphorylation

An intermediate tissue compartment, identified as a region of increased 2DG phosphorylation on autoradiograms (terminology discussed with Professor Guenter Mies, Max-Planck-Institute for Neurological Research, Germany) , displayed a small (sub-threshold) T_2^* signal change and lay inside the boundary of the ADC abnormality (Figures 4.3C and 4.4). This may point to residual oxygen utilisation on the border of the ADC abnormality in tissue with ADC and CBF values intermediate between the ischaemic core and T_2^*-defined penumbra (Figure 4.9). The presence of the region of increased 2DG phosphorylation within the ADC lesion suggests the tissue is still metabolically active, and may not be irreversibly injured *at this time point*, but could be critically injured and employing anaerobic glycolysis (Nedergaard and Astrup, 1986), which cannot sustain viability. As some oxygen is still being extracted from the blood, this suggests that some oxidative metabolism persists but it may indicate tissue destined for rapid, irreversible damage. This supports recent blood oxygen level-dependent MR studies proposing that the ADC lesion may not only incorporate tissue that is destined to die, but also severely injured, still viable tissue (Kidwell et al, 2002), and validates a number of previous studies that have reported reversibility of the ADC lesion following reperfusion (Mintorovitch et al, 1994; Minematsu et al, 1992; Kidwell et al, 2000). Hypermetabolic tissue displaying a small T_2^* percentage signal change may therefore indicate an intermediate compartment of the ischaemic penumbra situated within both the ADC abnormality and the perfusion

deficit, whose fate may be being determined by secondary insults after stroke, such as pre-terminal spreading depolarisations (Back et al, 1996), which may exhaust ATP levels in vulnerable cells.

4.4.3 Fate of the hypermetabolic region

The enhanced glucose metabolism after cerebral ischaemia has been ascribed to anaerobic glycolysis with lactate production contributing to irreversible damage to the tissue (Ginsberg et al 1977). From a number of studies, the ischaemic core has always been shown to be hypometabolic and always shows evidence of infarction (Nedergaard et al, 1988; Prado et al, 1988). There is also a suggestion that the region displaying low glucose utilisation may have little or no blood flow, and therefore little or no [^{14}C] 2DG can be delivered to the tissue. This study has shown that the ischaemic core is hypoperfused with evidence of very restricted but measureable CBF, and that some tracer must gain access to this region. Thus, it seems apparent that the hypometabolism is real, and a result of compromised cell activity, and not simply the failure to deliver the radioisotope. Specifically, the data have shown that the region of increased 2DG phosphorylation is situated between the ischaemic core and the region of significantly increased T_2^* signal change (the penumbra displaying glucose metabolism). This region has a negligible T_2^* signal change, suggesting that the region has switched to anaerobic glycolysis, which cannot sustain viability. During aerobic respiration, there is a yield of 36 ATP molecules per glucose molecule as opposed to only 2 ATP molecules per glucose for anaerobic glycolysis. This shows that there is very little ATP generated to sustain the cell in anaerobic conditions. The fate of the tissue may also be determined by secondary mechanisms post-stroke, including spreading depolarisations.

4.4.4 Spreading depolarisations as a contributor to increased glucose phosphorylation

This study has shown the flow-metabolism uncoupling phenomenon in which perfusion in the region of increased 2DG phosphorylation is critically reduced whilst glucose use is markedly increased (Figure 4.6). Many studies have shown increased glucose phosphorylation with 2DG autoradiography immediately peripheral to the infarct border (Nedergaard et al, 1986; Shigeno et al, 1983). Notable explanations for this phenomenon are that hypermetabolism occurs in this region, which requires increased glucose utilisation due to lack of oxygen, and also that anaerobic glycolysis is the predominant mechanism for

maintenance of brain metabolism due to the hypoperfused state of the tissue (Nedergaard, 1986).

There is a theory implicating metabolic stress as a determinant of the fate of the ischaemic penumbra. This stress is induced by cortical spreading depolarisations (CSDs) that stem from ischaemic depolarisations. These SD waves have been shown to originate from the boundary of the infarct core and traverse through the cortical penumbra (Mayevsky and Weiss, 1991; Iijima et al, 1992). Ischaemic depolarisations seem to induce cell damage due to the fact that, in ischaemic conditions, CBF in ischaemic tissue is unable to increase in response to heightened metabolic demand, and as a consequence, tissue oxygen tension decreases (Back et al, 1994) and high energy stores may become depleted (Takeda et al, 1993).

In experimental focal cerebral ischaemia, CSD incidence correlates with infarct size (Dijkhuizen et al, 1999). In the injured penumbra, where blood supply is compromised, CSD waves cause further reduction in tissue PO_2 and exacerbate metabolic stress–failure (Back et al, 1994; Somjen, 2001). Peri-infarct depolarisations (PIDs) in the initial hours after injury have been shown to cause a step-wise increase in the ischaemic tissue volume (Busch et al, 1996; Takano et al, 1996). Recurrent waves of depolarisation have been shown to extend from the ischaemic core to the penumbral region and beyond. CSD cause cells to depolarise and they require ATP to restore membrane potentials and ion concentration gradients, and peri-infarct depolarisations have been shown to recruit penumbral tissue into the ischaemic core (Hartings et al, 2003). The region of increased 2DG phosphorylation may represent the wave of spreading depolarisations and account for the progression of damage in the acute stroke period shown by the evolution of the ADC-derived lesion volume (Figure 4.11). Nedergaard and Astrup (1986) found that direct current (DC) potential was correlated to 2DG phosphorylation in this region. The 200% increase in glucose utilisation at the cortical infarct rim was associated with spontaneously recurring increases of extracellular potassium detected as DC potential deflections. This was in agreement with Branston and colleagues (1977) and Harris (1981), who also noted transient increases in extracellular potassium, which linearly correlated with clearance of potassium and blood flow. The transformation from aerobic to anaerobic glycolysis in the peri-infarct zone has gained credence because of repeated transient elevations of extracellular potassium detected in this region of increased 2DG phosphorylation (Branston et al, 1977). The increase in extracellular potassium affects the efficiency of the

ion transport, which in turn increases the metabolic rate (Shinohara, 1979), and as such, this displays the markedly high rate of glucose phosphorylation on the infarct rim.

In the intact brain, increased energy demand is coupled by an increase in cerebral blood flow, which allows equilibrium in energy state. In the periphery of brain infarcts, there is an uncoupling of flow and metabolism due to the restriction of blood flow. Thus, the peri-infarct depolarisations may compromise ion homeostasis which is detrimental to the brain tissue. For example, Ca^{2+} influx induced by PID in the peri-infarct region, will contribute to the downstream mechanisms in the ischaemic cascade resulting in cell injury that accompanies PIDs in the penumbra (Siesjo, 1992). Strong and colleagues (1983) found transient increases of potassium activity in the peri-infarct zone, and the frequency of these spreading depolarisations correlated with elevated glucose phosphorylation (Shinohara et al, 1979), as ATP-dependent ion pumps were overworked to sustain viability.

Tanaka and colleagues (1985) showed that, in the infarct rim, some regions displayed preserved flow-metabolism coupling, in that both local CBF (LCBF) and LCMRglc decreased proportionally. In this region, there was no evidence of histological damage. In contrast, regions having similar degree of flow reduction but increased 2DG accumulation displayed mild ischaemic damage. From this, they concluded that the flow-metabolism uncoupling contributes to infarct evolution.

Shiraishi and colleagues (1989) suggested that, during MCAO, high concentrations of excitatory amino acids may act on postsynaptic receptors which will continuously depolarise cells, without the cell actually firing. This causes glial metabolism to increase to metabolise the excitatory amino acids. Also, the increase in glucose uptake may be due to a shift toward anaerobic metabolism. As oxygen is limited around the rim of the infarct, glucose becomes the main nutrient for metabolism, although without oxygen, the Krebs cycle efficiency is limited. Lactate is therefore produced, and the amount of ATP molecules generated from each glucose molecule is significantly reduced. As a result, more glucose is taken up to compensate.

MR lactate spectroscopy co-registered with [^{14}C] 2DG would be one way in which to determine anaerobic glycolysis within the ischaemic hemisphere. In the current study, the region of increased 2DG phosphorylation, which we assume is metabolising anaerobically, has a negligible T_2^* signal (indicating a low oxygen extraction fraction and oxygen metabolism), but it has elevated glucose utilisation. This phenomenon has been shown to

disappear 6 hours after stroke (Nedergaard et al 1986). Since this is very inefficient method of metabolism, the tissue cannot maintain viability for an extended length of time with purely anaerobic respiration. Coregistration shows that the region of increased 2DG phosphorylation is on the boundary of the ADC lesion, implying severely injured tissue that will rapidly become incorporated into the irreversibly damaged region.

It has been shown that within a few minutes of severe ischaemia, there is a loss of electrical activity and disruption of ion homeostasis. This results in a significant increase in extracellular potassium concentrations with a concomitant increase in intracellular sodium and calcium concentrations (Hansen, 1981). The rise in intracellular calcium is responsible for the irreversible cell damage to mitochondrial function, the powerhouse for ATP production. At a later time point, as energy stores are affected, a depletion of phosphocreatine is also evident. Following the anaerobic metabolism of glucose in ischaemic brain tissue, excessive lactic acid is also produced which induces cellular acidosis (Raichle, 1983). Therefore, the decrease in oxygen delivery or other restrictions in mitochondrial activity, rather than glucose availability, are probably responsible for limiting oxidative metabolism (Sims and Anderson, 2002). This means that the decrease in oxygen delivery or impaired mitochondrial activity may be responsible for restricting oxidative metabolism, rather than glucose availability. There is a small positive change in T_2^* signal change to OC in the region of increased 2DG phosphorylation, suggesting that the tissue is still removing some oxygen from the blood, but a minority of intact mitochondria may allow oxidative metabolism to account for the slight increase in signal change.

Summary

The current study provides evidence of ongoing glucose metabolism in T_2^*OC-defined penumbra which was not significantly different from contralateral tissue, and significantly greater than infarct core. In addition, co-registration of 2DG autoradiography with MRI has provided detailed information on the adjacent tissue compartments within the ischaemic hemisphere, which show markedly different levels of glucose metabolism.

When compared to the conventional mismatch method, the Oxygen Challenge has introduced an additional parameter to improve the delineation of the ischaemic penumbra and provided further information on the metabolic characteristics of the tissue.

Chapter

5

Validation of T_2^*OC Based on Consequences of Reperfusion

5.1 Introduction

The mechanical or drug-induced restoration of blood flow represents the most effective intervention for acute ischaemic stroke that is ever likely to be discovered (Molina and Saver, 2005). In 1996, thrombolysis with recombinant tissue plasminogen activator was approved by the US Food and Drug Administration for acute ischaemic stroke of <3 hours duration. In May 2009, the American Heart Association/American Stroke Association recommended an extension of the window for acute ischaemic stroke, approving recombinant tissue plasminogen activator (alteplase) as a treatment up to 4.5 hours after symptom onset. The decision was primarily based on the findings from the third European Cooperative Acute Stroke Study trial (ECASS III), which confirmed a significant reduction in disability at the 90-day time period after recombinant tissue plasminogen activator treatment between 3 and 4.5 hours (Hacke et al, 2008). More recently, a time profile of benefit and harm for alteplase in a pooled analysis of eight randomized trials concluded that one in three patients had improved outcomes when treated between 1 and 3 hours from symptom onset, while one in six benefitted in the 3- to 4.5-hour time window. Significantly, risk may outweigh benefit beyond the 4.5-hour time point (Lees et al, 2010), and this was supported by a previous Cochrane meta-analysis (Wardlaw et al, 2009).

However, patient ineligibility means that fewer than 10% of all stroke patients can be thrombolysed (Cocho et al, 2005; Molina and Saver, 2005). There is no current MRI technique that accurately detects tissue viability and which could be used in routine clinical practice to identify patients likely to benefit from therapy such as thrombolysis, flow enhancement, or neuroprotection. The ability to determine a full index of tissue viability and haemodynamic status following stroke would significantly improve therapeutic intervention strategies for acute ischaemic stroke (Hacke et al, 1998). Alternative techniques that could determine tissue metabolic status would represent an advance on

current clinical imaging of the penumbra, establishing patient selection criteria for therapeutic strategies out-with current rigid time windows.

The previous chapter confirmed that T_2^*OC identified a compartment with a unique profile, defined by a significantly increased T_2^* percentage signal change. If this region is penumbra, the tissue should be capable of recovery if blood flow is restored, and this can be achieved by reversing the ischaemic insult by reperfusion. The aim of the current study was to test the validity of the T_2^*OC MRI technique based on the consequences of reperfusion. Our stated hypotheses were that T_2^*OC-defined penumbra should show signs of recovery following early restoration of flow and that the T_2^* response to OC following reperfusion should change to resemble the signal change in normal, non-ischaemic tissue. This was tested acutely after reperfusion and again at day 7. Evidence of tissue recovery in T_2^*OC-defined penumbra was determined from changes in CBF and ADC acutely following reperfusion. T_2^*OC maps during ischaemia were also coregistered with T_2-defined final infarct to determine whether tissue identified as penumbra had or had not become incorporated into final infarct.

5.2 Materials and methods

5.2.1 Rodent MCAO surgery

Male Sprague-Dawley rats (306±12g, n=8, Harlan, Bicester, UK) were initially anesthetised with 5% inhaled isoflurane in an induction chamber at room temperature. Following intubation, animals were artificially ventilated with 2% isoflurane delivered in air, slightly enriched with oxygen (30%) to maintain physiological stability throughout the experiment. Blood gases were maintained within the normal physiological range apart from increased PaO_2 during the OC. $PaCO_2$ was maintained between 35 and 45 mmHg to minimise cerebrovascular reactivity (Table 5.1). A rectal thermocouple provided continual monitoring of core body temperature that was maintained at 37°C±0.5°C.

Polyethylene catheters (Portex: external diameter 0.96mm; internal diameter 0.58mm; 70cm long) were placed in femoral arteries, to continuously monitor blood pressure and conduct blood gas analysis. MCAO was achieved by the intraluminal filament model, as described in Chapter 2.2.3. Ischaemia was induced for 109±20 minutes, which reflected the time taken to transfer the animal to the scanner and run the ischaemia scan series. The

monofilament was then removed. To ensure complete reperfusion, the ties around the common carotid and pterygopalatine branch were loosened to restore blood flow to MCA territory.

5.2.2 MRI scanning

Magnetic resonance imaging data were acquired on the system as described in Chapter 2.5.1.

Protocol

At ~1 hour after stroke, animals underwent MRI scanning that comprised DWI to detect ischaemic injury, T_2^*OC to detect penumbra, and ASL to provide CBF maps of ischaemia. Animals were removed from the magnet, and reperfusion was induced by withdrawal of the intraluminal filament. The scanning sequence was then repeated to confirm reperfusion and to study the consequences of reperfusion on the tissue defined as penumbra from the earlier DWI, T_2^*OC and ASL scans.

Ischaemia-induced damage will continue to evolve following reperfusion in this model and consequently histology or MRI at 24 hours will not predict final infarct size. Therefore, rats were recovered and rescanned at day 7 to define the final infarct. Choosing this late time point also avoids the confounding effects of brain swelling, which is present during the first days after stroke but has resolved by 7 days. This improves coregistration of final T_2 scans with acute scans. The animals also underwent T_2^*OC at this time point (Figure 5.1).

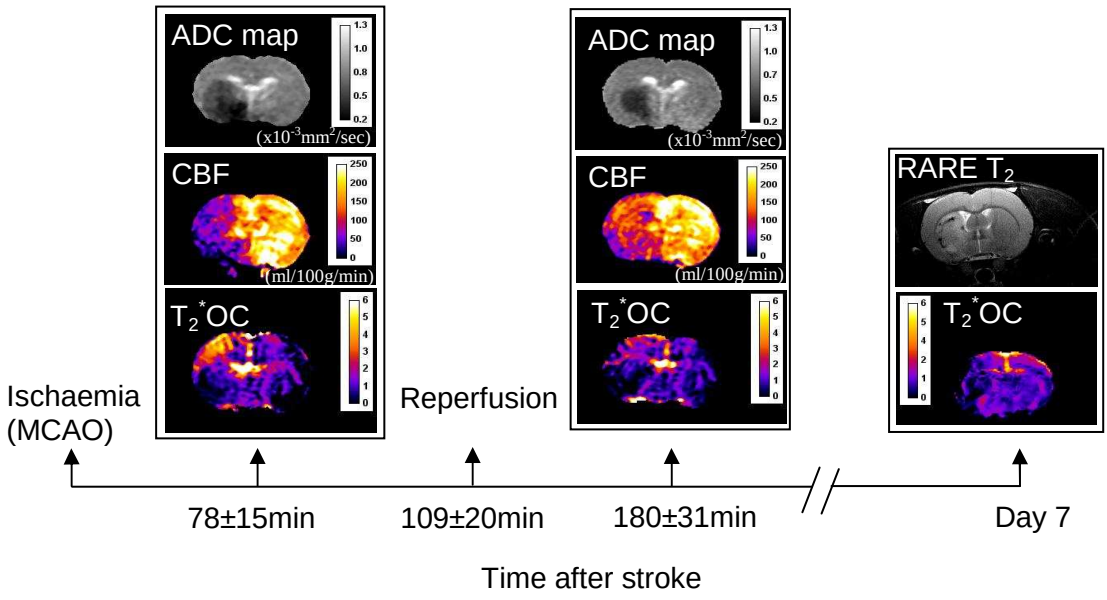

Figure 5.1 Time line of experimental protocol. Following stroke, the animals were placed in the magnet and a DWI scan was performed to identify ischaemic damage, ASL to generate fully quantitative blood flow maps and DWI/PWI mismatch images were produced for comparison. T_2^*OC was also performed during this period of ischaemia to derive T_2^* percentage signal change maps. Following MR scanning, the animals were removed from the magnet and reperfusion was performed by withdrawal of the intraluminal filament. The animals were then placed back in the magnet and the scanning sequence was repeated to identify the effect of reperfusion on the ischaemic brain. Following the reperfusion scanning series, the animals were removed from the magnet and recovered for 7 days post stroke when a T_2^*OC and a RARE T_2 was performed

Diffusion-weighted imaging and perfusion-weighted imaging

Diffusion-weighted and perfusion-weighted imaging was performed as described in Chapter 2.5.3 and 2.5.4. DW- and PW-imaging were also used to define penumbra from DWI/PWI mismatch (Figure 5.3A(vi)) and data were analysed on two selected coronal slices within the MCA territory. For analysis, the data for the rostral and caudal slices were combined. Arterial spin labelling scans were generated at 44±11 and 59±15 minutes after stroke for caudal and rostral slices, respectively. The scanning time for a single ASL slice was ~6 minutes and two slices were scanned throughout the MCA territory. Additionally, a T_1-weighted image (scan time 10 minutes) was performed to allow quantification of CBF in mL per 100g per minute.

T_2^*-weighted imaging

T_2^*-weighted imaging was performed as described in Chapter 2.5.6. Two coronal MRI slices (identified as rostral and caudal slices), which corresponded to territory supplied by the MCA, were selected for analysis. The paradigm for the T_2^*-weighted OC sequence was 4 minutes breathing air, followed by 6 minutes breathing 100% oxygen. This sequence was repeated at day 7 after stroke.

T_2-weighted imaging

During acute scanning and at 7 days following reperfusion, a sagittal RARE T_2 scan (as described in Chapter 2.5.5) was performed, in which the rhinal fissure was used as a neuroanatomical landmark to match the geometry as closely as possible with the acute scans (Figure 5.2A). A coronal RARE T_2 sequence was performed as described in Chapter 2.5.5 which enabled T_2-derived final infarct measurements (Figure 5.2B).

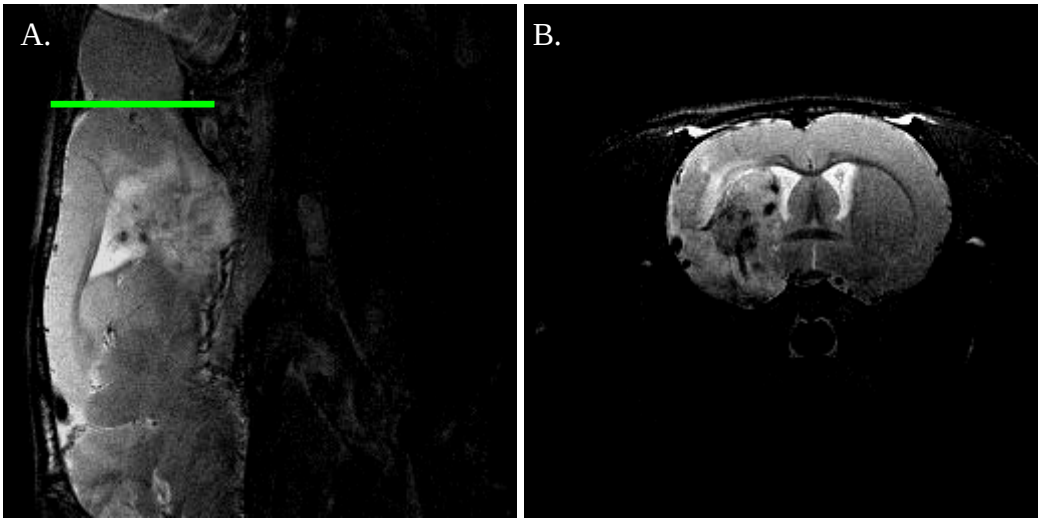

Figure 5.2. RARE T_2 scans performed in the sagittal plane (**A**) where the slices were aligned with the rhinal fissure (green line), and in the coronal plane (**B**), which enabled final infarct calculations. Ischaemic damage appears hyperintense in this scan sequence. There is also evidence of haemorrhage within the infarct, which appears as dark spots in the caudate nucleus and the cortex

5.2.3 MRI Data Analysis

Defining the ischaemic penumbra with DWI/PWI mismatch

Quantitative average ADC maps were generated as described in Chapter 2.5.3. A 16.5% reduction of mean contralateral ADC was used to determine the volume of ischaemic damage, which has been shown to match closely the final infarct size following permanent MCAO in Sprague-Dawley rats (Lo et al, 1997). Perfusion-weighted imaging was performed on caudal and rostral coronal slices within core MCA territory and the perfusion deficit area was calculated based on a 57% reduction of mean contralateral CBF (Meng et al, 2004). ADC and CBF maps were overlaid to identify the DWI/PWI mismatch area. Diffusion–perfusion mismatch was calculated as the difference between the perfusion deficit and the ADC lesion area on the corresponding slice. Volumes of DWI/PWI mismatch and thresholded T_2^*OC-defined penumbra were generated from the data from two coronal slices and the neuroanatomical location compared between the two techniques.

T_2^* oxygen challenge time course data and defining the ischaemic penumbra

The time course of the T_2^* signal change was analysed from ROIs (Figure 5.3A (iv)). T_2^* percentage signal change was calculated from time course graphs (Figure 5.4), where the average baseline signal was subtracted from the peak signal during OC. This value was then divided by the average baseline signal and multiplied by 100. T_2^* percentage signal change maps were generated using ImageJ software. The boundaries of penumbral tissue were defined using a threshold based on the empirical rule: the mean plus 2 SD of the T_2^* value of the contralateral hemisphere, excluding the ventricles (Figure 5.3A (iii).

Volumetric analysis of penumbra

Volumetric analysis of the perfusion deficit, ADC lesion, DWI/PWI mismatch, and T_2^*OC-defined penumbra was performed over the rostro-caudal extent of the ASL scans.

5.2.4 Regions of interest

During ROI placement on the ischaemia scans, I was blinded to the acute reperfusion and day 7 data and *vice versa*. ROIs were selected according to specific features on the images (Figure 5.3): (1) ischaemic core in caudate nucleus from the thresholded ADC lesion (Figure 5.3A (iv), red); (2) the contralateral caudate nucleus (excluding veins and ventricles) (pink), which was manually designated; (3) penumbra as defined by thresholded T_2^* percentage signal change (green); (4) equivalent contralateral cortex (sky blue); and (5) DWI/PWI mismatch (dark blue).

For the 7-day data, MRI-defined ROIs were defined and placed within; the final infarct according to the RARE T_2 scan; the thresholded T_2^*OC-defined penumbra identified from the acute ischaemic scan series; and two equivalent contralateral ROIs.

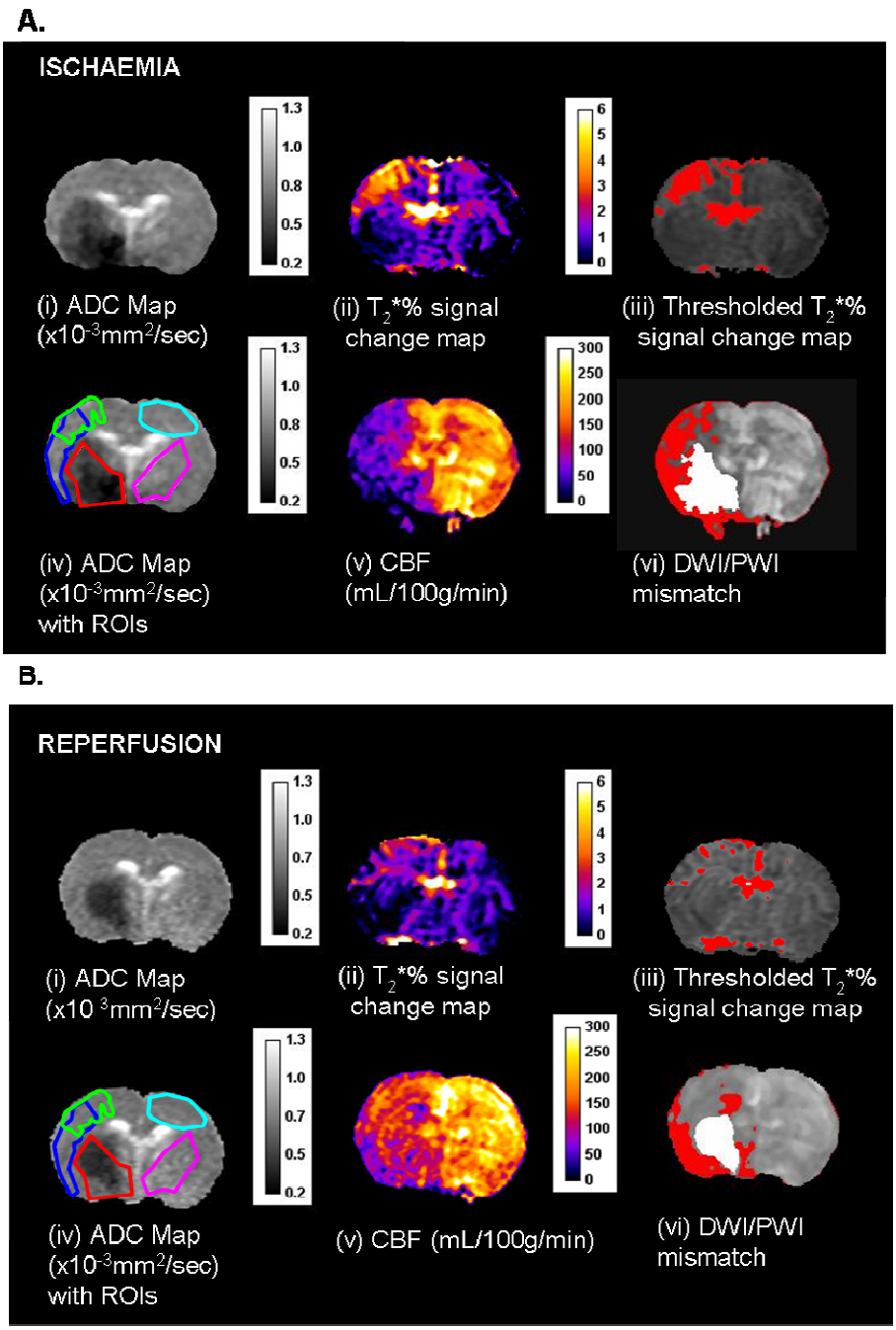

Figure 5.3 (**A**) Ischaemia scan series and (**B**) post-reperfusion scan series, with ROIs superimposed on the ADC maps (images Aiv and Biv); (ii) T_2^* oxygen challenge percentage signal change map, (iii) thresholded T_2^*OC map, (v) CBF map (mL per 100g per minute), and (vi) DWI/PWI overlay (mismatch tissue shown in red). ROIs were defined as follows:

Green ROI - the penumbra was defined by applying a threshold to display the greatest T_2^* percentage signal change excluding veins and ventricles (iii).

Red ROI - ischaemic core within the caudate nucleus, derived from the ADC lesion (i).

Sky blue ROI - the contralateral cortex, equivalent to OC-defined penumbra.

Cerise ROI - the contralateral caudate nucleus, equivalent to the ADC-derived lesion.

Dark blue ROI— DWI/PWI mismatch (vi) derived from the thresholded ADC (i) and CBF maps (v)

Coregistration

To coregister the acute and 7-day scans, linear coregistration was performed using Analyze (AnalyzeDirect, Inc. Overland Park, KS, USA). To align the data, ischaemia ASL and T_2^* images were warped to their corresponding DWI slices, and the reperfusion scan series and 7-day scans were warped to the same DWI slice as the ischaemic scan series. The processed data from the T_2^*OC and thresholded ADC and CBF maps were coregistered to (1) define ROIs and (2) identify the T_2^*OC-defined penumbral tissue. To correlate the T_2-defined infarct with the acute data, the data set at day 7 were also coregistered to the DWI scans generated from the ischaemic scan series.

5.2.5 Statistical analysis

All data are presented as mean±SD and were tested to confirm normal distribution using the D'Agostino and Pearson normality test. Data were normally distributed and as such, mean arterial blood pressure before and during OC was analysed by Student's paired *t*-test. T_2^* signal, ADC, and CBF values in different ROIs were analysed by one-way analysis of variance (ANOVA) followed by Student's paired *t*-test with a Bonferroni correction for multiple comparisons. A paired *t*-test was performed to compare changes in T_2^* signal, ADC, and CBF at the ischaemia and post-reperfusion time points.

5.3 Results

5.3.1 Acute data

5.3.1.1 Physiological variables

Oxygen challenge was performed twice during the acute scanning session. The mean time to commence OC was 78±15 minutes after MCAO for the scans performed during ischaemia and 180±31 minutes for the set of scans performed following reperfusion. Physiological variables were monitored throughout the experiment. Blood pressure and blood gases recorded immediately before OC for both the ischaemia and reperfusion scan series were within normal physiological levels (Table 5.1).

PHYSIOLOGICAL DATA				
	Values during ischaemia scans		**Values for reperfusion scans**	
	BASELINE	***DURING OC***	***BASELINE***	***DURING OC***
MABP	89.4±9	98.3±6*	86.9±9	93.5±10**
$PaCO_2$ (mmHg)	41.8±8		42.8±7	
PaO_2 (mmHg)	90±13		89.5±9	
Blood pH	7.324±0.05		7.302±0.03	

Table 5.1. Baseline physiological variables for the ischaemia scan series and the reperfusion scan series. MABP, mean arterial blood pressure. Data are expressed as mean±SD. * $p<0.05$ and ** $p<0.001$, Student's paired *t*-test

5.3.1.2 Acute T_2^* percentage signal change to OC

During MCAO (ischaemia scans), the T_2^* signal change during OC varied in magnitude across the hemisphere ipsilateral to the stroke (Figure 5.4A & C), with the smallest change in ischaemic core and the largest in the dorsolateral cortex (OC-defined penumbra). T_2^* signal increase in the penumbra ROI was significantly greater than in the contralateral cortical ROI ($p<0.01$; Figure 5.4C). In ischaemic core within the caudate nucleus, mean T_2^* signal during OC was significantly reduced compared with the contralateral caudate nucleus ROI ($p<0.05$).

Following reperfusion (mean OC scan time = 180±31 minutes following stroke onset and 71 minutes from initiation of reperfusion), T_2^* signal increase in the penumbral ROI reduced significantly from 8.4±4.1% to 3.25±0.81% ($p<0.001$, Figure 5.4B & D). In the DWI/PWI mismatch ROI, T_2^* percentage signal changed from 5.48±2.8% during ischaemia to 2.49±1.04% following reperfusion (Figure 5.4D). There were no significant T_2^* percentage signal changes from ischaemia to reperfusion in any of the other ROIs; T_2^* percentage signal change in ischaemic core caudate nucleus changed from 0.39±0.47% during ischaemia to 0.83±1.7% following reperfusion, contralateral cortex changed from 2.97±1.8% to 2.61±1.1%, and contralateral caudate nucleus changed from 3.35±2% to 2.59±1.3%.

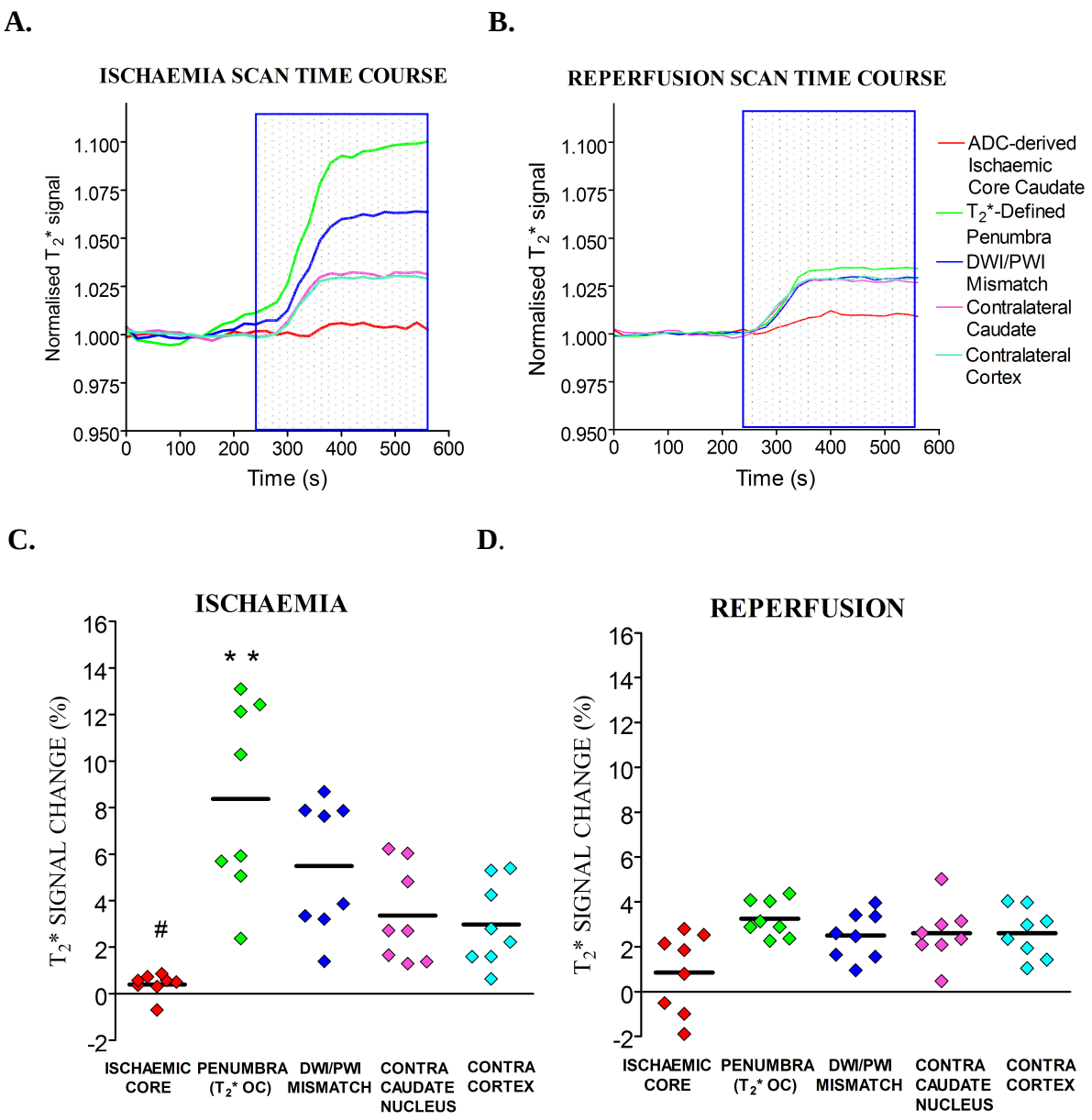

Figure 5.4. Mean T_2^* signal time course during ischaemia (**A**), and following reperfusion (**B**), mean T_2^* percentage signal change from baseline for ROIs during ischaemia (**C**) and following reperfusion (**D**) (n=8). (**A, B**) Positive T_2^* signal changes were recorded during oxygen challenge (OC) in contralateral caudate nucleus and cortex, the DWI/PWI mismatch, and the T_2^*OC-defined penumbra. All data were normalised to the average signal over the 4 minutes before OC from eight animals. The blue box represents the period of 100% oxygen inhalation (OC). (**C, D**) Horizontal lines represent means. ** $p<0.01$, relative to contralateral cortex ROI. # $p<0.05$, relative to contralateral caudate nucleus

5.3.1.3 Severity of ischaemia and tissue viability

During ischaemia, blood flow in the T_2^*OC-defined penumbra, DWI/PWI mismatch, and ischaemic core caudate nucleus were significantly reduced compared with the equivalent contralateral ROIs ($p<0.001$, Figure 5.5A). Cerebral blood flow values in the OC-defined penumbra were significantly higher than the DWI/PWI mismatch-defined penumbra ($p<0.05$). On reperfusion, mean CBF in ischaemic core caudate nucleus increased from 4.3±5.3 to 31±74 mL per 100g per minute, but remained significantly reduced compared with the equivalent contralateral ROI ($p<0.001$, Figure 5.5B). Mean CBF in the T_2^*OC-defined penumbra increased significantly from 41.94±13 to 116.5±25mL per 100g per minute ($p<0.001$, 5.5B). Mean CBF in DWI/PWI mismatch also increased significantly from 16.8±14 to 104.4±50mL per 100g per minute ($p<0.001$). Blood flow in contralateral caudate nucleus and cortex did not change significantly following reperfusion; 143±20 to 121±14 and 161±24 to 127±36 mL per 100g per minute, respectively.

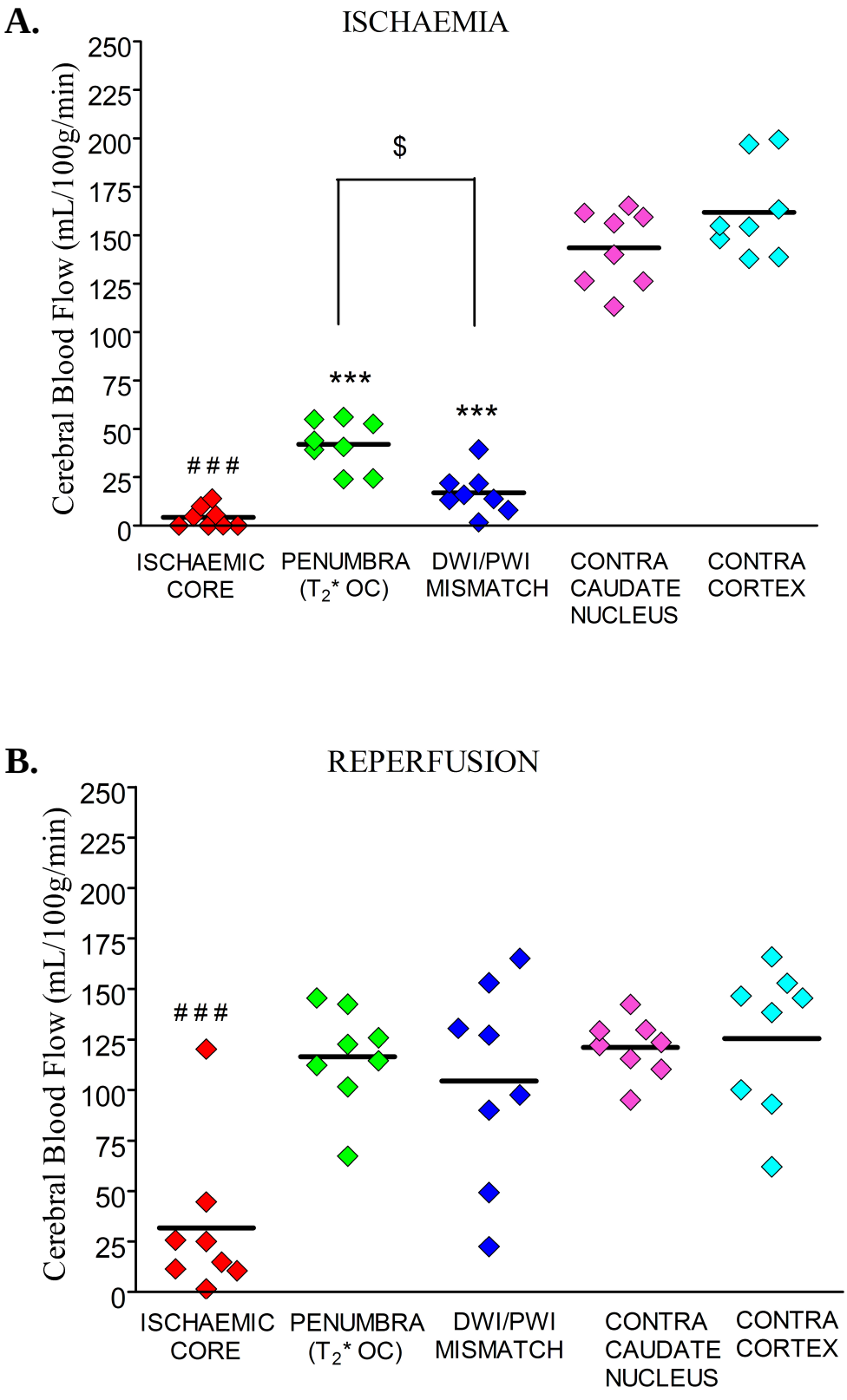

Figure 5.5. Mean CBF in selected ROIs during ischaemia (**A**) and following reperfusion (**B**). Horizontal lines represent means. *** p<0.001 relative to contralateral cortex ROI. # # # p<0.001 relative to contralateral caudate nucleus ROI. $ p<0.05

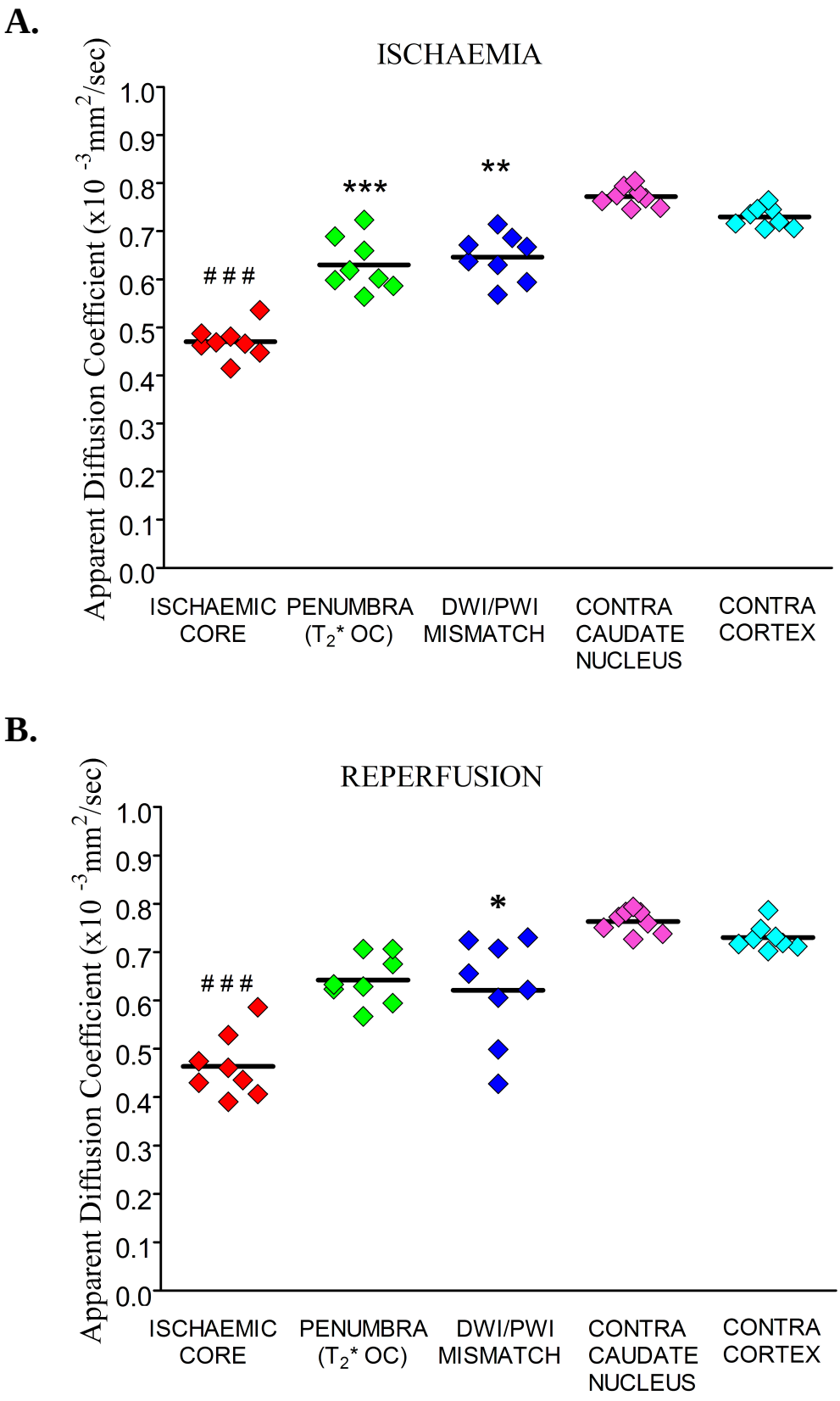

Figure 5.6. Mean ADC in selected ROIs during ischaemia (**A**) and following reperfusion (**B**). Horizontal lines represent means. *** p<0.001, ** p<0.01, * p<0.05 relative to contralateral cortex ROI. ### p<0.001, relative to contralateral caudate nucleus ROI

During ischaemia, ADC values (mean scan time was 72±8 minutes after stroke) in the T_2^*OC-defined penumbra, ischaemic core caudate nucleus and DWI/PWI mismatch were significantly reduced compared with the equivalent contralateral ROIs (Figures 5.3A(i) and 5.6A; $p<0.001$, $p<0.001$, and $p<0.01$, respectively). Following reperfusion, ADC values in the DWI/PWI mismatch and ischaemic core caudate nucleus ROIs remained significantly reduced when compared to equivalent contralateral ROIs following reperfusion. However, the ADC values in T_2^*OC-defined penumbra were not significantly different than the contralateral cortex ROI following reperfusion (Figure 5.6).

5.3.2 Day 7 data

5.3.2.1 T_2-defined infarct volume and T_2^*OC percentage signal change

In the surviving animals, infarcts were predominantly located sub-cortically with minimal cortical damage. The surviving animals (n=4, Figure 5.7B) tended to have a smaller ADC lesion volume during acute imaging than the animals that died prematurely (n=4) (Figure 5.7A). The animals that died prematurely did not survive beyond the 24 hour time point, suggesting that acute brain swelling was the most likely cause of death. Both ipsilateral and contralateral hemispheric volumes were calculated to show that there was no significant residual brain swelling at day 7 (622±27 and 624±30 mm^3 for the ipsilateral and contralateral hemispheric volumes, respectively).

T_2^* percentage signal change on day 7 in the OC-defined penumbra ROI (1.69±0.6%) was not significantly different from data for the equivalent contralateral cortex (1.72±0.6%; Figure 5.8B). The T_2^* signal change in the T_2-defined final infarct ROI was significantly reduced – displaying a negative signal (−0.88±0.6%) - compared with the equivalent contralateral caudate nucleus (1.72±0.6%) ($p<0.01$; Figure 5.8B). Figure 5.9 shows ADC maps and equivalent T_2^* percentage signal change maps from three slices within MCA territory during ischaemia, following reperfusion and at day 7. Figure 5.11 shows the effect of reperfusion on the ADC lesion over 3 slices in representative animal, as well as allowing comparison of the initial ADC lesion with the RARE T_2-derived final infarct.

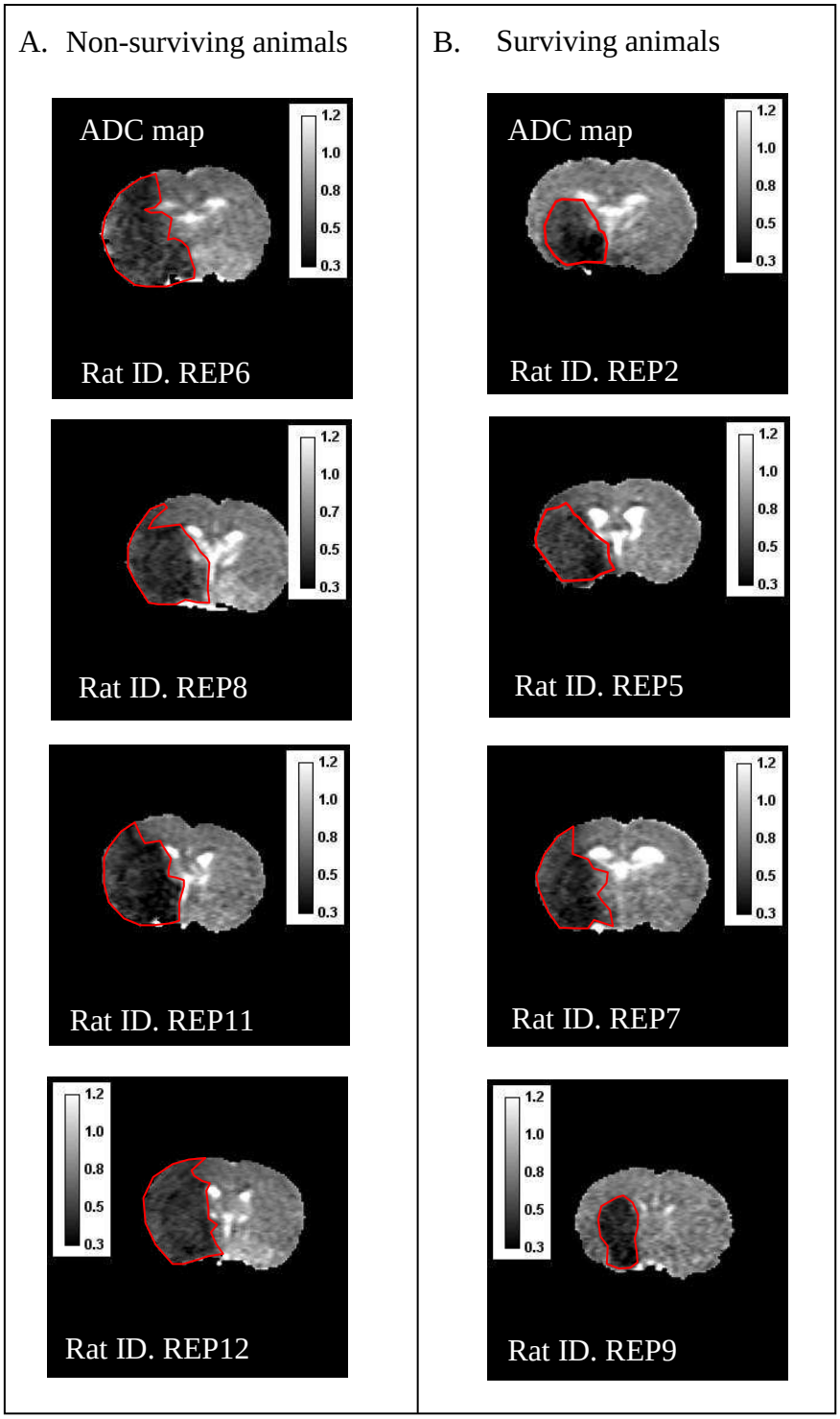

Figure 5.7. Illustrative ADC maps (slice 5) during the acute ischaemia scanning series of **A**. Animals that died before day 7 and **B**. Animals that survived up to day 7. The animals that survived up to day 7 tended to initially have smaller acute ADC lesions with less cortical damage. ADC scale bars in units of $x10^{-3}mm^2$. ADC lesions were derived using a 16.5% reduction in the mean contralateral ADC values excluding the ventricles (outlined in red)

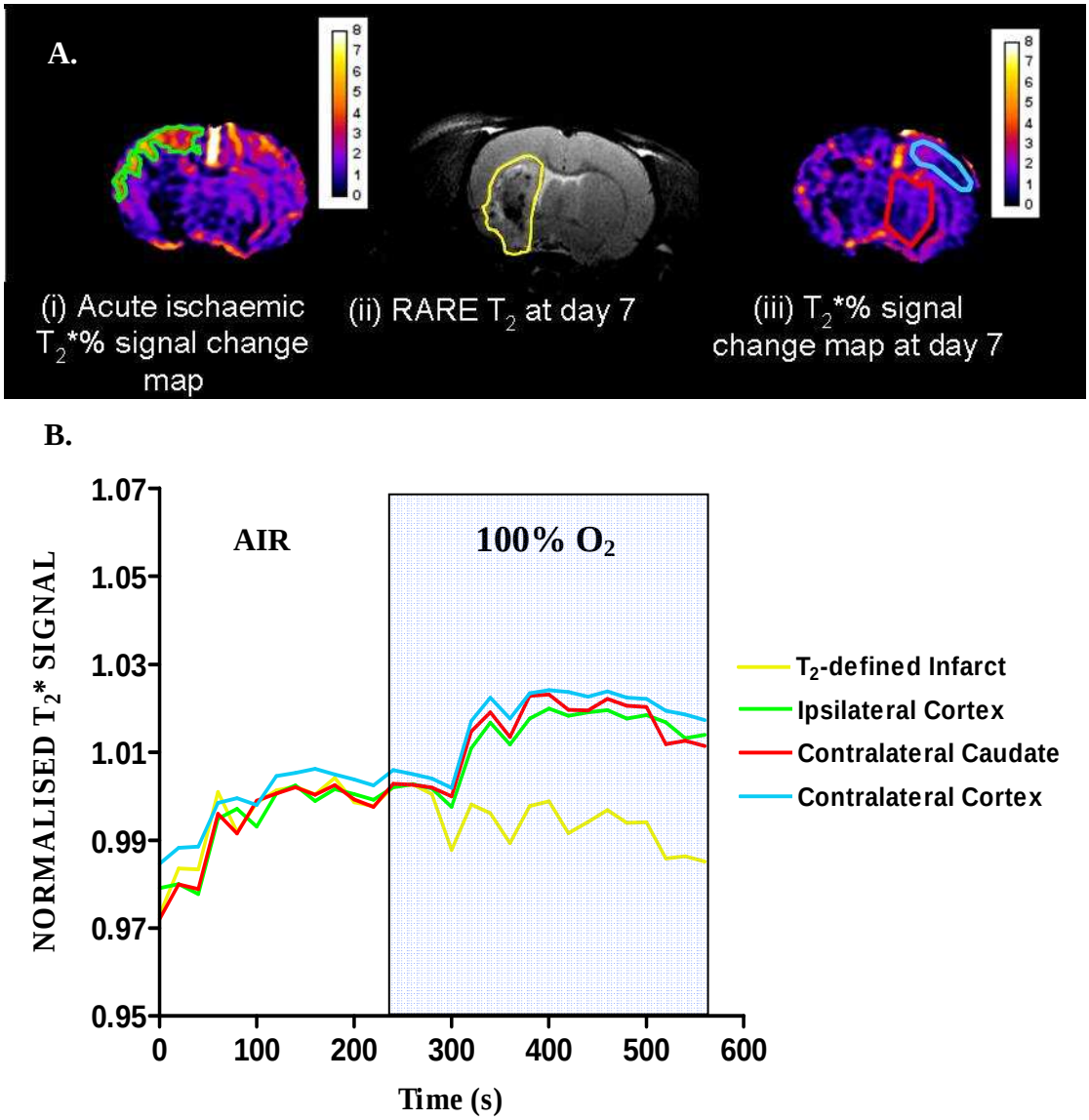

Figure 5.8. T_2^* percentage signal change at day 1 and day 7 in selected ROIs. (**A**) MRI ROIs derived from (i) acute T_2^*OC percentage signal change maps during ischaemia (ipsilateral cortex penumbra - green); (ii) RARE T_2 scans at day 7 after stroke (infarct ROI-yellow); and (iii) T_2^* percentage signal change maps at day 7 (contralateral cortex and caudate nucleus - sky blue and red, respectively). ROIs were superimposed onto day 7 T_2^* percentage signal change maps generated 7 days after stroke to generate T_2^* signal time course graphs (**B**). T_2^* time course graphs represent the mean normalised signal from four animals. All data were normalised to the average signal over the 4 minutes before oxygen challenge. Blue box represents the period of 100% oxygen inhalation

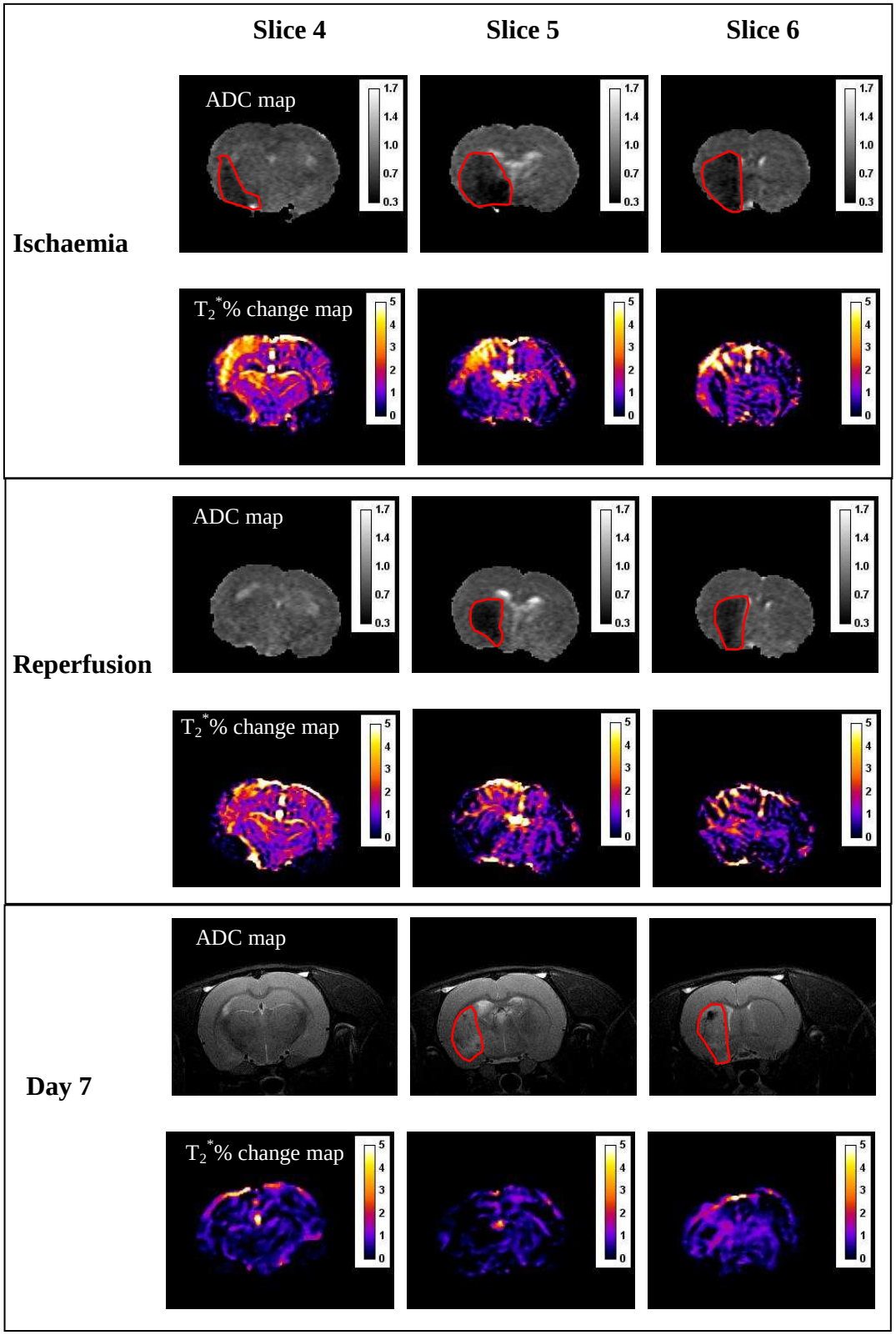

Figure 5.9. ADC maps and equivalent T_2^* percentage signal change maps from three slices within MCA territory during ischaemia (top), following reperfusion (middle) and at day 7 (bottom). ADC lesions were derived using a 16.5% reduction in the mean contralateral ADC values excluding the ventricles (outlined in red)

5.3.2.2 Evidence of penumbral salvage

Coregistration of the T_2^*OC-defined penumbra ROI (derived from the T_2^* percentage map during ischaemia) onto the RARE T_2 scan at day 7 (Figure 5.10), revealed that this region was not incorporated into the final infarct in any animal, providing evidence that T_2^*OC-defined penumbra had been salvaged by reperfusion.

5.3.2.3 Volumetric analysis of perfusion deficit, ADC lesion and penumbra

The volume of perfusion deficit, determined at 52.8±14.2 minutes after stroke, was 110±25 mm^3 and the ADC lesion volume determined at 72±8 minutes after stroke was 91.6±33 mm^3, generating a DWI/PWI mismatch volume of 20.2±15 mm^3. The thresholded T_2^*OC-defined penumbral volume, determined at 78±15 minutes was 17.3±9 mm^3. The mismatch- and T_2^*OC-defined penumbral volumes were ~22% and 19% of the volume of the ADC-defined ischaemic core, respectively. Although the volume of penumbral tissue was similar for the two methods, there were spatial differences with regards to the physical location (Figure 5.10(iv)).

The perfusion deficit volume in the four animals that survived to day 7 was 110.3±6 mm^3 determined at 53.5±12 minutes after stroke, and the ADC lesion volume was 88.6±21 mm^3 determined at 68.3±8.4 minutes after stroke. The DWI/PWI mismatch volume was 25.7±14 mm^3 and the thresholded T_2^*OC-defined penumbra, determined at 82.5±15 minutes was 18.9±8 mm^3. The mismatch- and T_2^*OC-defined penumbral volumes were ~29% and 22% of the volume of the ADC-defined ischaemic core, respectively. The T_2-defined final infarct volume at 7 days following MCAO was 71.7±22 mm^3.

5.3.2.4 Reperfusion reduces ADC-defined ischaemic damage

When comparing final infarct at 7 days with the ADC-derived lesion during ischaemia, ischaemic damage reduced from 116±64 mm^3 during ischaemia to 107±68 mm^3 at day 7 (Figure 5.11 and 5.12). This confirms the presence of penumbral tissue within the ADC defined lesion.

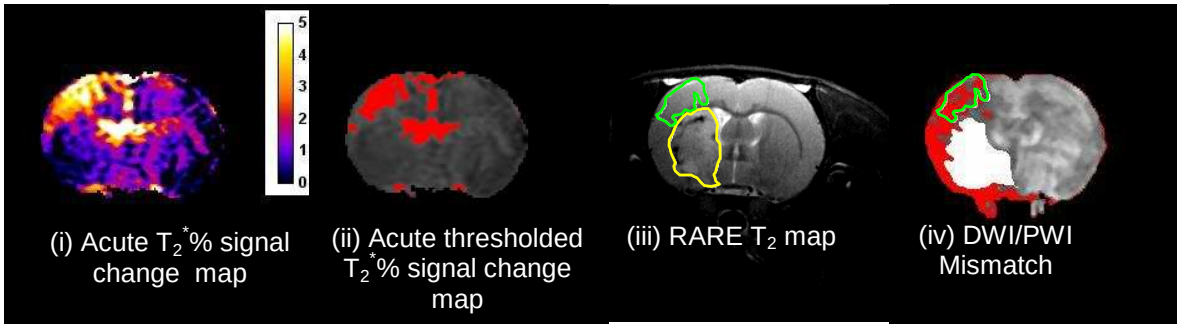

Figure 5.10. Comparison of neuroanatomical location of thresholded OC-defined penumbra in relation to T_2-defined final infarct and DWI/PWI mismatch. Acute T_2^* percentage signal change map (i) was thresholded to identify penumbra (ii) and superimposed upon the day 7 RARE T_2 (iii)—penumbra outlined in green. The final infarct is outlined in yellow. The T_2^*OC penumbra region of interest (ROI) was superimposed upon the DWI/PWI mismatch (iv) to compare the difference in the spatial locations of the mismatch and the T_2^*OC defined penumbra

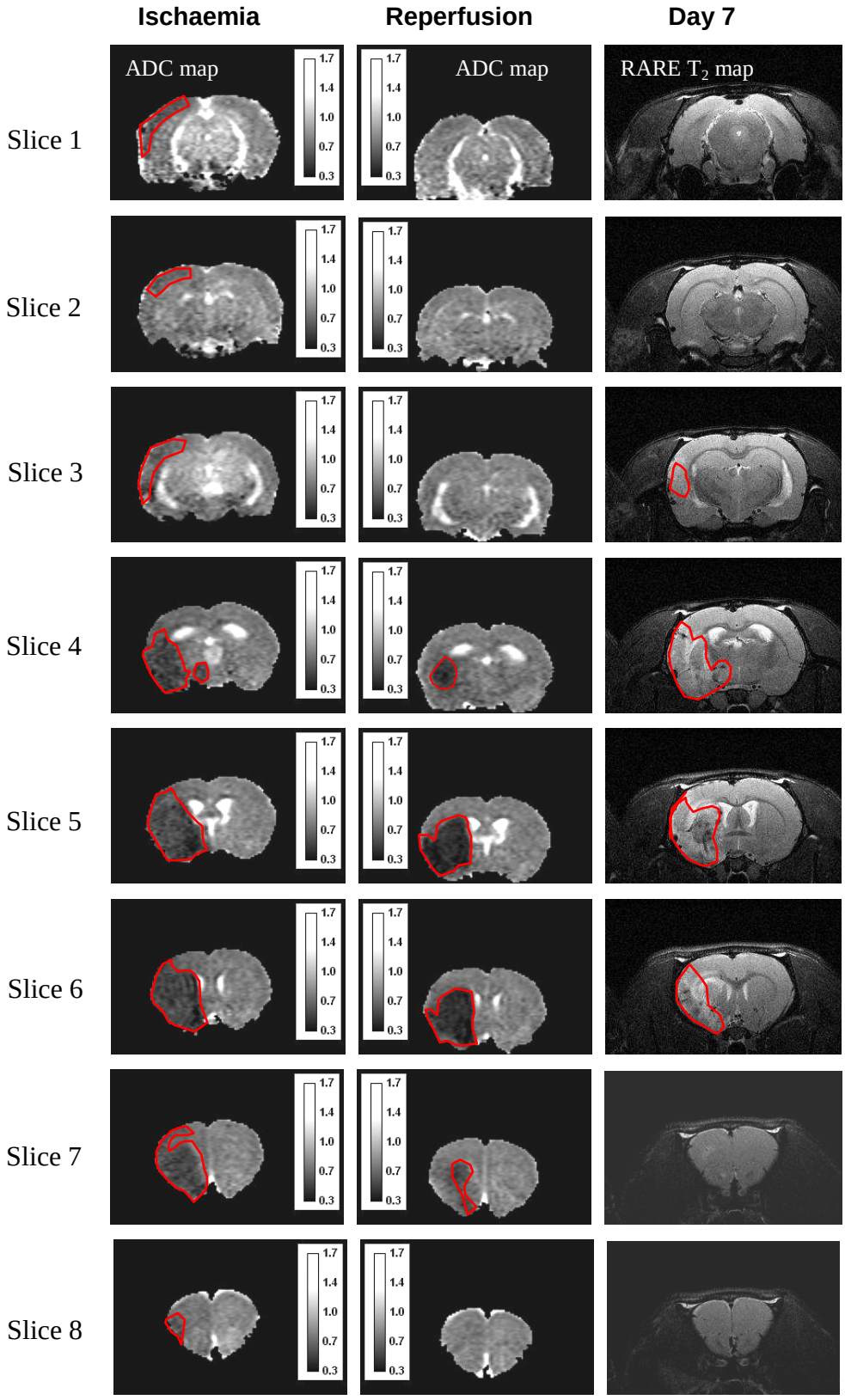

Figure 5.11. Ischaemic damage during ischaemia, post-reperfusion and at day 7 from a representative animal. ADC lesions were derived using the 16.5% reduction threshold (drawn in red), whereas the hyperintense region on the RARE T_2 scans were manually transcribed. ADC lesion volume decreased following reperfusion and final infarct was slightly reduced at day 7 compared to the ADC lesion post-reperfusion (Animal ID REP5, lesion volume shown in Figure 5.12)

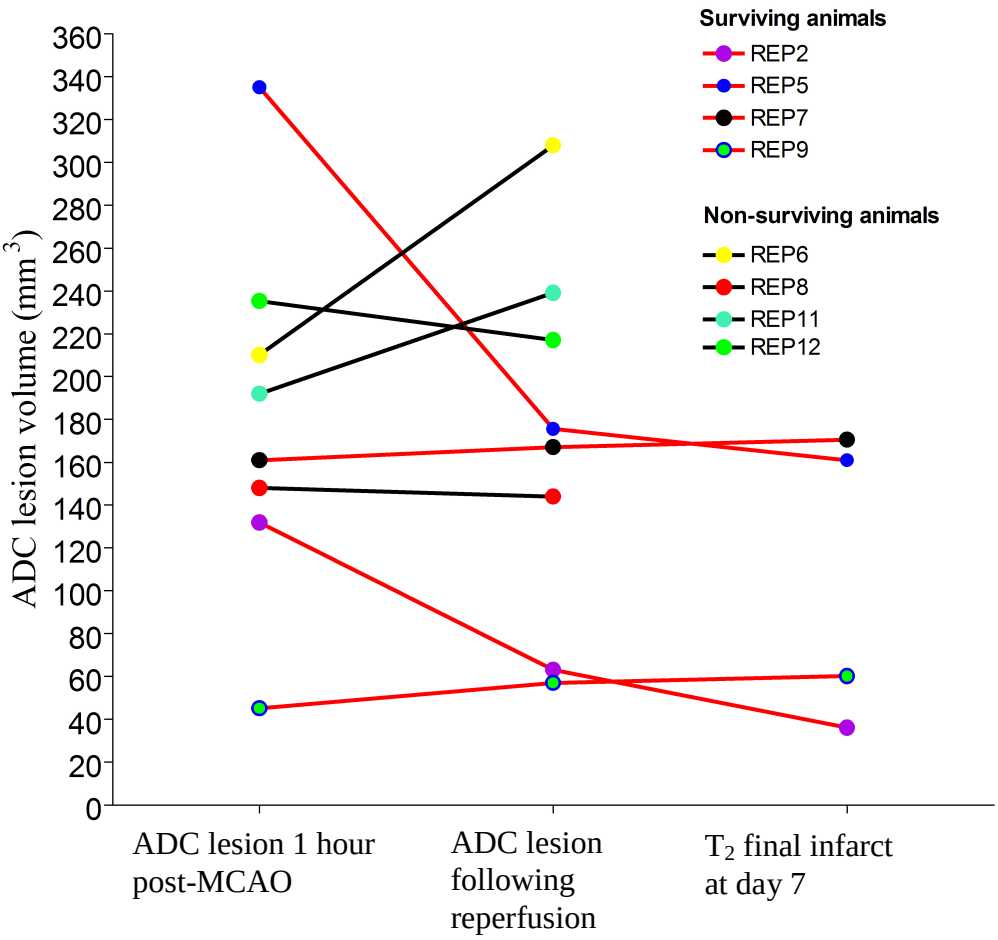

Figure 5.12. ADC lesion volume during ischaemia, following reperfusion and final infarct volume at day 7. Data with red lines represent the animals that survived up to day 7. Note that the lesion volume tended to either decrease or remain relatively static following reperfusion, and the injury did not expand between time of reperfusion and day 7. Data with black lines represent the animals that died before day 7 scans could be performed. Note that initial lesion volume in the animals that died tended to be greater than in the surviving animals, and that lesion volume continued to evolve despite reperfusion in two of the animals

5.4 Discussion

Depending on the duration and severity of the ischaemic insult, at least some of the tissue regarded as penumbra may recover if blood supply is promptly restored. If blood supply is restored and the tissue recovers, it should no longer demonstrate an increased OEF and its response to OC should be similar to non-ischaemic tissue. The validity of T_2^*OC by timely restoration of CBF and final infarct measurement to determine tissue salvage was evaluated.

The aim of this study was to test the validity of the technique by examining the fate of T_2^*OC-defined penumbra by timely restoration of CBF and final infarct measurement. Repeat T_2^*OC MRI sequences should reflect changes in the penumbra associated with restoration of flow and normalisation of T_2^* signal change consistent with tissue salvage. Evidence of recovery in the OC-defined penumbra was evaluated acutely by assessing changes in CBF and ADC following reperfusion and in the longer term on T_2-derived final infarct volume after 7 days.

There are varying definitions of penumbra, which have been devised using different techniques. The penumbra can be described as a region of decreased cerebral protein synthesis and preserved tissue ATP levels (Hossmann, 1993), unlike the ischaemic core, which experiences reductions in both protein synthesis and ATP. Following the progressive reduction in blood flow, decreased protein synthesis is one of the first biochemical or molecular changes that can be identified (Dienel et al, 1980; Bergstedt et al, 1993), declining when flow reduces below 50% (Mies et al, 1990). While this method may more accurately delineate penumbra, it requires a terminal autoradiographical technique, which cannot be used in recovery models of stroke. As such, the current definition of penumbra used for the study was tissue with reduced flow which has the capacity to recover when flow is promptly restored and this was evaluated from final infarct displayed on T_2 scans at 7 days post-stroke. Additionally, the pathophysiological mechanisms of ischaemic damage differ between permanent and transient MCAO. In permanent MCAO, peri-infarct depolarisations in oligaemic tissue are implicated in the evolution of penumbra into the infarct core, whereas in transient MCAO delayed secondary energy failure is responsible for evolution of damage (Olah et al, 2001).

5.4.1 Acute data

As expected, during ischaemia, the tissue demonstrating the greatest T_2^* increase to OC was localised to a cortical boundary zone between the MCA and anterior cerebral artery territories, which overlapped the DWI/PWI mismatch area. A smaller T_2^* response was recorded in non-ischaemic tissue, with negligible response within ischaemic core. These MR findings were consistent with our previous studies (Santosh et al, 2008; Robertson et al, 2011; Chapter 4 of the current thesis).

Restoration of blood flow to penumbral tissue will restore arterial oxygen levels back to normal with a resultant decrease in the OEF. The reduction in T_2^* signal change in T_2^*OC-defined penumbra following reperfusion is consistent with our stated hypothesis and provides evidence that the tissue is metabolising aerobically (Figure 5.4B). The extent of reperfusion was apparent on CBF maps, which demonstrated that blood flow in penumbral tissue attained levels similar to the contralateral cortex (Figure 5.5B). However, withdrawal of the intraluminal filament did not universally lead to complete reperfusion, as flow was still compromised in the ADC-defined ischaemic core (31.74±38 mL per 100g per minute, Figure 5.5B). Tissue recovery following reperfusion was evident in the OC-defined penumbra, in which the ADC values were above the ADC threshold of abnormality ($0.63\pm0.06 \times 10^{-3} mm^2/s$). In addition, reperfusion increased the ADC value of some tissue within the ischaemic core to above the predefined viability threshold (shown by change in lesion size following reperfusion) (Figure 5.3A(i) and B(i), and Figure 5.6).

5.4.2 Day 7 Data

T_2^*OC-defined penumbra

Our hypothesis stated that reperfused penumbral tissue should exhibit a normal T_2^* response to OC and this was confirmed on the day 7 T_2^* response (Figure 5.8B). There is evidence to suggest that the T_2^*OC technique is detecting true penumbral tissue. Penumbra must fulfil the fundamental criteria of being functionally reversible and responsive to therapeutic intervention. The region of tissue that displayed an increased T_2^* response (penumbra) in the acute scanning series, whose signal response then attenuated to a level similar to normal tissue following reperfusion, was shown to fully recover in that it did not become incorporated into the final infarct (Figure 5.10). During ischaemia, penumbra is capable of metabolising oxygen and extracting oxygen in the blood, aided by an increased

OEF. As such, during ischaemia, the oxyhaemoglobin: deoxyhaemoglobin ratio would alter in response to OC, in that high baseline deoxyhaemoglobin levels in penumbra convert to oxyhaemoglobin. This, in turn, increases the T_2^* signal response. Following reperfusion, blood flow and concomitant oxygen in the viable penumbral tissue is restored, which reduces the OEF and mirrors the T_2^* response seen in normal tissue. At day 7, this previously penumbral tissue remains out with the final infarct and has a similar T_2^* response to the contralateral hemisphere following OC (Figure 5.10 and 5.8B). As such, the reversibility of penumbra to normal tissue is detected by the T_2^*OC technique and confirmed by T_2-weighted scans.

Ischaemic core

Following reperfusion, irreversibly injured (ischaemic core) tissue should no longer metabolise oxygen or extract oxygen from the blood. Oxyhaemoglobin: deoxyhaemoglobin ratios would therefore be expected to remain static during OC. Within the T_2-defined infarct on day 7 after stroke, a negligible negative T_2^* signal change was observed during OC. The negative signal change recorded may be due to the presence of paramagnetic free oxygen dissolved within the plasma flowing through non-metabolising irreversibly damaged tissue, which will result in a reduction in T_2^* signal. Therefore, after 7 days, T_2^*OC enabled reperfused, non-metabolic tissue to be differentiated from metabolic tissue. Four out of the eight animals died before day 7. The high mortality appears to be most likely due to raised intracranial pressure associated with brain swelling as in these 4 animals the ADC lesion during ischaemia was larger than those animals that survived and the lesion continued to evolve following reperfusion.

5.4.3 Deleterious reperfusion events

In the hyperacute stage of stroke, a region of tissue normally supplied by the occluded artery cannot maintain normal oxygen metabolism when blood flow is reduced. This region is characterised by a decrease in CBF, with partially preserved $CMRO_2$ and LCMRglc. This is the early penumbral stage – often called misery perfusion – in which there is inadequate blood supply relative to metabolic demand (Baron et al, 1981). This phenomenon describes the state in which the tissue cannot receive adequate nutritive delivery whilst its energy reserves are rapidly becoming exhausted. The inadequacy to nourish the still-viable tissue outlines the *in limbo* nature of the ischaemic penumbra, in which full recovery of this tissue is still possible. According to PET studies, misery

perfusion is evident in 45-57% of patients studied within 4 days onset of acute stroke (Figure 5.13) (Baron et al, 1987).

On blood vessel recanalisation, misery perfusion in the ischaemic brain is followed by luxury perfusion which tends to be present during early reperfusion but is not maintained. Luxury perfusion is characterised by an oxygen supply in excess of demand, and its hallmark is a focal reduction of the OEF. It indicates full or partial re-establishment of perfusion within injured or already irreversibly damaged tissue. In luxury perfusion, the CBF may be increased (hyperperfusion), normal, or even decreased (relative to normal perfusion), although by definition in excess of what is required for prevailing $CMRO_2$, which itself may be normal, increased, or reduced. Hyperperfusion may compound the original insult by exacerbating cerebral oedema or by causing intraparenchymal haemorrhage. Therefore, despite a good likelihood of an excellent neurological outcome, reperfusion may paradoxically induce a series of pathophysiological responses which result in potentially fatal outcomes, including cerebral oedema or intracranial haemorrhage (The National Institute of Neurological Disorders and Stroke rT-PA Stroke Study Group (1997). Haemorrhagic transformations 24-36 hours following stroke are more frequent after reperfusion, regardless of the modality used (such as anti-thrombotics, mechanical recanalisation and intravenous lytics) (Khatri et al, 2007). Regarding animal models, reperfusion following a long period of ischaemia may actually increase final infarct size, compared to permanent blood vessel occlusion models (Aronowski et al, 1997; Yang and Betz, 1994). As such, thrombolytic therapy can potentially exacerbate ischaemic injury for certain patients, whilst dramatically improving clinical outcomes in others. The pathological cascade resulting from delayed reperfusion is often termed ‘reperfusion injury’.

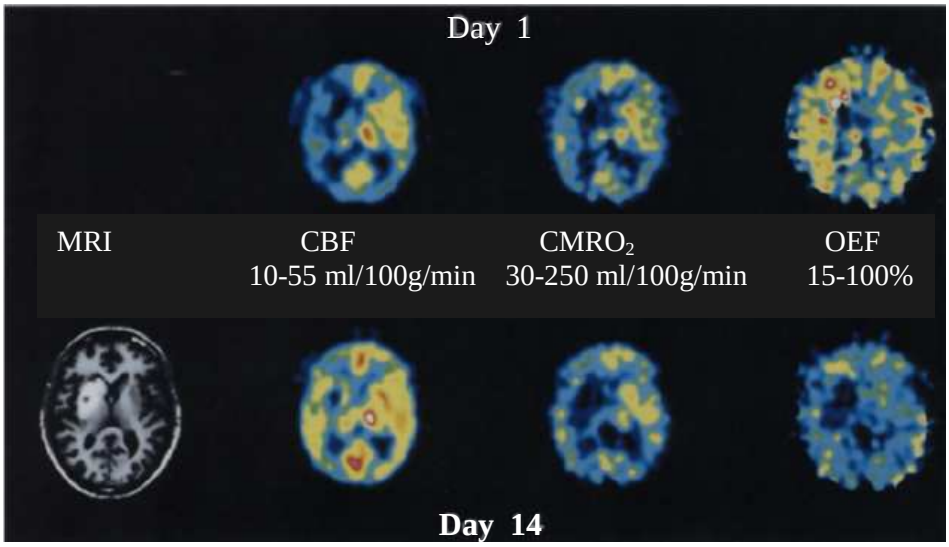

Figure 5.13. Evidence of misery perfusion in the acute stage (day 1), where there is impaired CBF and a preservation of oxygen metabolism (misery perfusion and increased oxygen extraction fraction) throughout whole MCA territory. After two weeks, CBF and $CMRO_2$ are proportionally decreased in this region, suggesting incorporation of penumbra into infarct (Adapted from Heiss and Herholz, 1994)

Reperfusion injury induces a cascade of harmful mechanisms that both introduce cellular dysfunction and increase cell death in tissues compromised by ischaemia. Reintroduction of oxygenated blood to the ischaemic region initiates the generation of oxygen free radicals and infiltration of neutrophils which, in addition to direct neuronal damage, may injure the endothelium and lead to subsequent haemorrhage (Fisher et al, 1990; Matsuo et al, 1995; Iadecola et al, 1996). Additionally, MCAO rat data have shown that inflammatory cells also contribute to increased apoptotic neuronal cell death (Chopp et al, 1996). An inflammatory response is known to originate from biochemical and cellular changes that cause oxidant production and complement activation (Jean et al, 1998). There are systemic and local responses to the onset of inflammation. This secondary brain damage arising from the acute inflammatory reaction may be due to cytokine production and molecular adhesive events. Leukocytes are recruited to the reperfused tissue which may induce microvessel occlusion and thus initiate a no-reflow phenomenon. So, following reperfusion, recirculation is inefficient (Ames et al, 1968) and likelihood of salvage is reduced.

Some subjects may have a more rapid recruitment of ischaemic tissue before reperfusion is performed, thereby leading to non-nutritional reperfusion, which may be due to the actual severity of the ischaemia. There is also a danger of pathophysiological effects following reperfusion, such as blood brain barrier disruption which leads to haemorrhagic transformation, or brain oedema (Molina and Alvarez-Sabin, 2009). However, the extent of reperfusion is now used as a surrogate marker for treatment efficacy, particularly with regards to thrombolytic therapy (Arnold et al, 2005).

5.4.4 Limitations of the study

Time to reperfusion varied slightly between rats due to the time taken to carry out the MRI scanning protocol during ischaemia. The duration of ischaemia was worth examining to note its contribution to mortality and explain why in some rats little or no tissue salvage was seen following reperfusion. The non-surviving animals had a mean reperfusion time of 113±25 min, whereas the surviving animals had a mean reperfusion time of 107±22 min. This non-significant difference suggests that duration of ischaemia was not the contributing factor. Reperfusion is associated with considerable brain swelling at the 24- to 48-hour time point. For this reason, only four of the 8 animals survived out to 7 days. This is a drawback of the intraluminal filament model, where the intact skull means there is no control of intracranial pressure. Also, the presence of iron-rich haemorrhages at day 7 may

undermine the T_2^*OC technique for identifying metabolic tissue following stroke at later time points.

Summary

An attenuation of the T_2^* percentage signal change to OC, following restoration of CBF, was consistent with tissue salvage in the T_2^*OC-defined cortical penumbra. Therefore, cortical tissue identified as penumbra using the OC technique is capable of recovery when blood flow is restored, which provides further evidence for the utility of T_2^*OC MRI for acute stroke management.

Chapter

6

Spatiotemporal mapping of the T_2^*OC- and DWI-PWI mismatch-defined penumbra

6.1 Introduction

When DWI/PWI mismatch was used to select patients for thrombolysis, it identified patterns that may define treatment responsiveness (DEFUSE study, Albers, Thijs & Wechsler et al, 2006) and it has been used to select patients for investigating an extended time window for thrombolytic therapy (Hacke, 2005). However, the technique has not been validated clinically and has a number of limitations. No DWI or ADC threshold has been determined which can differentiate between irreversibly damaged and potentially recoverable tissue (Guadagno et al, 2004) and when DWI/ADC thresholds are applied, the lesions identified can be fully or partially reversed by reperfusion in animal models and man (Kidwell et al, 2000). Interestingly, after reversal of the DWI lesion in humans following thrombolysis, secondary injuries may result in the return of the DWI lesion (Kidwell et al, 2000). As a consequence, thrombolysis may also benefit patients with no evidence of mismatch, since DWI lesions can potentially reverse. Also, defining a threshold for the perfusion deficit is equally difficult and may include benign oligaemic tissue which is not at risk (Butcher et al, 2005; Takasawa et al, 2008).

In animal stroke models, the amount of mismatch tissue has been shown to be very variable, and dependent upon the thresholds applied to ADC and CBF. Mismatch evolution varies between animal strains (Bardutzky et al, 2005) and the techniques applied to induce stroke (Henninger et al, 2006). These are crucial factors, as embolic MCAO models show the presence of penumbra for a long period of time compared to the intraluminal filament model (Zhang et al, 2001; Wang et al, 2001), suggesting that therapeutic time windows may be subjective.

Selection of patients for thrombolysis using DWI/PWI has been attempted (DEFUSE) and the phase II Echoplanar Imaging Thrombolytic Evaluation Trial (EPITHET) suggested that patients with large mismatch may have improved clinical outcomes following

thrombolysis, although the DIAS-2 study indicated otherwise (Donnan et al, 2009; Albers et al, 2006; Hacke et al, 2009; Davis et al, 2008). DIAS-2 defined the PWI perfusion deficit as >20% of the DWI lesion volume when presenting within 3-9 hours of symptom onset, whereas the DEFUSE and EPITHET volumetric measurements of mismatch were generated at a later time point. This highlighted the problem of quantifying CBF and mismatch, as there is no consensus over the thresholds to define the terms. Thresholds often tend to be generated from in-house measurements, and the introduction of standardised parameters may simplify findings between groups and studies.

The penumbra *per se* is defined not only as a region of perfusion deficit but also of some remaining metabolic activity. The absence of a marker of tissue metabolism for penumbral definition in current MRI paradigms renders comparability with standard PET findings difficult and leaves interpretation susceptible to the varied approaches used to define the perfusion deficit. As such, technological advancements are in place which introduce a measurement of metabolic activity to mismatch estimation, including MRI assessments of $CMRO_2$ (Xu et al, 2009) and MR-PET technology (Beyer and Pichler, 2009).

Aims

The previous studies have applied one T_2^*OC to identify penumbra and tested if this tissue compartment demonstrated the characteristics of penumbral tissue, i.e., ongoing glucose metabolism, and recovery on early reperfusion. Penumbral tissue would be expected to deteriorate and become incorporated into the irreversibly damaged ischaemic core over time if blood supply is not restored. In this study, I investigated how the T_2^*OC defined penumbra changed over time and then compared this with identification of penumbra as defined by PWI/DWI mismatch.

The main goals were:

(1) To map the temporal and spatial dynamics of tissue compartments in the ischaemic brain by applying thresholds according to its ADC, CBF and T_2^* status. Specifically, tissue compartments were defined by generating images using ADC and CBF criteria, CBF and T_2^* criteria, and ADC and T_2^* criteria.

(2) Identify and quantify the normal, ischaemic core and penumbral tissue compartments as defined by the aforementioned criteria over the first 4 hours following stroke.

6.2 Materials and methods

6.2.1 Rodent MCAO surgery

Male Sprague-Dawley rats (328±22g, n=6, Harlan, Bicester, UK) were initially anesthetized with 5% inhaled isoflurane in an induction chamber at room temperature. Following intubation, animals were artificially ventilated with 2% isoflurane delivered in air, slightly enriched with oxygen (30%) to maintain physiological stability throughout the experiment. Blood gases were maintained within the normal physiological range apart from increased arterial partial pressure of oxygen (PaO_2) during the OC. $PaCO_2$ was maintained between 35 and 45 mmHg to minimise cerebrovascular reactivity (Table 6.1). A rectal thermocouple provided continual monitoring of core body temperature that was maintained at 37°C±0.5°C. A polyethylene catheter (Portex: external diameter 0.96mm; internal diameter 0.58mm; 70cm long) was placed in the femoral artery, to continuously monitor blood pressure and conduct blood gas analysis. Middle cerebral artery occlusion (MCAO) was achieved by the intraluminal filament model, as described in Chapter 2.2.3.

6.2.2 MRI scanning

Scanning Protocol

Scanning was performed at three time points acutely (Figure 6.1) and once at the 24 hour time point. Firstly, at approximately 1 hour after stroke, animals underwent MRI scanning that comprised DWI to detect ischaemic injury, T_2^*OC to detect penumbra, and ASL to provide CBF maps of ischaemia. This scanning sequence was then repeated again at 2.5- and 4- hours following stroke. Rats were then recovered and rescanned at 24 hours post-stroke where RARE T_2-weighted imaging was performed to define the final infarct. The animals also underwent T_2^*OC and ASL at this time point.

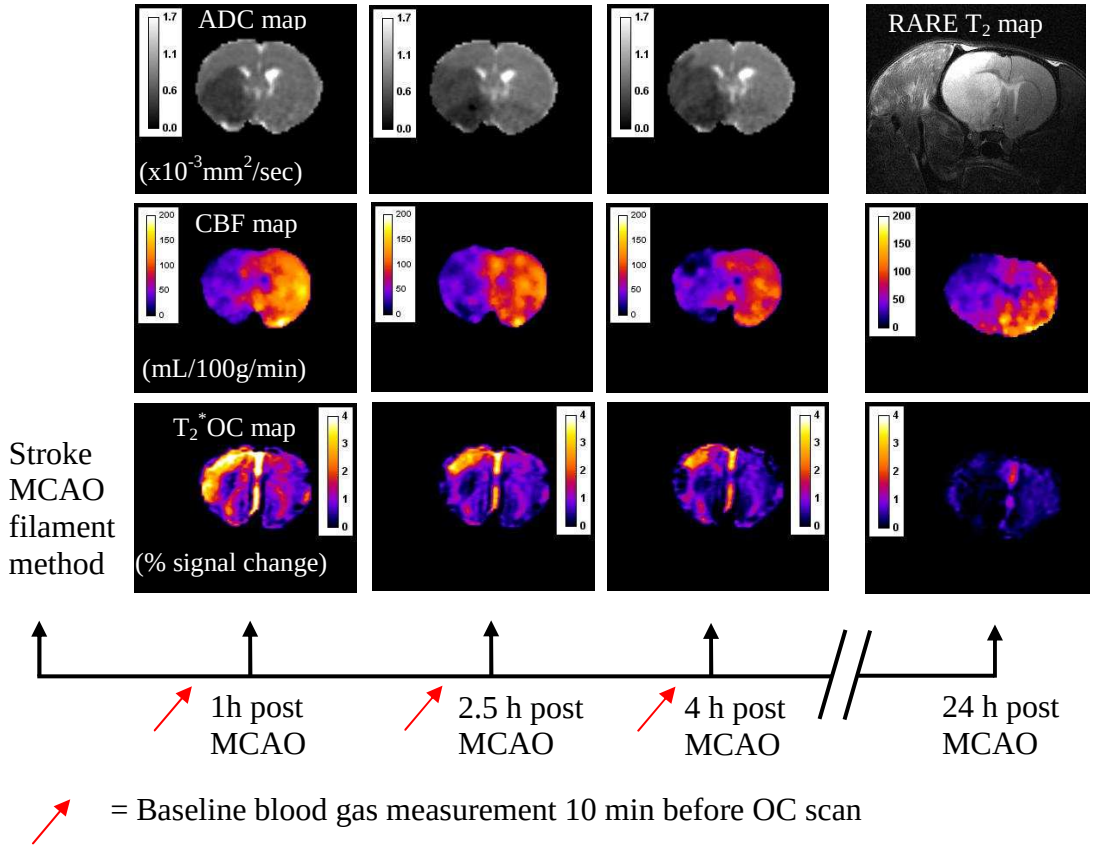

Figure 6.1 Time line of experimental protocol. Following stroke, the animals were placed in the magnet and a DWI scan was performed to identify ischaemic damage, ASL to generate fully quantitative blood flow maps and mismatch images were produced. T_2^*OC was also performed during this period of ischaemia to derive T_2^* percentage signal change maps. The scanning sequence was repeated twice, to allow T_2^*OC scanning at 2.5 hours and 4 hours post-MCAO. The animals were removed from the magnet and recovered up to 24 hours, and T_2^*OC and a RARE T_2 was performed

Diffusion-weighted imaging and perfusion-weighted imaging

Diffusion-weighted and perfusion-weighted imaging was performed as described in Chapter 2.5.3 and 2.5.4. DW- and PW-weighted imaging was used to define penumbra from DWI/PWI mismatch and data were analysed on four selected coronal slices within the MCA territory. The scanning time for a single ASL slice was ~6 minutes and four slices were scanned throughout the MCA territory. Additionally, a T_1-weighted image (scan time 10 minutes) was performed to allow quantification of CBF in mL per 100g per minute.

T_2^*-weighted imaging

T_2^*-weighted imaging was performed as described in Chapter 2.5.6. The same four coronal MRI slices throughout MCA territory used to generate CBF and ADC maps were selected for analysis. These slices were carefully selected to minimise the effect of susceptibility distortion around the ear canals. The paradigm for the T_2^*-weighted OC sequence was 5 minutes breathing air, followed by 5 minutes breathing 100% oxygen, and then 10 minutes breathing air. This sequence was repeated 24 hours after stroke.

T_2-weighted imaging

A coronal RARE T_2 sequence was performed as described in Chapter 2.5.5 which enabled T_2-derived final infarct measurements

6.2.3 MRI data analysis

T_2^* oxygen challenge time course data and defining the ischaemic penumbra

T_2^* percentage signal change was calculated from time course graphs, where the average baseline signal was subtracted from the peak signal during OC. This value was then divided by the average baseline signal and multiplied by 100. T_2^* percentage signal change maps were generated using ImageJ software. The boundaries of penumbral tissue were defined using a threshold based on the empirical rule: the mean plus 2 SD of the T_2^* value of the contralateral hemisphere, excluding the ventricles.

Defining the ischaemic penumbra with DWI/PWI mismatch

Quantitative ADC maps, in units of square millimetres per second, were calculated using the Stejskal–Tanner equation (Stejskal and Tanner, 1965). Apparent diffusion coefficient maps and CBF maps were generated using ImageJ and the ADC lesion and perfusion deficit, respectively, were thresholded using the empirical rule. Perfusion deficit area was calculated on each of the four PWI slices. Apparent diffusion coefficient and CBF maps were overlaid to identify the DWI/PWI mismatch area. DWI/PWI mismatch was calculated as the difference between the perfusion deficit and the ADC lesion area on the corresponding slice. Volumes of DWI/PWI mismatch and thresholded T_2^*OC-defined penumbra were generated from the data and the neuroanatomical location compared between the two techniques.

Coregistration

To coregister the T_2^*OC scans with the ADC and CBF scans at the three time points, linear coregistration was performed using Analyze. To align the data, T_2^* images were co-registered to their corresponding ADC slices, which allowed accurate pixel-by-pixel analysis.

Volumetric Analysis of Penumbra

The thresholds for ADC, CBF and T_2^* are defined as:
ADC – Mean contralateral hemisphere ADC values (excluding ventricles) **minus** 2SD
CBF – Mean contralateral hemisphere CBF values (excluding ventricles) **minus** 2SD
T_2^* - Mean contralateral hemisphere T_2^* (excluding large veins and ventricles) **plus** 2SD

Note that no lower limit of T_2^* was defined, and as such, normal tissue may have a T_2^* value above or below the T_2^* threshold, providing the region has normal ADC and CBF values (i.e., values above the ADC and CBF thresholds).

6.2.4 Pixel-by-pixel analysis

Pixel-by-pixel analysis provides an unbiased means of investigating the spatial and volumetric dynamic evolution of brain damage. Pixel-by-pixel analysis was generated using codes written in Matlab (MathWorks, Natick, MA, U.S.A.). Temporal changes in pixel distribution were analysed using pixel-by-pixel scatterplots and colour-coded images (such as in Figure 6.5) were derived to identify specific tissue compartments based on the ADC, CBF and T_2^* thresholds. Pixel-by-pixel analysis was performed to identify tissue regions based on ADC and CBF values (which are traditionally used to define DWI/PWI mismatch), the T_2^* and CBF values, and the T_2^* and ADC values.

Rat brain tissue was segmented into different compartments using an automated MatLab program written specially for this purpose by Dr Maria del Rosario Lopez-Gonzalez. The program inputs are the prepared images (i.e. cropped, and background values adjusted to -90 in the case of the CBF maps, 0 for the ADC maps and -1 for the T_2^*% signal change maps), and the threshold values of ADC, CBF and T_2^*. The program classifies the tissue using these threshold values for the 4 selected slices.

The program runs using interactive inputs from users during execution and runs by typing ‘t2’ in the command line; the program then asks the user for the input values/files, for example:

>> t2
Enter 1 or 2, for single or double threshold values: 1
Enter name of DWI map: DWI1.tif
Enter name of CBF map: CBF1.tif
Enter name of T_2^* map: PctChg.tif
Enter adc threshold value: 0.5
Enter cbf threshold value: 60
Enter T_2^* threshold value: 1

After execution, the program produces scatter plots of ADC vs CBF, T_2^* vs ADC and T_2^* vs CBF, colour coded maps of the segmented tissue, and histograms of ADC, CBF and T_2^* signal intensities. Additionally, the program gives the number of pixels per tissue compartment using ADC vs CBF, T_2^* vs ADC and T_2^* vs CBF maps which allows derivation of volumetric tissue compartment measurements.

For the ADC v CBF images, the four compartments were operationally defined as:
1. The '**normal**' region where both ADC and CBF values were above the thresholds;
2. The '**core**' region where both ADC and CBF values were below the thresholds;
3. The '**mismatch**' (or penumbral) region where the ADC value was above the threshold and the CBF value was below the threshold, and;
4. The **'negative mismatch'** region where the ADC value was below the threshold and CBF value was above the threshold (Figures 6.5 and 6.6)

For the T_2^* signal change to OC (T_2^*OC) v CBF images the four compartments were defined as:
1. The '**normal**' region where T_2^* signal change was below and CBF was above the thresholds;
2. A second '**normal**' region where both T_2^* signal change and CBF were above the thresholds;
3. The '**T_2^*OC defined penumbra**' region where the T_2^* signal change was above the threshold and the CBF value was below the threshold, and;
4. The '**core**' region where T_2^* signal change was below the threshold and CBF was below the threshold (Figures 6.7 and 6.8)

For the T_2^* signal change to OC v ADC images the four compartments were defined as:
1. The '**normal**' region where both T_2^* signal change and the ADC value were above the thresholds;
2. A second '**normal**' region where T_2^* signal change was below and ADC was above the thresholds;
3. The '**T_2^*OC defined penumbra'** region where the T_2^* signal change was above the threshold and ADC was below the threshold, and;
4. The '**core**' region where the T_2^* signal change was below the threshold and ADC was below the threshold (Figures 6.9 and 6.10)

It is important to note that it was not possible to exclude the ventricles and large veins prior to pixel-by-pixel analysis, and as such, these structures are included in the data.

Pixel-by-pixel tissue compartment volumetric analysis

For each acute time point, the tissue volume and mean±SD was calculated for each compartment for the three methods of tissue identification. The Matlab program also

quantifies the number of pixels within each tissue compartment, and so tissue area was calculated by the multiplying the number of pixels in a tissue compartment by the area of a pixel (0.0678 mm^2). Tissue volume was then generated by multiplying the areas by the tissue thickness (1.5 mm) (Figures 6.11, 6.12 and 6.13)

6.2.5 Quantifying final infarct at 24 hours

Infarct volume was calculated using ipsilateral brain swelling and contralateral compression corrections first described by Swanson and colleagues (1994) and Gerriets and colleagues (2004), respectively. Eight coronal RARE T_2 slices which matched the eight 4-hour acute ADC slices were selected, and the ipsilateral and contralateral hemisphere areas, as well as the final infarct area, were calculated by manual tracing using ImageJ. Infarct volumes were identified as regions of hyperintensity on the RARE T_2 scans. The volumes of the ipsilateral and contralateral hemispheres (HVi and HVc, respectively) and the lesion (LV) were calculated by summing the individual areas and the multiplying by slice thickness (1.5mm).

To correct for brain oedema and swelling, Swanson correction (Swanson et al, 1994) for lesion volume is as follows;

$$\textit{Swanson's correction for lesion volume} = (HVc) - (HVi\text{-}LV)$$

However, this correction factor does not account for contralateral compression, and so Gerriets' correction for compression was applied to calculate the lesion volume as a percentage of the ipsilateral hemisphere;

$$\textit{Corrected \%HLV} = ((HVc - HVi + LV) / HVc)) \times 100$$

A further compression correction factor to calculate the hemispheric lesion volume (Gerriets et al, 2004) was used;

$$\textit{Gerriets compression correction factor} = (HVi + HVc) / (2 \times HVc)$$

Therefore, to calculate the corrected lesion volume (cLV) that corrects for ipsilateral swelling (using the Swanson equation) and contralateral compression (using Gerriets' compression factor), the following equation was used;

$$cLV = Swanson\ lesion\ volume \times Gerriets\ compression\ correction\ factor$$

6.2.6 Statistical analysis

All data are presented as mean±SD. A one-way analysis of variance followed by Student's paired t-test with a Bonferroni correction for multiple comparisons was used to analyse the temporal evolution of the ADC-derived lesion volume. Comparison of physiological variables (pH, $PaCO_2$ and PaO_2) and the tissue volumes at the three time points were analysed using one-way analysis of variance followed by Student's paired t-test with a Bonferroni correction for multiple comparisons.

6.3 Results

6.3.1 Physiological variables

For the first scan series, the mean time to commence OC was 62±2.6 minutes after MCAO, and 150±1.7 minutes and 242±14 minutes post-MCAO for the 2.5 and 4 hour scan series, respectively. Physiological variables were recorded immediately before OC (Table 6.1). There were no significant differences in both $PaCO_2$ and PaO_2 at the three time points. A small but statistically significant ($p<0.0001$) increase in blood pH was recorded at 4 hours compared to the pH at the 1 hour and 2.5 hour time points but this had no physiological significance.

6.3.2 Evolution of ischaemic damage and concomitant loss of penumbra

By identifying the extent and change of ischaemic damage and penumbra over the 4 hours post-stroke, it was clear that the dynamic evolution of brain damage was not similar for all animals. From observation, for four out of the six animals, the ADC-derived ischaemic damage on the 4 selected coronal slices did not evolve markedly and the areas of penumbra did not measurably decrease over the time course of scanning (a sample animal is shown in Figure 6.2). An animal that did experience a dynamic increase in ADC-derived ischaemic damage with a concomitant loss of penumbral tissue is shown in Figure 6.3.

	1 hour scan series	2.5 hour scan series	4 hour scan series
pH	7.34±0.04	7.34±0.05	7.36±0.04***
pCO_2	44.5±5.7	45.33±10	42.42±5.7
pO_2	93.62±11	93.42±12	95.68±15

Table 6.1. Physiological variables in arterial blood samples at the three time points. Data expressed as mean±SD, *** p<0.0001, one-way analysis of variance followed by Student's paired t-test with a Bonferroni correction for multiple comparisons.

Time post-stroke (mins) when scans were run	**DWI scan**	**Slice 4 ASL**	**Slice 5 ASL**	**Slice 6 ASL**	**Slice 7 ASL**	**OC scan**
1 hr scan series	57±4.6	45.7±7.6	66±20	94±10	103±8	62±2.6
2.5 hr scan series	133±24	110±14	122±10	149±22	169±20	150±1.7
4 hr scan series	247±26	200±45	214±55	227±43	233±44	242±14

Table 6.2. Mean scan times (n=8) for the DWI, ASL and OC scans at the three scanning time points. Data expressed as mean minutes post-ischaemia±SD

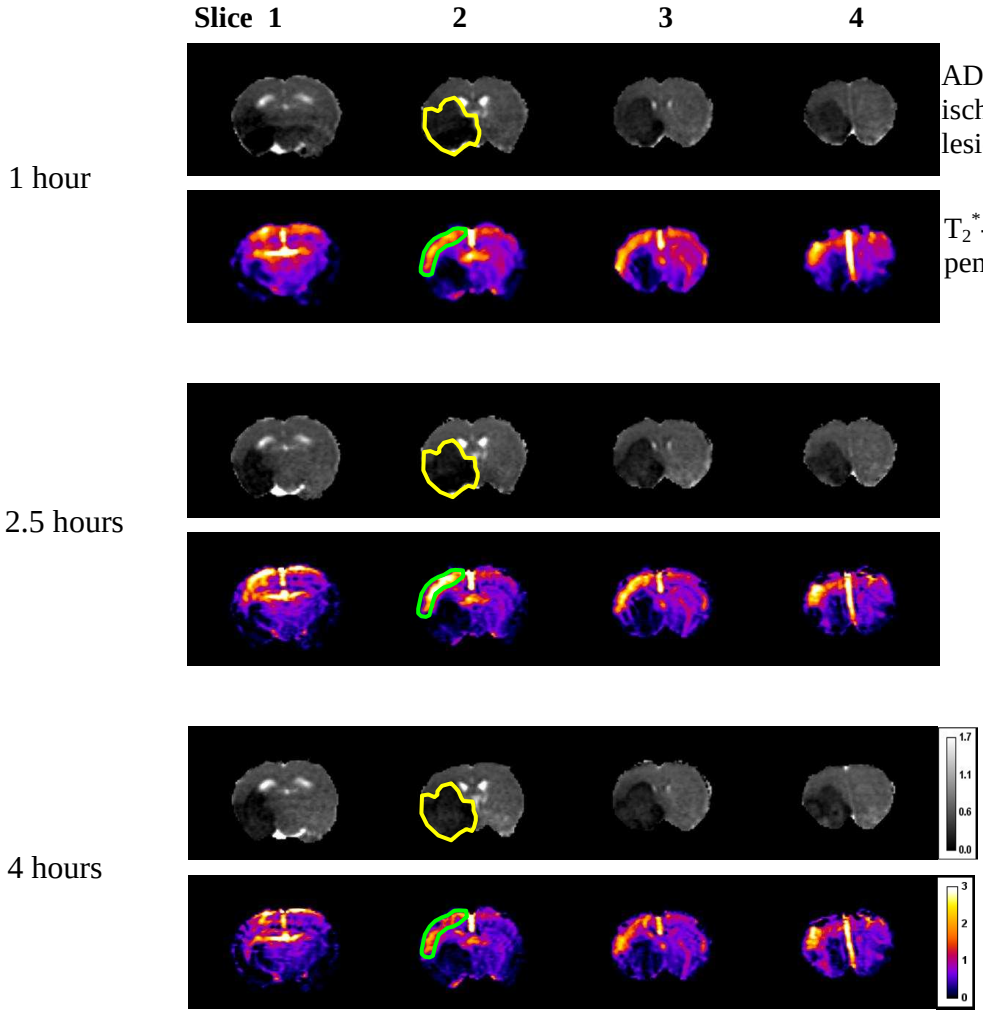

Figure 6.2. An example of an animal where the ADC lesion (drawn in yellow on slice 2 at each time point) and the T_2^*OC-defined penumbral tissue (drawn in green on slice 2 at each time point) did not increase and decrease significantly over time, respectively. ADC maps measured in $x10^{-3}mm^2$/sec and T_2^*OC maps scaled in units of percentage signal change

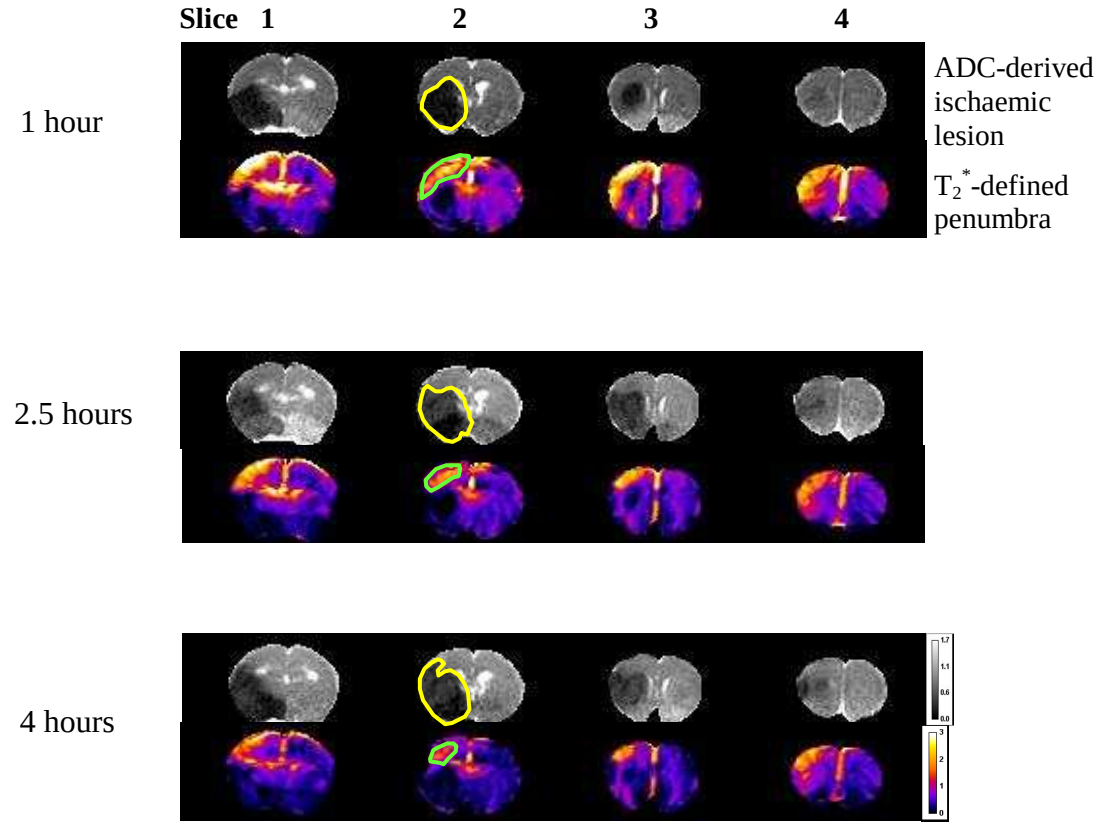

Figure 6.3. An example of an animal where the ADC lesion (drawn in yellow on slice 2 at each time point) and the T_2^*OC-defined penumbral tissue (drawn in green on slice 2 at each time point) increased and decreased over time, respectively. ADC maps measured in $x10^{-3}mm^2$/sec and T_2^*OC maps scaled in units of percentage signal change

6.3.3 Volumetric analysis of the thresholded T_2^*% signal change region

For comparative purposes, penumbra was firstly calculated using only the thresholded T_2^* percentage signal change region (Figure 6.4, and green line on Figure 6.13). At the one hour time point, the volume of tissue defined as penumbra was 45.9±31.2 mm^3, which reduced to 37.2±25 mm^3 at 2.5 hours and reduced again to 32.9.1±25 mm^3 at 4 hours post stroke. However this was not statistically significant, and there was no significant difference between the volumes at the 1 and 4 hour time points. This highlights that penumbral volume tended to remain relatively static over the course of the 4 hours in four of the animals, whereas decrease in penumbral volume occurred in two animals (animal IDs; Serial OC 7 and 10 on Figure 6.4).

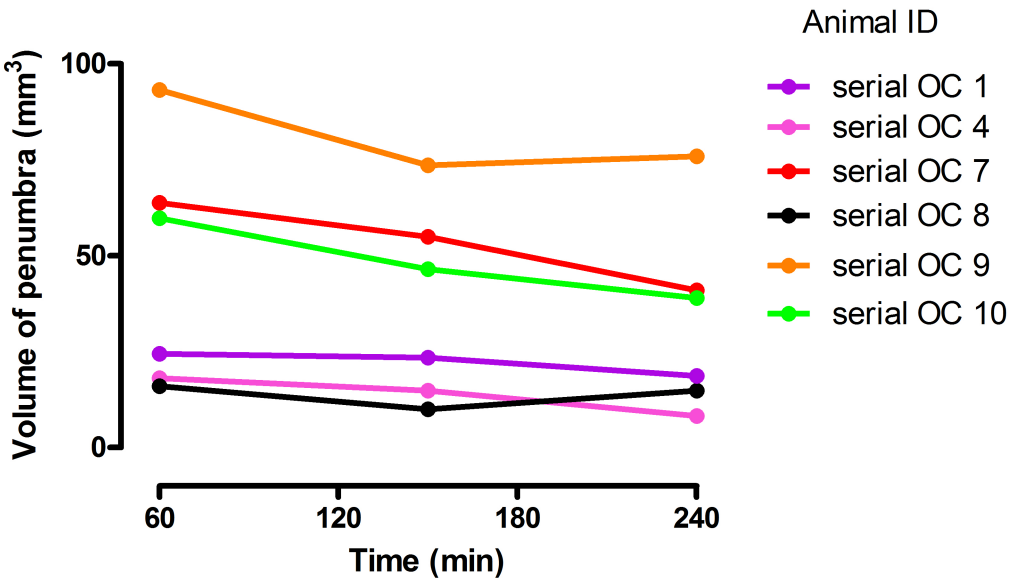

Figure 6.4. Penumbra calculated by measuring the volume of the thresholded T_2^*% signal change region for each animal (n=6). Penumbral volume remained relatively static over the 4 hour time point

6.3.4 Pixel-by-pixel analysis

ADC v CBF

The dynamics of ischaemic evolution was analysed on a pixel-by-pixel basis using the three methods of analysis. Figures 6.5 and 6.6 show representative ADC v CBF scatterplots and colour-coded maps of 4 slices from one animal at the three time points, with data subdivided into four quadrants which were defined by ADC and CBF thresholds. In the scatterplots, there were large clusters residing in the region defined as normal tissue (Region 3), the ischaemic core (Region 1) and penumbra (Region 4), with a small number of pixels residing in the tissue defined as negative mismatch (Region 2). The large pixel populations did not appear to evolve dynamically over time.

T_2^* v CBF

In the scatterplots (Figures 6.7 and 6.8), there were large clusters residing in the two regions defined as normal (Region 3 and 4) and the ischaemic core compartment (Region 1), with a smaller cluster in the region defined as penumbra (Region 2). The large pixel populations did not significantly evolve dynamically over time.

T_2^* v ADC

In the scatterplots (Figures 6.9 and 6.10), there were large clusters residing in the two regions defined as normal (Region 3 and 4) and the ischaemic core compartment (Region 1), with a smaller cluster in the region defined as penumbra (Region 2). The large pixel populations did not significantly evolve dynamically over time.

ADC v CBF

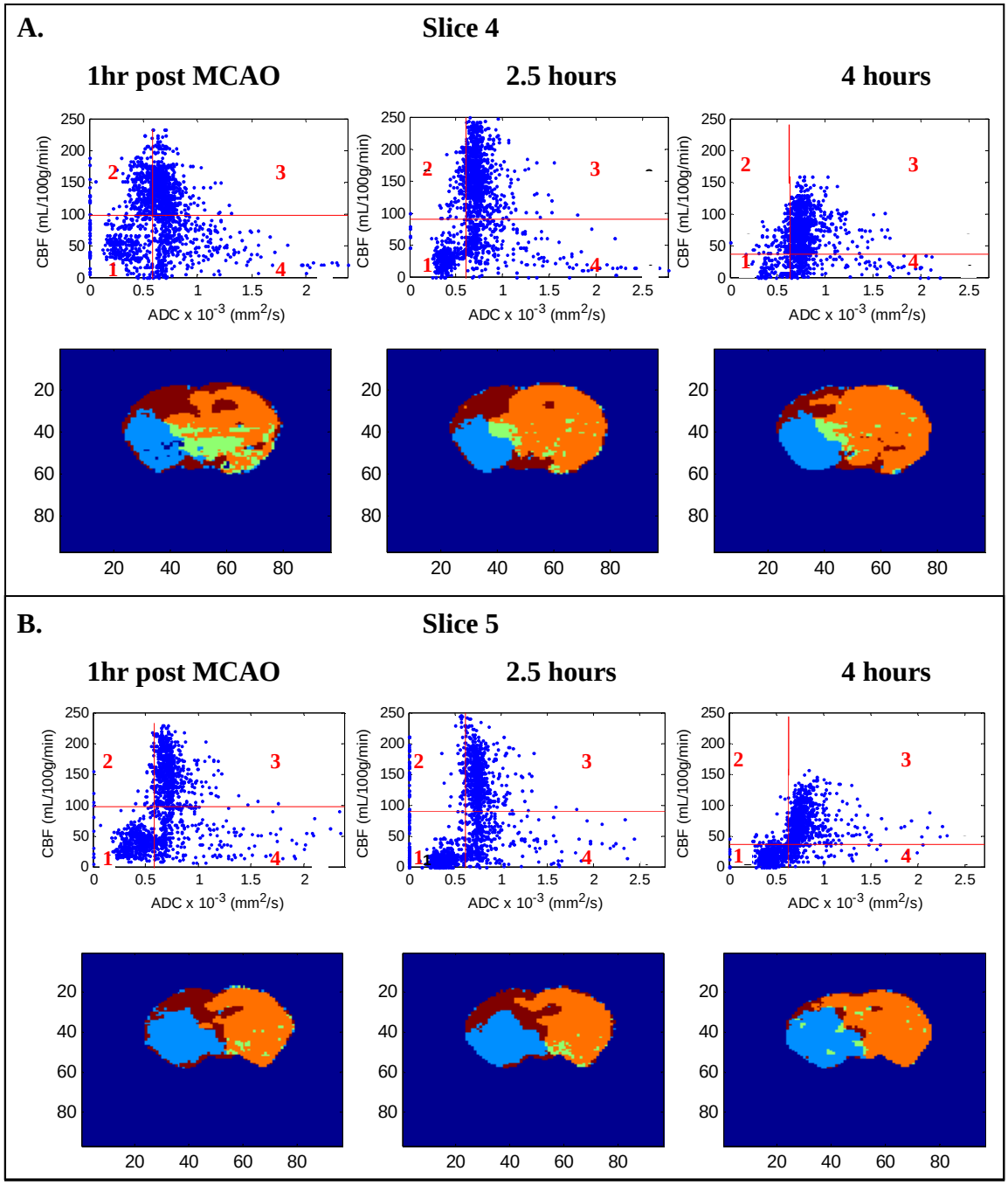

Figure 6.5. Pixel-by-pixel scatterplots and colour-coded maps of ADC v CBF in one animal for **A**. Slice 4 and **B**. Slice 5 at 1-, 2.5- and 4-hours post-pMCAO.

On scatterplots: Region 1: Ischaemic core Region 2: Negative mismatch
Region 3: Normal Region 4: Penumbra

On colour-coded maps:

Negative mismatch Ischaemic core
Penumbra Normal

Negative mismatch is evident on slice 4 due to a ghosting artefact on the ADC scans

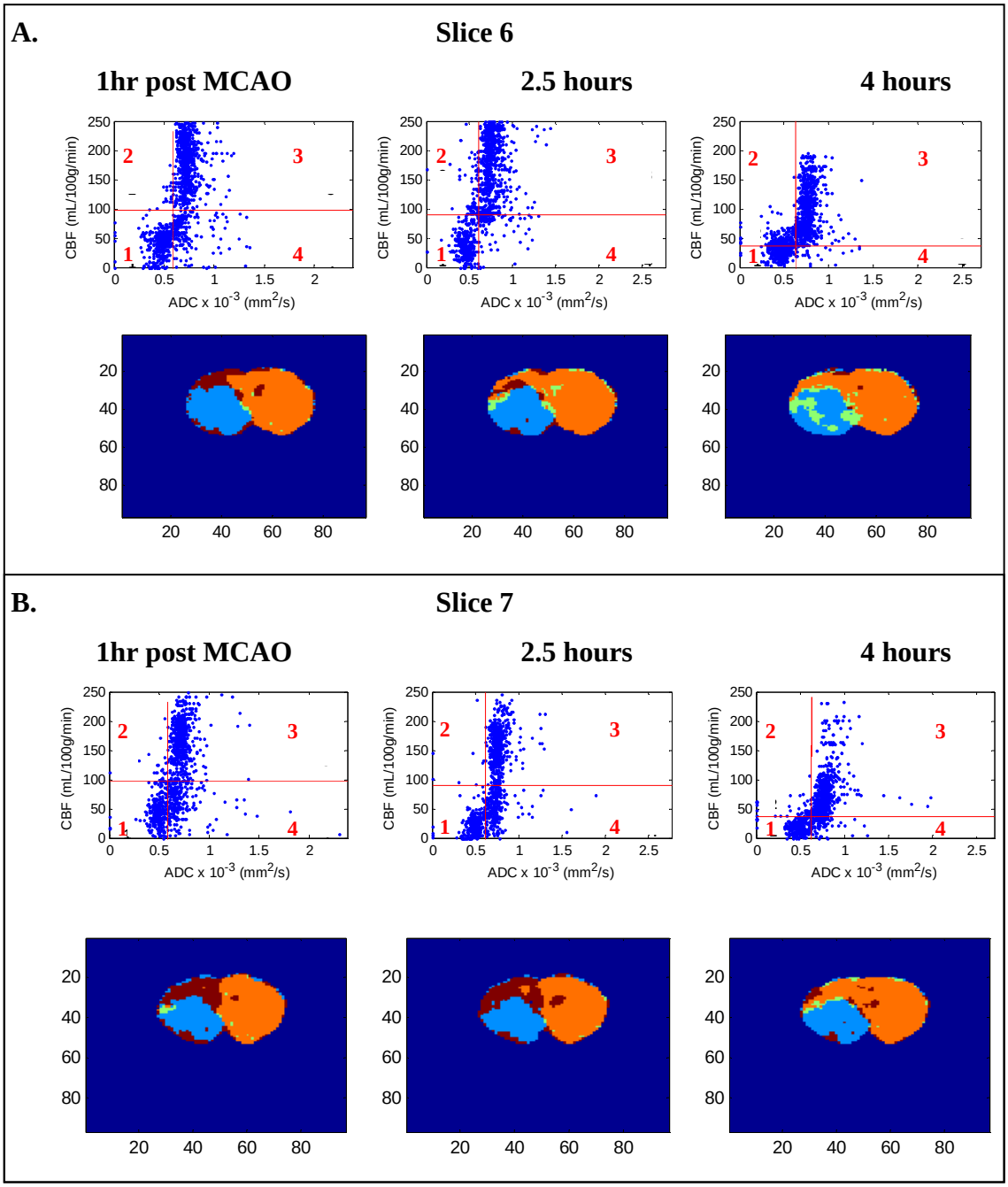

Figure 6.6. Pixel-by-pixel scatterplots and colour-coded maps of ADC v CBF in one animal for **A**. Slice 6 and **B**. Slice 7 at 1-, 2.5- and 4-hours post-pMCAO.

On scatterplots: Region 1: Ischaemic core Region 2: Negative mismatch
Region 3: Normal Region 4: Penumbra

On colour-coded maps:

Negative mismatch Ischaemic core
Penumbra Normal

T_2^* v CBF

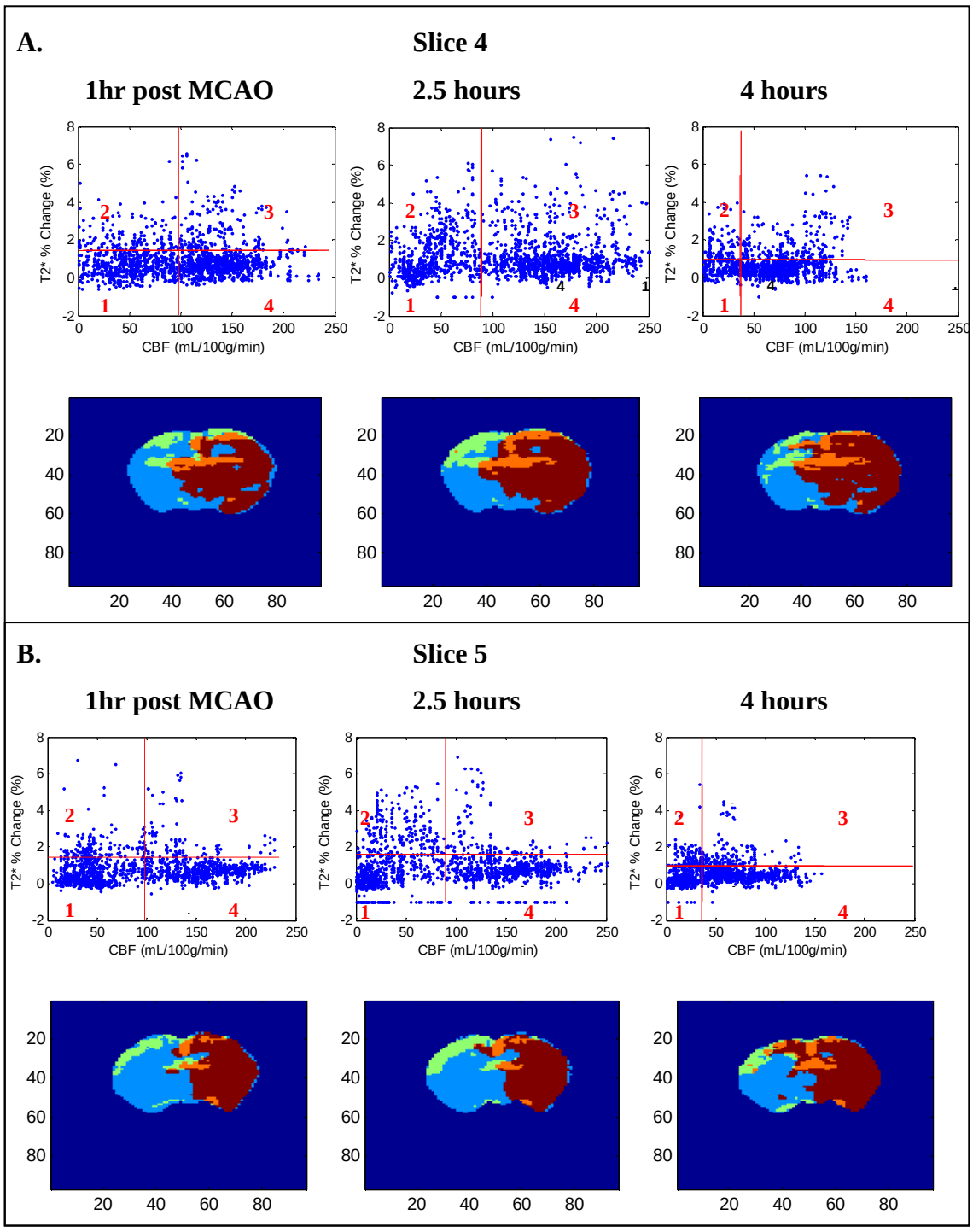

Figure 6.7. Pixel-by-pixel scatterplots and colour-coded maps of T_2^* v CBF in one animal for **A**. Slice 4 and **B**. Slice 5 at 1-, 2.5- and 4-hours post-pMCAO.

On scatterplots: Region 1: Ischaemic core Region 2: Penumbra

Region 3: Normal with ↑ T_2^* Region 4: Normal

On colour-coded maps:

- T_2^*OC-defined penumbra
- Ischaemic core
- Normal tissue (T_2^*% change below threshold)
- Normal tissue (statistically increased T_2^* % change)

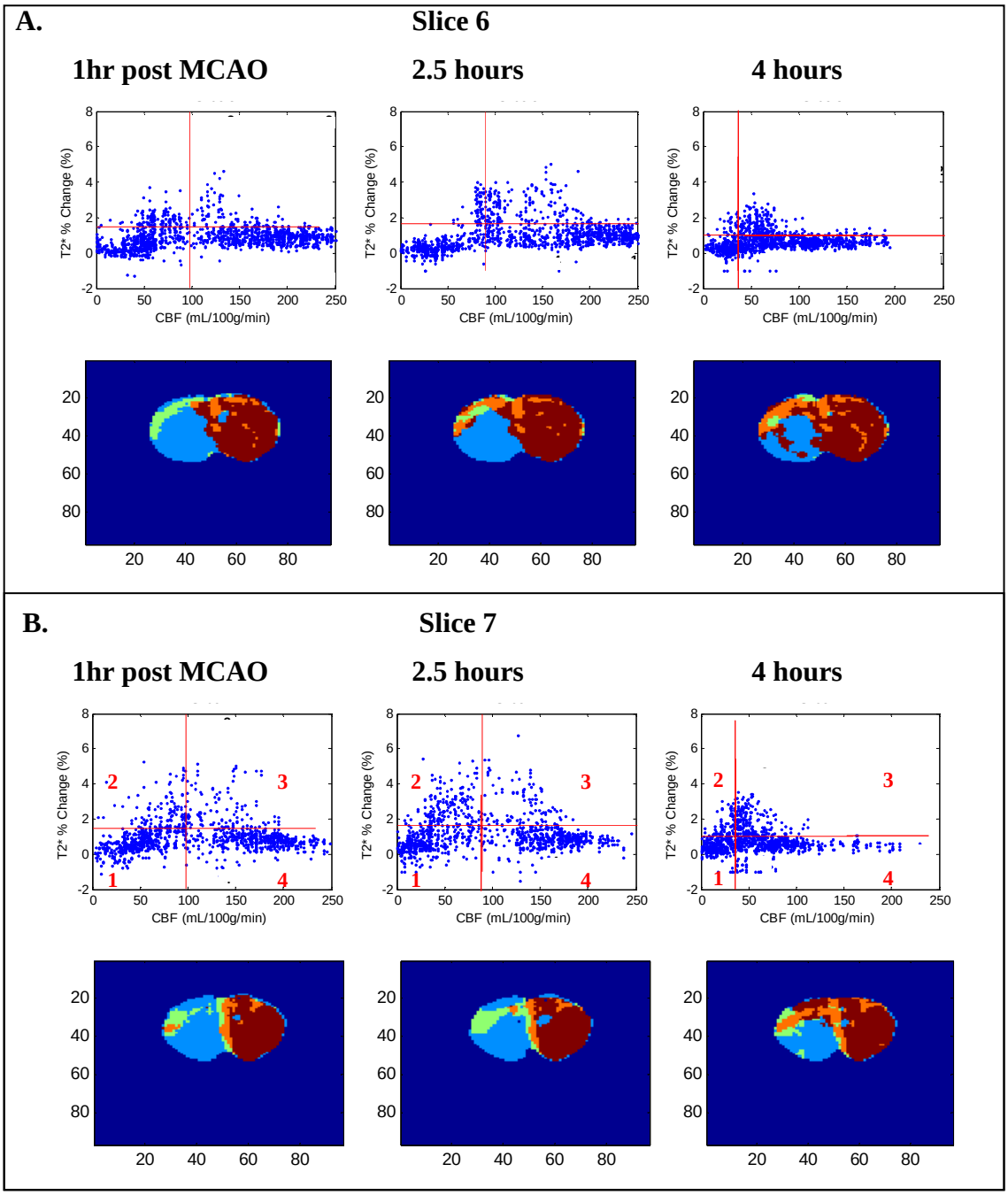

Figure 6.8. Pixel-by-pixel scatterplots and colour-coded maps of T_2^* v CBF in one animal for **A**. Slice 4 and **B**. Slice 5 at 1-, 2.5- and 4-hours post-pMCAO.

On scatterplots: Region 1: Ischaemic core Region 2: Penumbra

Region 3: Normal with ↑ T_2^* Region 4: Normal

On colour-coded maps:

- T_2^*OC-defined penumbra
- Ischaemic core
- Normal tissue (T_2^*% change below threshold)
- Normal tissue (statistically increased T_2^* % change)

T_2^* v ADC

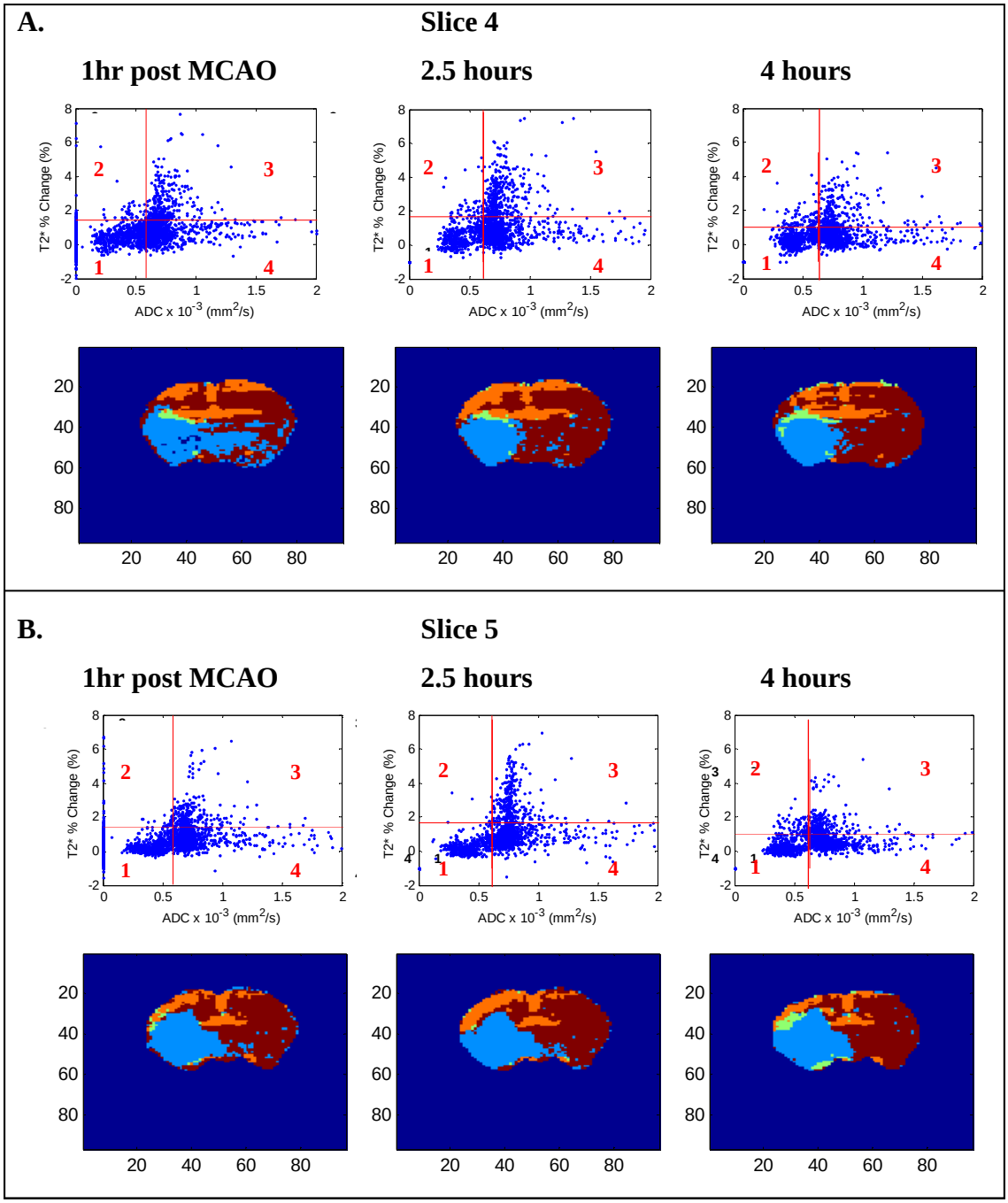

Figure 6.9. Pixel-by-pixel scatterplots and colour-coded maps of T_2^* v ADC in one animal for **A**. Slice 4 and **B**. Slice 5 at 1-, 2.5- and 4-hours post-pMCAO.

On scatterplots: Region 1: Ischaemic core Region 2: Penumbra

Region 3: Normal with ↑T_2^* Region 4: Normal

On colour-coded maps:

- T_2^*OC-defined penumbra
- Ischaemic core
- Normal tissue (T_2^*% change below threshold)
- Normal tissue with statistically increased T_2^* % signal change

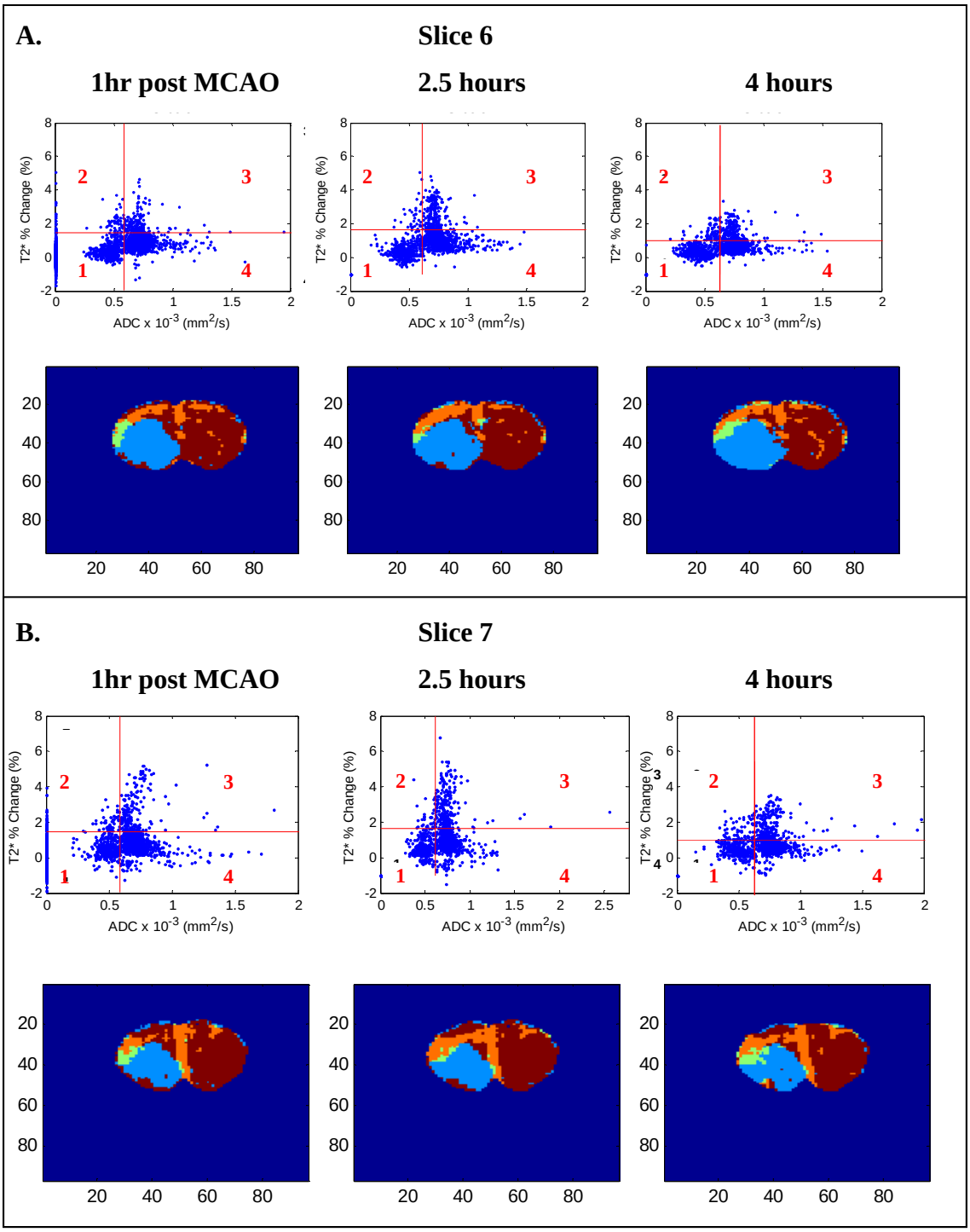

Figure 6.10. Pixel-by-pixel scatterplots and colour-coded maps of T_2^* v ADC in one animal for **A**. Slice 6 and **B**. Slice 7 at 1-, 2.5- and 4-hours post-pMCAO.

On scatterplots: Region 1: Ischaemic core Region 2: Penumbra

Region 3: Normal with ↑T_2^* Region 4: Normal

On colour-coded maps:

- T_2^*OC-defined penumbra
- Ischaemic core
- Normal tissue (T_2^*% change below threshold)
- Normal tissue with statistically increased T_2^* % signal change

6.3.5 Pixel-by-pixel tissue compartment volumetric analysis

ADC v CBF

Ischaemic core pixels

Using ADC v CBF pixel-by-pixel analysis, at the 1 hour time point, the volume of tissue identified as ischaemic core was 163.8±45 mm^3, which non-significantly increased to 186.6±31 mm^3 at 2.5 hours and then non-significantly reduced to 175±55 mm^3 at 4 hours (Figure 6.11).

Normal pixels

At the one hour time point, the volume of tissue identified as normal was 365±53 mm^3, which non-significantly increased to 372±37 mm^3 and then 397±45 mm^3 at the 2.5 hour and 4 hour time point, respectively (Figure 6.12).

Ischaemic penumbra

At the one hour time point, the volume of tissue defined as penumbra was 104±39 mm^3 which non-significantly decreased to 68±38 mm^3 and then 51±19 mm^3 at the 2.5 hour and 4 hour time point, respectively (Figure 6.13). There was a significant decrease in penumbral volume from the 1- to 4- hour time point ($p<0.05$)

T_2^* v CBF

Ischaemic core pixels

Using T_2^* v CBF pixel-by-pixel analysis, at the 1 hour time point, the volume of tissue identified as ischaemic core was 210±45 mm^3, which non-significantly increased to 213±42 mm^3 at 2.5 hours and then non-significantly reduced to 183±47 mm^3 at 4 hours (Figure 6.11).

Normal pixels

At the one hour time point, the volume of tissue identified as normal was 364±51 mm^3, which non-significantly reduced to 363±35 mm^3 and then non-significantly increased 393±43 mm^3 at the 2.5 hour and 4 hour time point, respectively (Figure 6.12).

Ischaemic penumbra

At the one hour time point, the volume of tissue defined as penumbra was 57±24 mm^3 which non-significantly decreased to 41±31 mm^3 and then non-significantly decreased to 37±12 mm^3 at the 2.5 hour and 4 hour time point, respectively (Figure 6.13).

T_2^* v ADC

Ischaemic core pixels

Using T_2^* v ADC pixel-by-pixel analysis, at the 1 hour time point, the volume of tissue identified as ischaemic core was 174±45 mm^3, which non-significantly increased to 203±33 mm^3 at 2.5 hours and then non-significantly reduced to 199±37 mm^3 at 4 hours (Figure 6.11).

Normal pixels

At the one hour time point, the volume of tissue identified as normal was 439±45 mm^3, which non-significantly reduced to 389±38 mm^3 and then non-significantly reduced to 384±35 mm^3 at the 2.5 hour and 4 hour time point, respectively (Figure 6.12).

Ischaemic penumbra

At the one hour time point, the volume of tissue defined as penumbra was 20±6 mm^3 which non-significantly increased to 26±18 mm^3 and then 36±10 mm^3 at the 2.5 hour and 4 hour time point, respectively (Figure 6.13).

Overall, as time evolved, the ischaemic core volume non-significantly increased from 1 to 4 hours using the ADC v CBF and T_2^* v CBF methods, and it non-significantly decreased with the T_2^* v ADC method. In the penumbral compartment, penumbral volume decreased over time using all three methods (significantly for the ADC v CBF, and non-significantly for the two T_2^* methods). The dynamic evolution of the normal tissue volume was well-matched (non-significant increase) when comparing the ADC v CBF and the T_2^* v CBF methods, whilst the evolution in the T_2^* v ADC method non-significantly decreased.

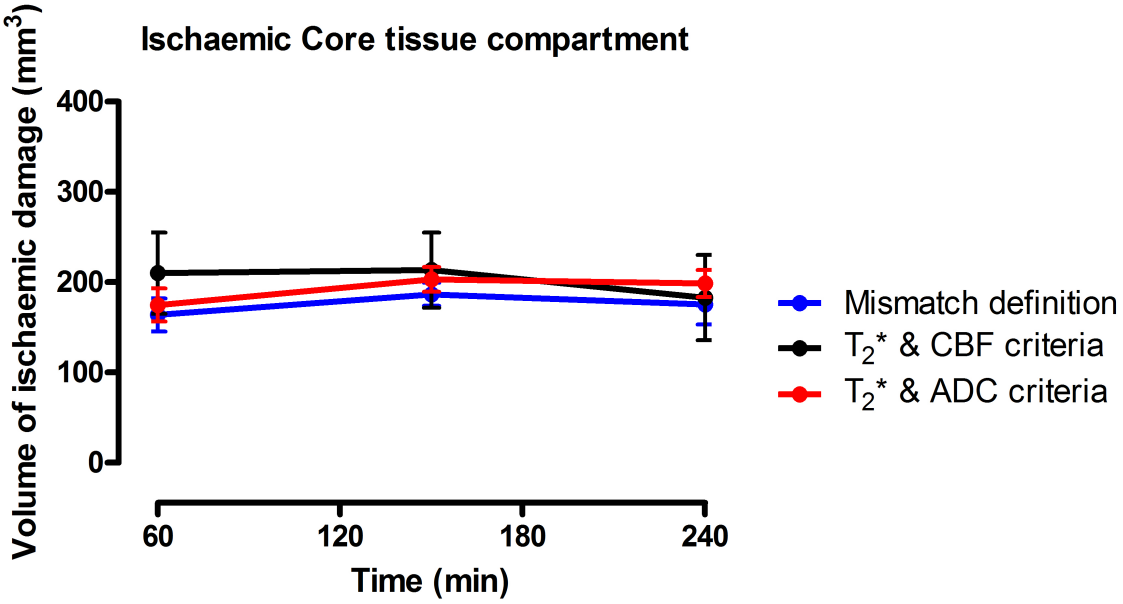

Figure 6.11. Volume of ischaemic core as defined by the three methods: **Blue** – traditional mismatch method where ADC and CBF values of pixels are below defined thresholds. **Black** – T_2^* v CBF criteria where T_2^* and ADC values are below pre-defined thresholds. **Red** – T_2^* v ADC criteria where T_2^* and CBF values are below thresholds. Data (n=6) expressed as mean±SD

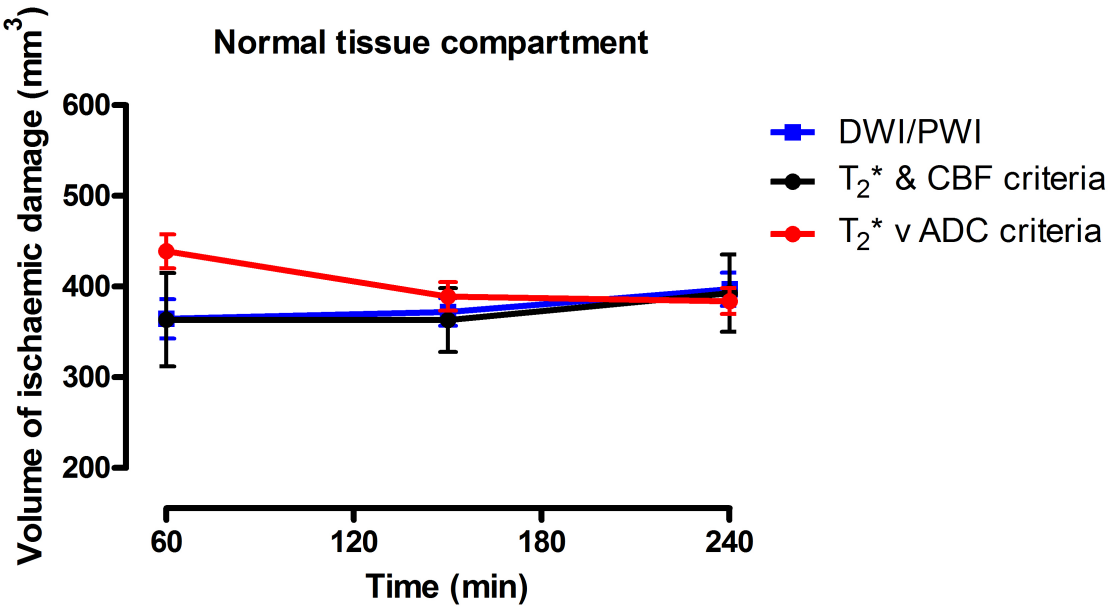

Figure 6.12. Volume of normal tissue across the two hemispheres as defined by the three methods:

Blue – traditional mismatch method with ADC and CBF above defined thresholds

Black –T_2^* v CBF criteria where CBF values are above pre-defined thresholds, whereas T_2^* may be above or below the set upper limit threshold.

Red – ADC values above pre-defined thresholds, whereas T_2^* is above and below the upper limit threshold. As such, this region also incorporates the perfusion deficit which may explain why it is larger initially. Data expressed as mean±SD

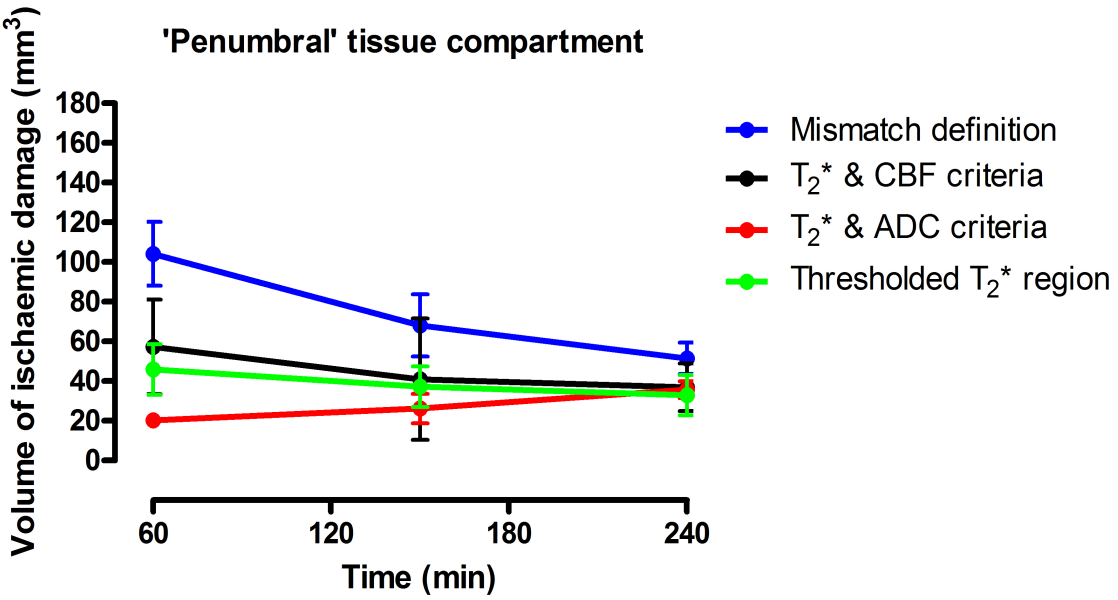

Figure 6.13. Volume of penumbral tissue is defined by three methods: **Blue** – traditional mismatch method where tissue has low CBF but ADC values above the ADC lesion threshold. Penumbral volume significantly decreased from the 1- to 4-hour time point ($p<0.05$). **Black** – T_2^* v CBF criteria where T_2^* is high and CBF is within the perfusion deficit. **Red** – T_2^* v ADC criteria where there is high T_2^* and ADC is low – evidence of penumbra within ADC lesion. **Green** – Penumbra calculated by measuring the volume of the thresholded T_2^*% signal change region. Data expressed as mean±SD

6.3.6 Evolution of ischaemic damage beyond 4 hours

There was evidence of increased T_2^* signal change to OC at the 4 hour time point, indicative of remaining penumbra (Figure 6.14), which suggests the potential progression of the ischaemic damage beyond 4 hours. This was was also supported by the DWI/PWI mismatch data. By analysing all 8 ADC slices at 4 hours and RARE T_2 slices at 24 hours (Figure 6.15), there was a significant progression in ischaemic damage beyond 4 hours, in which the mean ADC-derived volume of ischaemic damage at 4 hours was 267±55 mm^3, and the T_2-derived final infarct was 342±35 mm^3 (p=0.0278, Figure 6.16).

A second graph was generated showing the evolution of ischaemic damage for the 4 slices analysed in the pixel-by pixel analysis. This is because the 4 slices selected represent tissue that is almost fully supported by MCA territory, whereas the slices at the more rostro-caudal extent have better collateral supply and may initially have more penumbra that will ultimately become incorporated into the ischaemic core. There was a non-significant progression in ischaemic damage beyond 4 hours, in which the mean ADC-derived volume of ischaemic damage at 4 hours was 208±34 mm^3, and the T_2-derived final infarct was 228±33 mm^3 (Figure 6.17).

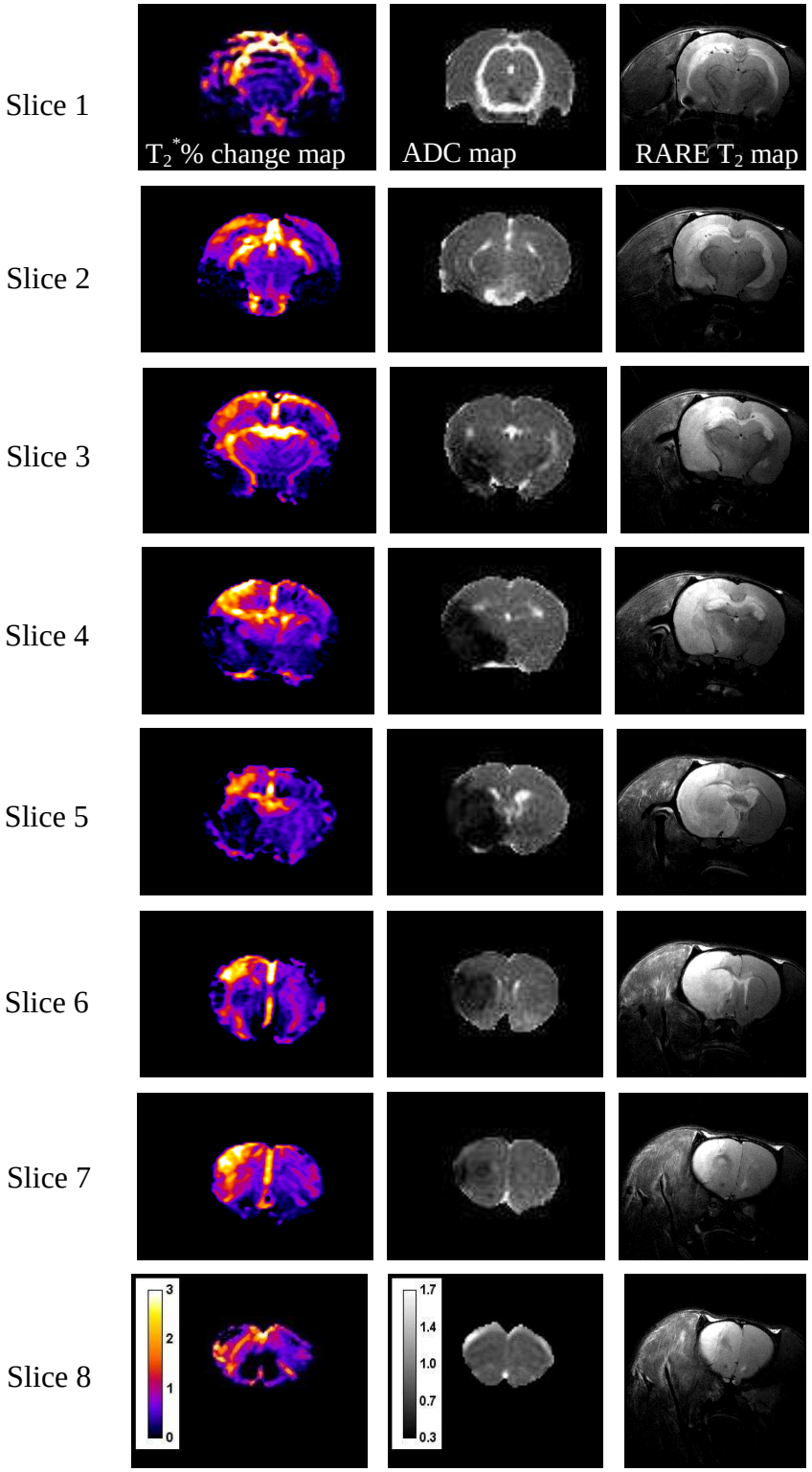

Figure 6.14. Evidence of T_2^*OC-defined penumbra at 4 hours post-pMCAO over 8 caudal-to-rostral slices with accompanying ADC maps, and RARE T_2 scans at 24h. Note larger areas of penumbra – displayed as high percentage signal change – in the rostral and caudal poles (slices 1-8). There is evidence of lesion expansion between 4h and 24h when observing ADC and RARE T_2 maps. T_2^* maps measured in units of percentage signal change. ADC maps measured in $x10^{-3}mm^2/sec$

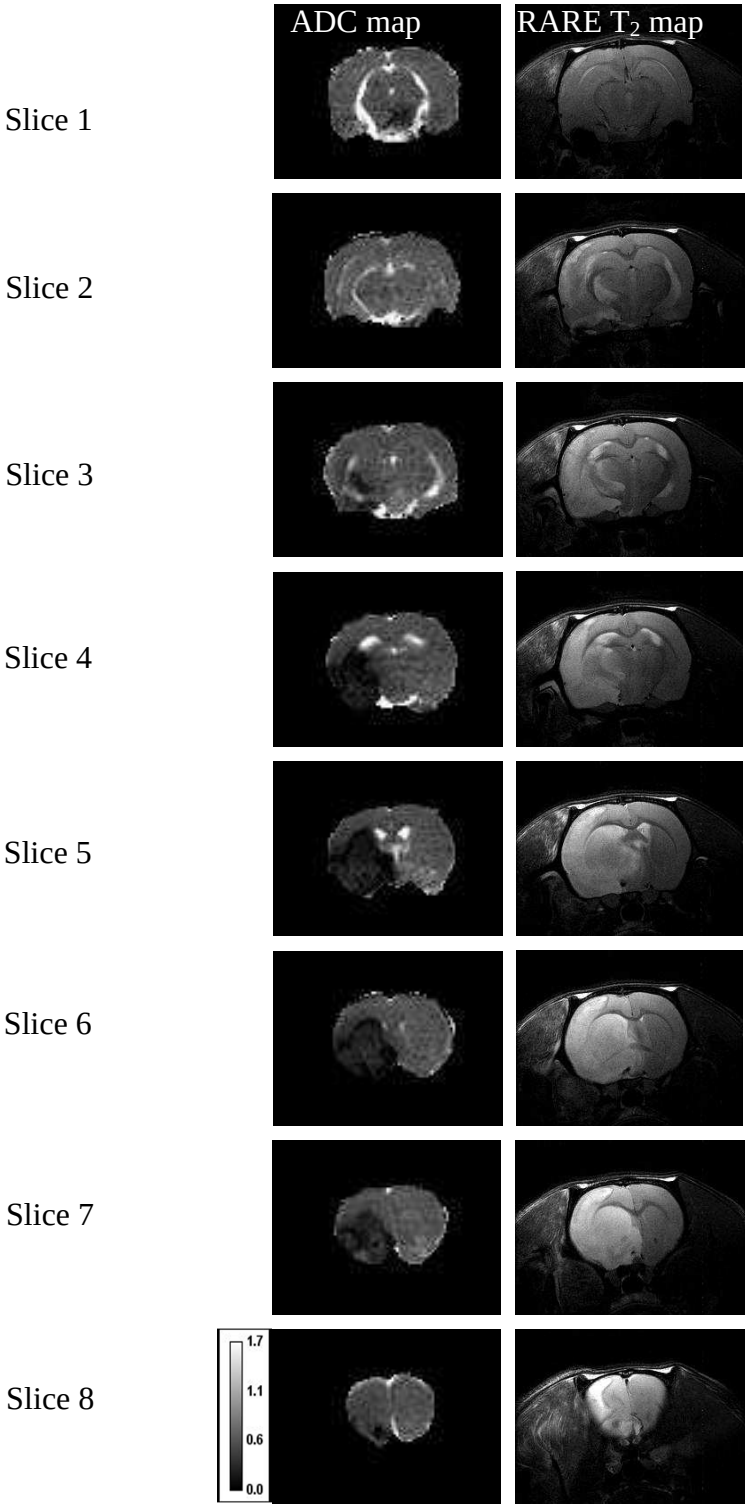

Figure 6.15. Representative rat showing four hour ADC (Left column) and 24 hour RARE T_2 (Right column) images across 8 coronal slices. ADC maps measured in $x10^{-3}mm^2/sec$

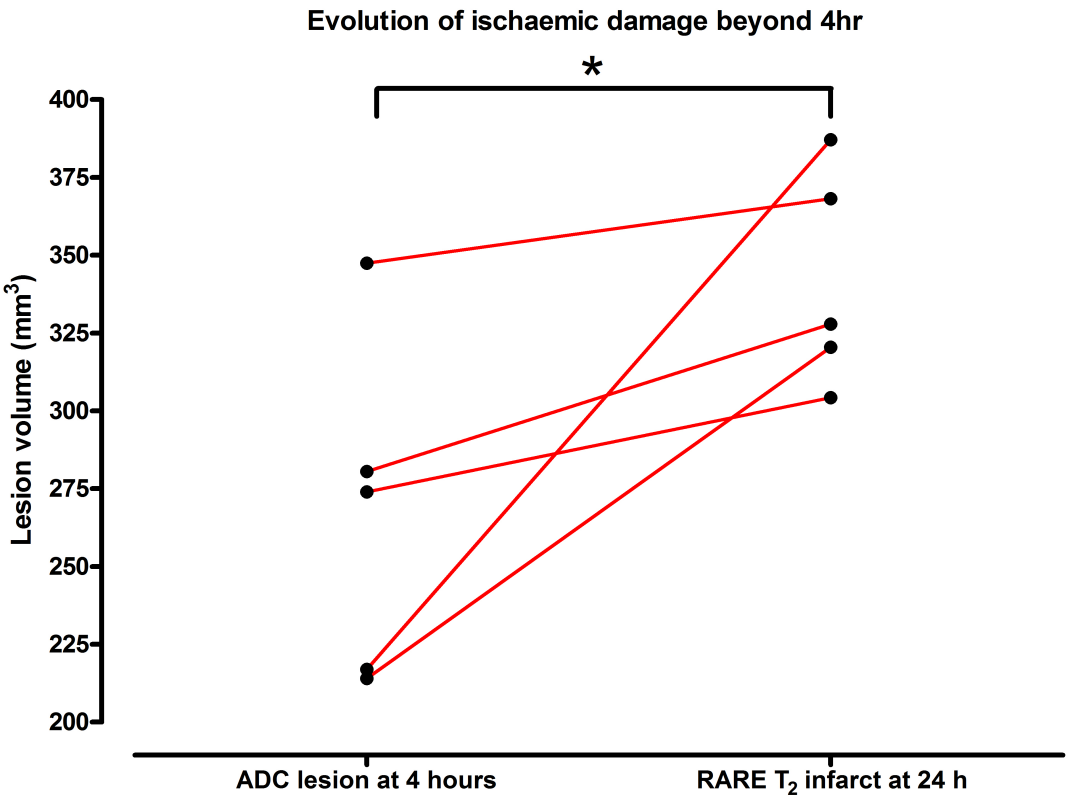

Figure 6.16. Evolution of ADC-derived and RARE T_2-derived ischaemic damage in the 5 surviving animals at 4 hours and 24 hours, respectively (* $p<0.05$) in all 8 coronal slices

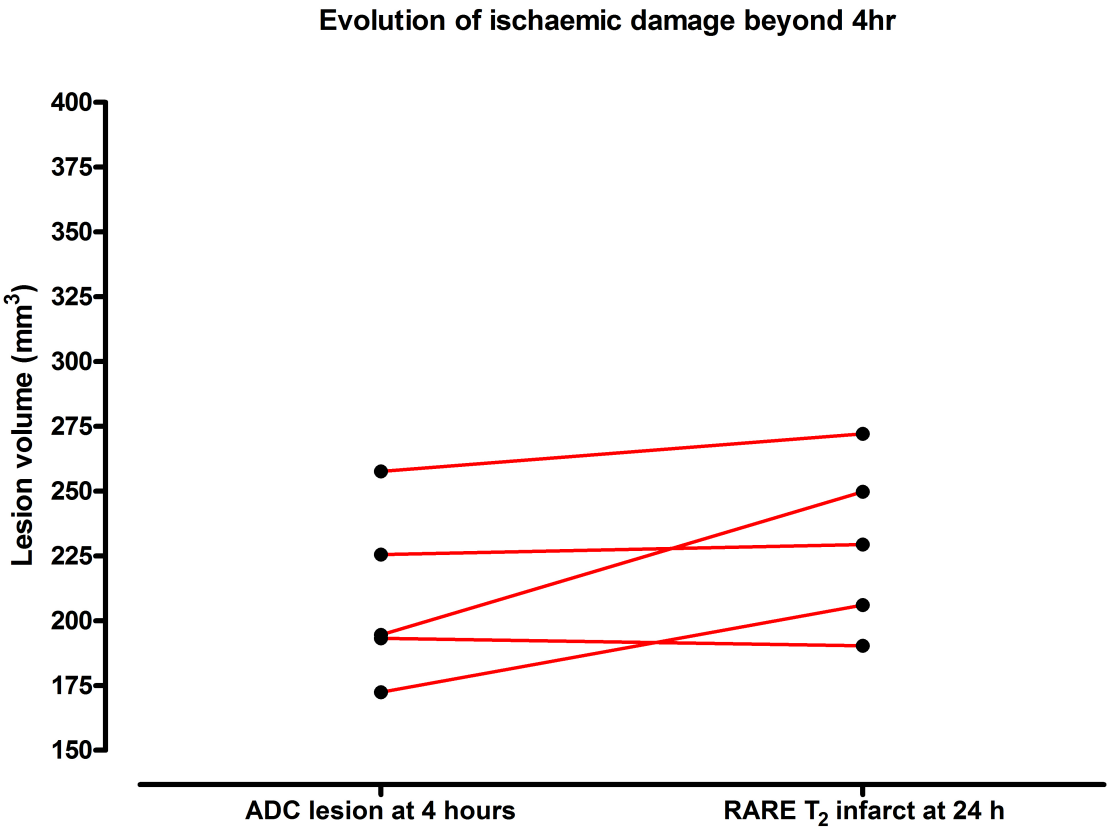

Figure 6.17. Evolution of ADC-derived and RARE T_2-derived ischaemic damage in the 4 selected central coronal slices for the 5 surviving animals at 4 hours and 24 hours, respectively. There was a negligible change in lesion volume, suggesting the damage progresses at the rostral and caudal poles where penumbra is more evident

6.4 Discussion

Quantitative evaluation of tissue volumes was achieved using pixel-by-pixel analysis, in which four pixel populations were defined using thresholds for ADC, CBF and T_2^*. From this, colour-coded images could be generated which enabled spatiotemporal mapping of ischaemic progression.

Pixel-by-pixel analysis

With pixel-by-pixel analysis, T_2^* as a parameter for penumbral identification identifies tissue that closely matches the region identified by mismatch. When the ADC lesion expands, the volume of penumbra decreases, whereas when the ADC lesion remains static, the T_2^*OC-defined penumbra remains static. T_2^*OC identified potential penumbra at the 4 hour time point, suggesting that the 4 hour time point does not represent maximal ischaemic damage. Volumetric comparison of the ADC lesion at 4 hours with the RARE T_2 final infarct at 24 hours showed that T_2^*OC did identify true penumbra at the 4 hour time point because the extent of damage increased at the 24h time point.

ADC v CBF

Using ADC and CBF parameters, it was shown that mismatch-derived penumbra was larger than penumbra defined using the two T_2^* methods (Figure 6.13). This may be because mismatch tissue also includes the ventricles on the contralateral and ipsilateral hemispheres, which show low values of CBF on the ASL sequences.

T_2^*OC V ADC

Since there was no lower limit threshold of T_2^* defined, it was possible to identify the penumbral tissue within the ADC lesion, which explains why this method displays the smallest volume of penumbra. However, this is an important finding, as it may reinforce the notion that the ADC lesion is not a true marker of irreversibly damaged tissue - it incorporates a region which is still metabolically active. Consequently, this explains why the tissue volume regarded as normal (Figure 6.12) is the largest using this criteria.

T_2^* v CBF

Using the T_2^* and CBF criterion may be the closest technique that we have to the PET criterion, which identifies tissue with reduced CBF, preserved oxygen consumption and

with increased OEF. This is a similar definition to the T_2^* v CBF criteria, which we believe identifies tissue with increased OEF and reduced CBF.

A limitation encountered in the current study is with the thresholds used for ADC, CBF and T_2^*. As there is no established T_2^*OC threshold, the empirical rule was used. Although this rule has no biological importance, it is a standard mathematical threshold used to identify values with statistical significance which states that, for normally distributed values, approximately 95% of the values lie within 2 standard deviations of the mean. This technique was also applied to the ADC and CBF images, partly because the established thresholds are known to be imprecise and inaccurate, and partly to fairly compare the three criteria used.

Limitations of DWI/PWI mismatch

Despite its limitations, the DWI/PWI mismatch model provides information on location and severity of ischaemia (derived from PWI), tissue viability status (ADC values derived from DWI), and therefore approximate location and size of penumbra. Perfusion-weighted imaging and DWI scans were therefore included in the scanning routine for comparison with T_2^*OC identification of penumbra. A number of studies have shown that differentiation between viable and nonviable tissue is difficult, using the diffusion abnormality (Kidwell et al, 2000; Fiehler et al, 2002), which correlates poorly with final infarct (Li et al, 1999). DWI lesions may be recoverable following prompt reperfusion in animal models and humans, and may not be destined for infarction (Schlaug et al, 1997; Mintorovitch et al, 1994; Kidwell et al, 2000). However, this tissue may become incorporated into the final infarct due to late secondary insults following reperfusion (Kidwell et al, 2002). This suggests that some patients with no evidence of mismatch may benefit from reperfusion therapies. Additionally, the perfusion deficit may incorporate tissue with benign oligaemia (destined to survive) even when optimal MRI thresholds (themselves as yet incompletely defined) are applied (Butcher et al, 2005). As such, the inner and outer margins of the penumbra may not be adequately delineated using the mismatch technique, which has been shown to frequently overestimate the final lesion size (Kucinski et al, 2005). By examining the evolution of the diffusion lesion and the perfusion deficit in patients left untreated, research has focussed on applying a multitude of ADC and perfusion thresholds which may enable delineation between tissue destined to die and tissue expected to survive (Kidwell et al, 2003).

MRI-defined DWI–PWI mismatch identifies penumbra in a similar, but not exact, neuroanatomical location. However, there are issues with the accuracy of this indirect technique which assumes that the DWI and ADC lesion signify irreversible damage and that tissue within perfusion deficit is ultimately destined to die. These underlying assumptions are undermined by reversibility of the DWI lesion with reperfusion, uncertainty over relevant perfusion thresholds and the inclusion of benign oligaemia within the perfusion deficit, and the variable metabolic state of DWI lesion voxels.

DWI and PWI thresholding

Many papers are based on the underlying assumption that maximal ischaemic damage in Sprague-Dawley rats occurs at three or four hours post stroke. Indeed, the 57% reduction for the CBF threshold of abnormality were derived by adjusting the respective threshold values so that the CBF-derived lesion volumes at 3 hours were equal to the 2,3,4-triphenyltetrazolium chloride (TTC) infarct volume at 24 hours (Meng et al, 2004). This 3 hour time point was also used by Lo and colleagues (1997) and Bardutzky et al (2005) as a means of establishing ADC thresholds. In-house observations by Dr. Tracey Baskerville has questioned this premise, and she found evidence of penumbral tissue at the 4 hour time point in both male and female rats (Figure 6.18) using the same pMCAO filament model. The current study has also reinforced the idea that penumbra exists beyond the 4 hour time point (Figures 6.14 and 6.15), and this questions the validity and accuracy of studies that rely on this thresholding technique.

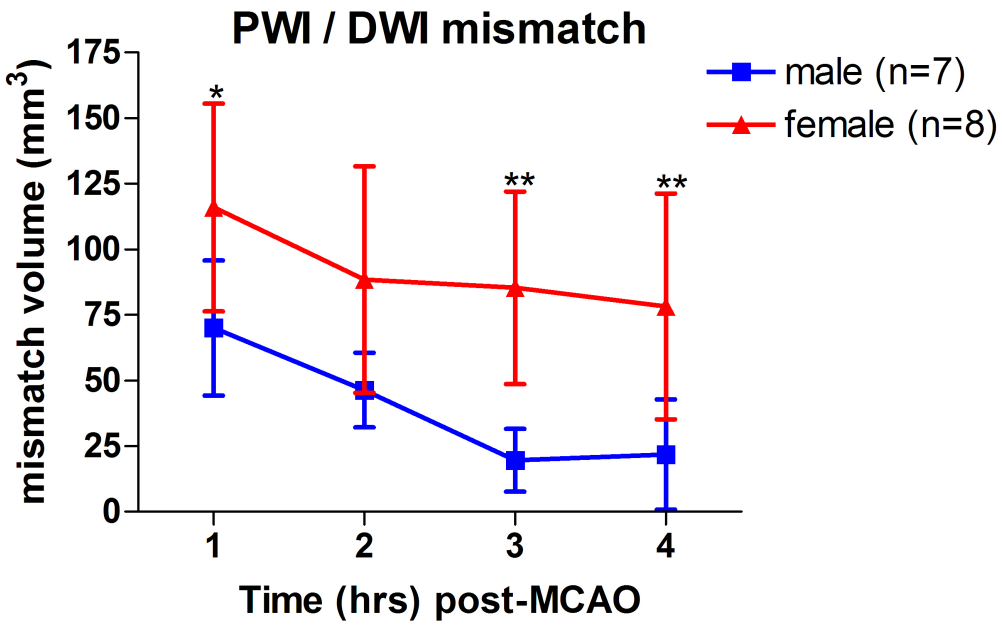

Figure 6.18. Volume of penumbra (PWI/DWI mismatch) in males and females at 1-4hrs after stroke onset. (ADC thresholds applied were 0.60 and 0.55 $x10^{-3}mm^2/s$ for males and females, respectively and a CBF threshold of 35 ml/100g/min for both sexes) ($^{*}P<0.05$, **P<0.01, Two-way ANOVA with Bonferroni post-tests)

Evidence of ischaemic damage beyond 4 hours

The progression of ischaemic damage may be due to secondary insults that occur following the return to consciousness, when animals are allowed a period of recovery prior to final infarct scanning. Firstly, when anaesthetic is removed, the animals could experience hypotensive or respiratory episodes which may compromise CBF and blood oxygen levels. This may therefore induce ischaemia and hypoxia, and increase waves of spreading depolarisation which thereby exacerbate ischaemic damage. Secondly, autoregulation would be expected to be impaired by stroke but physiological variables are carefully controlled under anaesthetic. Once consciousness returns, the autoregulatory state of the collateral pial vessels may lead to increased blood flow and oxygen to the injured penumbra which may cause secondary insults caused by increased free radical generation and oxidative stress.

Summary

The spatiotemporal behaviour of the T_2^*OC-defined penumbra was consistent with the pattern of progression shown by the established DWI/PWI mismatch technique. The animals that showed an increase in ischaemic damage and concomitant loss of mismatch over time displayed similar changes using the T_2^* criterion. Interestingly, mismatch volume that remained static over time also remained static in the T_2^*OC definitions. The current study validates the utility of T_2^*OC in its mapping of the spatiotemporal changes associated with penumbra, and suggests that mismatch overestimates penumbra and is unable to identify penumbra within the ADC lesion. Secondly, the current study also questions the accuracy and validity of studies that rely on ADC and CBF thresholds which assume maximal ischaemic damage at 3- or 4-hours post-stroke.

Chapter

7

General Discussion

Current flow restoration strategies for salvaging the ischaemic penumbra employ time from stroke onset, rather than positive identification of penumbra. It is clear that existing prerequisites for patient selection must be improved – the time of stroke onset is not always known, penumbra may not exist beyond 3 hours, or patients may present with penumbral tissue for up to 48 hours post-onset (Heiss, 1992). Despite the extension of the time window threshold for rT-PA thrombolysis from 3 to 4.5 hours post-symptom onset (Hacke et al, 2008), significant technological advances in neuroimaging have not successfully translated to the clinic since the seminal NINDS trial (1995). The advent of DWI/PWI mismatch (Schlaug et al, 1997) was initially promising in identifying ischaemic damage and penumbral tissue based on indirect diffusion and perfusion measures, but their employment in clinical trials have been unable to improve upon the time window for thrombolysis. The problem may arise from the fact that current PET-derived gold standard definitions of penumbra use metabolic indices such as OEF and $CMRO_2$, which are not fully incorporated into MR definitions. With this in mind, a paradigm shift in penumbral imaging is currently underway, in which MRI techniques based on a metabolic parameter are being developed for patient selection. The impracticalities of PET in the acute setting mean that MR techniques that incorporate PET definitions may introduce more accurate MR definitions and ultimately improve patient selection for clinical trials. Until an accurate means of quantifying the penumbra is available, the ability of clinical trials to identify effective therapies is not going to improve.

7.1 T_2^* Oxygen Challenge

The data provided in this thesis suggest that T_2^*OC provides information on metabolic state that could improve penumbral definition. It has been shown that BOLD MRI using T_2^* offers information on oxygen consumption and delivery (Baird & Warach, 1999; Kavec et al, 2001), but static T_2^*-weighted MRI under normoxic conditions has not adequately delineated penumbra in ischaemic stroke patients (Tamura et al, 2002; Grohn & Kauppinen, 2001), possibly because deoxyhaemoglobin is not rapidly cleared in ischaemic

conditions (Giesler, et al, 2006). Our new method using sequential T_2^*-weighted images with transient hyperoxia may dynamically alter the oxyhaemoglobin: deoxyhaemoglobin balance with the aim of distinguishing tissue compartments which have different metabolic activities and therefore different relative concentrations of deoxyhaemoglobin. By providing the additional measure of the rate of contribution of deoxyhaemoglobin to the measured pool, this may remove the potential confound observed by Geisler and colleagues.

The first validation study in this thesis used [^{14}C] 2-deoxyglucose autoradiography to determine the metabolic status of the tissue compartment identified as penumbra by the T_2^*OC MRI technique. The results indicated that glucose metabolism in the T_2^*OC-defined penumbra was comparable to contralateral values, whereas markedly different levels of glucose metabolism were evident in the ADC-derived ischaemic core and an adjacent region of increased 2DG phosphorylation. From this, it was concluded that metabolic information could be yielded from the ischaemic brain that may improve delineation of penumbral tissue which has its own unique metabolic profile. Secondly, as penumbral tissue must fulfil the fundamental criteria of being potentially salvageable and responsive to therapy, the consequences of reperfusion on the T_2^*OC-defined penumbra were tested. This confirmed that tissue identified as penumbra by T_2^*OC did not progress to infarction with prompt restoration of blood flow. Thirdly, the spatiotemporal characteristics of the T_2^*OC-defined penumbra were investigated and compared with the DWI/PWI mismatch definition of penumbra. This demonstrated that penumbra defined by T_2^*OC behaved in a similar manner to the penumbra defined by traditional mismatch criterion. As mismatch tissue volume reduced over time, T_2^*OC penumbra followed the same pattern, and conversely it remained static when mismatch remained static over time. Additionally, an interesting finding arose in the latter study which showed that ischaemic damage continues to progress beyond 4 hours following permanent MCAO, which may be relevant to the calculation of ADC and CBF thresholds.

From this thesis, it is clear that acute transient O_2 inhalation and sequential T_2^* weighted imaging delineates a region of tissue demonstrating the characteristics of penumbra which we believe is based on the OEF of the tissue and the change in deoxyhaemoglobin levels associated with OC. However, since neither OEF nor oxy:deoxyhaemoglobin ratios were measured in the studies we must also consider the contribution of additional components known to modulate the BOLD signal.

7.2 Components that may affect the T_2^* response

It is important to consider whether or not T_2^*-weighted signal changes to oxygen challenge reflect processes other than the change in tissue venous deoxyhaemoglobin concentration as a consequence of metabolism and OEF. The partial pressure of oxygen PaO_2 in the blood clearly influences the magnitude of the T_2^* response to hyperoxia (Chapter 3, Figure 3.8), while other factors sure as CBF, CBV and/or OEF may contribute to differentiating the ischaemic penumbra from surrounding tissue (Santosh et al, 2008; Robertson et al, 2011a and b).

7.2.1 Cerebral blood flow

Following ischaemia, one would expect a change in cerebral blood flow due to loss of autoregulation. It is well established that changes in CBF influence T_2^*-weighted signal intensity (Ogawa et al, 1990); this is the fundamental principle of functional MRI. It was not possible to examine real-time CBF changes in response to the hyperoxic challenge in the current studies, and as such, since only the baseline CBF was measured, the possibility that the T_2^*-weighted signal intensity changes reflect a change in CBF cannot be dismissed. The original OC paper (Santosh et al, 2008) used a pulsed ASL sequence on a single slice to investigate temporal changes in CBF during the OC (Figure 7.1). Oxygen challenge did not significantly influence relative CBF in the presumed penumbral zone, but it did induce a small decrease in CBF in the contralateral cortex in the rodent pMCAO model. In this thesis, correlation analysis for baseline CBF and T_2^* signals in 17 animals was performed, within T_2^*OC-defined penumbra, contralateral caudate nucleus, contralateral cortex and the ischaemic core (Figure 3.7). No correlation was found between T_2^* signal change and CBF in any of the regions of interest, reinforcing the view that T_2^* signal is not an indirect measure of CBF.

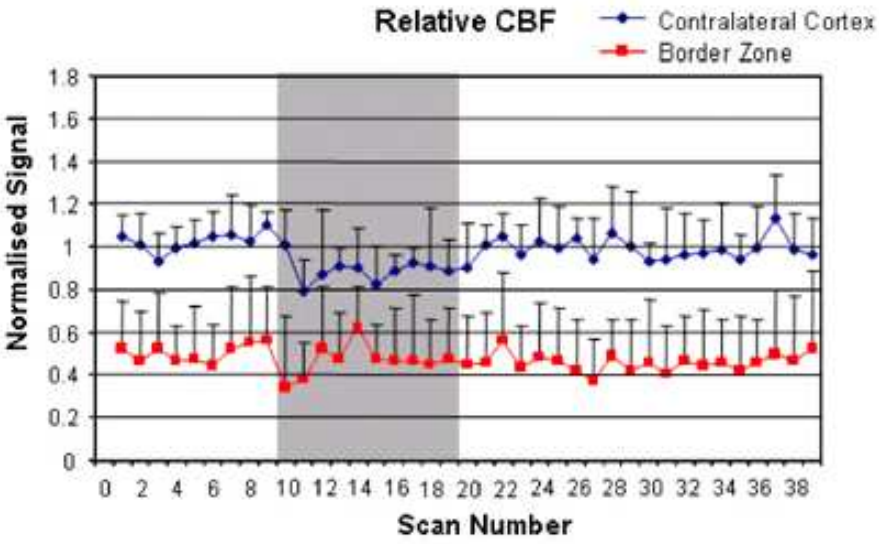

Figure 7.1. OC did not significantly influence CBF in the ipsilateral border zone (-0.008, 95% CI -0.066 to 0.081, p=0.78, red line) but induced a small decrease in CBF in the contralateral cortex (-0.10, 95% CI -0.199 to -0.001, *P*=0.048, blue line) following OC (shaded box)

In a subsequent (non-MRI) study from our department (Baskerville et al, 2011) CBF was measured during an OC protocol with intracerebral laser Doppler flowmetry probes (OxyFlo/Lite system) implanted into the ipsilateral (presumed penumbra) and contralateral cortex of rats exposed to pMCAO. These data have been superimposed alongside the T_2^* signal response (Figure 7.2). OC induced a small transient increase in CBF in coincident with a transient increase (from 83.28±4.99 to 98 ±8.78 mm Hg, $p<0.05$) in mean arterial blood pressure lasting ~2-3min. In comparison, the T_2^* signal increase to OC was maintained during the period of hyperoxia (5 mins) and returned back to baseline when hyperoxia was switched off. Therefore, the time course of this CBF response did not match the T_2^* signal response seen during OC, suggesting that the T_2^* signal change is not due simply to changes in CBF. In addition, it is known from hypercapnia studies that hypercapnia-induced CBF increases of 25-40% influence BOLD signal by as little as 2-3% (Rostrup et al, 2000; Rostrup et al, 2005). It is therefore unlikely that OC-induced changes in CBF had a significant influence on the BOLD T_2^* response. Although baseline CBF does not appear to influence the T_2^* response to OC, simultaneous measurement of CBF during T_2^* changes to OC would be required to fully clarify the effect of tissue perfusion on the T_2^* response to OC (see Chapter 7.3.2 section on NIRS).

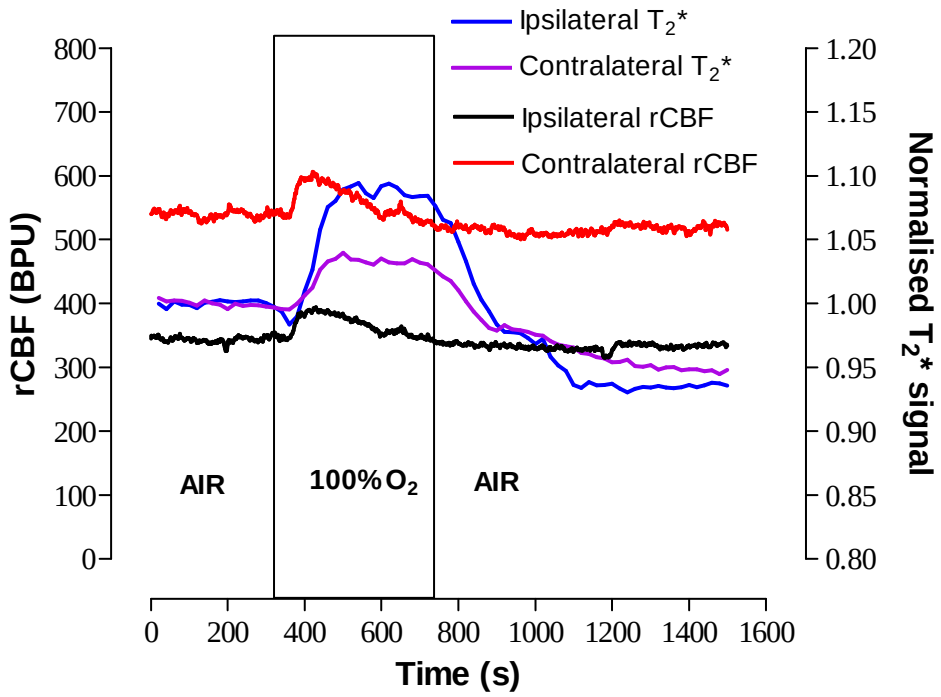

Figure 7.2. Representative traces of T_2^* and rCBF in presumed penumbra (ipsilateral) and contralateral cortex pO_2 and rCBF from a middle cerebral artery occlusion (MCAO) rat during oxygen challenge (OC) (Baskerville et al, 2011)

7.2.2 Cerebral blood volume

Buxton and colleagues (1998) proposed a model of the BOLD signal implicating the role of cerebral blood volume on the BOLD response. It showed that an increase in the BOLD signal can be caused both by a decrease in deoxyhaemoglobin content and by an increase in regional CBV (rCBV). It has been shown that the visual cortex and the cerebellum display high BOLD signal changes following hypercapnia, and these are regions which have high capillary densities and high basal CBV values (Kastrup et al, 1999). Resting state blood volume is one of the strongest determinants of the fMRI signal change magnitude, other than activation-induced oxygenation changes. Bandettini and Wong (1997) found that with oxygenation changes following activation, a voxel in the brain with a high blood volume will display a larger signal change than a voxel with a lower blood volume if all other circumstances were identical. Also, Bandettini and Wong (1995) showed an intricate link between CBV and oxygen saturation, in that increased blood volume with reduced blood oxygenation saturation causes the greatest BOLD signal magnitude, using a biophysical simulation (Figure 7.3).

Davis and colleagues (1998) examined baseline tissue deoxyhaemoglobin (dHb) content to determine its effect on the BOLD signal change to hypercapnia and to photic stimulation. In single slice experiments, the largest signal change values (up to 16%) were found in visual cortex, with smaller signal change (3–5%) in surrounding parietal and occipital cortex. This was thought to be due to the disproportionate concentration of venules in the visual cortex which would therefore have increased levels of deoxyhaemoglobin. They concluded that the changes in blood flow and oxidative metabolism were secondary to the baseline deoxyhaemoglobin levels with regards to BOLD sensitivity.

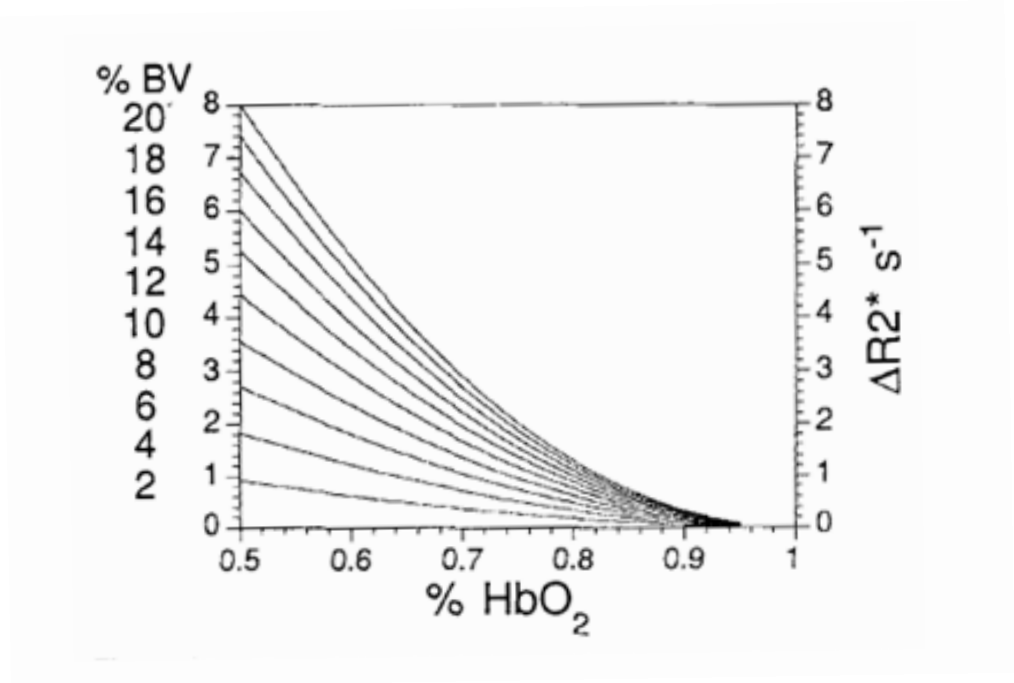

Figure 7.3. The relationship between signal change ($\Delta R2^{*s-1}$) and oxygen saturation ($\%HbO_2$) under different blood volumes (Taken from Bandettini and Wong, 1995)

Contradictory explanations have also been proposed which suggest a negligible CBV influence on the BOLD response. Kennan and colleagues (1997) isolated the contribution of blood volume changes to the BOLD signal by separating blood volume and magnetic susceptibility effects in response to respiratory challenges such as hypoxia and hyperoxia. A rat model was used to identify the source of signal variation when changing from 100% oxygen to 10% oxygen/90% nitrogen ventilation. They found that the change in blood magnetic susceptibility (i.e., the change from deoxy- to oxyhaemoglobin which has a large observed magnetic susceptibility effect) is the key contributor to the BOLD effect and not blood volume. They estimated that the maximal contribution from blood volume changes in hypoxia amounts to less than a 12% contribution to the observed relaxation rate changes in each region. This corresponds to a maximal estimate of the blood volume term since it is assumed that the blood is completely deoxygenated in the hypoxic state. If the blood is not fully deoxygenated relative to tissue then CBV effects will become smaller. This is in agreement with Prielmeir and colleagues (1994), who showed under hypoxia, oxygen saturation reached a minimum of about 40% which would reduce maximal blood volume contribution to only 7%.

CBV in stroke

Both PET (Powers, 1991) and MRI (Sorensen et al, 1996) studies have found inconsistencies in rCBV following stroke, in which CBV may remain unchanged, increased, or decreased in the ischaemic penumbra. Maeda and colleagues (1993) noted that, following middle cerebral artery occlusion in cats, the fall in CBF was compensated for by dilation of the vessels concerned, leading to an increased rCBV until the collateral circulation becomes insufficient. Within the infarct, autoregulatory mechanisms are altered, and both the rCBF and rCBV are usually decreased, and regions with reduced CBV may be regarded as irreversibly damaged. (Wintermark et al, 2002).

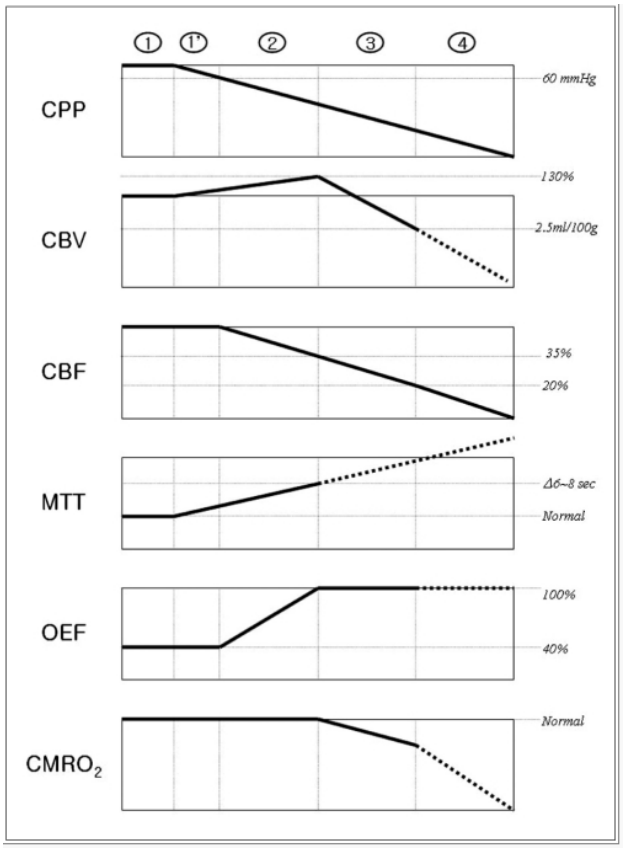

Area 1 is unaffected area
(1' is autoregulating)

Area 2 is benign oligaemia

Area 3 is ischaemic penumbra

Area 4 is ischaemic core.

Figure 7.4. Graphs representing the haemodynamic or metabolic response (Y-axis) to stroke in five different tissue compartments (the X-axis).
CPP = cerebral perfusion pressure; CBV = cerebral blood volume; CBF = cerebral blood flow; MTT = mean transit time; OEF = oxygen extraction fraction; and $CMRO_2$ = cerebral metabolic rate of oxygen (Taken from Lee et al (2005))

Lee and colleagues (2005) noted that both CBF and CBV are good predictors of tissue outcome. By using non-enhanced CT, if CBF and CBV are severely reduced or below detectable levels in a specific region, this tissue is expected to be irreversibly injured, whereas an estimate of tissue at risk is displayed as low CBF with normal to elevated CBV. One can then make assumptions that a good tissue outcome occurs when the region has elevated CBV in an area of perfusion deficit. Hossmann (1994) and Mayer and colleagues (2000) used thresholds of CBF and CBV to determine the fate of ischaemic tissue, in which the hypoperfused regions with high CBV and low CBF were more likely to experience a good tissue outcome compared to a similarly hypoperfused region with lower CBV values.

In humans, increases in rCBV in penumbra have also been shown using CT perfusion (Murphy et al, 2006), in which CBV in penumbra (2.15±0.43 ml/100g) was significantly higher than contralateral (1.78±0.30 ml/100g) and infarcted tissue (1.12±0.37 ml/100g), whilst CBF was significantly lower for infarct (13.3±3.75 ml/100g/min) than penumbra (25.0±3.82 ml/100g/min).

CBV in relation to Oxygen Challenge

The implications are that the vasculature within penumbra will contain more deoxyhaemoglobin than in normal or infarcted tissue if the regional CBV is increased, and therefore an amplified response in T_2^* % signal change to OC would be expected in this region. Therefore, one may speculate that CBV may have a large effect on the BOLD signal and its relative contribution may dominate the effect of other components influencing the T_2^* signal. Alternatively, if CBV modulates T_2^*OC response, then a brain region with increased CBV (induced by vasodilatation or otherwise, and not necessarily penumbra) would be expected to have an increased T_2^* response to OC.

7.3 Further validation techniques

7.3.1 Crossed cerebellar diaschisis

Diaschisis refers to the loss of excitation and consequent hypometabolism of tissue that is anatomically distant from the region of damage (von Monakow, 1914). A subtype of diaschisis known as crossed cerebellar diaschisis (CCD), which can occur following stroke

onset and lead to hypometabolism in the contralateral cerebellar hemisphere. Dr. Krishna Dani, neurologist at the Southern General Hospital, Glasgow, investigated the utility of T_2^*OC and perfusion imaging in the detection of hypometabolism in 12 subjects with clinically-defined cortical ischaemic stroke within middle cerebral artery territory, consented within 24 hours of onset. He found that the mean T_2^* percentage signal change to OC in the ipsilateral cerebellar hemisphere was significantly greater ($p=0.03$) than the values in the contralateral cerebellar hemisphere (5.1±2.7%, compared to 3.8±3.1%, data expressed as mean±SD, Figure 7.5). Interestingly, there was no significant difference in perfusion between cerebral hemispheres for any subject ($p=0.22$). This was the first study that did not require perfusion imaging to identify CCD using MRI, and it suggested that OC-derived cerebellar asymmetry reflected CCD. This study was very useful in confirming that OC has the potential to identify changes in metabolism, which we have hypothesised is the basis for the technique in defining the ischaemic penumbra.

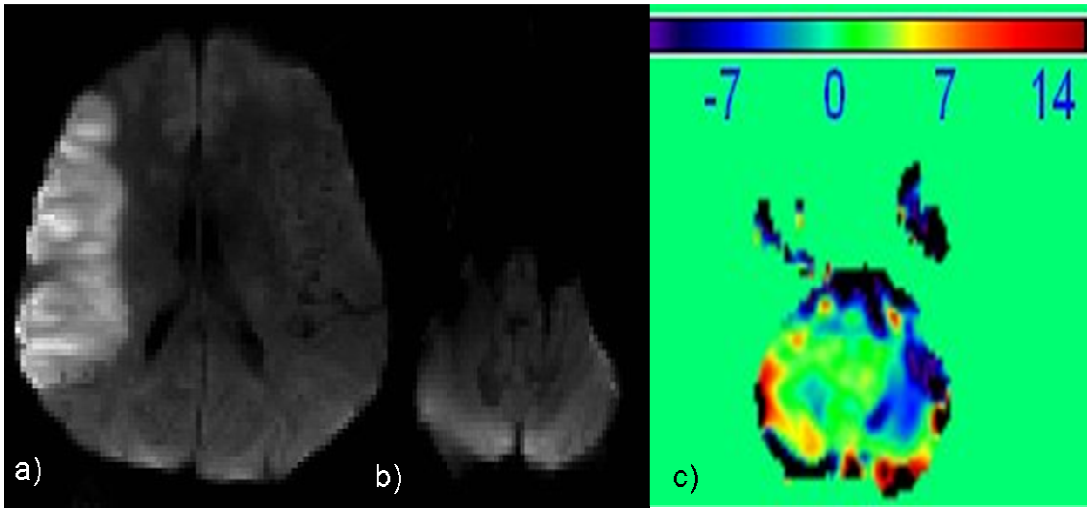

Figure 7.5. Attenuated T_2^* Response to oxygen challenge in the contralateral cerebellar hemisphere from a sample patient. **A**). Diffusion weighted imaging of the stroke lesion (identified as a region of hyperintensity), **B**). Diffusion weighted imaging in the cerebellum, in which no lesion is evident, and **C**). Attenuated T_2^* percentage signal change to oxygen challenge in the contralateral cerebellar hemisphere (displayed as dark blue). The colour scale is in units of percentage signal change

7.3.2 Near infrared spectroscopy (NIRS)

NIRS is a non-invasive technique for measurement of tissue absorbance of light at wavelengths in the spectral region from 700-1000 um, used to determine concentration changes of oxy- and deoxyhaemoglobin, cerebral blood volume and blood flow measurements. Since near infrared light penetrates biological tissues and even bone, such measurements can be performed through the intact skull. MRI-compatible NIRS systems have now been developed, making it possible to coregister brain haemodynamics by combining NIRS and fMRI, due to the fact that the fMRI BOLD signal is proportional to the changes in deoxyhaemoglobin concentration (Tak and Ye, 2009; Steinbrink et al, 2006). A setup which provides simultaneous NIRS and T_2^*OC MRI would provide data on the oxy- and deoxyhaemoglobin ratio, which is in turn influenced by OEF and would enable investigation of the extent to which the T_2^* percentage signal change to OC is due to changes in the relative concentration of oxy- and deoxyhaemoglobin in the blood. As this would provide real-time information on CBF and the amount of deoxyhaemoglobin being converted, it would confirm the contribution of the components influencing the BOLD signal.

7.4 Translation of T_2^* Oxygen Challenge to the clinic

Recently, Dani and colleagues (2010) demonstrated the first clinical application of OC during T_2^*-weighted MRI, detecting differences in vascular deoxyhaemoglobin levels between tissue compartments following stroke. The percentage signal change maps generated from the OC data could discriminate between gray and white matter on the contralateral hemisphere, consistent with the higher metabolic demand in gray matter. Regions of interest selected within the DWI lesion displayed a reduced T_2^* percentage signal change compared with the non-ischemic hemisphere. Of the four patients scanned in the hyperacute phase, three patients had a significantly higher T_2^* percentage signal change in penumbral tissue (defined by DWI/PWI mismatch) compared with normal tissue. This increase in T_2^* percentage signal change was less evident in patients scanned at later time points, in line with the likelihood that penumbral tissue may have been recruited into the irreversible ischemic core. These preliminary clinical data along with the CCD data support the potential for this novel MRI technique to delineate penumbral tissue in acute stroke by its metabolic status. Crucially, administration of oxygen with T_2^* scanning can be performed quickly and easily with widely available hardware. This technique may be used

acutely or more importantly to detect existing penumbral tissue in patients unable to present within the 3- to 4.5-hour time window for thrombolysis.

By exploiting the different magnetic properties of oxy- and deoxyhaemoglobin, the dynamic response to oxygen administration may detect tissue capacity for oxygen utilisation and define the ischaemic penumbra on the basis of oxygen extraction and metabolism. Both the pre-clinical and clinical data support the potential of T_2^*OC to discriminate tissue compartments in acute stroke based on metabolic status which thereby provides an alternative and improved means of defining the ischaemic penumbra.

Chapter

8

References

Aarts MM, Tymianski M (2005) TRPMs and neuronal cell death. Pflugers Arch 451;243-249

Aaslid R, Lindegaard KF, Sorteberg W, Nornes H (1989) Cerebral autoregulation dynamics in humans. Stroke 20:45–52

Adams HP (2005) Handbook of Cerebrovascular Diseases, Neurological Disease and Therapy. Vol. 66. Second edition, New York; Marcel Dekker, p73

Adamson J, Beswick A, Ebrahim S (2004) Is stroke the most common cause of disability? J Stroke Cerebrovasc Dis. 13:171-177

Adrain C, Creagh EM, Martin SJ (2002) Caspase Cascades in Apoptosis. Caspases-their role in cell death and cell survival. In: Caspases: their role in cell death and cell survival (Los M, Walczak H, eds),New York, NY: Landes Biosciences, 41-51.

Agranoff, AB (2006) Lacunar stroke. Retrieved December 3, 2007, from http://www.emedicine.com/pmr/topic63.htm

Aho K, Harmsen P, Hatano S, Marguardsen J, Smirnov VE, Strasser T (1980) Cerebrovascular disease in the community: results of a WHO Collaborative Study. Bull World Health Organ 58:113-130

Albers GW, Thijs VN, Wechsler L, Kemp S, Schlaug G, Skalabrin E, Bammer R, Kakuda W, Lansberg MG, Shuaib A, Coplin W, Hamilton S, Moseley M, Marks MP, for the DEFUSE Investigators (2006) Magnetic resonance imaging profiles predict clinical response to early reperfusion: The diffusion and perfusion imaging evaluation for understanding stroke evolution (DEFUSE) study. Annals of Neurology 60 (5):508-517

Albert, ML (2004) Death-defying immunity: do apoptotic cells influence antigen processing and presentation, Nat. Rev. Immunol. 4:223–231

Ames A, Wright L, Masayoshi K, Thurston J, Majno G (1968) Cerebral ischemia: The no-reflow phenomenon. Am J Pathol 52:437-443

Antiplatelet Trialists' Collaboration (1994) Collaborative overview of randomised trials of antiplatelet therapy I: prevention of death, myocardial infarction, and stroke by prolonged antiplatelet therapy in various categories of patients. BMJ 308:81-106

Arnold M, Nedeltchev K, Remonda L, Fischer U, Brekenfeld C, Keserue B, Schroth G, Mattle H (2005) Recanalisation of middle cerebral artery occlusion after intra-arterial thrombolysis: different recanalisation grading systems and clinical functional outcome. J Neurol Neurosurg Psychiatry 76(10):1373–1376

Aronowski J, Strong R, Grotta JC (1997) Reperfusion injury: demonstration of brain damage produced by reperfusion after transient focal ischemia in rats. J Cereb Blood Flow Metab 17:1048–1056

Astrup J, Symon L, Branston, NM, Lassen NA (1977) Cortical evoked potential and extracellular K+ and H+ at critical levels of brain ischemia. J. Cereb. Blood Flow Metab 20:1011-32

Astrup J, Siesjo BK, Branton NM, Lassen NA (1981) Thresholds in cerebral ischemia – the ischemic penumbra. Stroke 12:723-725

Back T, Ginsberg MD, Dietrich WD, Watson BD (1996) Induction of spreading depression in the ischemic hemisphere following experimental middle cerebral artery occlusion: effect on infarct morphology. J Cereb Blood Flow Metab 16:202–213.

Baird AE, Warach S (1999) Imaging developing brain infarction. Curr Opin Neurol 12:65–71

Bandera E, Botteri M, Minelli C, Sutton A, Abrams KR, Latronico N (2006) Cerebral blood flow threshold of ischemic penumbra and infarct core in acute ischemic stroke: a systematic review. Stroke 37:1334–9

Bandettini PA, Wong EC (1995) Effects of biophysical and physiologic parameters on brain activation-induced $R2^*$ and R2 changes: simulations using a deterministic diffusion model. International Journal of Imaging Systems and Technology 6 (2-3):133-152

Bandettini PA, Wong EC (1997) A hypercapnia-based normalization method for improved spatial localization of human brain activation with fMRI. NMR Biomed 10:197–203

Barber PA, Zhang J, Demchuk AM, Hill MD, Buchan AM (2001) Why are stroke patients excluded from TPA therapy?: An analysis of patient eligibility. Neurology 56:1015-1020

Barber PA, Davis SM, Darby DG, Desmond PM, Gerraty RP, Yang Q, Jolley D, Donnan GA, Tress BM (1999) Absent middle cerebral artery flow predicts the presence and evolution of the ischemic penumbra. Neurology 52:1125–1132

Bardutzky J, Shen Q, Henninger N, Bouley J, Duong TQ, Fisher M (2005) Differences in ischemic lesion evolution in different rat strains using diffusion and perfusion imaging. Stroke 36:2000-2005

Barnett H, Mohr JP, Stein B, Yatsch FM (eds) (1992) Stroke: Pathophysiology, Diagnosis and Management. 2nd ed. London, England: Churchill Livingstone:360-405

Baron JC, Bousser MG, Rey A, Guillard A, Comar D, Castaigne P (1981) Reversal of focal “misery-perfusion syndrome” by extra-intracranial arterial bypass in hemodynamic cerebral ischemia. A case study with 15O positron emission tomography, Stroke 12:454–459.

Baron JC (1999) Mapping the ischaemic penumbra with PET: implications for acute stroke treatment. Cerebrovasc Dis. 9:193–201

Baron JC, Rougemont D, Soussaline F, Bustany R,Crouzel C, Bousser MG, Comar D (1984) Local interrelationships of cerebral oxygen consumption and glucose utilization in normal subjects and in ischemic stroke patients: a positron tomography study. Journal of Cerebral Blood Flow & Metabolism 4:140–149

Baron JC, Bousser MG, Comar D, Soussaline F, Castaigne R (1981) Noninvasive tomographic study of cerebral blood flow and oxygen metabolism in vivo: potentials, limitations and clinical applications in cerebral ischemic disorders. Eur Neurol 20:273-284

Baron JC (1987) Ischemic stroke studied by 150-labeled compounds: misery perfusion and luxury perfusion. In: Clinical efficacy of positron emission tomography (Heiss WD, Pawlik G, Herholz K, Wienhard K, eds). Dordrecht: Martinus Nijhoff;15-23

Baron JC (2001) Perfusion thresholds in human cerebral ischemia: historical perspective and therapeutic implications. Cerebrovasc Dis 11(suppl 1):2-8

Baskerville TA, Deuchar G, McCabe C, Robertson C, Holmes WH, Santosh C, Macrae IM (2011) Influence of 100% and 40% oxygen on penumbral blood flow, oxygen level and T. 2^{*}-weighted MRI in a rat stroke model. In-Press to the Journal of Cerebral Blood Flow & Metabolism

Bederson JB, Pitts LH, Germano SM, Nishimura MC, Davis RL, Bartowski HM (1986) Evaluation of 2,3,5-triphenyltetrazolium chloride as a stain for detection and quantification of experimental cerebral infarction in rats. Stroke 17:1304–1308

Becker JU, Wira CR (2006) Stroke, Ischaemic. Retrieved November 29, 2007, from http://www.emedicine.com/emerg/topic558.htm

Belayev L, Zhao W, Busto R, Ginsberg MD (1997) Transient middle cerebral artery occlusion by intraluminal suture: three-dimensional autoradiographic image-analysis of local cerebral glucose metabolism–blood flow interrelationships during ischemia and early recirculation. J Cereb Blood Flow Metab 17:1266–1280

Bernard SA, Gray TW, Buist MD, Jones BM, Silvester W, Gutteridge G, Smith K (2002) Treatment of comatose survivors of out-of-hospital cardiac arrest with induced hypothermia. N. Engl. J. Med. 346:557–563

Beyer T, Pichler B (2009) A decade of combined imaging: from a PET attached to a CT to a PET inside an MR. Eur J Nucl Med Mol Imaging 36 Suppl 1:S1-2

Boas DA, Strangman G, Culver JP, Hoge RD, Jasdzewski G, Poldrack RA, Rosen BR, Mandeville JB (2003) Can the cerebral metabolic rate of oxygen be estimated with near-infrared spectroscopy? Phys Med Biol 48:2405–2418

Branston NM, Strong AJ & Symon L. (1977) Extracellular potassium activity, evoked potentials, and tissue blood flow. J Neurol Sci 32: 305−321.

Brüne, B (2003) Nitric oxide: NO apoptosis or turning it ON? Cell Death and Differentiation 10:864–869

Buchan AM, Gertler SZ, Li H, Xue D, Huang ZG, Chaundy KE, Barnes K, Lesiuk HJ (1994) A selective N-type ca2+ blocker prevents CA1 injury 24 hr following severe forebrain ischaemia and reduces infarction following focal ischaemia. J Cerebr Blood Flow and Metab 14:903-910

Busch E, Gyngell ML, Eis M, Hoehn-Berlage M, Hossmann KA (1996) Potassium-induced cortical spreading depressions during focal cerebral ischemia in rats: contribution to lesion growth assessed by diffusion-weighted NMR and biochemical imaging. J. Cereb. Blood Flow Metab. 16:1090–1099

Butcher KS, Parsons M, MacGregor L, Barber PA, Chalk J, Bladin C, Levi C, Kimber T, Schultz D, Fink J, Tress B, Donnan G, Davis S (2005) Refining the perfusion–diffusion mismatch hypothesis. Stroke 36:1153–1159

Buxton RB, Wong EC, Frank LR (1998) Dynamics of blood flow and oxygenation changes during brain activation: the balloon model. Magn. Reson. Med. 39 (6):855–864

Calamante F, Gadian DG, Connelly A (2002) Quantification of perfusion using bolus tracking magnetic resonance imaging in stroke: assumptions, limitations, and potential implications for clinical use. Stroke 33:1146–1151

Cenci MA, Wishaw IQ, Schallert T (2002) Animal models of neurological deficits: how relevant is the rat? Nature Neuroscience Reviews 3:574-578

Chen R, Balami JS, Esiri MM, Chen L, & Buchan AM (2010) Ischemic stroke in the elderly: an overview of evidence. Nature Reviews Neurology 6:256-265

Cho S, Park EM, Kim Y, Liu N, Gal J, Volpe BT, Joh TH (2001) Early c-Fos induction after cerebral ischemia: a possible neuroprotective role. J Cereb Blood Flow Metab 21:550-556

Chopp M, Li Y, Jiang N, Zhang RL, Prostak J: Antibodies against adhesion molecules reduce apoptosis after transient middle cerebral artery occlusion in rat brain. J Cereb Blood Flow Metab 16:578-584, 1996

Clarke, PGH (1990) Developmental cell death, morphological diversity, and multiple mechanisms. Anat. Embroyl. 181:195-213

Cranston, D (2007) Therapeutic ultrasound summer school: Cardiology and stroke, Cargese, April 10th – 13th 2007. Senior lecturer in surgeon and consultant urological surgeon, University of Oxford

Cohen ER, Ugurbil K, Kim SG (2002) Effect of basal conditions on the magnitude and dynamics of the blood dependent fMRI response. J Cereb Blood Flow Metab 22:1042–53

Corfield DR, Murphy K, Josephs O, Adams L, Turner R (2001) Does hypercapnia-induced cerebral vasodilation modulate the hemodynamic response to neural activation? NeuroImage 13:1207–1211

Csipo I, Montel AH, Hobbs JA, Morse PA, Brahmi Z (1998) Effect of Fas+ and Fas- target cells on the ability of NK cells to repeatedly fragment DNA and trigger lysis via the Fas lytic pathway. Apoptosis 3:105-114

Czosnyka M, Smielewski P, Piechnik S, Steiner LA, Pickard JD (2001) Cerebral autoregulation following head injury. J Neurosurg 95:756–63

Darby DG, Barber PA, Gerraty RP, Desmond PM, Yang Q, Parsons M, Li T, Tress BM, Davis SM (1999) Pathophysiological topography of acute ischemia by combined diffusion-weighted and perfusion MRI. Stroke 30:2043–2052

Davis D, Ulatowski J, Eleff S, Izuta M, Mori S, Shungu D, van Zijl PC (1994) Rapid monitoring of changes in water diffusion coefficients during reversible ischemia in cat and rat brain. Magn Reson Med 31(4) 454-460

Davis SM, Donnan GA, Parsons MW, Levi C, Butcher KS, Peeters A, Barber PA, Bladin C, De Silva DA, Byrnes G, Chalk JB, Fink JN, Kimber TE, Schultz D, Hand PJ, Frayne J, Hankey G, Muir K, Gerraty R, Tress BM, Desmond PM (2008) Effects of alteplase beyond 3 h after stroke in the Echoplanar Imaging Thrombolytic Evaluation Trial (EPITHET): a placebo-controlled randomised trial. Lancet Neurol 7:299–309

Dawson SL, Panerai RB, Potter JF (2003) Serial changes in static and dynamic cerebral autoregulation after acute ischaemic stroke. Cerebrovasc Dis 16:69–75.

Derouesne C, Cambon H, Yelnik A, Duydaerts C, Hauw JJ (1993) Infarcts in the middle cerebral artery territory. Acta Neurologica Scandinavica, 87:361-6

Dettmers C, Hartmann A, Rommel T, Krämer S, Pappata S, Young A, Hartmann S, Zierz S MacKenzie ET, Baron JC (1994) Immersion and perfusion staining with 2,3,5-triphenyltetrazolium chloride (TTC) compared to mitochondrial enzymes 6 hours after MCA-occlusion in primates. Neurol Res 16(3):205-8.

Dienel GA, Cruz NF, Mori K, Holden JE, Sokoloff L (1991) Direct measurement of the lambda of the lumped constant of the deoxyglucose method in rat brain: determination of lambda and lumped constant from tissue glucose concentration or equilibrium brain/plasma distribution ratio for methylglucose. J Cereb Blood Flow Metab 11(1):25-34.

Dienel GA, Pulsinelli WA, Duffy TE (1980) Regional protein synthesis in rat brain following acute hemispheric ischemia. J Neurochem 35(5):1216-26.

Diener HC, Cortens M, Ford G, Grotta J, Hacke W, Kaste M, Koudstaal PJ, Wessel T. (2000) Lubeluzole in acute ischemic stroke treatment: a double-blind study with an 8-hour inclusion window comparing a 10-mg daily dose of lubeluzole with placebo, Stroke 31, pp. 2541–2543

Dirnagl U, Iadecola C, Moskowitz MA (1999) Pathobiology of ischaemic stroke: an integrated view. Trends Neurosci 22:391-397

Dirnagl U, Kaplan B, Jacewicz M, Pulsinelli W (1989) Continuous measurement of cerebral cortical blood flow by laser-Doppler flowmetry in a rat stroke model. J. Cereb. Blood Flow Metab. 9:589-596

Dijkhuizen RM, Beekwilder JP, van der Worp HB, van der Sprenkel JWB, Tulleken KAF, Nicolay K (1999) Correlation between tissue depolarizations and damage in focal ischemic rat brain. Brain Res 840:194 –205.

Dohmen C, Bosche B, Graf R, Reithmeier T, Ernestus RI, Brinker G, Sobesky J, Heiss WD (2006) Identification and clinical Impact of impaired cerebrovascular autoregulation in patients with malignant middle cerebral artery infarction. Stroke 22:1–6

Donnan GA, Fisher M, Macleod M, Davis SM (2008) Stroke. Lancet 371 (9624): 1612–23

Donnan GA, Baron JC, Ma H, Davis SM (2009) Penumbral selection of patients for trials of acute stroke therapy. Lancet Neurol 8:261–9

Donnan GA, Baron JC, Davis SM, Sharp (2007) The ischemic penumbra: overview, definition and criteria. In: The Ischemic Penumbra (Donnan GA, Baron JC, Davis SM, Sharp, eds) Informa Healthcare USA, New York:7-20

Donnan, G.A (eds) (2007) The Ischemic Penumbra. Edition: illustrated
Published by CRC Press, 2007

Durukan A, Tatlisumak T (2007) Acute ischemic stroke: Overview of major experimental rodent models, pathophysiology, and therapy of focal cerebral ischemia. Pharmacology Biochemistry and Behavior 87(1):179-197

Duverger D, MacKenzie ET (1988) The quantification of cerebral infarction following focal ischaemia in the rat: influence of strain, arterial pressure, blood glucose concentration, and age. J. Cereb. Blood Flow Metab 8:449-461

Ebinger M, De Silva DA, Christensen S, Parsons MW, Markus R, Donnan GA, Davis SM (2009) Imaging the penumbra – strategies to detect tissue at risk after ischemic stroke J Clin Neurosci 16(2):178-187

Ellekjær H, Holmen J, Indredavik B, Terent A (1997) Epidemiology of Stroke in Innherred, Norway, 1994 to 1996 : Incidence and 30-Day Case-Fatality Rate. Stroke 28:2180–2184

Emerich DF, Dean RL, Bartus RT (2002) The role of leukocytes following cerebral ischemia: pathogenic variable or bystander reaction to emerging infarct? Exp Neurol 173:168–181

Enari M, Sakahira H, Yokoyama H, Okawa K, Iwamatsu A, Nagata S (1998) A caspase-activated DNase that degrades DNA during apoptosis, and its inhibitor ICAD. Nature 391:43-50

Fadok VA, Savill JS, Haslett C, Bratton DL, Doherty DE, Campbell PA, Henson PM (1992) Different populations of macrophages use either the vitronectin receptor or the phosphatidylserine receptor to recognize and remove apoptotic cells. J. Immunol 149(12):4029-35

Feigin VL (2005) Stroke epidemiology in the developing world. Lancet 365 (9478):2160–1

Feigin VL, Anderson CS, Rodgers A, Anderson NE, Gunn AJ (2002) The emerging role of induced hypothermia in the management of acute stroke. Journal of Clinical Neuroscience Volume 9, Issue 5:502-507

Felberg RA, Okon NJ, El-Mitwalli A, Burgin WS, Grotta JC, Alexandrov AV (2002) Early dramatic recovery during intravenous tissue plasminogen activator infusion: clinical pattern and outcome in acute middle cerebral artery stroke. Stroke 33:1301–7

Feril LB, Kondo T, Cui ZG, Tabuchi Y, Zhao QL, Ando H, Misaki T, Yoshikawa H, Umemura S (2005) Apoptosis induced by the sonomechanical effects of low intensity pulsed ultrasound in a human leukemia cell line. Cancer Letters 221 (2):145-152

Fiebach JB, Schellinger PD (2003) Local and Systemic Thrombolysis in Acute Stroke. Imaging Decisions MRI 7:26–30.

Fiehler J, Foth M, Kucinski T, Knab R, von Bezold M, Weillier C, Zeumer H, Rother J (2002) Severe ADC decreases do not predict irreversible tissue damage in humans. Stroke 33:79–86

Fink K, Zhu J, Namura S, Shimizu-Sasamata M, Endres M, Ma J, Dalkara T, Yuan J, Moskowitz MA (1998) Prolonged therapeutic window for ischemic brain damage caused by delayed caspase activation. J. Cereb. Blood Flow Metab. 18:1071–1076

Fisher M, Levine PH, Cohen RA (1990) A 21-aminosteroid reduces hydrogen peroxide generation by and chemiluminescence of stimulated human leukocytes. Stroke 21:1435-1438

Folbergova J, Memezawa H, Smith ML, Siesjo BK (1992) Focal and perifocal changes in tissue energy state during middle cerebral artery occlusion in normo- and hyperglycaemic rats. J. Cereb. Blood Flow Metab. 12:24-33

Furlan M, Marchal G, Viader F, Derlon JM, Baron JC (1996) Spontaneous neurological recovery after stroke and the fate of the ischemic penumbra. Ann Neurol. 40(2):216-26.

Fuster V, Stein B, Amboose JA, Badimon L, Badimon JJ, Chesebro JH (1990) Atherosclerotic plaque rupture and thrombosis: evolving concepts. Circulation 82 (supp II):47-59

Garcia JH, Khang-Loon H, Pantoni L, (1998) Pathology. In: Stroke pathophysiology, Diagnosis and management (Barnett H, Henry JM, Mohr JP, Stein BM, Yatsu FM, eds) Third Edition, Philadelphia, PA: Churchill Livingston

Geisler BS, Brandhoff F, Fiehler J, Saager C, Speck O, Rother J, Zeumer H, Kuncinski T (2006) Blood oxygen level-dependent MRI allows metabolic description of tissue at risk in acute stroke patients. Stroke 37:1778–1784

Gerriets T, Stolz E, Walberer M, Muller C, Rottger C, Kluge A, Kaps M, Fisher M, Bachmann G (2004) Complications and pitfalls in rat stroke models for middle cerebral artery occlusion: a comparison between the suture and the macrosphere model using magnetic resonance angiography. Stroke 35:2372–2377

Gido G, Kristian T, Siesjo BK (1997) Extracellular potassium in a neocortical core area after transient focal ischaemia. Stroke 28:206-10

Ginsberg MD (2009) Current status of neuroprotection for cerebral ischemia: synoptic overview. Stroke 40:S111-S114

Giller CA (1991) A bedside test for cerebral autoregulation using transcranial Doppler ultrasound. Acta Neurochir (Wien) 108:7–14

Gillum RF (1999) Risk factors for stroke in blacks: A critical review. American journal of epidemiology 150 no.12:1266-1274

Ginsberg MD, Pulsinelli WA (1994) The ischemic penumbra, injury thresholds and the therapeutic window for acute stroke. Ann. Neurology 36:553-554

Gjedde A, Wienhard K, Heiss WD, Kloster G, Diemer NH, Herholz K, Pawlik G (1985) Comparative regional analysis of 2-fluorodeoxyglucose and methylglucose uptake in brain of four stroke patients. With special reference to the regional estimation of the lumped constant. J Cereb Blood Flow Metab 5(2):163-78

Go AS (2009) The ACTIVE Pursuit of Stroke Prevention in Patients with Atrial Fibrillation. N Engl J Med 360:2127-2129

Gröhn OHJ, Kauppinen RA (2001), Assessment of brain tissue viability in acute ischemic stroke by BOLD MRI. NMR in Biomedicine 14:432–440

Gubitz G, Sandercock P, Counsell C (2003) Antiplatelet therapy for acute ischaemic stroke (Cochrane Review). In: The Cochrane Library, Issue 1, Oxford: Update Software

Goldstein LB (2000) Novel risk factors for stroke: homocysteine, inflammation and infection. Curr Atheroscler Rep 2:110-14

Grotta, J (1997) for the US and Canadian Lubeluzole Ischaemic Stroke Study Group. Lubeluzole treatment of acute ischaemic stroke. Stroke 28:2338-46

Guadagno JV, Warburton EA, Aigbirhio FI, Smielewski P, Fryer TD, Harding S, Price CJ, Gillard JH, Carpenter TA, Baron JC (2004) Does the acute diffusion-weighted imaging represent penumbra as well as core? A combined quantitative PET/MRI voxel-based study. J Cereb Blood Flow Metab 24:1249–1254

Guadagno JV, Jones PS, Fryer TD, Barret O, Aigbirhio FI, Carpenter TA, Price CJ, Gillard JH,Warburton EA, Baron JC (2006) Local relationships between restricted water diffusion and oxygen consumption in the ischemic human brain. Stroke 37:1741–8

Hacke W, Kaste M, Fieschi C, Toni D, Lesaffre E, von Kummer R, Boysen G, Bluhmki E, Höxter G, Mahagne MH, Hennerici M (1995) Intravenous thrombolysis with recombinant tissue plasminogen activator for acute hemispheric stroke: the European Cooperative Acute Stroke Study (ECASS). JAMA 274*:*1017-1025

Hacke W, Donnan G, Fieschi C, Kaste M, von Kummer R, Broderick JP, Brott T, Frankel M, Grotta JC, Haley EC, Kwiatkowski T, Levine SR, Lewandowski C, Lu M, Lyden P, Marler JR, Patel S, Tilley BC, Albers G, Bluhmki E, Wilhelm M, Hamilton S; ATLANTIS Trials Investigators; ECASS Trials Investigators; NINDS rt-PA Study Group Investigators. (2004) Better outcome with early stroke treatment: a pooled analysis of ATLANTIS, ECASS, and NINDS rt-PA Stroke Trials. Lancet 363(9411):768-74

Hacke W, Kaste M, Fieschi C, von Kummer R, Davalos A, Meier D, Larrue V, Bluhmki E, Davis S, Donnan G, Schneider D, Diez-Tejedor E, Trouillas P (1998) Randomised double-blind placebocontrolled trial of thrombolytic therapy with intravenous alteplase in acute ischaemic stroke (ECASS II). Second European-Australasian Acute Stroke Study Investigators. Lancet 352:1245–1251

Hacke W, Furlan AJ, Al-Rawi Y, Davalos A, Fiebach JB, Gruber F, Kaste M, Lipka LJ, Pedraza S, Ringleb PA, Rowley HA, Schneider D, Schwamm LH, Leal JS, Sohngen M, Teal PA, Wilhelm-Ogunbiyi K, Wintermark M, Warach S (2009) Intravenous desmoteplase in patients with acute ischaemic stroke selected by MRI perfusion–diffusion weighted imaging or perfusion CT (DIAS-2): a prospective, randomised, double-blind, placebo-controlled study. Lancet Neurol 8:141–50

Hacke W, Kaste M, Bluhmki E, Brozman M, Dávalos A, Guidetti D, Larrue V, Lees KR, Medeghri Z, Machnig T, Schneider D, von Kummer R, Wahlgren N, Toni D for the ECASS Investigators (2008) Thrombolysis with Alteplase 3 to 4.5 Hours after Acute Ischemic Stroke The New England Journal of Medicine vol. 359 no. 13:1317-1329

Hacke W, Albers G, Al-Rawi Y, Bogousslavsky J, Davalos A, Eliasziw M, Fischer M, Furlan A, Kaste M, Lees KR, Soehngen M, Warach S; DIAS Study Group (2005) The Desmoteplase in Acute Ischemic Stroke Trial (DIAS): a phase II MRI-based 9-hour window acute stroke thrombolysis trial with intravenous desmoteplase. Stroke 36:66–73

Hakim AM, Pokrupa RP, Villaneuva, J Diksic M, Evans AC, Thompson CJ, Meyer E, Yamamoto YL, Feindel WH (1987) The effect of spontaneous reperfusion on metabolic function in early human cerebral infarcts. Ann Neurol 21:279-289

Han BH, Xu D, Choi J, Han Y, Xanthoudakis S, Roy S, Tam J, Vaillancourt J, Colucci J, Siman R, Giroux A, Robertson GS, Zamboni R, Nicholson DW, Holtzman DM (2002) Selective, reversible caspase-3 inhibitor is neuroprotective and reveals distinct pathways of cell death after neonatal hypoxic-ischemic brain injury. J. Biol. Chem. 277:30128–30136

Hanisch UK (2002) Microglia as a source and target of cytokines. Glia 40:140–155

Hansen, AJ (1981) Extracellular ion concentrations in cerebral ischemia. In: The application of ion-selective microelectrodes (Zeuther T, eds) New York, Elsevier IN orth-Holland:239-254

Hara H, Friedlander RM, Gagliardini V, Ayata C, Fink K, Huang Z, Shimizu-Sasamata M, Yuan J, Moskowitz MA (1997) Inhibition of interleukin 1beta converting enzyme family proteases reduces ischemic and excitotoxic neuronal damage. Proc Natl Acad Sci U S A Mar 4; 94(5):2007-2012

Harms H, Wiegand F, Megow D, Prass K, Einhäupl KM, Dirnagl U (2000) Acute treatment of hypertension increases infarct sizes in spontaneously hypertensive rats. Neuroreport. 7, 11(2):355-9

Harper AM (1990) Physiological control of the cerebral circulation. In: Cerebral blood flow and metabolism (Harper AM, Jennett S, eds) Manchester University Press, Manchester and New York;4-25

Harris RJ, Symon L (1984) Extracellular pH, potassium and calcium activities in progressive ischaemia of rat cortex. J. Cereb. Blood Flow Metab. 1:203-09

Hart, R.G (2005) Cardioembolic stroke, Accessed 5th December 2007 at http://www.emedicine.com/neuro/topic45.htm

Hartings JA, Rolli ML, Lu XC, Tortella FC (2003) Delayed secondary phase of peri-infarct depolarizations after focal cerebral ischemia: relation to infarct growth and neuroprotection. J Neurosci 23:11602–11610

Hasegawa Y, Fisher M, Latour LL, Dardzinski BJ, Sotak CH. (1994) MRI diffusion mapping of reversible and irreversible ischaemic injury in focal brain ischaemia. Neurology 44, 1484-1490

Hata R, Mies G, Wiessner C, Fritze K, Hesselbarth D, Brinker G, Hossmann KA (1998) A reproducible model of middle cerebral artery occlusion in mice: hemodynamic, biochemical, and magnetic resonance imaging. J Cereb Blood Flow Metab. 18(4):367-75.

Hata R, Maeda K, Hermann D, Mies G, Hossmann KA (2000) Evolution of brain infarction after transient focal cerebral ischemia in mice. J Cereb Blood Flow Metab 20(6):937-46

Heckmann JG, Hilz MJ, Hagler H, Mück-Weymann M, Neundörfer B (1999) Transcranial Doppler sonography during acute 80 degrees head-down tilt (HDT) for the assessment of cerebral autoregulation in humans. Neurol Res 21:457–62

Heiss WD, Sobesky J, Hesselmann V (2004) Identifying thresholds for penumbra and irreversible tissue damage. Stroke 35 (11 Suppl 1):2671–4.

Heiss WD (2003) Best measure of ischemic penumbra: Positron emission tomography. Stroke 34:2534-2535

Heiss WD, Grond M, Thiel A, von Stockhausen H, Rudolf J, Ghaemi M, Löttgen J, Stenzel C, Pawlik G (1998) Tissue at Risk of Infarction Rescued by Early Reperfusion: A Positron Emission Tomography Study in Systemic Recombinant Tissue Plasminogen Activator Thrombolysis of Acute Stroke. Journal of Cerebral Blood Flow & Metabolism 18:1298–1307

Heiss WD, Herholz K (1994) Assessment of pathophysiology of stroke by positron emission tomography. Eur J Nuc Med 21:455-465

Heiss WD (2003) Best measure of ischemic penumbra: Positron emission tomography. Stroke 34:2534-2535

Heiss WD, Graf R (1994) The ischemic penumbra. Curr Opin Neurol 7:11-19

Heiss WD, Rosner G (1983) Functional recovery of cortical neurons as related to degree and duration of ischemia. Ann. Neurol. 14:294-301

Heiss WD, Graf R, Fujita T, Ohta F, Bauer B, Löttgen J, Wienhard K (1997) Early Detection of Irreversibly Damaged Ischemic Tissue by Flumazenil Positron Emission Tomography in Cats. *S*troke 28:2045-2052.

Henninger N, Sicard KM, Schmidt KF, Bardutzky J, Fisher M (2006) Comparison of ischemic lesion evolution in embolic versus mechanical middle cerebral artery occlusion in Sprague Dawley rats using diffusion and perfusion imaging. Stroke 37:1283–1287

Hoffman WE, Pelligrino D, Werner C, Kochs E, Albrecht RF, Schulte am Esch J (1992) Ketamine decreases plasma catecholamines and improves outcome for incomplete cerebral ischaemia in rats. Anaesthesiology 76:755-62

Hossmann KA (1994) Viability thresholds and the penumbra of focal ischemia. Ann Neurol 36:557-565

Hossmann KA, Schuier FJ (1980) Experimental brain infarcts in cats. I. Pathophysiological observations. Stroke 11:583-592

Hossmann KA, Mies G (2007) Multimodal mapping of the ischemic penumbra in animal models. In: The Ischemic Penumbra (Donnan GA, Baron JC, Davis SM, Sharp FR, eds), Informa Healthcare USA, New York:77-92

Howells DW, Porritt MJ, Rewell SS, O'Collins V, Sena ES, van der Worp HB, Traystman RJ, Macleod MR (2010) Different strokes for different folks: the rich diversity of animal models of focal cerebral ischemia. J Cereb Blood Flow Metab. 30(8):1412-31

Hsu CY, Lui TH, Xu J, Hogan EL, Chao J (1990) Lipid inflammatory mediators in ischemic brain edema and injury. In Lipid mediators in Ischemic Brain Damage and Experimental Epilepsy (Bazan NG, eds) New Trends Lipid Mediators Research, Karger, Basel, 4:85-112

Hudgins WR, Garcia JH (1970) Transorbital approach to the middle cerebral artery of the squirrel monkey: a technique for experimental cerebral infarction applicable to ultrastructural studies. Stroke 1:107–111.

Hungerhuber E (2006) Simultaneous bilateral laser Doppler fluxmetry and electrophysiological recording during middle cerebral artery occlusion in rats. Journal of Neuroscience Methods 154:109–115

Huppert, TJ, Hoge RD, Diamond SG, Franceschini MA, Boas DA (2006) A temporal comparison of BOLD, ASL, and NIRS hemodynamic responses to motor stimuli in adult humans. NeuroImage 29(2):368-382

Iadecola C, Zhang F, Casey R, Clark HB, Ross E (1996) Inducible nitric oxide synthase gene expression in vascular cells after transient focal cerebral ischemia. Stroke 27:1373-1380

Iijima T, Meis G, Hossmann KA (1992) Repeated negative deflections in rat cortex following middle cerebral artery occlusion are abolished by MK-801: effect on volume of ischemic injury. J Cereb Blood Flow Metab 12:727–733

Ikonomidou C, Mosinger JL, Salles KS, Labruyere J, Olney J (1989) Sensitivity of the developing rat brain to hypobaric/ischemic damage parallels sensitivity to N-methyl-D-aspartate neurotoxicity. J. Neurosci 9:2809-2816

Intercollegiate Working Party for Stroke. Concise Report on the National Sentinel Audit of Stroke 2001–2. Clinical Effectiveness & Evaluation Unit. Royal College of Physicians, London. Retrieved January 14 2011, from: http://www.rcplondon.ac.uk/college/ceeu/strokeconciseauditreport.pdf.

Jean WC, Spellman SR, Nussbaum ES, Low WC (1998) Reperfusion injury after focal cerebral ischemia: role of inflammation and the therapeutic horizon [review]. Neurosurgery 43:1382−1397

Johnston SC, Selvin S, Gress DR (1998) The burden, trends, and demographics of mortality from subarachnoid hemorrhage. Neurology 50:1413-8

Johnson PC (1964) Review of previous studies and current theories of autoregulation. Circulation Research Supplement I, XIV and XV:1.2-1.9

Kakuda W, Lansberg MG, Thijs VN, Kemp SM, Bammer R, Wechsler LR, Moseley ME, Parks MP, Albers GW (2008) Optimal definition for PWI/DWI mismatch in acute ischemic stroke patients. J Cereb Blood Flow Metab. 28(5):887-91

Kamenetsky M, Middelhaufe S, Bank EM, Levin LR, Buck J, Steegborn C. (2006) Molecular Details of cAMP Generation in Mammalian Cells: A Tale of Two Systems, Journal of Molecular Biology 362(4):623-639

Kammersgaard LP, Rasmussen BH, Jùrgensen HS, Reith J, Olsen TS (2000) Feasibility and safety of inducing modest hypothermia in awake patients with acute stroke through surface cooling: a case-control study. The Copenhagen Stroke Study. Stroke 31:2251-2256.

Kaste M, Fogelholm R, Rissanen A (1998) Economic burden of stroke and the evaluation of new therapies. Public Health 112(2):103-112

Kastrup, A., Kruger, G., Glover, G.H., Neumann-Haefelin, T. and Moseley, M.E., 1999. Regional variability of cerebral blood oxygenation response to hypercapnia. NeuroImage 10, pp. 675–681

Katzan IL, Hammer MD, Hixson ED, Furlan AJ, Abou-Chebl A, Nadzam DM (2004) Utilization of Intravenous Tissue Plasminogen activator for acute ischemic stroke. Arch Neurol. 61:346-350.

Kavec M, Grohn OH, Kettunen MI, Silvennoinen MJ, Penttonen M, Kauppinen RA (2001) Use of spin echo T2 BOLD in the assessment of misery perfusion at 1.5T. MAGMA 12:32–39

Kennan RP, Scanley BE, Gore JC (1997) Physiologic basis for BOLD MR signal changes due to hypoxia/hyperoxia: separation of blood volume and magnetic susceptibility effects. Magn Reson Med. 37(6):953-6.

Kerr JFR, Wyllie AH, Currie AR (1972) Apoptosis: a basic biological phenomenon with wide-ranging implications in tissue kinetics, Br J Cancer 26:239–257

Kesavadas C, Fiorelli M, Gupta AK, Pantano P, Bozzao L, Kapilamoorthy TR (2003) Diffusion weighted magnetic resonance imaging in acute ischemic stroke. Indian J Radiol Imaging 13:433-40

Kety SS, Schmidt CF (1948) The effects of altered arterial tensions of carbon dioxide and oxygen on cerebral blood flow and cerebral oxygen consumption of normal young men. J Clin Invest 27:484

Khatri P, Wechsler LR, Broderick JP (2007) Intracranial hemorrhage associated with revascularization therapies. Stroke 38(2):431-40

Kidwell CS, Liebeskind DS, Starkman S, Saver JL (2001) Trends in acute ischemic stroke trials through the 20th century. Stroke 32:1349–1359.

Kidwell CS, Saver JL, Mattiello J, Starkman S, Vinuela F, Duckwiler D, Gobin YP, Jahan R, Vespa P, Kalafut M, Alger JR (2000) Thrombolytic reversal of acute human cerebral ischemic injury shown by diffusion/perfusion magnetic resonance imaging. Ann Neurol 47:462–469

Kidwell CS, Saver JL, Starkman S, Duckwiler G, Jahan R, Vespa P, Villablanca JP, Liebeskind DS, Gobin YP, Vinuela F, Alger JR (2002) Late secondary ischemic injury in patients receiving intraarterial thrombolysis. Ann Neurol 52:698 –703

Kidwell CS, Alger JR, Saver JL (2003) Beyond mismatch: evolving paradigms in imaging the ischemic penumbra with multimodal magnetic resonance imaging. Stroke. 34(11):2729-35.

Kraemer N, Thomalla G, Soennichsen J, Fiehler J, Knab R, Kucinski T, Zeumer H, Rother J (2005) Magnetic resonance imaging and clinical patterns of patients with ‘spectacular shrinking deficit’ after acute middle cerebral artery stroke. Cerebrovasc Dis 20:285–90

Krieger DW, De Georgia MA, Abou-Chebl A, Andrefsky JC, Sila CA, Katzan IL, Mayberg MR, Furlan AJ. (2001) Cooling for acute ischemic brain damage (COOL AID): an open pilot study of induced hypothermia in acute ischemic stroke. Stroke 32:1847–1854.

Kristián T, Siesjö BK (1996) Role of calcium for neuronal development, maturation and cell death calcium-related damage in ischemia. Life Sciences 59(5-6):357-367

Kucinski T, Naumann D, Knab R, Schoder V, Wegener S, Fiehler J, Majumder A, Röther J, Zeumer H (2005) Tissue at risk is overestimated in perfusion-weighted imaging: MR imaging in acute stroke patients without vessel recanalization. Am J Neuroradiol 26:815–819

Kwong KK, Belliveau JW, Chesler DA, Goldberg IE, Weisskoff RM, Poncelet BP, Kennedy DN, Hoppel BE, Cohen MS, Turner R, Cheng H, Brady TJ, Rosen BJ (1992) Dynamic magnetic resonance imaging of human brain activity during primary sensory stimulation. Proc. Natl Acad. Sci. USA 89:5675–5679.

Lacy CR, Suh DC, Bueno M, Kostis JB (2001) Delay in presentation and evaluation for acute stroke: stroke time registry for outcomes knowledge and epidemiology (S.T.R.O.K.E.). Stroke. 32:63-69

Laing RJ, Jakubowski J, Laing RW (1993) Middle cerebral artery occlusion without craniectomy in rats. Which method works best? Stroke 24:294–297.

Latchaw RE, Yonas H, Hunter GJ, Yuh WT, Ueda T, Sorensen AG, Sunshine JL, Biller J, Wechsler L, Higashida R, Hademenos G (2003) Guidelines and recommendations for perfusion imaging in cerebral ischemia: a scientific statement for healthcare professionals by the writing group on perfusion imaging, from the Council on Cardiovascular Radiology of the American Heart Association. Stroke 34:1084–1104

Law R, Bukwirwa H (1999) The physiology of oxygen delivery. Update Anaesthesia 10:1–2

Lee DH, Kang DW, Ahn JS, Choi CG, Sang Joon Kim SJ, Suh DC (2005) Imaging of the Ischemic Penumbra in Acute Stroke. Korean J Radiol 6:64-74

Lee R (1995) Morphology of cerebral arteries. Pharmacology and Therapeutics 66:149-173

Lee JM, Bernstein A (1995) Apoptosis, cancer and the p53 tumour suppressor gene. Cancer metastasis review 14 (2):149-61

Lees KR, Bluhmki E, von Kummer R, Brott TG, Toni D, Grotta JC, Albers GW, Kaste M, Marler JR, Hamilton SA, Tilley BC, Davis SM, Donnan GA, Hacke W; ECASS, ATLANTIS, NINDS and EPITHET rt-PA Study Group, Allen K, Mau J, Meier D, del Zoppo G, De Silva DA, Butcher KS, Parsons MW, Barber PA, Levi C, Bladin C, Byrnes G (2010) Time to treatment with intravenous alteplase and outcome in stroke: an updated pooled analysis of ECASS, ATLANTIS, NINDS, and EPITHET trials. Lancet 15;375(9727):1695-703.

Levy DE, Brierly JB (1979) Delayed pentobarbital administration limits ischemic damage in gerbils. Ann Neurol 5:59-64

Li D, Waight DJ, Wang Y (1998) In vivo correlation between blood $T2^*$ and oxygen saturation, J. Magn. Reson. Imaging 8:1236–1239

Li F, Han SS, Tatlisumak T, Liu KF, Garcia JH, Sotak CH, Fisher M (1999) Reversal of acute apparent diffusion coefficient abnormalities and delayed neuronal death following transient focal cerebral ischemia in rats. Ann Neurol 46:333–342

Liebeskind DS (2004) Intracranial Hemorrhage. Retrieved December 5, 2007, from http://www.emedicine.com/neuro/topic177.htm

Lin W, Paczynski RP, Celik A, Kuppusamy K, Hsu CY, Powers WJ (1998) Experimental hypoxemic hypoxia in $R2^*$ of brain parenchyma accurately reflect the combined effects of changes in arterial and cerebral venous oxygen saturation. Magn. Reson. Med. 39:474–481.

Linskey ME, Jungreis CA, Yonas H, Hirsch WL, Sekhar LN, Horton JA, Janosky JE (1994) Stroke risk after abrupt internal carotid artery sacrifice: accuracy of preoperative assessment with balloon test occlusion and stable xenon-enhanced CT. AJNR Am J Neuroradiol 15:829-843

Lipton P (1999) Ischemic cell death in brain neurons. Physiological review 79, vol 4: 1431-1568

Lipton P (2007) Pathologically-activated therapeutics for neuroprotection: mechanism of NMDA receptor block by memantine and S-nitrosylation. Curr. Drug Targets 8:621-632

Lo EH, Dalkara T, Moskowitz MA (2003) Mechanisms, challenges and opportunities in stroke, Nature Reviews Neuroscience 4:399-414

Lo EH, Pierce AR, Mandeville JB, Rosen BR (1997) Neuroprotection with NBQX in rat focal cerebral ischemia. Effects on ADC probability distribution functions and diffusion–perfusion relationships. Stroke 28:439–447

McAuley MA (1995) Rodent models of focal ischaemia. Cerebrovascular brain metabolism review 7(2):153-180

Mackay J, Mensah GA (2004) The atlas of heart disease and stroke, Contributor World Health Organization Staff, Myriad Editions Limited Staff, Center for Disease Control Staff. World Health Organization:52-53

Maeda M, Itoh S, Ide H, Matsuda T, Kobayashi H, Kubota T, et al. Acute stroke in cats: comparison of dynamic susceptibility-contrast MR imaging with T2- and diffusion-weighted MR imaging. Radiology. 1993;189:227–232

Magistretti PJ (2006) Neuron-glia metabolic coupling and plasticity. J Exp Biol 209:2304–2311

Majno G, Joris I (1995) Apoptosis, oncosis and necrosis. An overview of cell death. Am. J. Pathol. 146:3-15

Makar TK, Nedergaard M, Preuss A, Gelbard AS, Perumal AS, Cooper AJ (1994) Vitamin E, ascorbate, glutathione, glutathione disulfide, and enzymes of glutathione metabolism in cultures of chick astrocytes and neurons: evidence that astrocytes play an important role in antioxidative processes in the brain. J. Neurochem. 62:45–53

Mandir AS, Poitras MF, Berliner AR, Herring WJ, Guastella DB, Feldman A, Poirer GG, Wang ZQ, Dawson TM, Dawson VL (2000) NMDA but not non-NMDA exocitoxicity is mediated by poly(ADP-ribose) polymerase. J. Neurosci 20:8005-11

Mant J, Wade, D Winner S (2004) Stroke, Health Care Needs Assessment, Chapter 3:141-243.

Marchal G, Serrati C, Rioux P, Petit-Taboué MC, Viader F, de la Sayette V, Le Doze F, Lochon P, Derlon JM, Orgogozo JM (1993) PET imaging of cerebral perfusion and oxygen consumption in acute ischaemic stroke: relation to outcome. Lancet 341:925-7

Marieb EN (1998) The central nervous system. In: Human anatomy and physiology (Marieb EN, eds). Benjamin/Cummings Science Publishing, California:404-455

Markus H (2001) The pathophysiology of stroke. The British Journal of Cardiology 8(10):586-589

Markus R, Reutens DC, Kazui S Read S, Wright P, Chambers BR, Sachinidis JI, Tochon-Danguy HJ, Donnan GA (2003) Topography and temporal evolution of hypoxic viable tissue identified by 18F-fluoromisonidazole positron emission tomography in humans after ischemic stroke. Stroke 34:2646–2652

Matsuo Y, Kihara T, Ikeda N, Ninomiya M, Onodera H, Kogure K (1995) Role of neutrophils in radical production during ischemia and reperfusion of the rat brain: Effect of neutrophil depletion on extracellular ascorbyl radical formation. J Cereb Blood Flow Metab 15:941-947

Mayer TE, Hamann GF, Baranczyk J, Rosengarten B, Klotz E, Wiesmann M, Missler U, Schulte-Altedorneburg G, Brueckmann HJ (2000) Dynamic CT perfusion imaging of acute stroke. AJNR Am J Neuroradiol. 21:1441–1449

Mayevsky A, Weiss H (1991) Cerebral blood flow and oxygen consumption in cortical spreading depression J Cereb Blood Flow Metab 11:829–836

Meng X, Fisher M, Shen Q, Sotak CH, Duong TQ (2004) Characterizing the diffusion/perfusion mismatch in experimental focal cerebral ischemia. Ann Neurol 55:207-212.

Menon RS, Ogawa S, Hu X, Strupp JP, Anderson P, Uğurbil K (1995) BOLD based Functional MRI at 4 Tesla includes a capillary bed contribution: Echo planar imaging correlates with previous optical imaging using intrinsic signals. Magn. Reson. Med. 33:453–59

Menon RS, Ogawa S, Tank DW, Ugurbil K (1993) 4 Tesla gradient recalled echo characteristics of photic stimulation induced signal changes in the human primary visual cortex. Magn. Reson. Med. 30:380–86

Mies G, Iijima T, Hossmann KA (1993) Correlation between peri-infarct DC shifts and ischaemic neuronal damage in rat. NeuroReport 4:709–711

Minamisawa H, Nordström CH, Smith ML, Siesjö BK (1990) The influence of mild body and brain hypothermia on ischemic brain damage. J Cereb Blood Flow Metab. 10(3):365-74

Minematsu K, Li L, Sotak C, Davis M, Fisher M (1992) Reversible focal ischemic injury demonstrated by diffusion-weighted magnetic resonance imaging in rats. Stroke 23:1304-1311

Mintorovitch J, Yang GY, Shimizu H, Kucharczyk J, Chan PH, Weinstein PR (1994) Diffusion-weighted magnetic resonance imaging of acute focal cerebral ischemia: comparison of signal intensity with changes in brain water and Na1,K(1)-ATPase activity. J Cereb Blood Flow Metab. 14:332–336

Moffat BA, Chenevert TL, Hall DE, Rehemtulla A, Ross BD (2005) Continuous arterial spin labeling using a train of adiabatic inversion pulses. J Magn Reson Imaging 21:290–296

Molina CA, Saver JL (2005) Extending Reperfusion Therapy for Acute Ischemic Stroke: Emerging Pharmacological, Mechanical, and Imaging Strategies. Stroke. 36:2311-2320

Molina CA, Alvarez-Sabin J (2009) Recanalization and Reperfusion Therapies for Acute Ischemic Stroke. Cerebrovasc Dis 27(Suppl. 1):162-167

Mrsulja BB, Ueki Y, Lust WD (1986) Regional metabolite profiles in early stages of ischaemia in the gerbil. Metab. Brain Dis 1:205-220

Moustafa RR, Baron JC (2007) Perfusion thresholds in cerebral ischemia. In: The Ischemic Penumbra (Donnan GA, Baron JC, Davis SM, Sharp FR, eds), Informa Healthcare USA, New York:22-35

Muir KW, Santosh C (2005) Imaging of acute stroke and transient ischaemic attack J Neurol Neurosurg Psychiatry 76:19-28

Muir KW, Buchan A, von Kummer R, Rother J, Baron JC (2006) Imaging of acute stroke. Lancet Neurol 5(9):755-68. Review.

Murphy BD, Fox AJ, Lee DH, Sahlas DJ, Black SE, Hogan MJ, Coutts SB, Demchuk AM, Goyal M, Aviv RI, Symons S, Gulka IB, Beletsky V, Pelz D, Hachinski V, Chan R, Lee TY (2006) Identification of penumbra and infarct in acute ischemic stroke using computed tomography perfusion-derived blood flow and blood volume measurements. Stroke. 37:1771-1777.

Neumann-Haefelin T, Wittsack H, Wenserski F, Siebler M, Seitz RJ, Mödder U, Freund HJ (1999) Diffusion- and perfusion-weighted MRI: The DWI-PWI mismatch region in acute stroke. Stroke 30:1591-1597

National Health Service Executive (1996). Burden of disease. NHSE

National Institute of Neurological Disorders and Stroke (NINDS) (1999). Stroke: Hope Through Research. National Institutes of Health. Retrieved November 29, 2007, from: http://www.ninds.nih.gov/disorders/stroke/detail_stroke.htm

National Institute of Neurological Disorders and Stroke (NINDS) (1999) Stroke Information Page. Retrieved December 5, 2010, from: http://www.ninds.nih.gov/disorders/stroke/stroke.htm#What_is_the_prognosis

Nedergaard M, Astrup J. Infarct rim: effect of hyperglycemia on direct current potential and [14C]2-deoxyglucose phosphorylation (1986). J Cereb Blood Flow Metab 6(5):607-15

Nedergaard M, Diemer NH (1988) Experimental cerebral ischemia: barbiturate resistant increase in regional glucose utilization. J Cereb Blood Flow Metab 8:763-766

Nedergaard M, Gjedde A, Diemer NH (1986) Focal ischemia of the rat brain: Autoradiographic determination of cerebral glucose utilization, glucose content, and blood flow. J. Cereb Blood Flow and Metab 6:414-424

Nestler EJ, Hyman SE, Malenka RC (eds) (2001) Molecular Neuropharmacology: A Foundation for Clinical Neuroscience, McGraw-Hill Professional, pp404

Neumann J, Gunzer M, Gutzeit HO, Ullrich O, Reymann KG, Dinkel K (2006) Microglia provide neuroprotection after ischaemia. FASEB J. 20(6):714-6

Neurology Channel, Stroke: Treatment, Rehab, Prognosis, Prevention of Stroke (2007) Retrieved December 14, 2010, from: http://www.neurologychannel.com/stroke/treatment.shtml

NINDS rt-PA Stroke Study Group (1995) Tissue plasminogen activator for acute ischemic stroke. The National Institute of Neurological Disorders and Stroke rt-PA Stroke Study Group. N Engl J Med. 333:1581–1587

Obata T, Thomas TL, Miller K, Luh WM, Wong EC, Frank LR, Buxton RB (2004) Discrepancies between BOLD and flow dynamics in primary and supplementary motor areas: applications of the balloon model to the interpretation of BOLD transients. NeuroImage 21:144–153

Obrenovitch TP, Garofalo O, Harris RJ, Bordi L, Ono M, Momma F, Bachelard HS, Symon L (1988) Brain tissue concentrations of ATP, phosphocreatine, lactate, and tissue pH in relation to reduced cerebral blood flow following experimental acute middle cerebral artery occlusion. J Cereb Blood Flow Metab 8:16-23

Ogawa S, Lee TM, Kay AR, Tank DW (1990) Brain magnetic resonance imaging with contrast dependent on blood oxygenation. Proc Natl Acad Sci, 87:9868–9872

Ogawa S, Lee TM, Nayak AS, Glynn P (1990) Oxygenation-sensitive contrast in magnetic resonance image of rodent brain at high magnetic fields. Magnetic Resonance in Medicine, 14:68–78

Ogawa S, Tank DW, Menon R, Ellermann JM, Kim SG, Merkle H, Ugurbil K (1992) Intrinsic signal changes accompanying sensory stimulation: functional brain mapping with magnetic resonance imaging. Proc Natl Acad Sci, 89:5951–5955

Ogawa S, Tank DW, Menon R, Ellermann JM, Kim SG, Merkle H, Ugurbil K (1993) Functional brain mapping by blood oxygen-level dependent contrast magnetic resonance imaging: a comparison of signal characteristics with a biophysical model, Biophys. J. 64:803–812

Olah L, Wecker S, Hoehn M (2001) Relation of apparent diffusion coefficient changes and metabolic disturbances after 1 hour of focal cerebral ischemia and at different reperfusion phases in rats.J Cereb Blood Flow Metab 21(4):430-9.

Oliff HS, Coyle P, Weber E (1997) Rat strain and vendor differences in collateral anastomoses. J Cereb Blood Flow Metab. 17:571–578.

Pabello NG, Tracy SJ, Snyder-Keller A, Keller RW (2005) Regional expression of constitutive and inducible transcription factors following transient focal ischemia in the neonatal rat: influence of hypothermia. Brain Res 15:11–21

Parsons MW, Barber PA, Chalk J, Darby DG, Rose S, Desmond PM, Gerraty RP, Tress BM, Wright PM, Donnan GA, Davis SM (2002) Diffusion- and perfusion-weighted MRI response to thrombolysis in stroke. Annals of Neurology 51 (1):28-37

Paulson OB (1972) Intracranial hypertension Anaesthesiology 36:1-3

Petersen S, Peto V, Scarborough P, Rayner M (2005) Coronary heart disease statistics. British Heart Foundation

Phan TG, Wright PM, Markus R, Howells DW, Davis SM, Donnan GA (2002) Salvaging the ischaemic penumbra: more than just reperfusion? Clin Exp Pharmacol Physiol 29:1–10

Pignataro G, Studer FE, Wilz A, Simon RP, Boison D (2006) Neuroprotection in ischemic mouse brain induced by stem cell-derived brain implants. J Cereb Blood Flow Metab 27(5):919-27

Posse S, Kemna LJ, Elghahwagi B, Wiese S, Kiselev VG (2001) Effect of graded hypo- and hypercapnia on fMRI contrast in visual cortex: Quantification of T2 changes by multiecho EPI. Magn Reson Med 46:264–271

Poustchi-Amin M, Mirowitz SA, Brown JJ, McKinstry RC, Li T (2001) Principles and Applications of Echo-planar Imaging: A Review for the General Radiologist. RadioGraphics *21:767-779*

Powers WJ (1991) Cerebral hemodynamics in ischemic cerebrovascular disease. Ann. Neurol. 29**:**231–240

Powers WJ (1993) Acute hypertension after stroke: the scientific basis for treatment decisions. Neurology 43:461-467

Prado R, Ginsberg MD, Dietrich WD, Watson BD, Busto R (1988) Hyperglycaemia increases infarct size in collaterally perfused but not end-arterial vascular territories. J Cereb Blood Flow Metab 8:186-192

Preston E, Sutherland G, Finsten A (1993) Three openings of the blood-brain barrier produced by forebrain ischemia in the rat, Neuroscience letters 149:75-78

Prielmeier F, Nagatomo Y, Frahm J (1994) Cerebral blood oxygenation in rat brain during hypoxic hypoxia. Quantitative MRI of effective transverse relaxation rates. Magn Reson Med. 31(6):678-81.

Pullicino PM (1993) Pathogenesis of lacunar infarcts and small deep infarcts. Adv Neuro 62:125-140

Raff M (1998) Cell suicide for beginners. Nature 396:119-122.

Raichle ME (1983) The Pathophysiology of Brain Ischemia Ann Neurol 13:2-10

Ramsay SC, Murphy K, Shea SA, Friston KJ, Lammertsma AA, Clark JC, Adams L, Guz A, Frackowiak RS (1993) Changes in global cerebral blood flow in humans: effect on regional cerebral blood flow during neural activation task. J Physiol 471:521–534

Rapoport SI (1976) Pathological alterations of the blood-brain barrier. In: Blood-Brain Barrier in Physiology and Medicine (Rapoport SI, eds) Raven, New York:129-152.

Read SJ, Hirano T, Abbott DF, Sachinidis JI, Tochon-Danguy HJ, Chan JG, Egan GF, Scott AM, Bladin CF, Mckay WJ, Donnan GA (2007) Identifying hypoxic tissue after acute ischemic stroke using PET and 18Ffluoromisonidazole. Neurology 51:1617–1621

Rha JH, Saver JL (2007) The impact of recanalization on ischemic stroke outcome: a meta-analysis. Stroke 38:967–973

Ridker PM (2002) Inflammatory biomarkers, statins, and the risk of stroke: cracking a clinical conundrum. Circulation 105:2583-85

Roberts HC, Dillon WP, Furlan AJ, Wechsler LR, Rowley HA, Fischbein NJ, Higashida RT, Kase C, Schulz GA, Lu Y, Firszt CM (2002) Computed tomographic findings in patients undergoing intra-arterial thrombolysis for acute ischemic stroke due to middle cerebral artery occlusion: results from the PROACT II trial. Stroke 33:1557–65

Robertson CA, McCabe C, Gallagher L, Lopez-Gonzalez R, Holmes W, Condon B, Muir KW, Santosh C, Macrae IM (2011a) Stroke Penumbra Defined by an MRI-based Oxygen Challenge Technique: 1.Validation using [^{14}C] 2-Deoxyglucose Autoradiography. Journal of Cerebral Blood Flow & Metabolism (in press).

Robertson CA, McCabe C, Gallagher L, Lopez-Gonzalez R, Holmes W, Condon B, Muir KW, Santosh C, Macrae IM (2011b) Stroke Penumbra Defined by an MRI-based Oxygen Challenge Technique: 2. Validation based on the consequences of reperfusion. Journal of Cerebral Blood Flow & Metabolism (in press)

Rostrup E, Larsson HBW, Knudsen GM, Born AP, Paulson OB (2005) Changes in BOLD and ADC weighted imaging in acute hypoxia and altitude adaptation. Neuroimage 28:947–955

Rostrup E, Larsson HBW, Toft PB, Garde K, Henriksen O (1995) Signal changes in gradient echo images of human brain induced by hypo- and hyperoxia. NMR Biomed, 8:41–47

Rostrup E, Larsson HBW, Toft PB, Garde K. Thomsen P, Ring L, Søndergaard, Henriksen O (1994) Functional MRI of CO2 induced increase in cerebral perfusion. NMR Biomed, 7:29–34

Rothwell PM, Coull AJ, Silver LE Fairhead JF, Giles MF, Lovelock CE, Redgrave JN, Bull LM, Welch SJ, Cuthbertson FC, Binney LE, Gutnikov SA, Anslow P, Banning AP, Mant D, Mehta Z (2005) Population-based study of event-rate, incidence, case fatality, and mortality for all acute vascular events in all arterial territories (Oxford Vascular Study), Lancet 366:1773–1783

Roussel SA, van Bruggen N, King MD, Gadian DG (1995) Identification of collaterally perfused areas following focal ischemia in rat by comparison of gradient echo and diffusion weighted MRI. J Cereb Blood Flow Metab 15:578–586

Roy CS, Sherrington CS (1890) On the Regulation of the Blood-supply of the Brain. Journal of Physiology 11 (1-2):85–158

Rudd AG, Hoffman A, Irwin P, Lowe D, Pearson MG (2005) Stroke Unit Care and Outcome, Results from the 2001 National Sentinel Audit of Stroke (England, Wales, and Northern Ireland), Stroke. 36:103-106

Sacco RL, DeRosa JT, Haley EC, Levin B, Ordronneau P, Phillips SJ, Rundek T, Snipes RG, Thompson JL for the GAIN Americas Investigators (2001) Glycine antagonist in neuroprotection for patients with acute stroke. GAIN Americas: a randomized controlled trial, JAMA 285:719–1728

Saita K, Chen M, Spratt NJ, Porritt MJ, Liberatore GT, Read SJ, Levi CR, Donnan GA, Ackermann U, Tochon-Danguy HJ, Sachinidis JI, Howells DW (2004). Imaging the penumbra with 18Ffluoromisonidazole in a rat model of ischemic stroke. Stroke 35:975–80

Saka RO, McGuire A, Wolfe CDA (2007) Economic burden of stroke in England. King's College London. Retrieved November 29, 2007, from: http://www.nao.org.uk/publications/nao_reports/05-06/0506452_economic_analysis.pdf

Salisbury HR, Banks BJ, Footitt DR, Winner SJ, Reynolds DJ (1998) Delay in presentation of patients with acute stroke to hospital in Oxford. QJM. 91(9):635-640

Saver JL (2004) Number needed to treat estimates incorporating effects over the entire range of clinical outcomes. Arch Neurol. 61:1066-70

Schellinger PD, Fiebach JB, Hacke W (2003) Imaging-Based Decision Making in Thrombolytic Therapy for Ischemic Stroke Stroke 34:575 -583

Schellinger PD, Thomalla G, Fiehler J, Kohrmann M, Molina CA, Neumann-Haefelin T, Ribo T, Singer OC, Zaro-Weber O, Sobesky J (2007) MRI-Based and CT-Based Thrombolytic Therapy in Acute Stroke Within and Beyond Established Time Windows: An Analysis of 1210 Patients. Stroke 38(10):2640 - 2645

Schlaug G, Siewert B, Benfield A, Edelman RR, Warach S (1997) Time course of the apparent diffusion coefficient (ADC) abnormality in human stroke. Neurology 49:113–119

Schramm P, Schellinger PD, Fiebach JB, Heiland S, Jansen O, Knauth M, Hacke W, Sartor K (2002) Comparison of CT and CT angiography source images with diffusion-weighted imaging in patients with acute stroke within 6 hours after onset, Stroke 33:2426–2432

Shah, S., Pathophysiology of stroke. Retrieved December 3, 2007, from http://www.uic.edu/com/ferne/pdf/pathophys0501.pdf

Sharp FR, Lu A, Tang Y, Millhorn DE (2000) Multiple molecular penumbras after focal cerebral ischemia. J Cereb Blood Flow Metab 20:1011–1032

Shen Q, Fisher M, Sotak CH, Duong TQ (2004) Effects of reperfusion on ADC and CBF pixel-by-pixel dynamics in stroke: characterizing tissue fates using quantitative diffusion and perfusion imaging. J Cereb Blood Flow Metab 24:280–290

Shigeno T, Teasdale GM, Kirkham D, et al: Effect of naloxone on cerebral glucose metabolism in normal rats and rats with focal cerebral ischaemia. J Cereb Blood Flow Metab 3 (Suppl 1):$528-$529, 1983

Shinohara M, Dollinger B, Brown G, Rapoport S, Sokoloff L (1979) Cerebral glucose utilization: local changes during and after recovery from spreading cortical depression Science 203(4376):188-190

Siesjo BK (eds) (1978) Brain Energy Metalolism. New York: John Wiley & Sons; 1978

Siesjo BK, Katsura K, Kristian T (1996) Acidosis-related damage, Adv Neurol 71:209–233

Sims NR, Anderson MF (2002) Mitochondrial contributions to tissue damage in stroke Neurochemistry International 40:511–526

Somjen GG (2001) Mechanisms of spreading depression and hypoxic spreading depression-like depolarization. Physiol Rev 81:1065–1096

Sorensen AG, Buonanno FS, Gonzalez RG, Schwamm LH, Lev MH, Huang-Hellinger FR, Reese TG, Weisskoff RM, Davis TL, Suwanwela N, Can U, Moreira JA, Copen WA, Look RB, Finklestein SP, Rosen BR, Koroshetz WJ (1996) Hyperacute stroke: evaluation with combined multisection diffusion-weighted and hemodynamically weighted echo-planar MR imaging. Radiology 199:391–401

Stan E, McNames J, Kohles SS, Biber C, Biberic N, Leech N, Mangan RW, KcKinney TJ, Surdu M, Goldstein B (2004) Mechanical vasoconstriction for a cerebral myogenic autoregulatory model. Proceedings of the 26th annual international conference of the IEEE EMBS, San Francisco, CA, USA, September 1-5

Steinbrink J, Villringer A, Kempf F, Haux D, Boden S, Obrig H (2006) Illuminating the BOLD signal: combined fMRI-fNIRS studies. Magn Reson Imaging 24(4):495-505

Strandgaard S, Paulson OB (1990) Pathophysiology of stroke, Journal of cardiovascular pharmacology 15 (suppl. 1):38-42

Strebel S, Lam AM, Matta B, Mayberg TS, Aaslid R, Newell DW (1995) Dynamic and static cerebral autoregulation during isoflurane, desflurane, and propofol anesthesia. Anesthesiology 83: pp66–76

Stroke Unit Trialists' Collaboration. Organised inpatient (stroke unit) care for stroke (Cochrane Review). In: The Cochrane Library, Issue 4, 2002. Oxford: Update Software.

Strong AJ, Fabricius M, Boutelle MG, Hibbins SJ, Hopwood SE, Jones R, Parkin MC, Lauritzen M (2002) Spreading and synchronous depressions of cortical activity in acutely injured human brain. Stroke 33:2738−2743

Strong AJ, Smith SE, Whittington DJ, Mel drum BS, Parsons AA, Krupinski J, Hunter AJ, Patel S (2000) Factors influencing the frequency of fluorescence transients as markers of peri-infarct depolarizations in focal cerebral ischemia. Stroke 31:214−222

Sudlow CL, Warlow CP (1997) Comparable studies of the incidence of stroke and its pathological types: results from and international collaboration. Stroke 28:491-9

Swanson RA, Morton MT, Tsao-Wu G, Savalos RA, Davidson C, Sharp FR (1990) A semiautomated method for measuring brain infarct volume. J Cereb Blood Flow Metab. 10:290–293

Symon L, Pasztor E, Branston NM (1974) The distribution and density of reduced cerebral blood flow following acute middle cerebral artery occlusion: An experimental study by the technique of hydrogen clearance in baboons. Stroke 5:355-364

Tak S, Ye J (2009) Quantification of CMRO2 and CBF using Simultaneous NIRS and fMRI. NeuroImage 3:212

Takano K, Latour LL, Formato JE, Carano R, Helmer KG, Hasegawa Y, Sotak CH, Fisher M (1996) The role of spreading depression in focal ischemia evaluated by diffusion mapping. Ann Neurol 39:308–318

Takasawa M, Jones PS, Guadagno JV, Christensen S, Fryer TD, Harding S, Gillard JH, Williams GB, Aigbirhio FI, Warburton EA, Ostergaard L, Baron JC (2008) How reliable is perfusion MR in acute stroke? Validation and determination of the penumbra threshold against quantitative PET. Stroke 39:870–7

Takasawa M, Beech JS, Fryer TD, Hong YT, Hughes JL, Igase K, Jones PS, Smith R, Aigbirhio FI, Menon DK, Clark JC, Baron JC (2007) Imaging of brain hypoxia in permanent and temporary middle cerebral artery occlusion in the rat using 18F-fluoromisonidazole and positron emission tomography: a pilot study. J Cereb Blood Flow Metab 27:679–89

Tamura A, Kawai K, Takagi K (1996) Animal models used in cerebral ischemia and stroke research. In Clinical Pharmacology of Cebrebral Ischemia. Totowa: Humana Press. Chapter 11:265-294.

Tamura H, Hatazawa J, Toyoshima H, Shimosegawa E, Okudera T (2002) Detection of deoxygenation-related signal change in acute ischemic stroke patients by $T2^{*}$-weighted magnetic resonance imaging. Stroke;33:967

Tamura A, Graham DI, McCulloch J, Teasdale GM. (1981) Focal cerebral ischaemia in the rat: 1. Description of technique and early neuropathological consequences following middle cerebral artery occlusion. J Cereb Blood Flow Metab 1:53-60

The ATLANTIS, ECASS, NINDS rt-PA Study Group Investigators (2004) Better outcome with early stroke treatment: a pooled analysis of ATLANTIS, ECASS, and NINDS rt-PA Stroke Trials. Lancet 363(9411):768-74

The Hypothermia after Cardiac Arrest Study Group (2002) Mild therapeutic hypothermia to improve the neurologic outcome after cardiac arrest. N. Engl. J. Med. 346:549–556

The Intercollegiate Working Party for Stroke (2002). National clinical guidelines for stroke. London: Royal College of Physicians. Retrieved April 26, 2011, from: http://www.rcplondon.ac.uk/pubs/books/stroke/stroke_guidelines_2ed.pdf

The National Institute of Neurological Disorders and Stroke rt-PA Stroke Study Group. (1995) Tissue plasminogen activator for acute ischemic stroke. N Engl J Med 333(24):1581-7

The National Institute of Neurological Disorders and Stroke rT-PA Stroke Study Group (1997) Intracerebral hemorrhage after intravenous rT-PA therapy for ischemic stroke. Stroke 28:2109– 2118

The NINDS t-PA Stroke Study Group (1997) After Intravenous t-PA Therapy for Ischemic Stroke. Stroke 28:2109-2118.

Tohyama Y, Sako K, Yonemasu Y (1998) Hypothermia attenuates hyperglycolysis in the periphery of ischemic core in rat brain. Exp Brain Res 122:333–338

Tortora GJ, Grabowski SR (eds) (2000) Principles of anatomy and physiology. John Wiley and Sons Inc. New York, 9th Edition, pp94

Turner R, Le Bihan D, Moonen CT, Despres D, Frank J (1991) Echo-planar time course MRI of cat brain oxygenation changes. Magnetic Resonance in Medicine 22:159–166

Uchino K, Alexandrov AV, Garami Z, El-Mitwalli A, Morgenstern LB, Grotta JC (2005) Safety and feasibility of a lower dose intravenous TPA therapy for ischemic stroke beyond the first three hours. Cerebrovasc Dis 19:260–6

Volkow ND, Rosen B, Farde L (1997) Imaging the living human brain: magnetic resonance imaging and positron emission tomography. Proc. Natl. Acad. Sci. USA 94:2787–88

von Kummer R, Bourquain H, Bastianello S, Bozzao L, Manelfe C, Meier D, Hacke W (2001) Early prediction of irreversible brain damage after ischemic stroke at CT. Radiology 219:95-10

von Monakow C (1914) Lokalisation im Grosshirn und der Abbau der Funktion durch kortikale Herde. Bergmann, Wiesbaden.

Wahlgren NG, Ranasinha KW, Rosolacci T, Franke CL, van Erven PM, Ashwood T, Claesson L (1999) and for the CLASS Study Group, Clomethiazole Acute Stroke Study (CLASS): results of a randomized, controlled trial of clomethizaole versus placebo in 1360 acute stroke patients, Stroke 30:21–28.

Wang CX, Todd KG, Yang Y, Gordon T, Shuaib A (2001) Patency of cerebral microvessels after focal embolic stroke in the rat. J Cereb Blood Flow Metab. 21:413– 421

Warach S (2001) Tissue viability thresholds in acute stroke: the 4- factor model. Stroke 32:2460-2461

Wardlaw JM, Murray V, Berge E, Del Zoppo GJ (2009) Thrombolysis for acute ischaemic stroke. Cochrane Database Syst Rev. Oct 7(4)

Wardlaw JM, del Zoppo G, Yamaguchi T (2003) Thrombolysis for acute ischaemic stroke (Cochrane Review). In: The Cochrane Library, Issue 1, Oxford: Update Software

Warlow CP, Dennis MS, van Gijn J, et al (2001) What caused this transient or persisting ischaemic event? In: Stroke: A practical guide to management (Warlow CP, Dennis MS, van Gijn J, et al, eds). Oxford: Blackwell Science:223-300

Warlow C, Sudlow C, Dennis M, Wardlaw J, Sandercock P (2003) Stroke, Lancet 362:1211-24

Weinberger J, Cohen G (1983) Nerve terminal damage in cerebral ischemia: greater susceptibility of catecholamine nerve terminals relative to serotonin nerve terminals. Stroke 14:986–989

Weishaupt D, Kochli VD, Marincek B (2006) How does MRI work? An introduction to the physics and function of magnetic resonance imaging, second edition, Springer-Verlag Berlin Heidelberg New York:91

Welch KMA, Barkley GL(1986) Biochemistry and pharmacology of cerebral ischaemia, In: Stroke: Pathophysiology, diagnosis and management (Barnett HJM, Stein BM, Mohr JP, Yatsu FM, eds), volume 1, Third Edition, Philadelphia, PA: Churchill Livingston, pp75-90

Welty TE, Horner TG (1990) Pathophysiology and treatment of subarachnoid hemorrhage. Clin Pharm 9(1), pp35-9

Winn RH, Dacey RG, Mayberg MR (1989) Cerebral circulation. In Textbook of physiology (Volume 2) (Patton HD, Fuchs AF, Hille B, Scher AM, Steiner R, eds). W. B. Saunders Company, Philadelpia:952-960

Wintermark M, Flanders AE, Velthuis B, Meuli R, van Leeuwen M, Goldsher D, Pineda C, Serena J, van der Schaaf I, Waaijer A, Anderson J, Nesbit G, Gabriely I, Medina V, Quiles A, Pohlman S, Quist M, Schnyder P, Bogousslavsky J, Dillon WP, Pedraza S (2006) Perfusion-CT assessment of infarct core and penumbra: receiver operating characteristic curve analysis in 130 patients suspected of acute hemispheric stroke. Stroke 37: 979-985

Wintermark M, Bogousslavsky J (2003) Imaging of acute ischemic brain injury: the return of computed tomography. Curr Opin Neurol 16:59-63

Wintermark M, Reichhart M, Thiran JP, Maeder P, Chalaron M, Schnyder P, Bogousslavsky J, Meuli R (2002) Prognostic accuracy of cerebral blood flow measurement by perfusion computed tomography, at the time of emergency room admission, in acute stroke patients. Ann Neurol. 51(4):417-32

Wong KS, Lam WWM, Liang E, Huang YN, Chan YL, Kay R (1996) Variability of Magnetic Resonance Angiography and Computed Tomography Angiography in Grading Middle Cerebral Artery Stenosis. Stroke 27:1084-1087

Wu A, Fujikawa DG (2002) Effects of AMPA-receptor and voltage-sensitive sodium channel blockade on high potassium-induced glutamate release and neuronal death in vivo. Brain Res 946:119–129.

Xu F, Ge Y, Lu H (2009) Noninvasive quantification of whole-brain cerebral metabolicrate of oxygen (CMRO2) by MRI. Magn Reson Med 62:141-8

Yang GY, Betz AL (1994) Reperfusion-induced injury to the blood-brain barrier after middle cerebral artery occlusion in rats. Stroke 25:1658–1665

Yao H, Ginsberg MD, Eveleth DD, Lamanna C, Watson BD, Busto R (1995) Local cerebral glucose utilization and cytoskeletal proteolysis as indices of evolving focal ischemic injury in core and penumbra. J. Cereb. Blood Flow Metab. 15:398-408

Yau P (2004) Apoptosis, The Science Creative Quarterly, Issue 3. Retrieved January 10, 2008, from: http://www.scq.ubc.ca/apoptosis

Yonas H, Johnson DW and Pindzola RR (1995) Xenon-enhanced CT of cerebral blood flow. Sci Am 2:58–67

Youman P, Wilson K, Harraf F, Kalra L (2003) The Economic Burden of Stroke in the United Kingdom, PharmacoEconomics 21(1):43-50(8)

Zaman AG, Helft G, Worthley SG, Badimon JJ (2000) The role of plaque rupture and thrombosis in coronary artery disease. Atherosclerosis 149(2):251-266

Zaro-Weber O, Moeller-Hartmann W, Heiss WD, Sobesky J (2009) The performance of MRI-based cerebral blood flow measurements in acute and subacute stroke compared with 15O-water positron emission tomography. Identification of penumbral flow. Stroke 40:2413–2421

Zhang L, Zhang ZG, Zhang RL, Lu M, Adams J, Elliott PJ, Chopp M (2001) Postischemic (6-hour) treatment with recombinant human tissue plasminogen activator and proteasome inhibitor PS-519 reduces infarction in a rat model of embolic focal cerebral ischemia. Stroke 32:2926 –2931

Zhao W, Belayev L, Ginsberg MD (1997) Transient middle cerebral artery occlusion by intraluminal suture. II. Neurological deficits and pixel-based correlation of histopathology with local blood flow and glucose utilization. J. Cereb. Blood Flow Metab. 17:1281-1290